

Sheffield Hallam University

Clay-polyvinylalcohol nanocomposites: Competitive adsorption of polyvinylalcohol and plasticizers onto Na-bentonite.

KHAIRUDDIN, .

Available from the Sheffield Hallam University Research Archive (SHURA) at:

<http://shura.shu.ac.uk/19908/>

A Sheffield Hallam University thesis

This thesis is protected by copyright which belongs to the author.

The content must not be changed in any way or sold commercially in any format or medium without the formal permission of the author.

When referring to this work, full bibliographic details including the author, title, awarding institution and date of the thesis must be given.

Please visit <http://shura.shu.ac.uk/19908/> and <http://shura.shu.ac.uk/information.html> for further details about copyright and re-use permissions.

Learning and Information Services
Adsetts Centre, City Campus
Sheffield S1 1WD

26-10-00

102 070 940 5



REFERENCE

ProQuest Number: 10697214

All rights reserved

INFORMATION TO ALL USERS

The quality of this reproduction is dependent upon the quality of the copy submitted.

In the unlikely event that the author did not send a complete manuscript and there are missing pages, these will be noted. Also, if material had to be removed, a note will indicate the deletion.



ProQuest 10697214

Published by ProQuest LLC (2017). Copyright of the Dissertation is held by the Author.

All rights reserved.

This work is protected against unauthorized copying under Title 17, United States Code
Microform Edition © ProQuest LLC.

ProQuest LLC.
789 East Eisenhower Parkway
P.O. Box 1346
Ann Arbor, MI 48106 – 1346

**Clay-polyvinylalcohol nanocomposites:
Competitive adsorption of polyvinylalcohol and
plasticizers onto Na-bentonite**

Khairuddin

**A thesis submitted in partial fulfilment of the requirements of
Sheffield Hallam University
for the degree of Doctor of Philosophy**

February 2012

Declaration

The work described in this thesis was carryout out by the author in the Materials and Engineering Research Institute at Sheffield Hallam University, between October 2008 and May 2011. The author declares that this work has not been submitted for any other degree. The work is original except where acknowledged by reference.

Author:

(Khairuddin)

Director of Studies:

(Dr. Francis Clegg)

Supervisor:

(Prof Christopher Breen)

Abstract

Competitive adsorption of poly(vinyl alcohol) (PVOH) and plasticizers (PEG Mw 600 and 2000, M600 and quaternized M600) onto Na-bentonite has been studied. Preliminary experiments showed that as the concentration of plasticizers or PVOH increased, the amount adsorbed by clay increased and followed a Langmuir-type adsorption. The order of affinity to clay was PVOH, PEG2000, M600 and PEG600. Step changes occurred in the gallery with increasing amounts of plasticizer offered as it expanded from a depleted single layer through to a full single layer, then a combined single and bilayer system, and finally a full bilayer system. For PVOH, multi-layers were observed, as well as mostly exfoliated structures when the PVOH concentration was > 75 wt%. The extent of change in the d-spacings of PEG600/clay and PVOH/clay systems were shown to be greatly affected by thermal treatment and exposure to different relative humidities at low organic loadings (<17 wt%), and less at high loadings (>23 wt%). The thermal stability of PEG600 or PVOH in clay was dependant on the loading and so related to the type of structure. Desorption of organic from clay by washing up to ten times with water showed that not all organic was removed since the d-spacing of organic/clay did not collapsed to that of clay alone.

In the competitive adsorption studies, both plasticizers (PEG600 or M600) and PVOH were present within the clay gallery, the amounts of plasticizer and PVOH present increased with the amount of plasticizer and PVOH offered. The amount of PVOH adsorbed by clay was slightly increased by the presence of 1-30pph PEG600, but reduced in the presence of 30 pph M600 and 1, 10 and 30 pph QM600, whilst the amount of PEG600 or M600 adsorbed by clay was reduced when the amount of PVOH offered was increased. Samples prepared by mixing PEG600 with clay first before adding PVOH consistently exhibited slightly higher d_{001} -spacings and peak intensities when compared to the corresponding samples prepared by either mixing PEG600 and PVOH before adding clay or mixing PVOH with clay first before adding PEG600. The differences are assigned to their molecular arrangements rather than quantities adsorbed.

The tensile storage modulus, β , α temperature and E_a of PVOH/clay systems increased as the amount of clay increased whilst the opposed trend was observed for the toughness and damping properties. Introduction of clay into PVOH resulted in a reduced water permeability in the nanocomposites since an 8 times reduction was observed when clay content was 50 wt%. The opposite trend was observed when 20 wt% PEG600 was introduced to the PVOH since it increased the water permeability by 4.4 times. Introduction of clay to PVOH/PEG600 reduced the water permeability and ≈ 23 wt% clay was needed to return the WVTR value to that of PVOH alone. Besides clay, the crystallinity of PVOH was shown to reduce the water permeability of the nanocomposites. The levels of PVOH crystallinity were identified using FTIR from the intensity ratio of the bands at 1142 cm^{-1} and 2942 cm^{-1} ; the ratio increased with heating temperature and clay content but decreased with time when exposed to 85% relative humidity. In addition, the intensity of the XRD peak at $\approx 19^\circ 2\theta$, which relates to PVOH crystallinity increased with temperature and decreased with exposure time for all films. The sample crystallinity was greatly affected by water content, however, the induced crystallinity was not completely lost after being maintained at 23°C and 85 % RH for 51 days.

Dedicated to:

my wife (Nurul) and my sons (Farhan, Salim and Dzaki)

Acknowledgement

I would like to thank all the people who have helped and inspired me during my doctoral study at the Materials and Engineering Research Institute, Sheffield Hallam University.

First and foremost I would like to thank my Director of Studies, Dr Francis Clegg, for his guidance during my research and study. He has supported me throughout with his patience and knowledge whilst allowing me the room to work in my own way. I attribute the level of my PhD to his encouragement and effort and without him this thesis, too, would not have been completed or written. One simply could not wish for a better or friendlier Director of Studies.

I offer my sincerest gratitude to my supervisor, Prof Christopher Breen, for making this PhD project possible. In retrospect, I am amazed by his confidence to hire me as his PhD research student. I received precious experiences by attending many world class conferences and during my study he made every effort to make me succeed. In addition, he was always accessible and willing to help.

Prof Mo Song from Loughborough University and Dr. Chris Sammon deserved special thanks as my external and internal examiners. They broadened my perspective on data analysis particular to my PhD work. They helped me enjoy the viva and gave nice conversation.

I would to thank Prof Chris Care and Prof Bob Akid, the former and current Directors of MERI, and all MERI staff including Rachael Toogood, Indira and Corrie Houton for providing the support and help I have needed during my study.

Special acknowledgement also goes to Prof Doug Cleaver, Head of Postgraduate Studies, for a constant source of encouragement during my study.

I would like to thank the many technicians in the various laboratories and workshops who have aided me over the years, including Robert Burton for running the XRD and analysing my samples using XRF and Deeba Zahoor who helped tutor me in TGA, DSC and FTIR as well checking I followed the safety regulations in practical work. In particular, I would like to thank Kevin Osborne who allowed me to use his lab as part of the preparation of quaternized M600. He also kindly analysed my samples using Proton NMR.

It is also a pleasure to thank PCAS group members including; Michael Barwood, Victoria Boyes, Dr Marianne Labet, Dr. Fabio Papini, Dr. Subodh Sabnis, Dr. Prakash Muthudoss, Scott Bannister and Hakan Keles. I am also grateful to all my buddies in room 508 (Norfolk Building) including Dr. Salah Gnefid, Dr. Mousa May, Dr. Ante Hecimovic, Dr. Ganesh Kamath, Sampan Seth, Daniel Loch, Stephen Dodds, Chinh Nguyen, Arunprabhu Arunachalam Sugumaran, Vikas Jawla and Itai Vutabwarova. They made the environment a convivial place to work in.

In my daily life in Sheffield I have been blessed with the friendly and cheerful members of the Indonesian Society. They made me and my family's life like that in Indonesia. In particular, I would like to thank Indonesian Embassy in London for giving me the necessary support and help whilst I and my family lived in the UK.

The funding support for the PhD study came from the Indonesian Government through a DIKTI scholarship and is greatly appreciated. Without this scholarship,

my ambition to study abroad could not be realized. I would like to thank the Rector of Sebelas Maret University who gave me the opportunity. Thanks also to my colleagues in Physics Department at Sebelas Maret University who took responsibility for teaching during my PhD study.

My deepest gratitude goes to my family for their unflagging love and support throughout my life; this thesis is simply impossible without them. I am indebted to my mother Madiana and my father H. MS. Tadjuddin. Although they are no longer with us, they are forever remembered. I am sure they share our joy and happiness in heaven. The support and prayers of my parents in-law Hj. Nurtini and H. Jafar Dzakaria, my step mother Siti Hadijah, and great family of H.MS Tadjuddin and H. Jafar Dzakaria were a bridge for my success. My brother H Dar and his family deserve special gratitude, they were available to give a hand anytime. I feel proud of my wife, Nurul, for her constant support, love and encouragement to pursue this degree. My tough times are made easy by the presence of my lovely sons: Farhan, Salim and Dzaki.

Last but not least, thanks be to God for my life through all tests in the past 3 years. You have made my life more bountiful. May your name be exalted, honoured and glorified.

Content

1. Introduction	1
1.1. Background and justification of research	2
1.2. Aim of the project	5
1.3. References	8
2. Literature review	13
2.1. Clay	14
2.2. Poly(vinyl alcohol)(PVOH)	17
2.3. Poly(ethylene glycol)(PEG)	21
2.4. Poly(propylene glycol)(PPG)	22
2.5. Polytheramines	23
2.6. Polymer clay nanocomposites	24
2.6.1. Structure of polymer clay nanocomposites	25
2.6.2. Permeability in polymer clay nanocomposites	26
2.6.3. Preparation techniques	28
2.6.4. Poly(vinyl alcohol)(PVOH)/clay nanocomposites	29
2.6.5. Poly(ethylene glycol)(PEG)/clay nanocomposites	34
2.6.6. Polytheramines/clay nanocomposites	40
2.7. References	45
3. Techniques	56
3.1. X-ray diffraction (XRD)	57
3.2. Thermogravimetric analysis (TGA)	60
3.3. Adsorption isotherms (centrifugation approach)	62
3.4. Thermogravimetric mass spectroscopy (TGMS)	64

3.5. Water vapour transmission rate (WVTR)	65
3.6. Dynamic mechanical analysis (DMA)	66
3.7. Fourier transform infrared spectroscopy (FTIR)	67
3.8. X-ray fluorescence (XRF)	68
3.9. Nuclear magnetic resonance (NMR)	68
3.10. References	69
4. Experimental	71
4.1. PVOH/clay nanocomposites	72
4.2. PEG, PPG, M600/clay nanocomposites	72
4.3. PVOH/PEG600/clay nanocomposites	73
4.4. Quaternized M600/clay nanocomposites	73
4.5. PVOH/QM600/clay nanocomposites	74
4.6. References	76
5. Competitive and synergistic adsorption of PVOH and PEG600 on clay	77
5.1. Clay dispersion	78
5.1.1. PVOH/clay binary system	78
5.1.2. Effect of thermal treatment and relative humidity on the d-spacing of in PVOH/clay composites	83
5.1.3. PEG600/clay binary system	88

5.1.4. Effect of thermal treatment and relative humidity on the d-spacings of PEG600/clay composites	91
5.1.5. PVOH/PEG600/clay tertiary system and different sequence of mixing	94
5.1.6. Effect of thermal treatment and relative humidity on the clay dispersion in PVOH/PEG600 clay nanocomposite	101
5.2. Thermal stability	105
5.2.1. Effect of clay concentration on the thermal stability of PVOH/clay composites	105
5.2.2. Effect of clay concentration on the thermal stability of PEG600/clay composites	112
5.2.3. Effect of clay concentration on the thermal stability of PVOH/ PEG600/clay composites	115
5.3. Competitive adsorption and effect of different route of mixing	119
5.3.1. Quantification of the amount of PVOH and PEG600 adsorbed by clay	119
5.3.2. Adsorption of PVOH onto clay from aqueous solution	120
5.3.3. Adsorption of PEG600 onto clay from aqueous solution	124
5.3.4. Competitive and synergistic adsorption of PVOH and PEG600 onto clay from aqueous solution	129
5.3.5. Effect of sequence of addition on the adsorption of PVOH and PEG600 onto clay from aqueous solution	136
5.4. References	140

6. Adsorption of PEG2000, M600 and QM600 in the absence and presence of PVOH onto clay	143
6.1. Adsorption of PEG2000 or M600 onto clay from aqueous solution in the absence of PVOH	144
6.2. Comparison of PVOH and plasticizers adsorption onto clay in binary systems from aqueous solution	147
6.3. Adsorption of Quaternized M600 (QM600) onto clay from aqueous solution in the absence of PVOH	151
6.4. Competitive adsorption of PVOH and M600 onto clay from aqueous solution	157
6.4.1. Quantification of the amount of PVOH and M600 adsorbed by clay	157
6.4.2. Adsorption of PVOH and M600 onto clay from aqueous solution	158
6.5. Adsorption of PVOH from aqueous onto cation-exchanged QM600-clay	164
6.6. Comparison of PVOH adsorption from aqueous solution in the presence of PEG600, M600, and QM600	170
6.7. Desorption of organics from aqueous solution	178
6.8. References	184
7. Physical and barrier properties of PVOH films in the absence and presence of clay and PEG600	186
7.1. Mechanical properties of PVOH/clay films	187
7.2. Water vapour barrier properties of PVOH and PVOH/clay films in the absence and presence of PEG600	194

7.2.1. PVOH/clay films in the absence of PEG600	194
7.2.2. PVOH/clay films in the presence of PEG600 and its comparison in the absence of PEG600	196
7.3. Effect of PVOH crystallinity on water vapour barrier properties in the absence and presence of clay	199
7.4. References	212
8. Conclusion and future works	215
8.1. Introduction	216
8.2. Competitive and synergistic adsorption of PVOH and PEG600 on clay	216
8.3. Adsorption of PEG2000, M600 and QM600 in the absence and presence of PVOH onto clay	218
8.4. Physical and barrier properties of PVOH films in the absence and presence of clay and PEG600	220
8.5. Future works	222
8.6. References	225
Appendix	226
A1. Award and presentation in seminar and conferences	227
A2. Conference and seminar attended	229

List of figures

Figure 2.1. Structure of 2:1 layered silicates	14
Figure 2.2. Swelling of clay in the presence of water	15
Figure 2.3. Various arrangements of clay layers in dry state (a) and in water (b-c)	16
Figure 2.4. Structure for the intercalated surfactants	17
Figure 2.5. Molecular structure (a) and Sakurada's structural model (b) of Poly(vinyl alcohol) (PVOH)	19
Figure 2.6. Molecular structure of poly(ethylene glycol) (PEG)	22
Figure 2.7. Molecular structure of polypropylene glycol (PPG)	23
Figure 2.8. Molecular structure of Jeffamine M series	23
Figure 2.9. The different ways in which clay layers can be dispersed within a polymer matrix (not to scale)	26
Figure 2.10. Schematic illustration of tortuosity for a diffusing penetrant introduced to exfoliated clay, layered in a polymer matrix. (A) Filled polymer and (B) Unfilled polymer	27
Figure 3.1. Schematic of x-ray diffractometer	58
Figure 3.2. Schematic depicting the expected X-ray diffraction patterns for various types of clay/polymer structures	58
Figure 3.3. Schematic diagram of a TGA instrument	61

Figure 3.4. Diagrammatic representation of TGA and derivative TG (DTG)

data curve 61

Figure 3.5. Schematic experiment of centrifugation approach 64

Figure 5.1. XRD traces from PVOH/Clay composites at low

PVOH content 79

Figure 5.2. XRD traces from PVOH/Clay composites at intermediate

PVOH content 80

Figure 5.3. XRD traces from PVOH/Clay nanocomposites at high

PVOH content 80

Figure 5.4. Summary of d-spacings from XRD traces of PVOH/Clay

nanocomposites 82

Figure 5.5. The influence of thermal treatment and relative humidity on the
diffraction patterns of sodium clay 83

Figure 5.6. The influence of thermal treatment and relative humidity on the
diffraction patterns of PVOH/clay nanocomposites 85

Figure 5.7. Summary of d-spacings from PVOH/clay composites under the
influence of thermal treatment and relative humidity 87

Figure 5.8. XRD traces for PEG600/Clay nanocomposites at low PEG600
content 89

Figure 5.9. XRD traces for PEG600/Clay nanocomposites at low PEG600
content 89

Figure 5.10. Summary of d-spacings observed in the XRD traces of PEG600/Clay composites	90
Figure 5.11. Influence of thermal treatment and relative humidity on the diffraction patterns of PEG600/clay composites	92
Figure 5.12. Summary of d-spacings of PEG600/clay composites under the influence of thermal treatment and relative humidity	93
Figure 5.13. XRD patterns from tertiary systems of PEG600/PVOH/clay composites for moderate PVOH content (10 pph)	95
Figure 5.14. The d-spacing of PEG600/PVOH/clay composites when PVOH content of 2 pph (a), 5 pph (b), 10 pph (c), 15 pph (d) and 50 pph (e) along d-spacing of PEG600/clay	97
Figure 5.15. XRD patterns from PEG600/PVOH/clay composites	99
Figure 5.16. The d-spacings of PEG600/PVOH/clay composites prepared in route 1 (R1), route 2 (R2) and route 3 (R3) when PVOH content is (a) 2 pph, (b) 10 pph, (c) 15 pph and (d) 50 pph along with the d-spacings of PEG600/clay	100
Figure 5.17. Influence of thermal treatment and relative humidity on the d-spacings of PEG600/PVOH/clay composites prepared via route 1, a-c) contain low PVOH levels (2 pph), d-f) contain medium PVOH levels (10 pph) (continued on next page)	102

Figure 5.18. a) selected XRD patterns collected from samples prepared via route 3 and at various temperatures and humidities.	
Selected XRD traces of composites heated at 150 °C prepared via b) route 1 and c) route 3	103
Figure 5.19. Thermograms (a) and their negative derivatives (b) of PVOH/clay composites and PVOH film	108
Figure 5.20. Weight loss in a) the first region (35-150 °C), b) second region (200 – 385 °C), c) third region (400-550 °C) and the sum of second and third regions for clay, PVOH and PVOH/clay mixtures	109
Figure 5.21. Mass chromatograms for volatile degradation products during the thermal degradation of PVOH	110
Figure 5.22. Summary of thermal stability (derivative peak maxima) of a) the 2 nd peak and b) the 3 rd peak for PVOH and PVOH/clay	111
Figure 5.23. a) Thermograms and b) their derivatives of PEG600/clay composites and PEG600	113
Figure 5.24. a) Weight loss in the first peak (35-150 °C) and b) second peak (150-460 °C) for clay, PEG600 and PEG600/clay composites	113

Figure 5.25. Summary of thermal stability (derivative peak maxima) for PEG600 and PEG600/clay composites	114
Figure 5.26. Negative derivative thermograms for PEG600, PVOH, PEG600/PVOH, PEG600/clay and PVOH/clay	116
Figure 5.27. Mass chromatograms obtained from volatile degradation products during the thermal degradation of a PEG600/PVOH mixture (50 wt %)	116
Figure 5.28. Derivative thermograms for PEG600/PVOH/clay nanocomposites with fixed amounts of PVOH (a) and PEG600 (b)	118
Figure 5.29. Weight losses from the 1st maximum as a function of actual PVOH content in PEG600/PVOH mixtures	120
Figure 5.30. XRD patterns of PVOH/Clay a) 2-25 wt% PVOH and b) 23-95 wt% PVOH composites prepared from suspension (full line) and from sediment (dashed line) after centrifugation	122
Figure 5.31. Summary of d-spacings observed in the XRD traces of PVOH/Clay composites prepared from full suspension (BC) and sediment (AC)	123
Figure 5.32. Adsorption data of PVOH onto clay from aqueous solution calculated via the centrifugation approach	123

Figure 5.33. The XRD patterns of PEG600/Clay a) 1-17 wt% and b) 23-95 wt% composites prepared from full suspension (full line) and from sediment (dashed line)	125
Figure 5.34. Summary of d-spacings observed in the XRD traces of PEG600/Clay composites prepared from full suspension (BC) and sediment (AC)	126
Figure 5.35. Adsorption data of PEG600 onto clay from aqueous solution (via centrifugation approach)	127
Figure 5.36. Adsorption isotherms of either PEG600 or PVOH on clay as a function “free organic” concentration in solution for concentrations up to a) 0.5 g/ml and b) 0.015 g/ml	128
Figure 5.37. The XRD patterns and d-spacings of PEG600/PVOH/Clay nanocomposites when amount of clay is 100 pph and PEG600 are a) 1 pph, b) 10 pph and c) 30 pph prepared from suspension (BC) and from sediment (AC)	131
Figure 5.38. Competitive adsorption data of PVOH and PEG600 onto clay from aqueous solution in tertiary systems (TS) (a) and its comparison with binary system (BS) when the amount of PEG600 is constant; 1 (b), 10 (c), and 30 pph (d). G refers to organic adsorbed by clay and F refers to organic in the supernatant	132

Figure 5.39. Summary of competitive adsorption data of PEG600 and PVOH onto clay from aqueous solution for binary (BS) and tertiary systems (TS). TS (PEG-1) represents the adsorption of PVOH in the presence of 1 pph PEG600 in the tertiary system. TS (PVOH-2) represents the adsorption of PEG600 in the presence of 2 pph PVOH in the tertiary system

133

Figure 5.40. Typical XRD patterns from PEG600/PVOH/clay composites prepared by routes 1, 2 and 3. For each route the amount of PEG600, PVOH and clay are 10, 50 and 100 pph, respectively and prepared from full suspension or from sediment after centrifugation

136

Figure 5.41. Competitive adsorption of PEG600 and PVOH onto clay from aqueous solution for route 1 (R1), route 2 (R2) and route 3 (R3) in tertiary system (continued on next page)

137

Figure 6.1. XRD patterns of a) PEG2000/clay and b) M600/clay composites prepared from full suspension (full lined traces: BC) or sediment after centrifugation (dashed traces: AC). Their respective d-spacings are plotted against concentration of c) PEG2000 or d) M600

145

Figure 6.2. Data from adsorption experiment (centrifugation approach) of PEG2000 and M600 onto clay from aqueous solution

146

Figure 6.3. XRD traces of organic/clay binary systems for PEG600, M600, PEG2000 and PVOH from films prepared from sediment after centrifugation. Traces are offset for clarity	148
Figure 6.4. Comparison of adsorption data for organic gallery and free organic as a function of organic offered	149
Figure 6.5. Organic uptake by clay as a function of “free organic” concentration ranges up to a) 0.5 g/ml and b) 0.005 g/ml	150
Figure 6.6. FTIR spectra of M600, QM600 and QM600 heated at 60 °C	154
Figure 6.7. Amounts of QM600 exchanged as a function of QM600 offered expressed as CEC (a) and gram/gram of clay (b) and determined by either TGA or XRF measurement	155
Figure 6.8. XRD patterns of QM600 exchanged clay	156
Figure 6.9. DTG’s of M600, PVOH and PEG600/PVOH mixtures	158
Figure 6.10. XRD patterns and d-spacings of M600/PVOH/Clay nanocomposites prepared from suspension (BC) and from sediment (AC) when amounts of clay is 100 pph and M600 are a) 1 pph, b) 10 pph and c) 30 pph	160
Figure 6.11. Competitive adsorption data of PVOH and M600 onto clay from aqueous solution in tertiary system (TS) (a) and its comparison with PVOH/clay binary system when the amount of M600 is constant; 1 (b), 10 (c), and 30 pph (d)	161

Figure 6.12. Competitive adsorption data of M600 and PVOH onto clay from aqueous solution. TS represents the tertiary systems, whereas BS represents the binary systems, the associated numbers represent the concentrations of PVOH or M600 offered 163

Figure 6.13. The XRD patterns and d-spacing of QM600/PVOH/Clay composites where the amount of clay is 100 pph and QM600 is constant, i.e. a) 2, b)10 pph and c) 30 pph, respectively prepared from suspension (BC) and from sediment (AC) 166

Figure 6.14. Adsorption of PVOH onto clay from aqueous solution in the present of QM600 (a) and its comparison with binary system (BS) when the amount of QM600 is constant; 2 (b), 10 (c), and 30 pph (d) 167

Figure 6.15. Competitive adsorption of PVOH onto clay from aqueous solution in the present of QM600 (tertiary system-TS) and its comparison with that in the binary system (BS) 170

Figure 6.16. Comparison of XRD traces from PEG600/PVOH/clay, M600/PVOH/clay and QM600/PVOH/clay films prepared from sediment (AC films). The amounts of PEG600 and M600 are fixed at 1pph and that of QM600 at 2 pph in a) all plasticizer concentrations are fixed at 10 pph in b) and 30pph in c) 172

Figure 6.17. Comparison of the combined amounts of PVOH and plasticizer adsorbed onto clay from aqueous solution in the presence of fixed amounts of PEG600, M600, and QM600 i.e. a) 1 pph for PEG600 and M600 and 2 pph for QM600, b) 10 pph and c) 30 pph 173

Figure 6.18. Competitive adsorption data of PVOH and plasticizer onto clay from aqueous solution in the presence of fixed amounts of PEG600, M600, and QM600 i.e. a) 1 pph for PEG600 and M600 and 2 pph for QM600, b) 10 pph and c) 30 pph. The amounts in solution are not presented 175

Figure 6.19. Adsorption data of a) PVOH from aqueous solution in the presence of varying plasticizer (PEG600, M600 and QM600) concentrations and b) adsorption data of PEG600 and M600 from aqueous solution in the presence of varying PVOH concentrations 177

Figure 6.20. XRD traces of a) PEG600 and b) PPG725 after being offered at 16.7 wt% loading (from full suspension) and after being washed 1 – 10 times (from sediment after centrifugation) 179

Figure 6.21. XRD traces of a) PPG2000 and b) PVOH after being offered at 16.7 wt% loading (from full suspension) and after being washed 1 – 10 times (from sediment after centrifugation) 180

Figure 6.22. a) Amounts of PEG600, PPG725, PPG2000 and PVOH adsorbed on clay before and after washing (numbers in graph represent the final wt% of organic remaining on the clay) and b) concentrations of PEG600, PPG725, PPG2000 and PVOH removed from the organic/clay complexes during successive washings 181

Figure 7.1. a) Tensile storage modulus, E' and b) $\log E'$ for PVOH and PVOH/clay composites as a function of temperature (Frequency 1 Hz). The samples were equilibrated in the humidity oven at 23 °C

and 85 % relative humidity (RH) for 24 hours before performing the DMA experiment	189
Figure 7.2. Tan δ of PVOH and PVOH/clay nanocomposites as a function of temperature (Frequency 1 Hz)	191
Figure 7.3. a) Tan δ at transition (T_g) measured at peak height and b) peak temperature (T_g) as function of clay content	192
Figure 7.4. Logarithmic frequency as a function of temperature (a) and activation energy E_a as function of clay content (b)	192
Figure 7.5. Amount of water (g) transmitted through PVOH and PVOH/clay nanocomposites	195
Figure 7.6. Water vapour transmission rates for PVOH and PVOH/clay nanocomposites	195
Figure 7.7. Amount of water transmitted through PVOH(80-x)/clay(x wt%)/PEG600(20) films	198
Figure 7.8. Water vapour transmission rate (WVTR) values for PVOH/PEG600/clay nanocomposites films	198
Figure 7.9. Comparison WVTR from PVOH/clay and PVOH/clay/PEG600 after normalisation to that of PVOH alone	199
Figure 7.10. Water vapour transmission rate (WVTR) values for PVOH/clay composites	201
Figure 7.11. FTIR spectra collected on D1 of PVOH films treated at different temperature	203

Figure 7.12. FTIR spectra of PVOH films heated at 200 °C on D1, D3 and D52	203
Figure 7.13. FTIR spectra of PVOH, PVOH/clay 5 wt% and PVOH/clay 10 wt% heated at 200 °C on D1	204
Figure 7.14. intensity ratios of 1142 to 2942 cm^{-1} bands from PVOH (a) and PVOH/clay 5 wt% (b) and PVOH/clay 10 wt% (c) as a function of time (days)	205
Figure 7.15. XRD traces of unheated and heated PVOH films on D1	207
Figure 7.16. XRD traces of PVOH films heated at 200 °C on D1, D3 and D52	207
Figure 7.17. XRD traces of PVOH and PVOH/clay 5 wt% and PVOH/clay 10 wt% heated at 200 °C on D1	208
Figure 7.18. a) Percentage weight change from initial weight (≈ 0.14 g) of a) PVOH, b) PVOH/clay 5 wt% and c) PVOH/clay 10 wt% films	209

Term used in this work

MMT: monmorillonite

PVOH: Poly(vinyl alcohol)

PEG: Poly(ethylene glycol)

PPG: Poly(propylene glycol)

XRD: X-ray diffraction

TGA: Thermogravimetric analysis

TGMS: Thermogravimetric mass spectroscopy

WVTR: Water vapour transmission rate

DMA: Dynamic mechanical analysis

FTIR: Fourier transform infrared spectroscopy

XRF: X-ray fluorescence

NMR: Nuclear magnetic resonance

1.1. Background and justification of research

Polymer clay nanocomposites have attracted great attention in the last decade since they simultaneously impart significant improvements in mechanical, barrier and fire retardant properties when compared with those of the pure polymer [1.1,1.2]. It is well known that the addition of as little as 5 wt% clay can give the same level of mechanical and thermal improvement as those typically achieved with loadings of 20-40 wt% of micron size fillers such as glass fibre, talc, calcium carbonate or carbon black [1.3].

Na-bentonite is a naturally occurring clay of the smectite family having a 2:1 layered structure; each layer (or sheet) is 1 nm thick and consists of an octahedral sheet of alumina sandwiched between two tetrahedral sheets of silica [1.4,1.5]. It is hydrophilic and disperses readily into water soluble polymers such as poly(vinyl alcohol) (PVOH) [1.6-1.9], poly(ethylene oxide) [1.10-1.12] and starch [1.13,1.14]. Therefore, it is relatively straightforward to cast self-supporting films of these polymer nanocomposites from water. However, these hydroxylated polymers tend to be brittle and successful production of polymer films or coatings may require the addition of a suitable plasticizer. Sequestering of plasticizer by the clay may lead to brittle films and in addition the dispersion of clay may be affected by the plasticizer.

Currently, there is a debate about how polymer-plasticizer-clay mixtures interact and in turn how it affects their properties. For example, the incorporation of clay increased the crystallinity of poly(lactic Acid) (PLA) [1.15-1.20] when the nanocomposites were intercalated, but the opposite effect was observed when they were exfoliated [1.15-1.18]. In other systems, it was reported that clay promoted crystallization of PVOH [1.8], polypropylene [1.21]

and nylon-6 [1.22], whilst the opposite effect was reported for PEO [1.12,1.23]. Poly(ethylene glycol) (PEG), as plasticizer, was shown to increase the crystallinity of PLA [1.18,1.19,1.20,1.24] by enhancing a higher mobility of PLA chains and promoting crystallization kinetics, whilst Ozkog [1.19] reported that PEG nearly had no effect on the crystallinity of PLA. In another system, Jang [1.25] reported that the plasticizer glycerine reduced the crystallinity of PVOH. Lower crystallinities of polymer can lead to an increase in their biodegradation rate, but reduce both their water vapour barrier properties and modulus. Generally, plasticizer is used to improve the flexibility of material, but it can also promote exfoliation of clay [1.19,1.20]. When polymer and plasticizer are mixed with clay to produce nanocomposites, preferential adsorption of the polymer and/or plasticizer into the clay gallery can occur [1.20,1.26]. It can be difficult to quantify the amounts of plasticizer and polymer that reside in or outside the clay gallery, but their quantification is very important as the polymer-plasticizer compositions determine the final properties of the nanocomposites.

Most adsorption studies of polymer or plasticizer on clay reported so far in the literature [1.6,1.7,1.10,1.11] have only focused on binary systems, i.e. polymer/clay or plasticizer/clay mixtures. Also the results were not correlated with mechanical and barrier properties of the systems under study. A study of the competitive adsorption of PEG's with different molecular weight on clay was reported by Chen [1.26], again there was no information on how adsorption of the polymer on clay affected the properties of the nanocomposites. Moreover, theoretical descriptions for these systems are limited [1.27,1.28]. Therefore, comprehensive studies of synergistic and competitive adsorption covering different polymer-clay-plasticizer compositions, their sequence of mixing, and how they affect the mechanical and barrier properties is much sought after.

In this project, PVOH has been selected as a 'model' hydrophilic polymer in an attempt to investigate its competitive adsorption with different plasticizers into the clay gallery. Furthermore, the mechanical and barrier properties of these composites have been assessed since the dispersion of clay in PVOH with plasticizers can be affected by creating intercalated rather than exfoliated structures [1.8,1.9]. PVOH is of interest since it is used as a barrier film for food packaging applications due to its; excellent oxygen barrier properties, flexibility, transparency, toughness, biodegradability as well as being relatively cheap when compared with other barrier polymers [1.29].

The largest demanding application of polymers is for packaging, which shares 42% of 100 million tonnes of today's polymer global market [1.30]. Incorporation of clay in polymers used for food packaging is performed mostly to improve gas and water barrier permeability [1.30]. It is reported that clay shares nearly 70% of the market volume of nanoparticles used in food packaging. The barrier improvement is due to tortuous effects of clay forcing the gas permeant to travel a longer path as it diffuses through the film and also influence of the clay on the crystallinity of polymer. In a particular commercial application, it is reported that clay can cut water and gas permeability of polyethylene terephthalate (PET) by as much as 75% [1.31]. Recently, Priolo [1.32] developed a transparent, super gas barrier with polyethylenimine (PEI)-poly(acrylic acid)(PAA)-montmorillonite (MMT) nanocomposites that can cut oxygen permeability by almost 100 %. The addition of clay to polymer not only improves polymer performance but also has economical and environmental advantages such as; the reduction in use of raw materials due to improved stiffness and also savings in the cost of transportation, the reduced storage of crushed empty containers whilst waiting for recycling, reductions in CO₂

emissions, and improvements in biodegradability of polymers such as PLA, polybutyrene succinate (PBS) and polycaprolactone (PCL). Positive impact of clay on human health was reported by de Abreu [1.33] who found that incorporation of clay into polyamide was able to slow down the rate of migration of substances such as caprolactam, 5-chloro-2-(2,4-dichlorophenoxy)phenol (triclosan) and trans,trans-1,4-diphenyl-1,3-butadiene (DPBD) from polyamide into the food by up to six times.

1.2. Aim of the project

The principle aim of this project is to understand the competitive and synergistic interaction between clay-PVOH-plasticizer mixtures, for example, which molecule has greater affinity for the adsorption sites of the clay gallery. Such understanding will be reviewed to help improve the mechanical and barrier properties of PVOH. To achieve this, several techniques will be used such as X-ray diffraction (XRD), adsorption studies via a centrifugation approach, thermogravimetric analysis (TGA) and dynamic mechanical analysis (DMA). Particular emphasis was given to TGA since this technique indirectly allowed the amounts of polymer and plasticizer adsorbed onto the clay to be quantified. The degradation profile of each component within a mixture was sufficiently resolved to allow an accurate and calibrated method for quantification to be established. The thermal stability and degradation of these composites were also investigated using thermogravimetry mass spectroscopy (TG-MS).

This first chapter outlines the background and justification for the research together with aims and objectives. The literature is reviewed and

discussed in Chapter 2, which covers details of the materials investigated within the project and a survey of the relevant work published on polymer/clay nanocomposites. Detail of the techniques used in this project are presented in Chapter 3 and include; TGA, XRD, adsorption isotherms (centrifugation approach), TGMS, water vapour transmission rate (WVTR), DMA, Fourier transform infrared (FTIR), X-ray fluorescence (XRF) spectroscopy and proton nuclear magnetic resonance (^1H NMR). The sample preparation of polymer clay nanocomposites via solution casting, the synthesis of quaternized polyetheramine and its subsequent cation exchange reaction onto Na montmorillonite is presented in Chapter 4.

The competitive and synergistic adsorption of PEG600 and PVOH on clay has been investigated and results are presented in Chapter 5. This includes an investigation of clay dispersion and subsequent thermal stability of PVOH or PEG600/clay composites. The amount of water in the systems has also been assessed and controlled by varying temperature and humidity. In the competitive study between PVOH and plasticizer with clay, particular attention has been given to the dispersion of clay and how it is effected by different routes of mixing. Quantified amounts of PVOH and/or PEG600 adsorbed by clay in the binary and tertiary systems have also been investigated.

The adsorption of different plasticizers, such as PEG with molecular weight (Mw) of 2000 (PEG2000), polyetheramine (M600) and quaternised polyetheramine (QM600) in the absence and presence of PVOH onto clay is presented in Chapter 6, this allows the the effects of plasticizer molecular weight (Mw), polarity and solubility to be studied. The effect of anchoring quaternised polyetheramine onto clay on PVOH adsorption has also been investigated. The desorption of organics such as PEG600, polypropylene glycol

with MW of 725 and 2000 (PPG725 and PPG2000) and PVOH from clay is also presented to demonstrate the mobility or immobility of these components from clay.

The physical and barrier properties of PVOH films in the absence and presence of clay and/or PEG600 is presented in Chapter 7. PVOH is sensitive to water vapour and as a result can affect its ability to act as an oxygen barrier. PVOH is typically laminated between materials with good water barrier properties so that the PVOH film remains free from water and hence impermeable to oxygen. The effect of water content on the crystallinity of PVOH films and their ability to act as water barriers has been assessed. The rate at which the extent of crystallinity decreases when held at controlled temperature and relative humidity was investigated. Finally, conclusions from the research and future work are discussed in Chapter 8.

1.3. References

- [1.1]. Kojima, Y., Usuki, A., Kawasumi, M., Okada, A., Kurauchi, T.T. and Kamigaito. O. J. (1993). Synthesis of nylon 6–clay hybrid by montmorillonite intercalated with ϵ -caprolactam. *Journal of polymer science, part A, polymer chemistry*, **31**(4), 983-986.
- [1.2]. Kawasumi, M. (2004). The discovery of polymer clay hybrids. *Journal of polymer science, part A, polymer chemistry*, **42** (4), 819-824.
- [1.3]. Okada, A. and Usuki, A. (2006). Twenty years of polymer-clay nanocomposites. *Macromolecular materials and engineering*, **291** (12), 1449-1476.
- [1.4]. Grim, R.E. (1953). Clay mineralogy. New York, McGraw-Hill.
- [1.5] Brindley SW, Brown G, editors (1980). Crystal structure of clay minerals and their X-ray diffraction. London, Mineralogical Society.
- [1.6]. Chang, S. H., Ryan, M.E., Gupta, R.K. and Swiatkiewicz, B. (1991). The adsorption of water-soluble polymers on mica, talc limestone, and various clay minerals. *Colloids and surfaces*, **59** (0), 59-70.
- [1.7]. De Bussette, S.G. and Ferreiro, E.A. (2004). Adsorption of poly(vinyl alcohol) on montmorillonite. *Clays and clay minerals*, **52** (3), 334-340.
- [1.8]. Strawhecker, K.E. and Manias, E. (2000). Structure and properties of poly (vinyl alcohol)/Na montmorillonite nanocomposites. *Chemistry of materials*, **12** (10), 2943-2949.
- [1.9]. Doeppers, L.M. (2004). Preparation and characterisation of poly(ethylene terephthalate) and poly(vinyl alcohol)/clay nanocomposites. *Ph.D thesis*, Sheffield Hallam University-UK.

[1.10]. Parfitt, R.L. and Greenland, D.J. (1970). The adsorption of poly(ethylene glycol) on clay minerals. *Clay minerals*, **8** (3), 305.

[1.11]. Chen, B. and Evans, J. R. G. (2005). X-ray diffraction studies and phase volume determinations in poly (ethylene glycol)-montmorillonite nanocomposites. *Polymer International*, **54** (5), 807-813.

[1.12]. Strwahecker, K.E. and Manias, E. (2003). Crystallization behavior of poly (ethylene oxide) in the presence of na montmorillonite fillers. *Chemistry of materials*, **15** (4) , 844-849.

[1.13]. Tang, X. and Alavi, S. (2011). Recent advances in starch, polyvinyl alcohol based polymer blends, nanocomposites and their biodegradability. *Carbohydrate polymers*, **85** (1), 7-16.

[1.14]. Amass, W., Amass, A. and Tighe, B. (1998). A review of biodegradable polymers: Uses, current developments in the synthesis and characterization of biodegradable polyesters, blends of biodegradable polymers and recent advances in biodegradation studies. *Polymer international*, **47** (2), 89-144.

[1.15]. Krikorian, V. and Pochan, D.J. (2003). Poly (l-lactic acid)/Layered silicate nanocomposite: Fabrication, characterization, and properties. *Chemistry of materials*, **15** (22), 4317-4324.

[1.16]. Krikorian, V. and Pochan, D.J. (2004). Unusual crystallization behavior of organoclay reinforced poly(l-lactic acid) nanocomposites. *Macromolecules*, **37** (17), 6480-6491.

[1.17]. Krikorian, V. and Pochan, D.J.(2005). Crystallization behavior of poly(l-lactic acid) nanocomposites: Nucleation and growth probed by infrared spectroscopy. *Macromolecules*, **38** (15), 6520-6527

[1.18]. Ray, S. S. and Okamoto, M. (2003). Biodegradable polylactide and its nanocomposites: Opening a new dimension for plastics and composites. *Macromolecular rapid communications*, **24** (14), 815-840.

[1.19]. Ozkog, G. and Kemaloglu, S. (2009). Morphology, biodegradability, mechanical, and thermal properties of nanocomposite films based on PLA and plasticized PLA. *Journal of applied polymer science*, **114** (4), 2481-2487.

[1.20]. Pluta, M., Paul, M.M., Alexandre, M., and Dubois, P. (2006). Plasticized polylactide/clay nanocomposites. I. the role of filler content and its surface organo-modification on the physico-chemical properties. *Journal of polymer science-B-polymer physics edition*, **44** (2), 299-311.

[1.21]. Maiti, P., Nam, P.H., Okamoto, M., Kotaka, D., Hasegawa, N. and Usuki, A. (2002). The effect of crystallization on the structure and morphology of polypropylene/clay nanocomposites. *Polymer engineering and science*, **42** (9), 1864–1871.

[1.22]. Lincoln, D.M., Vaia, R.A., Wang, Z.G., Hsiao, B.S. and Krishnamoorti, R. (2001). Temperature dependence of polymer crystalline morphology in nylon 6/ montmorillonite nanocomposites. *Polymer*, **42** (25), 9975-9985.

[1.23]. Liao, B., Song, M., Liang, H. and Pang, Y. (2001). Polymer-layered silicate nanocomposites. 1. A study of poly(ethylene oxide)/Na⁺-montmorillonite nanocomposites as polyelectrolytes and polyethylene-block-poly(ethylene

glycol) copolymer/Na⁺-montmorillonite nanocomposites as fillers for reinforcement of polyethylene. *Polymer*, **42** (25), 10007-10011.

[1.24]. Pillin, I., Montrealy, N. and Grohens, Y. (2006). Thermo-mechanical characterization of plasticized PLA: Is the miscibility the only significant factor?. *Polymer*, **47** (13), 4676-4682.

[1.25]. Jang, J. and Lee, D.K.(2003). Plasticizer effect on the melting and crystallization behavior of polyvinyl alcohol. *Polymer*, **44** (26), 8139-8146.

[1.26]. Chen, B. and Evans, J.R.G. (2004). Preferential intercalation in polymer-clay nanocomposites. *The journal of physical chemistry B*, **108** (39), 14986-14990.

[1.27]. Vaia R. A. and Giannelis, E. P. (1997). Lattice Model of Polymer Melt Intercalation in Organically-Modified Layered Silicates. *Macromolecules*, **30** (25), 7990-7999.

[1.28]. Balazs, A. C., Singh, C. and Zhulina, E. (1998). Modelling the interactions between polymers and clay surfaces through self-consistent field theory. *Macromolecules*, **31** (23), 8370-8381.

[1.29]. Jang, J. and Lee, D.K.(2003). Plasticizer effect on the melting and crystallization behavior of polyvinyl alcohol. *Polymer*, **44** (26), 8139-8146; References therein.

[1.30]. Silvestre, C., Duraccio, D. and Cimmino, S.(2011). Food packaging based on polymer nanomaterials. *Progress in polymer science*, **36** (12), 1766-1782

[1.31]. Lagaron, J.M., Sanchez-Garcia, M.D., Gimenez, E. (2007). Novel PET nanocomposites of interest in food packaging applications and comparative

barrier performance with biopolyester nanocomposites. *Journal of plastic film and sheeting*, **23** (2), 133–148.

[1.32]. Priolo, M.A., Gamboa, D., Holder, K.M., and Grunlan, J.C. (2010). Super gas barrier of transparent polymer-clay multilayer ultrathin films. *Nanoletters*, **10** (12), 4970–4974

[1.33]. de Abreu, D.A.P., Cruz, J.M., Angulo, I., Losada, P.P. (2010). Mass transport studies of different additives in polyamide and exfoliated nanocomposite polyamide films for food industry. *Packaging technology and science*, **23** (2), 59–68.

2.1. Clay

Clay is one of many inorganic nano-particles that are recognized as possible additives to enhance polymer performance; others include synthetic polymer nanofibres, cellulose nano-whiskers or carbon nanotubes. Clay has attracted more positive attention from the packaging industry due to their availability and low cost but more importantly due to the significant enhancements they impart and their relatively simple processability [2.1].

Clay minerals are a subclass of phyllosilicate minerals within the silicate family, which have flat hexagonal sheets of silicate tetrahedra with a Si:O ratio of 2:5. The other subclass of phyllosilicates include groups of serpentine, mica, and chlorite [2.2]. Clay minerals have main members such as smectite, talc, vermiculite and kaolin.

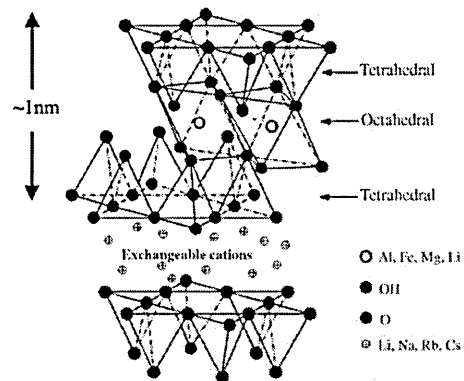


Figure 2.1. Structure of 2:1 layered silicates [2.3]

Montmorillonite (MMT), which has an idealised chemical formula of $\text{Na}_{0.3}(\text{Al}_{1.7}\text{Mg}_{0.3})\text{Si}_4\text{O}_{10}(\text{OH})_2$, is a member of the smectite family and is found in bentonite deposits. Smectites are a group of 2:1 layered minerals (Figure 2.1), which means that one clay layer consists of one alumina-octahedral sheet sandwiched between two silica-tetrahedral sheets [2.4,2.5]. The clay layer is

about 1 nm in thickness and 100-200 nm in diameter. In nature, isomorphous substitution can take place in the alumina-octahedral sheet by replacing Al^{3+} with Mg^{2+} . In nature, the negative excess is compensated by inorganic cations, such as Na^+ or Ca^{2+} , which are located in the domains between adjacent clay layers leading to a regular van der Waals gap called the gallery or interlayer. It is generally accepted that 80% of the exchange cations occupy sites within the gallery, and 20% are on the edges of the clay layer. One characteristic of clay is given by the cation exchange capacity (CEC), i.e. the total amount of cations that can be exchanged by other cations. The quantity is expressed in milliequivalents (meq) per 100 grams. MMT has a CEC in the range between 80-150 meq/100 g.

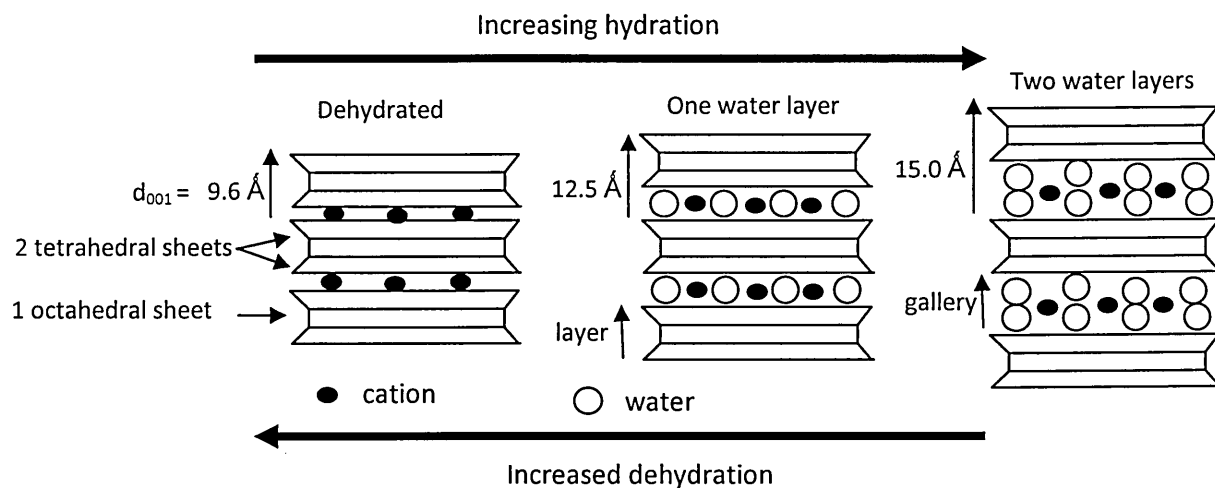


Figure 2.2. Swelling of clay in the presence of water

MMT is hydrophilic and its water content is variable, it can increase greatly in volume when it adsorbs water. A schematic representation of the dehydration and swelling processes of clay layers is given in Figure 2.2. The spacing (d_{001}), i.e. the regular distance between layers, of MMT is 9.6 \AA when no water is present in the gallery (dehydrated), it increases to 12.5 \AA when one

layer of water is present, and becomes 15.0 Å when two layers of water are present. Such dehydration-swelling processes are reversible provided the temperature does not exceed 300 °C [2.6]. This hydrophilic character of MMT promotes dispersion of the clay layers in water soluble polymer such as poly(vinyl alcohol) (PVOH), poly(ethylene oxide) (PEO) and starch.

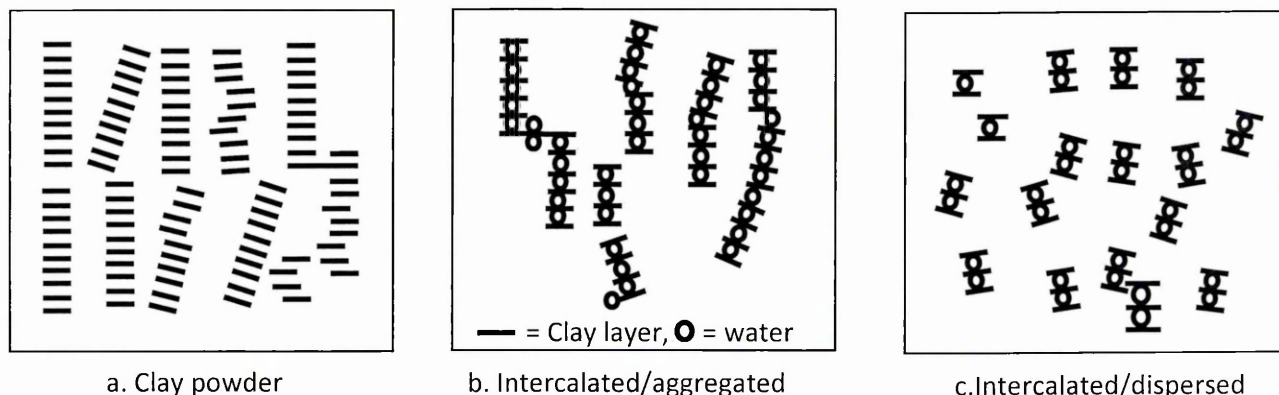


Figure 2.3. Various arrangements of clay layers in dry state (a) and in water (b-c)

The interaction between clay and water determines how the clay layers are arranged. In the dry state (clay powder), clay platelets exist in face-to-face stacks like a deck of playing cards, but clay platelets begin to change when exposed to water. Figure 2.3 shows various arrangements of clay layers including the dry state: clay powder, and in water: intercalated/aggregated and intercalated/dispersed.

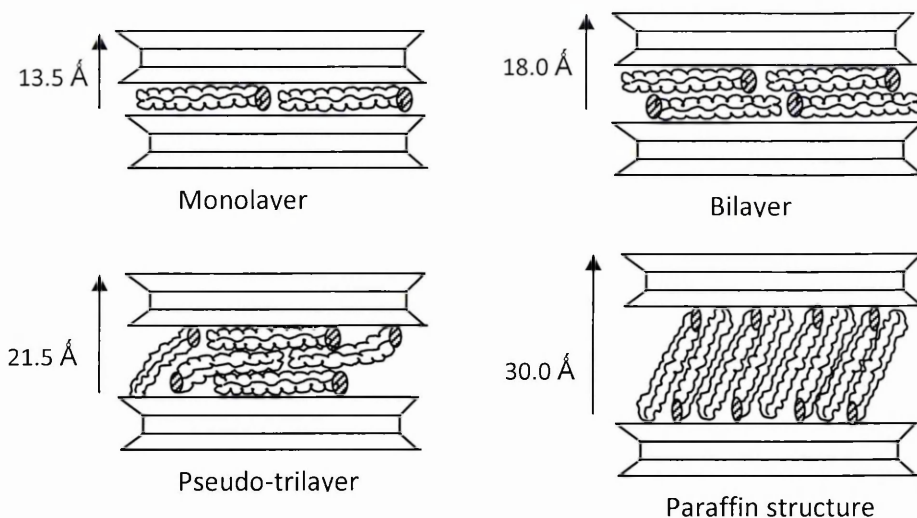


Figure 2.4. Structure for the intercalated surfactants

Generally, polymers are not compatible with clay and so nanocomposites can be difficult to form [2.7]. The compatibility between polymer and clay can be improved by converting the hydrophilic silicate surface to one that is more organophilic. The clay modification can be performed by ion-exchange reactions with cationic alkylammonium surfactants. The cationic surfactant lowers the surface energy of the inorganic host and improves the wetting characteristics with the polymer matrix, enabling the polymer to enter the gallery and produce a larger interlayer spacing. Figure 2.4 shows a proposed model of the structure for the intercalated surfactants including monolayer, bilayer, pseudo-trilayer, and paraffin structure [2.8]. These structures are analogous to the structures described in this thesis of polymer and plasticizer that are intercalated in the gallery of unmodified clay.

2.2. Poly(vinyl alcohol) (PVOH)

Poly(vinyl alcohol) (PVOH) was discovered by Klatté in 1915. It is manufactured by polymerization of vinyl acetate which then undergoes

hydrolysis [2.9]. It has different product names such as ethenol, polyviol, vinol, alvyl, alcotex, covol, gelvatol, lemol, and mowiol [2.7]. It is a semi-crystalline and hydroxylated polymer, odourless and non-toxic. According to data published in 2006 [2.10], over one million metric tons of PVOH was consumed and that China produced and consumed half of the world consumption.

PVOH has been developed as a barrier film for food packaging application since PVOH has excellent gas barrier properties, offers flexibility, transparency, toughness, biodegradability as well as having a lower cost than other barrier polymers [2.11]. Other uses of PVOH are in paper and paperboard; as binders for pigmented paper coatings, as membranes for column packing materials for the separation of aqueous solutions [2.12], and as carbon dioxide barrier in polyethylene terephthalate (PET) bottles [2.13].

Water is the most common solvent for PVOH. In order to fully dissolve PVOH, the water has to be heated to 90 °C [2.14,2.15]. Other suitable solvents for PVOH are diethyl triamine [2.16], dimethyl sulphoxide [2.17], formamide, dimethyl formamide and phosphoric acid trisdimethylamide [2.9]. At temperature above 100 °C, PVOH can also be dissolved in multivalent alcohols such as glycerine, glycol, and ethanol-amines [2.9].

The idealised molecular structure of PVOH is given in Figure 2.5a [2.18]. Due to the polarity of PVOH chains, they tend to have mutual orientation both in aqueous solution and in the solid state as described by Sakurada's model in Figure 2.5b [2.9]. The crystalline area in the model is shown by the interweaving polymer chains that lie parallel to one another. The tendency of the chains to form crystalline areas increases with the regularity of the chain structure. Such orientation of the chains will be counteracted by the presence of acetyl groups

(COCH₃) in the molecule as PVOH is not always 100% hydrolysed. For fully hydrolysed grades typical degrees of hydrolysis are between 97.2–99.8%. Both syndiotactic (alternate) and atactic (random) forms are both possible for the steric structure of PVOH [2.19], with atactic structure being predominant [2.9].

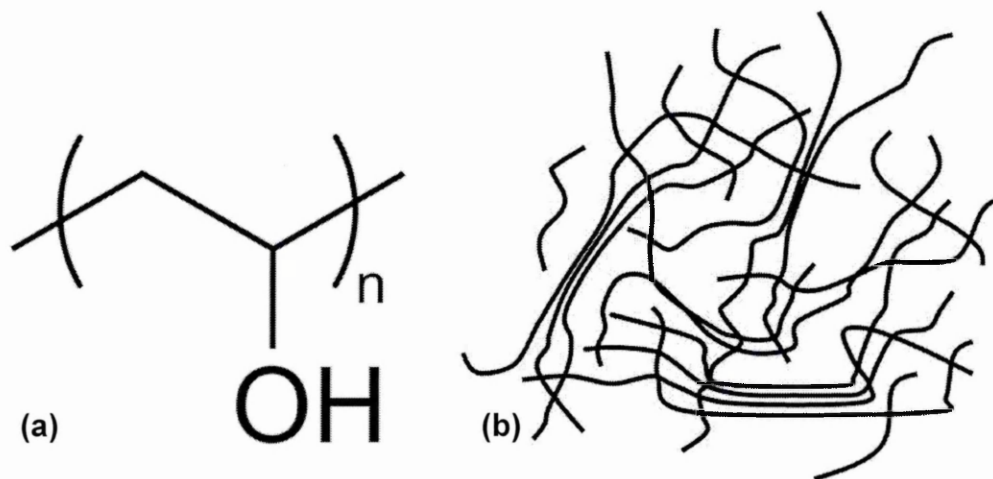


Figure 2.5. Molecular structure (a) and Sakurada's structural model (b) of Poly(vinyl alcohol) (PVOH)

PVOH has glass transition temperatures (T_g) ranging between 40 and 80 °C, melting temperatures (T_m) ranging between 180 and 240 °C, and decomposes rapidly above 200 °C [2.17]. The T_g and T_m value depends on the type and thermal history of the sample. Fully hydrolysed PVOH is completely water soluble above its 'dry' glass transition temperature of 85 °C [2.20]. The solubility and swellability of PVOH are greatly influenced by the degree of crystallization. In fully hydrolysed PVOH, heat treatment produces an increase in crystallization which, in turn, impairs its solubility in water [2.9].

Anhydrous PVOH films are stiff and brittle and so their flexibility can be improved by adding plasticizer. Any plasticizers have to be compatible with the polymer so as to reduce migration out of the polymer film. Since PVOH has a polar character, only compounds with highly polar groups are suitable as plasticizers for PVOH. In addition the volatility of the plasticizer should be as low

as possible in order to reduce loss. Ethylene glycol, di- and triethylene glycol, polyethylene glycols (PEG) with low molar mass, glycerine, trimethylol propane, neopentyl glycol, triethanolamine, and ethoxylated phosphates are among the common plasticizers and are typically used in quantities of up to 30% relative to PVOH [2.9]. Although water has a plasticizing effect on PVOH such that PVOH films stored in moist air become flexible, water cannot be considered an ideal plasticizer due to its high volatility.

PVOH has a strong inter and intra molecular hydrogen bonding network and under normal conditions PVOH films, especially those of higher viscosity grades, have a high tear strength and good elongation at break values [2.21]. These properties are affected to a considerable extent by the moisture content of the PVOH film, since water acts as plasticizer [2.22]. As the water vapour content of the air increases, the value for elongation at break increases, while the tensile strength decreases. The presence of water provides a lubrication effect that promotes chain mobility by disrupting the polymer-polymer hydrogen bonding. The increased chain mobility reduces the glass transition temperature [2.20, 2.22].

Holland [2.23] showed that the elimination of water (from hydroxyl side groups) was considered as the main contribution to thermal degradation of PVOH when in the solid state ($< T_m$), which results in a reduction of the amount of hydrogen bonding, the T_m and the degree of crystallinity. In the molten state ($> T_m$), the thermal degradation contributed to the elimination of water and the production of volatile saturated and unsaturated aldehydes and ketones at ~ 290 °C.

Assender [2.24] reported that PVOH samples prepared by drying at 50 °C overnight were found to increase in both crystallinity (in the range 38-50 %)

and crystal perfection when the annealing temperatures were increased from 120 to 230 °C. The presence of water had an effect on reducing the glass transition and also on enhancement of the crystallisation process resulting in a greater level of crystallinity upon annealing.

The effect of plasticizers on PVOH properties has been investigated by several researchers. Jang [2.25] reported that glycerine reduced the melting temperature (T_m) and crystallinity of PVOH according to the amount of glycerine content and regardless of the degree of hydrolysis. These effects diminished gradually at glycerine contents above 40 pph. Mohsin [2.26] found that sorbitol reduced the glass transition temperature (T_g), melting temperature (T_m), degradation temperature (T_d), and also elastic modulus according to the amount of sorbitol.

2.3. Poly(ethylene glycol) (PEG)

Poly(ethylene glycol) (PEG) which has the molecular structure shown in Figure 2.6 [2.18] is also known as poly(ethylene oxide) (PEO) or polyoxyethylene (POE) [2.27]. The three names are chemically synonymous, but historically PEG refers to oligomers and polymers with a molecular mass below 20,000 g/mol, PEO to polymers with a molecular mass above 20,000 g/mol, and POE to a polymer of any molecular mass. It is commercially available over a wide range of molecular weights from 100 g/mol to 10,000,000 g/mol. Pure PEG has been characterised as a clear viscous liquid (molecular weight less than 200), a wax-like substance (molecular weight 200 - 2000) and as an opaque white crystalline solid (molecular weight > 2000) [2.28]. PEG is readily soluble in water, but solubility decreases with increasing molecular weight. PEG is a non-toxic compound and is used in pharmaceuticals

compositions and as a food additive, and so is suitable for food packaging applications [2.29].

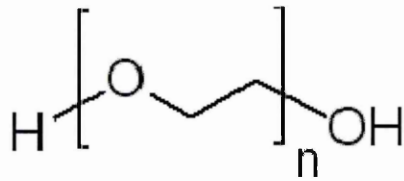


Figure 2.6. Molecular structure of poly(ethylene glycol) (PEG)

PEG with low molar mass can be used as plasticizer for polymers by reducing intra-molecular hydrogen bonds. The compatibility of PEG with PVOH increases sharply as the molar mass of the PVOH decreases [2.9]. PEG can also enhance the degradability of biopolymers such as polylactide (PLA) [2.30] and is combined with clay in the application of water based drilling fluids where clay is the major phase [2.31].

2.4. Polypropylene glycol (PPG)

Polypropylene glycol (PPG) which has the molecular structure shown in Figure 2.7 is also known as polypropylene oxide. Conventional PPG has an atactic structure. PPG is a liquid molecular weight dependant at room temperature, less soluble in water, and so potentially not as good a plasticizer for PVOH as compared to PEG. Secondary hydroxyl groups in PPG are less reactive than primary hydroxyl groups in PEG [2.27]. PPG is a non-toxic compound and is used as a solvent for vegetable oils, sterilizer or pasteurizer for nutmeats, notably almonds [2.32], and so is assumed suitable for food packaging applications. The other uses are as a surfactant, dispersant in

leather finishing; a primary ingredient in the manufacture of paintballs; and a foaming suppressant in industrial processes [2.33].

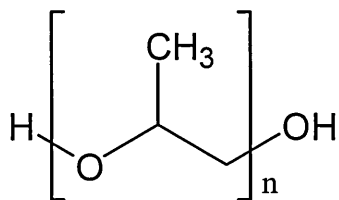


Figure 2.7. Molecular structure of polypropylene glycol (PPG)

2.5. Polyetheramines

Polyetheramines are polymers having primary amino groups attached at the ends of a polyether backbone where the polyether backbone is usually based on either propylene oxide (PO), ethylene oxide (EO), or mixed PO/EO. The family of polyetheramines, based on this core structure, can consist of monoamines, diamines or triamines. Polyetheramines produced by Huntsman are named Jeffamine polyetheramines, and the structure of Jeffamine monoamines (Jeffamine M series) is shown in Figure 2.8, where the ratio of x and y defines the type of the series and the dominance of the polyether backbone. For example, the x/y ratio of Jeffamine monoamines with Mw 600 (M600) is 1/9, and so predominately PPG based (more hydrophobic), whereas Jeffamine M2070 has the x/y ratio is 31/10, and so predominately PEG based (more hydrophilic) [2.34].

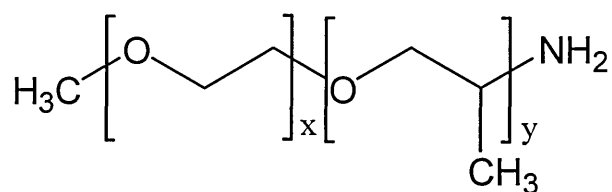


Figure 2.8. Molecular structure of Jeffamine M series

Polyetheramines are generally used to increase flexibility, toughness, hydrophilicity or hydrophobicity, and to control moisture absorption. They also offer various reactivities, have good temperature stability, low viscosity, colours and vapour pressures.

2.6. Polymer clay nanocomposites

Polymer clay nanocomposites are mixtures of polymer and clay, representing a radical alternative to conventional polymer composites [2.3]. The first successful example of polymer-clay nanocomposites was developed by scientists at Toyota Central Research Laboratories in 1986 for nylon-clay nanocomposites [2.35].

Polymer-clay nanocomposites can offer a unique property profile by simultaneously enhancing mechanical, barrier and fire resistant properties by adding as little as 5 wt% clay with respect to the pristine polymer. This reduces the component weight since traditional fillers are added at 20-40 wt%. The nanocomposites may also offer extra benefits such as transparency, better surface properties (acting as a good substrate to provide better interaction with the incoming material (layer) such as in multilayer coating or intumescent coating) and recyclability. The main reason for these improved properties resides in the clay properties as opposed to conventional fillers [2.36]. The clay particles have one dimension in the nanometer (from 1 to 100 nm) range and when dispersed offer a much higher surface area for polymer-filler interactions than in conventional composites. A uniform dispersion means that the clay layers have some regular order whereas a random dispersion there is no

regularity between clay particles. Nanomaterials according to the European Commission are materials whose main constituents have a dimension of between 1 and 100 billionth of a metre [2.37]. The very large organic/clay interface changes the molecular mobility, the relaxation behaviour and the consequent thermal and mechanical properties of the resulting nanocomposite material. Nanocomposites as packaging offer an increase in the shelf life of many food products and benefits for safety food to prevent the growth of bacteria and organisms.

2.6.1. Structure of polymer/clay nanocomposites

There are four key variables that affect the properties of nanocomposite material: type of clay, clay pre-treatment (organic modification), the type of polymer and the preparation technique used to disperse the clay in the polymer matrix [2.38].

The types of clay dispersion in polymers can be identified as i) microcomposite, ii) intercalated and iii) exfoliated as depicted in Figure 2.9 [2.36]. The type of clay dispersion in the polymer matrix plays an important role in the final properties of the nanocomposites since it determines how the clay interacts with the matrix. If good thermal properties are desired, then ordered/intercalated dispersions are often desired, whereas best mechanical properties are obtained with disordered/exfoliated systems. Good barrier properties also require that the plane of the clay surface lies perpendicular to the path of the diffusant.

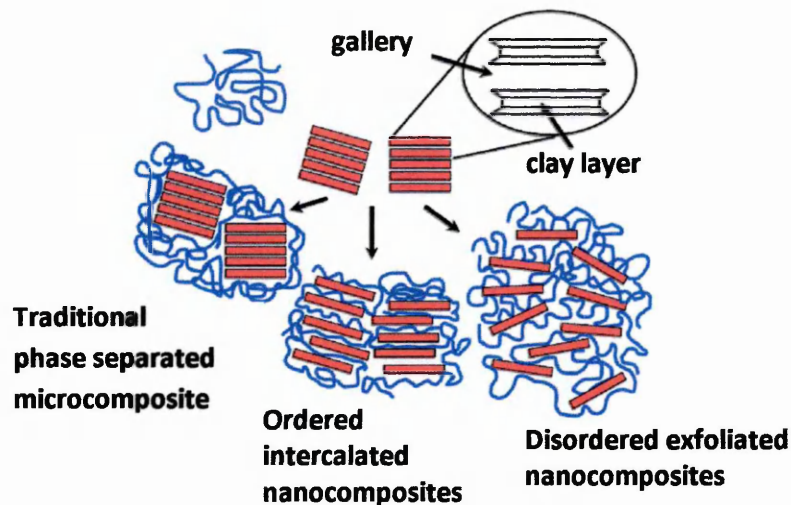


Figure 2.9. The different ways in which clay layers can be dispersed within a polymer matrix (not to scale)

The two major types of nanocomposites; intercalated and exfoliated can often be found in different regions of a nanocomposite material. For ordered-intercalated systems, the spacing between individual clay layers, called the d-spacing, increases from its intrinsic value as polymer chains or monomer molecules diffuse into the clay galleries. Such intercalated nanocomposites show diffraction peaks in their XRD patterns. In exfoliated systems the individual clay layers are separated from the intercalated tactoids and are dispersed in the matrix polymer with no apparent inter-particle interactions. The exfoliated nanocomposites do not show any XRD diffraction peaks that could be attributed to ordered clay layers [2.3].

2.6.2. Permeability in polymer/clay nanocomposites

Polymer nanocomposites exhibit better barrier performance to diffusing penetrants in comparison with unmodified polymers [2.40-2.43]. For example, introduction of 3 wt% clay reduced oxygen permeability of PLA by 66 % [2.40], 2 wt% clay reduced gas permeability of polyimide by 50 % [2.41], 4.8 wt % clay

reduced the water permeability of poly(ϵ -caprolactone) by five fold [2.42], and 4-6 wt% clay reduced the water permeability of PVOH by 40 % [2.43]. These improvements are based on the tortuosity arguments, wherein the permeating molecules must travel a longer diffusive path in the presence of clay layers as illustrated (simple model) in Figure 2.10.

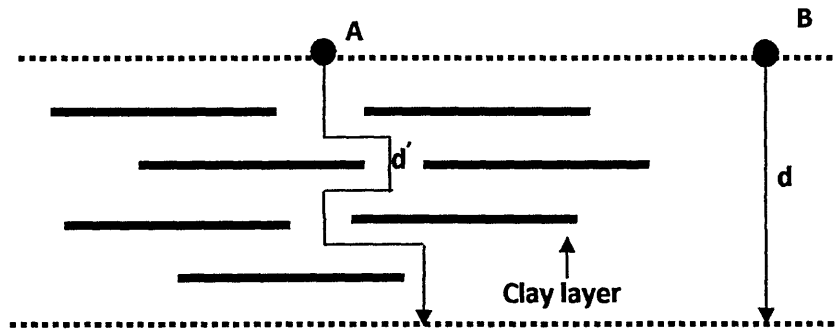


Figure 2.10. Schematic illustration of tortuosity for a diffusing penetrant introduced to exfoliated clay, layered in a polymer matrix. (A) Filled polymer and (B) Unfilled polymer

The tortuosity factor (τ) is defined as the ratio of the actual distance (d') that permeating molecules must travel to the shortest distance (d) that it would have travelled in the absence of the clay [2.44]. It is expressed in terms of the length (L), width (W), and volume fraction of the sheets (Φ_s) as

$$\tau = \frac{d'}{d} = 1 + \frac{L}{2W} \Phi_s \quad (2.1)$$

The effect of tortuosity on the permeability is expressed as

$$\frac{P_s}{P_p} = \frac{1-\Phi_s}{\tau} \quad (2.2)$$

where P_s and P_p represent the permeabilities of the polymer-clay nanocomposite and pure polymer, respectively. In general, clay layers have L ranging from 30 to 2000 nm with a width of 1 nm.

2.6.3. Preparation techniques

A number of polymer-clay nanocomposite preparation methods have been reported in the literature [2.38,2.45-2.50]. The choice of the preparation method usually depends on the properties of the polymer matrix and the type of clay. The three most common methods to prepare clay nanocomposites are 1) intercalation of a suitable monomer and subsequent in situ polymerization, 2) intercalation of polymer from solution, and 3) polymer-melt intercalation. Solution intercalation methods employing non-aqueous systems are less desirable in commercial applications since suitable compatible clay/polymer/solvent systems are not always available [2.48]. Moreover, there are additional costs associated with the solvents, their disposal, and their impact on the environment [2.49].

For in situ polymerization methods, the monomer is used directly as a solubilising agent for swelling the clay. Subsequent polymerization takes place after combining the clay and monomer, thus allowing formation of polymer chains between clay layers [2.47]. Nanocomposites prepared by this route have been reported for thermoplastic materials like polyimides, poly(ϵ -caprolactone), polystyrene and polyolefins as well as thermosets, such as epoxy, unsaturated polyester resins, and elastomeric materials like rubber or elastomeric epoxies and polyurethanes [2.50].

For solution-intercalation methods, a suitable solvent that can both solubilise the polymer and swell the clay is required. When the clay is dispersed within a solution of the polymer, the polymer chains can adsorb onto the clay layers and displace the solvent within the gallery of the clay [2.47]. Typically, nanocomposites prepared by the solution intercalation mechanism are achieved

with water soluble polymers such as poly(vinyl alcohol), poly(ethylene oxide), poly(vinylpyrrolidone) or poly(acrylic acid) [2.50].

Melt intercalation of polymers into clay is a powerful approach to prepare polymer-clay nanocomposites because it is simple, economical and environmentally friendly. In this method, the polymer and clay is heated above the melting point of the polymer and mixed [2.47] under high shear forces. If the clay surface is sufficiently compatible with the polymer, intercalation and exfoliation can occur in the melt due to entropic and enthalpic factors without the need of any solvent. Melt intercalation has been applied to a wide range of polymers such as polystyrene, nylon-6, polypropylene, rubbers or poly (ethylene oxide) and copolymers of ethylene and vinyl acetate or styrene and butadiene [2.50].

2.6.4. Poly(vinyl alcohol) (PVOH)/clay nanocomposites

PVOH can easily adsorb onto MMT [2.51,2.52]. When clay was dispersed in aqueous PVOH solution, the clay was kept in colloidal dispersion by the steric interaction of the polymer chains and the clay layers. Removal of some solvent from such solutions created a gel embedded with clay layers. Some re-aggregation of the clay layers were observed when the gel was dried further to form polymer films. The extent of this re-ordering was found to depend on the drying conditions.

Strawhecker [2.43] investigated the structure and properties of PVOH/MMT nanocomposites. Their samples, prepared by drying for 2 days at 40 °C, were investigated by using tensile and water vapour transmission rate

(WVTR) experiments. After further drying at 80-90 °C for 1 day the samples were analysed using transmission electron microscopy (TEM), XRD, differential scanning calorimetry (DSC) and thermogravimetric analysis (TGA). They observed that both the d-spacings and their spatial distributions decreased systematically with increasing MMT load (40 to 90 wt%). The existence of both intercalated and exfoliated clay layers throughout the polymer matrix especially in low (≤ 10 wt%) and moderate (10-20 wt%) MMT loadings were consistently observed by TEM together with XRD. The T_g (≈ 70 °C) and T_m (≈ 225 °C) signals shown by DSC traces weakened gradually as clay loading increased and disappeared for MMT loading above 60 wt% suggesting no melting endotherms were found for the confined polymer. Compared to the pristine PVOH, the composites with MMT loading below 40 wt% showed a higher T_m , which gradually increased at the expense of the bulk PVOH crystal phase. This higher T_m in the composites was shown by XRD traces where the 101 and 10 $\bar{1}$ peak concurrently decreased in intensity and were replaced by what appeared to be a single peak at 19.5 °2 θ when MMT loading achieved 20 wt%. The location of crystal with higher T_m in PVOH/MMT was further shown by using atomic force microscopy (AFM) [2.53]. They believed the higher T_m was due to the strong specific interactions between the clay surface and the polymer and that they were initiated and grown in the vicinity of the silicate surface with a crystal size of about 2 μm . Those found in the PVOH film were about 5 μm or larger. The mechanical properties showed that the Young modulus increased sharply at very low MMT loading and then levelled off above 4 wt% MMT loading, and was about 3.5-4 times the value for bulk PVOH. This enhancement of Young modulus was at the expense of a 20% decrease in toughness but no change in the stress at break was observed compared to the neat PVOH. The other

superior properties of the composites were shown by the decrease in water permeability by about 40 % for 4-6 wt% MMT loading and by the increase in thermal stability by about 75 °C for 10 wt% of MMT loading. Moreover, the high transparency of the PVOH was retained at MMT loading under 10 wt% as evidenced by UV/vis measurements (400-700 nm).

Adsorption of PVOH onto MMT layers was investigated by Chang [2.51]. PVOH (Mw 90,000)/MMT suspension was stirred at 25 °C for various times, and then centrifuged at 15,000 rpm for 30 minutes. They found that 8 hours was needed for adsorption of PVOH onto MMT to reach equilibrium. They also observed that the amount of PVOH adsorbed when dry MMT was added directly to aqueous PVOH was higher than when clay was first conditioned in suspension. Later, Chiellini [2.52] investigated the adsorption of PVOH onto MMT centrifuged at 10,000 rpm and found that the amount adsorbed increased with time and then levelled off after about 7 weeks (Mw 30,000 and degree of hydrolysis 98%), and depended almost linearly on the concentration of the starting PVOH solution. Higher temperatures (within the range 20-50 °C) were shown to increase the amount of PVOH adsorbed by MMT. Higher hydrolysis degrees (within the range 72-98 %) and lower-molecular weight PVOH fractions (in the case with hydrolysis degree of 88 % and Mw range 61,000-161,000) were preferentially adsorbed. The adsorption process was considered irreversible as evidenced by no detectable amount of PVOH being released from MMT samples.

De Bussetti [2.54] found that the adsorption of PVOH on Ca-MMT decreased with increasing suspension pH, whilst adsorption on Na-MMT was not affected by the pH of the suspension. The adsorption of PVOH on MMT

followed a H-type isotherm suggesting that PVOH was adsorbed in large quantities and densely packed. The PVOH adsorption was an irreversible process and was adsorbed not only in the gallery but also on the clay surface. They also reported that it was not possible to remove the PVOH from the clay surface by adding HCl to the suspension. Interaction via H-bonding between the hydroxyl groups of the PVOH and the clay's inter-lamellar silanol groups (-SiO-) [2.55,2.56] was the reason preventing the PVOH molecules from being ejected easily from the surface by the action of chemical agents such HCl, NaCl and sodium pyrophosphate.

A substantial enhancement in the mechanical properties of MMT-PVOH nanocomposites was reported by Soundararajah [2.57]. They found that the tensile strength and young modulus of MMT-PVOH nanocomposites increased more than 60%, while the tearing energy doubled to that of neat PVOH. The degree of exfoliated MMT was believed to contribute to the enhancements.

Besides tortuosity arguments due to clay fillers, the free volume fraction may be another dominant factor for the barrier properties in polymer materials containing clay nanoparticles. Cui [2.58] investigated the relation between free volume (which relates to amorphous fraction) and barrier properties in miscible blends of poly(vinyl alcohol) and nylon 6/MMT clay nanocomposites (NYC). The gasoline permeability of the NYC/PVOH blends decreased with increasing PVOH content. The PVOH content dependence on macroscopic barrier property is similar to that on the microscopic free volume (permeability coefficient). A similarity was found between barrier properties versus PVOH content and free volume parameters versus PVOH content. The relation between the free volume fraction (ratio of free volume to the total volume of polymer) and permeability coefficient could be described exactly as an

exponent function, implying that microscopic free volume plays an important role on determining macroscopic barrier properties.

Adoor [2.59] prepared PVOH based (Mw 125,000) mixed matrix membranes with 5 and 10 wt% sodium MMT using the solvent method and tested for pervaporation dehydration of aqueous mixtures of isopropanol and 1, 4-dioxane. Pervaporation is a technique for separating aqueous–organic mixtures as well as organic–organic mixtures whilst the mixed matrix membranes refer to PVOH/MMT membranes. They observed that pervaporation performances were superior over that of the pristine PVOH (unfilled) membrane in terms of flux and separation factors. The increased hydrophilic nature due to MMT and the formation of PVOH/MMT mixed matrix membranes were offered as reasons for the increased separation of water over the organic components in the feed mixtures.

Ahn [2.60] investigated the extended lifetime of pentacene thin-film transistors (TFT) with a PVOH/clay nanocomposite passivation layer fabricated by a solvent method and spin casting. Using only 3 wt% of clay to PVOH showed an extended TFT lifetime of 2860 hours when compared to conventional PVOH passivation (1540 hours). It was believed that a polymer/clay nanocomposite approach could potentially improve the barrier effect of most organic passivation layers and thus TFT lifetimes.

Jia [2.61] prepared PVOH/kaolinite nanocomposites via in situ polymerization. With 8 wt% kaolinite the glass transition temperature changed from 61.2 to 81.6 °C and the melting temperature changed from 227.5 to 214.7 °C and was attributed to intercalation of PVOH into kaolinite. The PVOH-

kaolinite matrix also showed a higher thermal decomposition temperature and greater amounts of carbonaceous char.

PVOH (Mw 106,000)/MMT nanocomposites prepared under the effect of electron beam irradiation at a constant dose of 20 kGy was investigated by Alla [2.62]. They found that the introduction of MMT clay led to an improved water resistance of up to 300% with 4 wt% clay, mechanical properties such as tensile strength increased up to 185.7% with 3 wt% clay and elongation at break increased up to 145.7% with 4 wt% clay. Moreover, the intercalation of PVOH with clay suppressed the glass transition temperature, but did not affect the melting temperature as shown by DSC.

Sengwa [2.63] observed that PEO Mw 60,000 and PVOH Mw 70,000 blends showed poor miscibility in their film form as shown by the existence of the separate clusters of PEO and PVOH using high resolution optical microscopic. Their miscibility was improved when the blends were mixed with MMT. It is believed that the extent of miscibility was due to hydrogen bonded bridging through exfoliated MMT clay layers. They also observed that MMT reduced the polymer chain mobility.

Ip [2.64] found that MMT from Arumpo had better ability to intercalate PVOH than that from Unimin. The intercalation of PVOH on MMT was improved by acidification followed by washing the MMT.

2.6.5. Poly(ethylene glycol) (PEG) clay nanocomposites

The effect of plasticizer on the binary system of PEG (Mw 300) /poly(3-hydroxybutyrate)(PHB) (Mw 380,000) was investigated by Parra [2.65]. It was found that PHB/PEG films were transparent and more flexible when compared

to the pure, brittle PHB film. The initial decomposition temperatures of these films were very similar, indicating that the addition of up to 10% plasticizer did not alter the thermal stability of the final blends. An increase in the PEG content did reduce the tensile strength and increase the elongation at break when compared to pure PHB.

The effect of PEG (Mw 1000) on the properties of PLA (Mw 186,000) - MMT (Cloisite 30B) nanocomposites was investigated by Ozkog [2.66]. They found that the level of clay dispersion improved by the addition of PEG. The addition of 20% PEG to neat PLA resulted in the T_g decreasing by $\sim 30^\circ\text{C}$, but the reduction was only slightly recovered ($\sim 4^\circ\text{C}$) by further incorporation of clay. The addition of clay to neat PLA decreased ($\sim 20^\circ\text{C}$) the T_c and promoted a new form of polymer crystal. The addition of PEG reduced the T_m of PLA but the T_m recovered to the initial value of PLA when 5 wt% clay was added. The addition of 3 wt% clay into neat-PLA did not affect the tensile strength. The addition of 3 wt% clay to plasticized PLA improved the modulus by $\sim 36\%$, but the strain at break value was lowered by about 40%. The biodegradation rate of PLA was retarded with the addition of PEG and/or clay.

Pillin [2.29] found that the addition of PEG reduced the T_g and T_m of PLA. The reduction in T_g and T_m decreased with increasing PEG molecular weight (200-1000) and with decreasing PEG content (within the range 10-30 wt%). PEG also resulted a higher crystallinity of PLA which was believed due to a higher mobility of PLA chains. Moreover, the addition of PEG reduced both tensile modulus and stress at break of PLA.

Pluta [2.30] investigated PLA (Mw 81,800)/clay nanocomposites plasticized with PEG (Mw 1000). They showed that plasticization reduced the T_g

of PLA by ~ 26.3 °C for unfilled PLA and by ~ 21 °C for the PLA-clay nanocomposites, on the other hand; plasticization reduced the T_m by ~ 5 °C for both plasticized PLA and PLA-clay nanocomposites. Both PEG and PLA were found to intercalate within the clay galleries.

Bujdak [2.67] investigated the effect of the clay layer charge on the intercalation of PEO Mw 7500, 100000 and 5000000. They found that the amount of intercalated PEO increased with layer charge but then decreased when the layer charge reached 71 meq/100 g. The amount of water continuously increased in the presence of PEO indicating that the PEO oxygen atoms did not directly associate with the exchange cations, but were mostly coordinated to water molecules and surface oxygen atoms of clay.

Parfitt [2.68] found that the affinity of PEG for clay surfaces increased with molecular weight (Mw 200-20000).. Higher molecular weight PEG created higher d-spacings. The effect of the exchangeable cation on the adsorption followed the order Cs>Na>Ca>Al, which indicated the cation retained its hydration shell and did not form a direct association with the adsorbed PEG molecules but via the ether oxygen atoms and water molecules in the primary hydration shell of the exchangeable cation, to give a water bridge.

Chen [2.69] studied preferential intercalation in PEG-MMT nanocomposites. They found that impurity cations (Ca and K) that were present before being purified by sodium cations did not affect the extent of PEG uptake. From a 60 wt% PEG + 40 wt% MMT mixture, only 30 wt% PEG was taken up by the clay; 20 wt% was located in the gallery (called absorption) whereas 10 wt% was located at the clay layer edge and surface (called adsorption). Further investigation showed that of the 30 wt% PEG adsorbed by MMT, 25 wt% was

PEG35000 and 5 wt% was PEG4000. The preferential intercalation of MMT to higher PEG molecular weight may be explained by Budjak [2.67] who reported that the low Mw PEG has a larger number of hydrophilic end groups than that of the high Mw PEG and should facilitate the preferential intercalation of the latter on the relatively hydrophobic regions between interlayer cations. Moreover, the macromolecules prefer a conformation that allows for maximum segment-surface interaction as molecules with higher Mw have fewer molecule chains and can have more conformation per unit mass, yet result in the same total energy.

The effect of size and surface area of two different clay types (laponite and montmorillonite) on the structure and characteristics of PEO Mw 1,000,000/clay (40 wt%) nanocomposites in the form of multilayer films was investigated by Stefanescu [2.70,2.71]. XRD measurements showed that higher amounts of MMT resulted in an improved final orientation of the clay platelets, parallel to the plane of multilayer films. DSC demonstrated that both clays suppressed the crystallinity of PEO. Further investigation showed that gradually replacing MMT with equivalent amount of laponite resulted in a gradual decrease of PEO crystallinity and became completely amorphous in the samples when the amount of laponite was 60 wt% (no MMT was present).

Chaiko [2.72] reported a new mechanism for the formation of intercalated PEG/clay nanocomposites. Samples were prepared by dispersing PEG (Mw 1450) along with etidromic acid (1-hydroxyethane 1,1-diphosphonic acid) in different clays (hectorite, saponite and MMT), the slurries were washed, cast and dried to produce very flexible and transparent films with a highly ordered intercalated structure showing a total of 13 (00l) reflections. The oxygen

permeability in PEG/MMT films was 650000 times lower than that of PEG. The extreme low gas transport in PEG/MMT films was believed to be due to not only tortuosity effects but also extreme polymer constraint in the clay gallery. A saponite nanocomposite containing excess polymer showed phase separation consisting of a mixture of intercalated structures with d-spacing of 17.7 Å and a three-dimensional polymer crystal phase with diffraction peaks at 4.63 Å (19.2 °2θ) and 3.83 Å (23.3 °2θ). For H⁺ exchanged saponite, the d-spacing was shown to increase with increase in polymer loading. A molecular weight dependency was observed in the PEG/H⁺-saponite nanocomposites containing > 27 wt% polymer indicating an oxonium-exchange mechanism (protonation of the terminal –OH group of the adsorbed PEG due to the presence of H⁺ ions in the exchange sites of the clay) where the 4.63 and 3.82 Å reflections are absent (i.e. all PEG was absorbed by the clay). This new formation of two dimensional crystalline phase has a melting point 5-7 °C higher than that of the unconfined polymer and is consistent with the increase in melt transition observed by Strawhecker [2.43].

Thiyagarajan [2.73] reported that in the absence of salt the radius of gyration (R_g) of PEG increased with increasing M_w , but decreased with an increase in PEG concentration. In the presence of either Na₃PO₄ or Na₂CO₃, PEG chains aggregate (form leads to biphasic formation) whereas in the presence of NaNO₃, they behave like a random coil with no evidence of aggregation. The aggregation size increased with an increase in salt concentration until a discontinuity appeared at the point of biphasic formation [5 wt%], wherein the polymers in the PEG rich phase form an entangled mesh in which the identities of individual polymers are lost. In the monophasic regime, the aggregates were elongated with a radius of about 19 Å.

Strawhecker [2.74] reported the effect of MMT on the crystallisation behaviour of PEO (Mw 136,000). They found that the introduction of MMT (below 10 wt%) hindered the PEO crystallisation as shown by a reduction in the T_c or a slowdown in the crystal growth rate, however, it did not affect the overall crystallinity of PEO. The hindering effect of MMT on PEO crystallisation was compensated by the huge increase in the nucleation density resulting in smaller and non-isotropic PEO crystallites. These additional nuclei, which occurred within the bulk of PEO homogenous nucleation, caused the PEO overall crystallization kinetics (i.e. product of nucleation rate and crystal growth rate) to become faster with an increase in MMT loading. While the usual behaviour of semi-crystalline polymers such as PVOH [2.43], polypropylene [2.75] and nylon-6 [2.76] shows that fillers normally result in heterogeneous nucleation, promoting crystals in their vicinity, the slowdown of PEO crystallisation with the introduction of MMT indicates that the strong coordination of PEO to the Na^+ cations surfaces promotes amorphization (ether crown-like) of PEO conformations. Previously, Liao [2.77] reported that the crystallinity of PEO (Mw 20,000)/MMT (35/65 wt%) nanocomposites prepared by melt intercalation decreased with increasing annealing time.

Chen [2.798] reported that a d-spacing of 1.82 nm in PEG (Mw 300–20,000)/MMT nanocomposites prepared by solution-casting method was both independent of Mw and the method of drying. The d-spacing of the nanocomposites prepared by melt intercalation also gave a d-spacing of 1.82 nm, irrespective of PEG molecular weight or mixing time. Further investigation of the nanocomposite structure using TEM showed that both intercalation and exfoliation structures existed in PEG (Mw 4000)/MMT nanocomposites. The amount of PEG (Mw 1500) uptake by clay was shown to increase linearly with

concentration at low concentration and remained at ~19 wt% when the concentration was higher than 0.023 g ml^{-1} . Free PEG (Mw 1500) was even obtained when small amounts (0.01 g ml^{-1}) of PEG was added. Moreover, the confined polymer in the clay galleries prepared by melt intercalation exerted a density of 670 kg m^{-3} , which is significantly lower than the bulk density of 1100 kg m^{-3} . This indicates that the clay lowers the packing density of the PEG by not allowing the PEG molecules to orient together. They also observed that the disappearance of -OH and interlayer water in clay when PEG entered the gallery indicating that melt processing method adopts a similar mechanism as that for the solution method, which is co-incident with Budjak [2.67].

2.6.6. Polyetheramines clay nanocomposites

Lin [2.79] tailored the d-spacing of MMT with 2 different polyetheramine salts prepared with one equivalent of HCl in water. Intercalation of telechelic poly(propylene glycol)-bis(2-aminopropyl ether) (POP) with Mw's of 230, 400, 2000 and 4000 in MMT achieved d-spacings of 15, 19.4, 58 and 92 Å, and organic encapsulation's of 23, 35, 62, and 72 wt%, respectively. The organophilicity of POP/MMT also increased with increasing Mw of POP as shown by both MMT/POP2000 and MMT/POP4000 being able to swell and disperse in toluene easily by simple mixing, while POP230 and POP400 derived silicates are dispersible only in polar ethanol solvent. For MMT/poly(ethylene glycol)-bis(2-aminopropyl ether) (POE) Mw 2000 only a d-spacing of 19.4 Å and an organic encapsulation of 43 wt% was achieved. These results suggested that the high affinity of the POE backbone for Na^+ cations on the silicate surface may hinder incoming amines for the completion of the ionic exchange reaction.

Moreover, they found that the crystallinity of POE Mw 2000 was significantly reduced in the silicate gallery compared to that of the pristine POE. This result is consistent with previous work of confined PEG in clay reported by Chen [2.78] and Vaia [2.80].

Chou [2.81] reported the intercalation of polyoxyethylene (POE) and poly(oxypropylene) (POP)-backboned amines on MMT via an ionic exchange reaction between ammonium salts ($-\text{NH}_3^+\text{Cl}^-$) and sodium ion of MMT. In their studies, the PM amines were α,ω -diamines of poly(oxypropylene)-block-poly(oxyethylene)-block-poly(oxypropylene) with Mw's 2000 (PM-D2000) and 6000 (PM-D6000). The POP amines are the POP-backbones diamines of Mw's 230, 400, 2000 and 4000 (POP-D230, POP-D400, POP-D2000 and POP-D4000, respectively) and the analogous triamines of POP-T400, POP-T3000 and POP-T5000. They observed that the d-spacings of PM-D2000 and PM-D6000 in clay were independent of molecular weight (≈ 19 & 19.8 Å for PM-D2000 and PM-D6000) and that only low ionic exchange conversions (33 and 13%, respectively) occurred. In contrast to PM amines, the hydrophobic POP amines showed increases in interlayer spacing as a function of molecular weight (i.e. 15, 19.4, 58, and 92 Å) and that high ionic exchange conversions (i.e. 77, 76, 74 and 65 %) for POP230, POP-D400, POP-D2000 and POP-D4000, respectively were noted. For POP-T, the ion exchange conversions were 47, 64 and 52 % with interlayer spacings of 16, 62.6 and 82 Å for POP-T400, POP-T3000 and POP-T5000, respectively. In the case of POP-T5000 treated with 1-3 equivalents of HCl and then subjected to intercalation, the d-spacings decreased with increasing number of HCl equivalents i.e. from 82 to 74 and then 61 Å for 1, 2, and 3 equivalents of HCl, respectively.

Lin [2.82] found that the intercalation of amine salts from poly(oxypropylene) diamines in MMT had a critical point in molecular weight for dramatic enhancement in d-spacing. It changed to 58 Å for POP (Mw 2000) with an amount equivalent to 1 x CEC and to 92 Å for POP Mw 4000 with an amount equivalent to 0.8 x CEC. The d-spacing for poly(oxybutylene) (POB - Mw 2000) with an amount equivalent to 0.8 x CEC was 54.4 Å. A lower critical point (of poly(oxybutylene) amines/CEC equivalent ratio) for POB2000 and POP4000 than that of POP2000 reflected their higher backbone hydrophobicity and this was supported by good solvophilicity in toluene when the critical point was achieved. In contrast, the d-spacing for POE (Mw 2000) was only 20 Å and independent of the amounts intercalated. In the case of POP (Mw 2000)/MMT, the d-spacing was found to be 47 Å and 58 Å for two and one equivalent of HCl, respectively. These results indicated that the orientation and stretching of POP molecules in the confined area of the interlayer were influenced by two non-covalent forces, the ionic telechelic amine/MMT association and the hydrophobic effect of POP backbone.

Lin [2.83] investigated a self-aligning mechanism of poly(oxyalkylene) diamine salts when intercalated into MMT. The POP amines included α,ω -diamine of poly(oxypropylene) with Mw 2000 and the PM-amines were α,ω -diamine of poly(oxypropylene)-block-poly(oxyethylene)-block-poly(oxypropylene) with Mw 2000. Scanning electron microscopy (SEM) showed that the self-alignment resulted in individual rod dimensions ranging from 100 to 800 nm wide and 2-10 μm long when POP-amine salt loadings were below an equivalent of 0.8 x CEC (19 Å basal spacing and below 46 wt% organic). No rod formation was observed on the pristine Na^+ -MMT and POP-amine/MMT complex with an amount equivalent to 1 x CEC (58 Å basal spacing

and 63 wt% organic) indicating that pristine MMT without organic modification failed to self-assemble into long rods and POP/MMT with an abundant POP-amine fraction could not form directional array either. The self-assembly ability of POP (Mw 2000) in MMT improved when the non-protonated species was introduced to the Na⁺-MMT that was already acidified to H⁺-MMT by treatment with excess HCl. The resulting product was an organoclay, with the sodium cations replaced, having 19 Å basal and 26 wt% organic where the length of the individual rods was as great as 40 μm. Using the same method, PM Mw 2000 was intercalated into H⁺-MMT and resulted in a similar d-spacing (19 Å) and 26 wt% organic, however, no rod morphology was observed. These results suggest that the self-aligning ability is attributed to the incorporation of organic sectors into silicate interlayers and a balance of the hydrophilic/hydrophobic forces.

Lu [2.84] reported the necessary structural requirements of polyether polyols for their successful intercalation into Na⁺-MMT. The composites were prepared by mixing a range of polyether polyols with MMT by shear stirring at 11,000 rpm under an argon atmosphere. The amount of polymer adsorbed by clay was obtained by centrifugation approach. They found that homopolyetherols such as PPG2000 and polytetrahydrofuran (PTHF2000) could not be intercalated into the galleries of MMT, but PEG4000, diols2000 and block-type co-polyetherols with oxyethylene (EO) sequences (Triol1100, 6000, and SAN Triol 4500) could and resulted in 15-30 wt% being intercalated. Five or six units of EO sequences were necessary for intercalation, and it was believed to be the right number for the polyetherols to coordinate around the sodium ions in a crown-ether type complexion.

Lin [2.85] studied the compatibility of poly(oxypropylene) amine (POP amine) intercalated MMT with epoxy. The POP amine/MMT structures (Mw 400, 2000, and 4000, namely; Jeffamine D400, D2000, and D4000, respectively) exhibited d-spacings of 19.4, 58 and 92 Å, respectively. The epoxy nanocomposites prepared with 10 wt% D2000/MMT showed an exfoliated structure and an improvement in tensile strength (2.8 vs 0.3 Mpa), flexural modulus (9.6 vs 3.1 Mpa) and elongation (81.2 vs 25.3 %).

Liao [2.77] reported that the compatibility of polyethylene (PE) with Na⁺-MMT was improved by blending PE with PE-block-PEG copolymer/Na⁺-MMT complexes as shown by the higher tensile strength of PE blended with PE-PEG copolymer/Na⁺-MMT than that of PE blended with Na⁺-MMT.

2.7. References

- [2.1]. Sorrentino, A., Gorrasi, G. and Vittoria, V. (2007). Potential perspectives of bio-nanocomposites for food packaging applications. *Trends in food science & technology*, **18** (2), 84-95.
- [2.2]. Deer, W.A., Howie, R.A. and Zussman, J. (1992). An introduction to the rock-forming minerals (2nd ed.). London, Longman.
- [2.3]. Ray, S.S. and Okamoto, M. (2003). Polymer/layered silicate nanocomposites: A review from preparation to processing. *Progress in polymer science*, **28** (11), 1539-1641.
- [2.4]. Grim RE (1953). Clay mineralogy. New York, McGraw-Hill.
- [2.5]. Brindley, S.W and Brown G, editors (1980). Crystal structure of clay minerals and their X-ray diffraction. London, Mineralogical Society.
- [2.6]. Del Pennino, U., Mazzega, E., Valleri, S., Alietti, A., Brigatti, M.F. and Poppi, L. (1981). Interlayer water and swelling properties of monoionic montmorillonites. *Journal of colloid and interface science*, **84** (2), 301-309.
- [2.7]. Lebaron, P.C., Wang, Z. and Pinnavaia, T.J. (1999). Polymer-layered silicate nanocomposites: An overview. *Applied clay science*, **15** (1-2), 11-29.
- [2.8]. Vaia, R. A., Teukolsky, R. K. and Giannelis, E. P. (1994). Interlayer Structure and Molecular Environment of Alkylammonium Layered Silicates. *Chemistry of materials*, **6**(7), 1017-1022
- [2.9]. www2.cbm.uam.es/confocal/Manuales/Mowiol.pdf
- [2.10]. SRI Consulting CEH Report Polyvinyl Alcohol, published March 2007, abstract retrieved July 30, 2008

[2.11]. Jang, J. and Lee, D.K. (2003). Plasticizer effect on the melting and crystallization behavior of polyvinyl alcohol. *Polymer*, **44** (26), 8139-8146;

References therein.

[2.12]. Murakami, R., Hachisako, H., Yamada, K. and Motozato, Y. (1995).

Properties of poly (vinyl alcohol)/silica hybrid gel particles. *Journal of materials science letters*, **14** (13), 937-938.

[2.13]. Farha, S.K. and Chappaqua, N.Y. (1995). Polyethylene terephthalate-containing laminate. US patent no. 5,472,753

[2.14]. Ngui, M. O. and Mallapragada S. K. (1999). Mechanistic investigation of drying regimes during solvent removal from poly(vinyl alcohol) films. *Journal of applied polymer science*, **72** (14), 1913-1920.

[2.15]. Ngui, M. O. and Mallapragada, S. K. (1998). Understanding isothermal semicrystalline polymer drying: Mathematical models and experimental characterization. *Journal of polymer science part B polymer physics*, **36** (15), 2771-2780.

[2.16]. Hass, H.C. and Makas, A.S. (1960). A note for syndiotactic polyvinyl Alcohol. *Journal of Polymer Science*, **46** (148), 524-28

[2.17]. Tanigami T., Yano, K., Yamaura, K., Matsuzawa, S. (1995). Anomalous swelling of poly(vinyl alcohol) film in mixed solvent of dimethyl sulfoxide and water. *Polymer*, **36** (15), 2941-2946

[2.18]. Sigma-Aldrich (2011)[online]. Last accessed 15 September 2011 at: <http://www.sigmaaldrich.com/>

- [2.19]. Krimm, S., Liang, C.Y. and Sutherland, G. (1956). Infrared spectra of high polymers. V. polyvinyl alcohol. *Journal of polymer science*, **22** (101), 227-247.
- [2.20]. Hodge, R.M., Bastow, T.J., Edward, G.H., Simon, G.P and Hill, A.J. (1996). Free volume and the mechanism of plasticization in water-swollen poly (vinyl alcohol). *Macromolecules*, **29** (25), 8137-8143.
- [1.21]. Wang, X., Fang, D., Yoon, K., Hsiao, B. S. and Chu B. J. (2006). High performance ultrafiltration composite membranes based on poly(vinyl alcohol) hydrogel coating on crosslinked nanofibrous poly(vinyl alcohol) scaffold. *Journal of membrane science*, **278** (1-2), 261-268
- [2.22]. Konidari, M.V., Papadokostaki, K.G. and Sanopoulou, M. (2011). Moisture-induced effects on the tensile mechanical properties and glass-transition temperature of poly(vinyl alcohol) films. *Journal of applied polymer science*, **120** (6), 3381-3386.
- [2.23]. Holland, B. J. and Hay, J. N. (2001). The thermal degradation of poly(vinyl alcohol). *Polymer*, **42** (16), 6775-6783.
- [2.24]. Assender, H.E. and Windle, A.H. (1998). Crystallinity in poly(vinyl alcohol). 1. an X-ray diffraction study of atactic PVOH. *Polymer*, **39** (18), 4295-4302.
- [2.25]. Jang, J. and Lee, D.K. (2003). Plasticizer effect on the melting and crystallization behavior of polyvinyl alcohol. *Polymer*, **44** (26), 8139-8146.
- [2.26]. Mohsin, M., Hossin, A. and Haik, Y. (2011). Thermomechanical properties of poly(vinyl alcohol) plasticized with varying ratios of sorbitol. *Materials science and engineering: A*, **528** (3), 925-930.

[2.27]. Wikipedia (2011). [online]. Last accessed 15 September 2011 at:
www.wikipedia.org

[2.28]. Chemindustry (2011) [online]. Last accessed 15 September 2011 at:
http://chemindustry.ru/Polyethylene_Glycol.php

[2.29]. Pillin, I., Montrelay, N. and Grohens, Y. (2006). Thermo-mechanical characterization of plasticized PLA: Is the miscibility the only significant factor? *Polymer*, **47** (13), 4676-4682.

[2.30]. Pluta, M., Paul, M.M., Alexandre, M., and Dubois, P. (2006). Plasticized polylactide/clay nanocomposites. I. the role of filler content and its surface organo-modification on the physico-chemical properties. *Journal of polymer science-B-polymer physics edition*, **44** (2), 299-311.

[2.31]. Rossi, S., Luckham, P.F. and Tadros, T.F. (2003). Influence of non-ionic polymers on the rheological behaviour of Na⁺-montmorillonite clay suspensions. part II. homopolymer ethyleneoxide and polypropylene oxide-polyethylene oxide ABA copolymers. *Colloids and surfaces A: Physicochemical and engineering aspects*, **215** (1-3), 1-10.

[2.32]. ReferenceAnswers (2011) [online]. Last accessed 15 September 2011 at <http://www.answers.com>

[2.33]. Britannica (2011) [online]. Last accessed 15 September 2011 at <http://www.britannica.com>

[2.34]. Huntsman (2011) [online]. Last accessed 15 September 2011 at:
<http://www.huntsman.com>

- [2.35]. Kawasumi, M. (2004). The discovery of polymer-clay hybrids. *Journal of polymer science, part A, polymer chemistry*, **42** (4), 819-824.
- [2.36]. Chen, J. S., Poliks, M.D., Ober, C.K., Zhang, Y., Wiesner, U., and Giannelis, E. (2002). Study of the interlayer expansion mechanism and thermal-mechanical properties of surface-initiated epoxy nanocomposites. *Polymer*, **43** (18), 4895-4904
- [2.37]. European Commission (2011) [online] at <http://ec.europa.eu/enterprise/newsroom/infocentre/detail.cfm?id=5500&lang=en>
- [2.38]. Ray, S.S. and Bousmina, M. (2005). Biodegradable polymers and their layered silicate nanocomposites: In greening the 21st century materials world. *Progress in materials science*, **50** (8), 962-1079.
- [2.39]. PCAS Group-MERI-SHU (2010) [online]. Last accessed 27 October 2010 at: <http://www.shu.ac.uk/research/meri/pcas/composites/index.html>
- [2.40]. Maiti, P. et al. (2002). New Poly(lactide)/Layered Silicate Nanocomposites: Role of Organoclays. *Chemistry of materials*, **14** (11), 4654-4661
- [2.41]. Yano, K., Usuki, A., Okada, A., Kurauchi, T. and Kamigaito, O. (1993). Synthesis and Properties of Polyimide-Clay Hybrid. *Journal of polymer science part A: polymer chemistry*, **31** (10), 2493-2498.
- [2.42]. Giannelis, E. P. (1996). Polymer Layered Silicate Nanocomposites. *Advanced materials*, **8** (1), 29-35.

- [2.43]. Strawhecker, K.E. and Manias, E. (2000). Structure and properties of poly (vinyl alcohol)/Na montmorillonite nanocomposites. *Chemistry of materials*, **12** (10), 2943-2949.
- [2.44]. Bharadwaj, R. K. (2001). Modeling the barrier properties of polymer-layered silicate nanocomposites. *Macromolecules*, **34** (26), 9189-9192.
- [2.45]. Ray, S. S. and Okamoto, M. (2003). Biodegradable polylactide and its nanocomposites: Opening a new dimension for plastics and composites. *Macromolecular rapid communications*, **24** (14), 815-840.
- [2.46]. Wang, Y., Zhang, L., Tang, C. and Yu, D. (2000). Preparation and characterization of rubber-clay nanocomposites. *Journal of applied polymer science*, **78** (11), 1878-1883.
- [2.47]. Zanetti, M., Lomakin, S. and Camino, G. (2000). Polymer layered silicate nanocomposites. *Macromolecular materials and engineering*. **279** (1), 1-9.
- [2.48]. Schmidt, D. F., Clement, F. and Giannelis, E. P. (2006). On the origins of silicate dispersion in polysiloxane/layered-silicate nanocomposites. *Advanced functional materials*, **16** (3), 417-425.
- [2.49]. Nguyen, Q. T. and Baird, D. G. (2006). Preparation of polymer-clay nanocomposites and their properties. *Advances in polymer technology*, **25** (4), 270-285.
- [2.50]. Alexandre, M. and Dubois, P. (2000). Polymer-layered silicate nanocomposites: Preparation, properties and uses of a new class of materials. *Materials science & engineering R*, **28** (1-2), 1-63.

- [2.51]. Chang, S. H., Ryan, M.E., Gupta, R.K. and Swiatkiewicz, B. (1991). The adsorption of water-soluble polymers on mica, talc limestone, and various clay minerals. *Colloids and surfaces*, **59**, 59-70.
- [2.52]. Chiellini, E., Corti, A., Politi, B. and Solaro, R. (2000). Adsorption/desorption of polyvinyl alcohol on solid substrates and relevant biodegradation. *Journal of polymers and the environment*, **8** (2), 67-79.
- [2.53]. Strawhecker, K.E. and Manias, E. (2001). AFM of poly (vinyl alcohol) crystals next to an inorganic surface. *Macromolecules*, **34** (24), 8475-8482.
- [2.54]. De Bussette, S.G. and Ferreiro, E.A. (2004). Adsorption of poly(vinyl alcohol) on montmorillonite. *Clays and clay minerals*, **52** (3), 334-340
- [2.55]. Carrado, K. A., Thiyagarajan, P. and Elder, D. L. (1996). Polyvinyl alcohol-clay complexes formed by direct synthesis. *Clays and clay minerals*, **44** (4), 506-514.
- [2.56]. Bajpai, A. K. and Vishwakarma, N. (2003). Adsorption of polyvinylalcohol onto fuller's earth surfaces. *Colloids and surfaces A: Physicochemical and engineering aspects*, **220** (1-3), 117-130
- [2.57]. Soundararajah, Q.Y., Karunaratne, B.S.B. and Rajapakse, R.M.G. (2009). Mechanical properties of poly (vinyl alcohol) montmorillonite nanocomposites. *Journal of composite materials*, **44** (3), 303-311.
- [2.58]. Cui, L., Yeh, J.T., Wang, K., Tsai, F.C. and Fu, Q. (2009). Relation of free volume and barrier properties in the miscible blends of poly (vinyl alcohol) and nylon 6-clay nanocomposites film. *Journal of membrane science*, **327** (1-2), 226-233

- [2.59]. Adoor, S. G., Sairam, M., Manjeshwar, L.S., Raju, K.V.S.N. and Aminabhavi, T.M. (2006). Sodium montmorillonite clay loaded novel mixed matrix membranes of poly (vinyl alcohol) for pervaporation dehydration of aqueous mixtures of isopropanol and 1, 4-dioxane. *Journal of membrane science*, **285** (1-2), 182-195.
- [2.60]. Ahn, T., Suk, H.J., Won, J. and Yi, M.H. (2009). Extended lifetime of pentacene thin-film transistor with polyvinyl alcohol (PVA)/layered silicate nanocomposite passivation layer. *Microelectronic engineering*, **86** (1), 41-46.
- [2.61]. Jia, X., Li, Y., Zhang, B., Cheng, Q. and Zhang, S. (2008). Preparation of poly (vinyl alcohol)/kaolinite nanocomposites via in situ polymerization. *Materials research bulletin*, **43** (3), 611-617.
- [2.62]. Alla, S. G. A., El-din, H. M. N. and El-naggar, A. W. M. (2006). Electron beam synthesis and characterization of poly (vinyl alcohol)/montmorillonite nanocomposites. *Journal of applied polymer science*, **102** (2), 1129-1138.
- [2.63] Sengwa, R. J., Choudhary, S. and Sankhla, S. (2010). Dielectric properties of montmorillonite clay filled poly(vinyl alcohol)/poly(ethylene oxide) blend nanocomposites. *Composites science and technology*, **70** (11), 1621-1627.
- [2.64]. Ip, K. H., Stuart, B.H., Thomas, P.S. and Ray, A. (2011). Characterisation of poly(vinyl alcohol)–montmorillonite composites with higher clay contents. *Polymer testing*, **30** (7), 732-736.
- [2.65]. Parra, D. F., Fusaro, J., Gaboardi, F. and Rosa, D.S. (2006). Influence of poly (ethylene glycol) on the thermal, mechanical, morphological, physical–

chemical and biodegradation properties of poly (3-hydroxybutyrate). *Polymer degradation and stability*, **91** (9), 1954-1959.

[2.66]. Ozkog, G. and Kemalolu, S. (2009). Morphology, biodegradability, mechanical, and thermal properties of nanocomposite films based on PLA and plasticized PLA. *Journal of applied polymer science*, **114** (4), 2481-2487.

[2.67]. Bujdak, J., Hackett, E., and P. Giannelis, E.P (2000). Effect of layer charge on the intercalation of poly(ethylene oxide) in layered silicates: Implications on nanocomposite polymer electrolytes. *Chemistry of materials*, **12** (8), 2168-2174.

[2.68]. Parfitt, R.L. and Greenland, D.J. (1970). The adsorption of poly(ethylene glycol) on clay minerals. *Clay Minerals* **8** (3), 305-315.

[2.69]. Chen, B. and Evans, J.R.G (2004). Preferential intercalation in polymer-clay nanocomposites. *The journal of physical chemistry B*, **108** (39), 14986-14990.

[2.70]. Stefanescu, E. A., Stefanescu, A., Daly, W.H., Negulescu, I.I. (2008). Hybrid polymer-clay nanocomposites: A mechanical study on gels and multilayered films. *Polymer*, **49** (17), 3785-3794.

[2.71]. Stefanescu, E. A., Daly, W.H. and Negulescu, I.I (2008). Hybrid Polymer/Clay nanocomposites: Effect of clay size on the structure of multilayered films. *Macromolecular materials and engineering*, **293** (8), 651-656.

[2.72]. Chaiko, D.J. (2003). New poly(ethylene oxide)-Clay composites. *Chemistry of materials*, **15** (5), 1105-1110.

[2.73]. Thiyagarajan, P., Chaiko, D. J. and Hjelm, R. P. (1995). A neutron scattering study of poly(ethylene glycol) in electrolyte solutions.

Macromolecules, **28** (23), 7730-7736.

[2.74]. Strawhecker, K.E. and Manias, E. (2003). Crystallization behavior of poly(ethylene oxide) in the presence of Na-montmorillonite fillers. *Chemistry of materials*, **15** (4), 844-849.

[2.75]. Maiti, P., Nam, P.H., Okamoto, M., Kotaka, D., Hasegawa, N. and Usuki, A. (2002). The effect of crystallization on the structure and morphology of polypropylene/clay nanocomposites. *Polymer engineering and science*, **42** (9), 1864–1871.

[2.76]. Lincoln, D.M., Vaia, R.A., Wang, Z.G., Hsiao, B.S. and Krishnamoorti, R. (2001). Temperature dependence of polymer crystalline morphology in nylon 6/montmorillonite nanocomposites. *Polymer*, **42** (25), 9975-9985.

[2.77]. Liao, B., Song, M., Liang, H. and Pang, Y. (2001). Polymer-layered silicate nanocomposites. 1. A study of poly(ethylene oxide)/Na⁺-montmorillonite nanocomposites as polyelectrolytes and poly(ethylene-block-poly(ethylene glycol) copolymer)/Na⁺-montmorillonite nanocomposites as fillers for reinforcement of polyethylene. *Polymer*, **42** (25), 10007-10011.

[2.78]. Chen, B. and Evans, J. R. G. (2005). X-ray diffraction studies and phase volume determinations in poly(ethylene glycol)-montmorillonite nanocomposites. *Polymer international*, **54** (5), 807-813.

[2.79]. Lin, J.J., Cheng, I.J., Wang, R., and Lee, R.J. (2001). Tailoring basal spacings of montmorillonite by poly(oxyalkylene)diamine intercalation. *Macromolecules*, **34** (26), 8832-8834.

[2.80]. Vaia, R. A., Sauer, B.B., Tse, O.K. and Giannelis, E.P. (1997). Relaxations of confined chains in polymer nanocomposites: Glass transition properties of poly (ethylene oxide) intercalated in montmorillonite. *Journal of polymer science part B: polymer physics*, **35** (1), 59-67

[2.81]. Chou, C.C., Shieu, F.S., and Lin, J.J. (2003). Preparation, organophilicity, and self-assembly of poly(oxypropylene)amine-Clay hybrids. *Macromolecules*, **36** (7), 2187-2189.

[2.82]. Lin, J. J., Chen, I. J. and Chou, C. C. (2003). Critical conformational change of poly (oxypropylene) diamines in layered aluminosilicate confinement. *Macromolecular rapid communications*, **24** (8), 492-495.

[2.83]. Lin, J. J., Chou, C. C. and Lin, J. L. (2004). Lengthy rod formation from a poly (oxyalkylene) amine-intercalated smectite clay by a self-aligning mechanism. *Macromolecular rapid communications*, **25** (11), 1109-1112.

[2.84]. Lu, Y., Kong, S.T., Deiseroth, H.J. and Mormann, W. (2008). Structural requirements for the intercalation of polyether polyols into sodium-montmorillonite: The role of oxyethylene sequences. *Macromolecular materials and engineering*, **293** (11), 900-906.

[2.85]. Lin, J. J., Cheng, I. J. and Chu, C. C. (2003). High compatibility of the poly (oxypropylene) amine-intercalated montmorillonite for epoxy. *Polymer journal*, **35** (5), 411-416.

3.1. X-ray diffraction (XRD)

X-rays are a high frequency form of electromagnetic radiation (in the range 3×10^{16} to 3×10^{19} Hz corresponding to a wavelength of 100 to 0.1 Å) that is produced when atoms of any substance such as copper are hit by high speed electrons. X-radiation is also called Rontgen radiation after Wilhem Conrad Rontgen who discovered them in 1895, and who called them x-rays to signify an unknown type of radiation [3.1]. X-rays have certain properties: they travel in straight lines, are exponentially absorbed by matter with the exponent being proportional to the mass of the absorbing material, they darken photographic plates, and create shadows of absorbing material on photosensitive paper [3.2].

X-ray diffraction is a non-destructive technique that is often used to determine the crystalline structure of a material. The phenomenon of it was found by von Laue, a German physicist, who argued that it was possible to diffract x-rays by means of crystals if the wavelength of x-rays was about equal to the inter-atomic distance in crystals. Later, W.H. Bragg and his son W.L. Bragg derived an expression for the necessary conditions for x-ray diffraction to occur in much simpler mathematical terms than von Laue had used in the same year (1912) [3.3]. Within the following year they were able to solve the structure of NaCl, KCl, KBr and KI.

Bragg proposed planes of particles behaving like reflecting planes that were capable of scattering constructive interference in certain directions. W.L. Bragg formulated the description of x-ray diffraction, known as Bragg's law, as follows:

$$n\lambda = 2d \sin\theta \quad (3.1)$$

where n is the order of diffraction, λ is the x-ray wavelength, d is the distance between reflecting the planes and θ is the angle of diffraction.

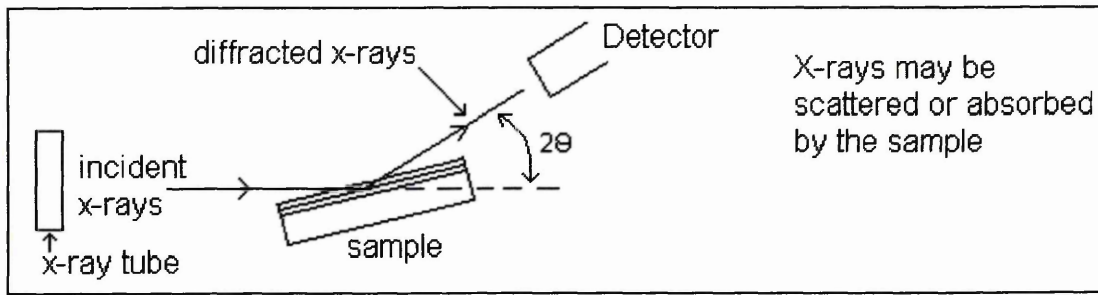


Figure 3.1. Schematic of x-ray diffractometer

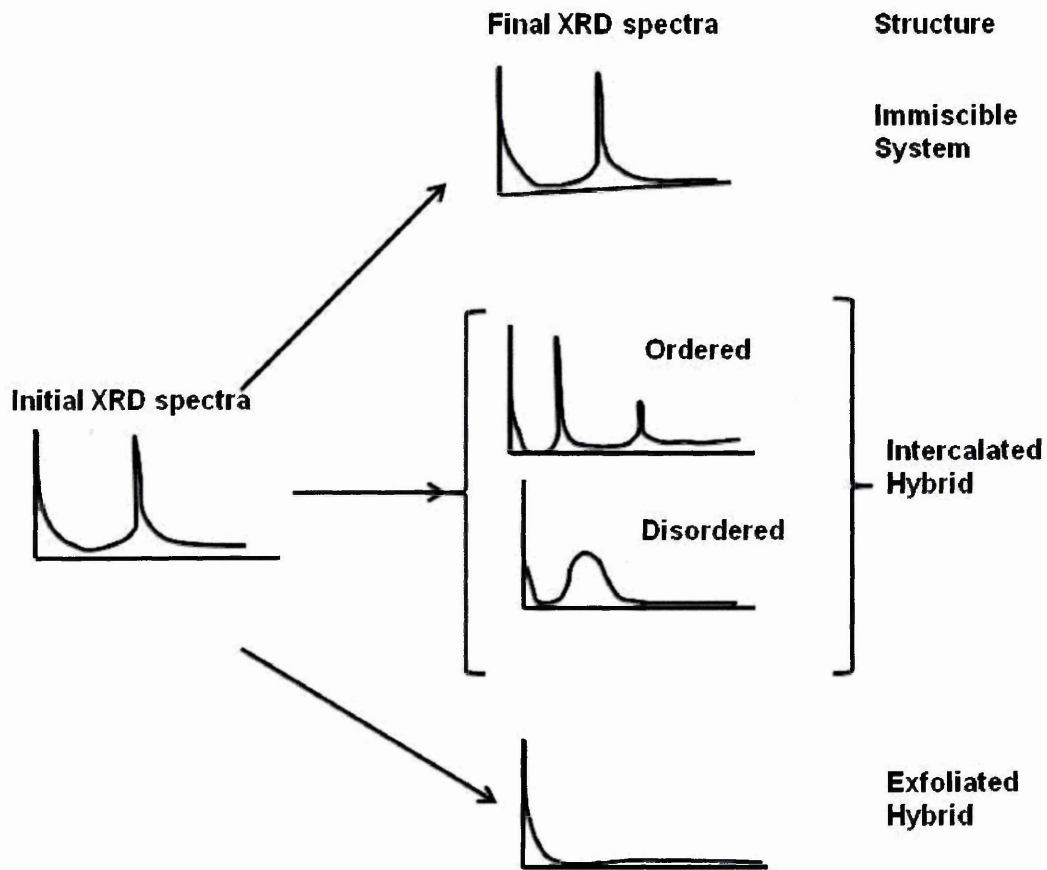


Figure 3.2. Schematic depicting the expected X-ray diffraction patterns for various types of clay/polymer structures.

In this thesis, Bragg-Bentano parafofocussing geometry is employed to analyse the samples. A simplified schematic of the x-ray diffractometer is given in Figure 3.1. In the analysis of polymer/clay nanocomposites, the use of x-ray diffraction relies on the established procedures developed for the identification and characterisation of layered silicate minerals. The crystal structures such as unit cell type and their dimensions are then obtained from the diffraction pattern. The 00/ basal reflections are generally used to characterise the morphology of polymer/clay nanocomposites [3.4]. The interlayer spacing of clay is calculated from the position of the 001 peak using Bragg's law after re-arrangement as given below:

$$d = \frac{n\lambda}{2 \sin\theta} \quad (3.2)$$

The XRD interpretation of clay dispersion in a polymer matrix can be described in Figure 3.2 [3.5]. The shift to lower angles represents an increase in d-spacing. The orders of reflection become more intense the more ordered it becomes. The influence of polymer intercalation on the order of the silicate is indicated by changes in the intensity and shape of the basal reflection (001). Increased order is shown by a decrease in peak width and increase in peak intensity. This provides an index of the degree of co-planarity of the silicate layers in an intercalated hybrid. The XRD trace of microcomposites is attributed to a single peak whereas an exfoliated hybrid is attributed to an XRD silent trace, i.e. no d_{001} peaks are observed. All XRD measurements conducted in this report used $\text{CuK}\alpha_1$ as the source of x-rays (1.54186 Å) at 40 mA and 40 kV.

A divergent slit of 0.5° , anti scatter slit of 1° , and mask of 15 were used. Data was collected using step size of 0.02° and a scan time of 1 s per step.

3.2. Thermogravimetric analysis (TGA)

Thermogravimetric analysis (TGA) is a technique used to measure the weight change of sample due to the formation of volatile products in relation to change in temperature. It is commonly used in research to determine polymer characteristics such as degradation temperatures, absorbed moisture contents and levels of inorganic and organic components or solvent residues [3.6].

The schematic of a typical TGA instrument is shown in Figure 3.3. It mainly consists of a balance and counter balance, furnace, sample holder, and thermocouple. A non-oxidative degradation (pyrolysis) is performed under inert gas flow, while the use of air or oxygen allows oxidative degradation of samples. During the measurement, a sample weighing a few milligrams is placed in a refractory crucible and the weight is recorded by means of a sensitive balance. The sample measurement can be performed from room temperature up to 1000°C . Factors such sample size, particle size distribution, packing density, sample holder, use of inert atmosphere, gas flow rate, and heating rate may affect the shape of the weight loss curve [3.7].

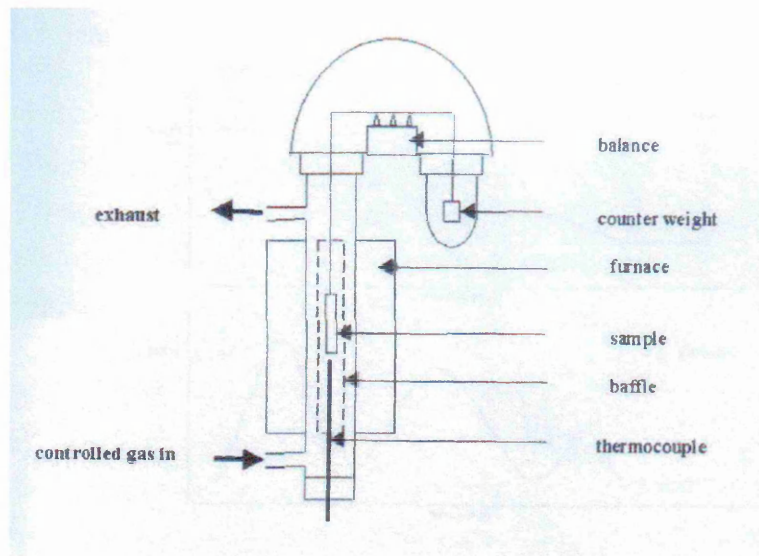


Figure 3.3. Schematic diagram of a TGA instrument.

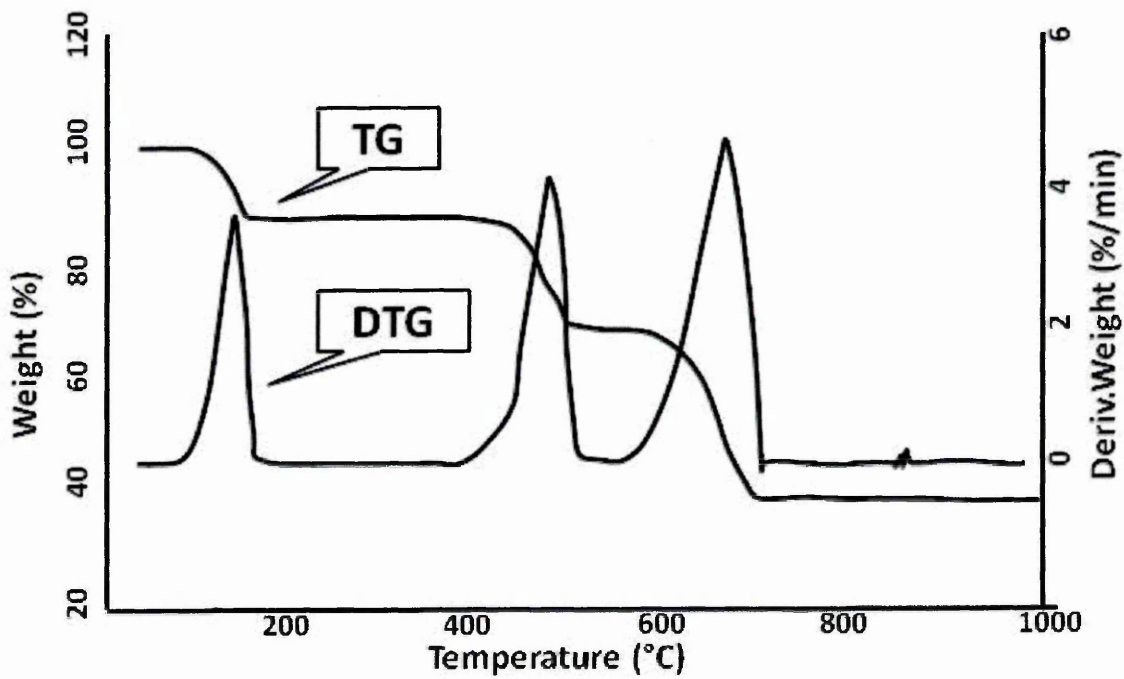


Figure 3.4. Diagrammatic representation of TGA and derivative TG (DTG) data curve.

Data is given by weight loss as a function of temperature and is called a thermogram (TG). The negative, derivative weight loss curve (typical curve shown in Figure 3.4) can also be used to show the rate at which weight is lost.

Significant weight losses are therefore represented as peaks in the DTG curve. Generally, the incorporation of clay into a polymer matrix has been found to enhance thermal stability by acting as a superior insulator and mass transport barrier to the volatile products generated during decomposition [3.8].

All TGA measurements were performed on a Mettler Toledo TG50 Thermogravimetric Analyser using an alumina crucible. Data was recorded at a heating rate of 20 °C/min between 35 and 800 °C after an initial isothermal stage where the sample was kept at 35 °C for 15 minutes. The analysis was performed under a nitrogen atmosphere with a flow rate of 10 ml/min.

3.3. Adsorption Isotherms (Centrifugation approach)

Centrifugation is a technique which uses centrifugal force (*g*-force) to isolate suspended particles from their surrounding medium in a liquid suspension [3.9]. It exploits the fact that many particles in a liquid suspension, given time, will eventually settle at the bottom of a container due to gravity (1 *x g*). However, the length of time required for such separations can be impractical. Extremely small particles will not separate at all in solution, unless subjected to high centrifugal force. When a suspension is rotated at a certain speed (revolutions per minute (RPM)), centrifugal force causes the particles to move radially away from the axis of rotation. The force on the particles compared to gravity is called Relative Centrifugal Force (RCF). For example, an RCF of 500 *x g* indicates that the centrifugal force applied is 500 times greater than that of Earth's gravitational force. The RCF value is determined by the following formula:

$$RCF = 11.17 (r) \left(\frac{n}{1000} \right)^2 \quad (3.3)$$

where r is the radius in centimetres from the centreline of the rotor to the point in the tube where RCF value is required, and n is the rotor speed in rpm.

In this research, a centrifugation approach is used to quantify the amount of organic that adsorbs on the clay of organic-clay suspension. The instrument is a SORVALL RC6 with SA-600 rotor capable of holding 50 ml Nalgene polycarbonate oak ridge round-bottom tubes [3.10]. The prepared organic (polymer and/or plasticizer)/clay suspensions (see Chapter Experimental 4.1) were placed in the tubes and centrifuged at 15,000 rpm for 1.5 hours. After centrifugation, materials were separated into two phases: i) sediment; the adsorbed organic and sedimented clay gathered at the bottom of the tube and ii) supernatant, any remaining non-adsorbed organic and suspension medium (water). Sediment and supernatant were dried separately at 47 °C for 24 h. The amount of organic in the supernatant was measured gravimetrically using a four-place balance. The amount of organic in the sediment adsorbed by clay was calculated by the amount of organic offered to the clay minus the amount determined in the supernatant (free organic). A schematic of the centrifugation experiment is shown in Figure 3.5. In the competitive study, TGA is used to determine the amount of PVOH and plasticizer (e.g. PEG600 or M600) in the supernatant, detail about the calculation is given in Chapters 5 and 6.

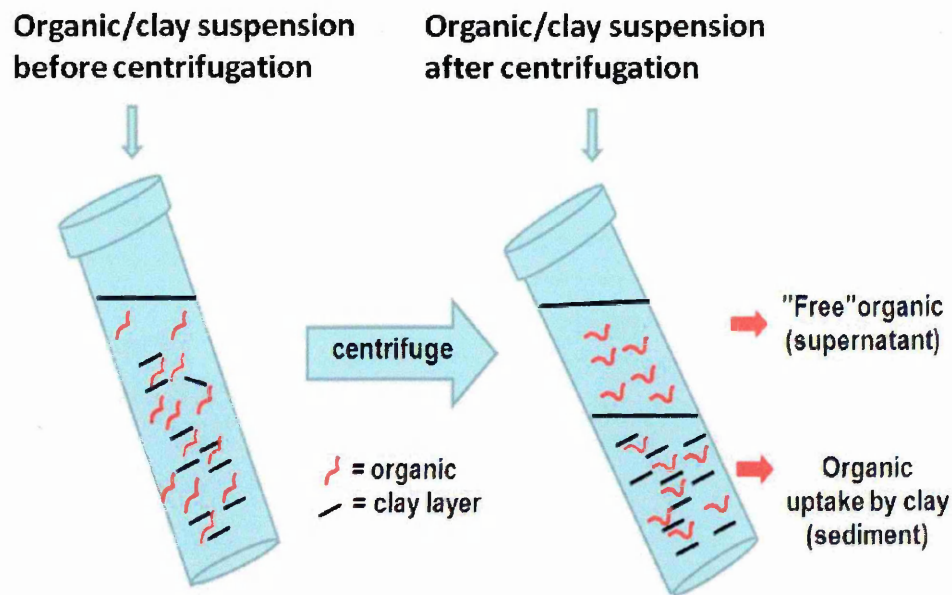


Figure 3.5. Schematic experiment of centrifugation approach.

3.4. Thermogravimetric mass spectrometry (TGMS)

TGMS is a technique which can be used to determine the elemental composition of a sample or molecule [3.11]. It involves ionizing chemical compounds to produce charged molecules or molecular fragments and then measurement of their mass to charge ratio. TGMS instruments are mainly composed of a furnace (TG/DTA), an ion source, a mass analyser, and a detector. The furnace is used to heat the sample in the same manner as that described above in the TGA section (Section 3.2) and results in the desorption of species or the creation of volatile decomposition products. The ion source is used to convert the evolved gas phase molecules into ions. The mass analyzer then separates the ions by their mass to charge ratio by applying electromagnetic fields. Finally, the detector is used to account the number of ions hitting the detector over a period of time.

3.5. Water vapour transmission rate (WVTR)

Water vapour transmission rate (WVTR) or "permeability" of sheet material is defined as the mass of water vapour transmitted through a unit area in a unit time under specified conditions of temperature and humidity, and is expressed in grams per square metre per 24 hours ($\text{g}/(\text{m}^2\cdot\text{day})$). The use of this method is not generally recommended if the transmission rate is expected to be less than $1 \text{ g}/(\text{m}^2\cdot\text{day})$, for materials thicker than $3000 \mu\text{m}$ or films that shrink to an appreciable extent under the test conditions used.

An experimental procedure to measure the WVTR is conducted using dishes/cups containing a desiccant such as silica gel, activated charcoal, calcium sulphate or calcium chloride which is closed by the material to be tested. The cups are placed in a controlled atmosphere (humidity oven). The cups are weighted at suitable intervals of time and the WVTR is determined from the increase in mass when this increase has become proportional to the time interval. The WVTR result is calculated from the following formula [3.11]:

$$\text{WVTR} = (240 \times m) / (S \times t) \quad (3.4)$$

where t is the total duration in hours, m is the increase in mass in milligrams of the assembly during the time t , and S is exposure surface area of cups. In this research, aluminium cups supplied by Sheen Instruments with an exposure surface of 25 cm^2 were used. Silica gel (9.5 g for each cup) that had been dried overnight in oven at 100°C was used as desiccant. Nanocomposite films were equilibrated in the humidity oven at 23°C and 85 % relative humidity (RH) for 24 hours before performing the WVTR measurement.

3.6. Dynamic mechanical analysis (DMA)

Dynamic mechanical analysis (DMA) is a technique where an oscillation force with a set frequency is applied to a sample and reports changes in stiffness and damping [3.13]. It works by applying a sinusoidal deformation to a sample of known geometry by a controlled stress or a controlled strain. For a controlled stress, the sample will deform at a certain amount which is related to its stiffness.

The stiffness and damping are represented as modulus and tan delta. The modulus can be expressed as the storage modulus (in-phase component), which is related to elastic behaviour of the sample and the loss modulus (out-phase component), which is related to the viscous behaviour of the sample. The ratio of the loss modulus E'' to the storage modulus E' is the tan delta and called damping, which is a measurement of the energy dissipation of a material under cyclic load.

As the modulus values change with temperature, transition in a material can be seen as change in the E' or tan delta curves. DMA can measure the glass transition, melting temperature and other transitions that occur in the glassy or rubbery plateau of a material. The glass transition (T_g) value is detected as the onset of E' drop, the peak of the tan delta, or the peak of the E'' curve. To ensure that the transition is a T_g , it is performed by running a multi frequency scan, this is because T_g is frequency dependant.

All DMA measurements were conducted using a Perkin Elmer DMA8000 instrument in tension mode using the following conditions: frequency 1 and 10 Hz (i.e. multi frequency scan); ratio tension 1.2; heating rate 2 °C/minute; displacement 0.01 mm and temperature range -50 to 130 °C. The dimension of the specimen samples were approximately 65 μm in thickness, 7-8 mm in width,

and 10 mm in length. The activation energies of the relaxation processes involved were calculated using an Arrhenius-type equation from the maximum values of the loss modulus at the two mentioned frequencies [3.14].

3.7. Fourier Transform Infrared Spectroscopy (FTIR)

Fourier transform infrared spectroscopy (FTIR) is a technique which is used to obtain an infrared (IR) spectrum of absorption, emission or photoconductivity of a solid, liquid or gas [3.15]. IR spectroscopy exploits the fact that molecules absorb IR light at specific frequencies that are characteristic of the vibrational energy levels of various functional groups in a sample. The IR absorption occurs at resonant frequency i.e. when the frequency of the absorbed radiation is the same as the frequency of the bond or group that vibrates with respect to other molecules. The vibrational energy levels are distinctive for every molecule and its isomer and so the IR spectrum has often been referred to as the fingerprint of a molecule.

The infrared spectrum is usually divided into three regions; the higher energy near IR ($14000\text{--}4000\text{ cm}^{-1}$ or $0.8 - 2.5\text{ }\mu\text{m}$ wavelength), which may be used to study harmonic vibrations, the mid IR ($4000\text{--}400\text{ cm}^{-1}$ or $2.5 - 25\text{ }\mu\text{m}$), which may be used to study the fundamental vibrations and associated rotational-vibrational structure, and the low energy far IR ($400\text{--}10\text{ cm}^{-1}$ or $25\text{--}1000\text{ }\mu\text{m}$), which may be used to study rotational spectroscopy.

A Thermo Nicolet NEXUS spectrometer along with a MCT (mercury cadmium telluride) detector cooled by liquid nitrogen was used for all the FTIR analysis. The spectrometer was coupled with a single reflection diamond ATR cell (Graseby Specac, U.K). This setup has the trade name "Golden Gate". PVOH film was placed on top of the crystal diamond and the spectra of the films

taken. The wavelength of interest ranges from 700 to 4000 cm^{-1} and was collected with resolution of 4 cm^{-1} and 64 scans. Omnic software was used to collect and analyse the spectra.

3.8. X-ray Fluorescence (XRF)

XRF is a fast, non-destructive and multi elemental technique used for qualitative and quantitative elemental analysis of samples [3.16]. It is based on x-rays emitted by atoms of a material that have been excited by bombardment with high-energy x-rays or gamma rays. The x-ray spectrum acquired during the emission process reveals a number of characteristic peaks. The energy of the peaks leads to the identification of the element presents in the sample (qualitative analysis), whilst the peak intensities relate to the relevant or absolute elemental concentration (semi quantitative or quantitative analysis).

3.9. Nuclear magnetic resonance (NMR) spectroscopy

NMR spectroscopy is a research technique that utilizes the phenomenon of nuclei magnetic resonance to obtain chemical information of molecules [3.17]. In this project ^1H NMR was used to evidence and evaluate modifications of the functional group of M600 and QM600, where ^1H NMR spectra were recorded on Bruker Avance ^{III} at 400 MHz spectrometers with TMS (tetramethyl silane - $\text{Si}(\text{CH}_3)_4$) as an internal standard. Deuterated chloroform (CDCl_3) and deuterated water (D_2O) were used as solvents in the NMR spectroscopy measurements. M600 is soluble in chloroform but not in water, whilst QM600 is soluble in water, but only moderately soluble in chloroform.

3.10. References

- [3.1]. Garcia, K. (2002). Wilhelm Roentgen and the Discovery of X-Rays (Unlocking the Secrets of Science). Mitchell Lane Publishers.
- [3.2]. 'Elements of x-ray diffraction', 3rd edition, (Eds. Cullity BD, Stock SR) (2001). London, Prentice Hall.
- [3.3]. Waseda, Y., Matsubara, E., and Shinoda, K. (2011). X ray Diffraction Crystallography: Introduction, Examples and Solved Problems. Germany, Springer.
- [3.4]. Vaia, R.A. and Liu, W. (2002). X-ray powder diffraction of polymer/layered silicate nanocomposites: Model and practice. *Journal of polymer science part B: polymer physics*, **40** (15), 1590-1600.
- [3.5]. Vaia, R. A., Vasudevan, S., Krawiec, W., Scanlon, L.G. and Giannelis, E.P. (1995). New polymer electrolyte nanocomposites: Melt intercalation of poly (ethylene oxide) in mica-type silicates. *Advanced materials*, **7** (2), 154-156.
- [3.6]. Mansfield, E, Kar, A., Quinn, T. P., Hooker, S. A. (2010). Quartz Crystal Microbalances for Microscale Thermogravimetric Analysis. *Analytical Chemistry*, **82** (24), 9977-9982.
- [3.7]. Dodd, J.W. and Tonge, K.H. Editors (1987). Thermal methods. London, John Wiley & Sons.
- [3.8]. Ray, S. S. and Okamoto, M. (2003). Biodegradable polylactide and its nanocomposites: Opening a new dimension for plastics and composites. *Macromolecular rapid communications*, **24** (14), 815-840.
- [3.9]. Kendro: Basic of centrifugation (2011) [online]. Last visit on 25 October 2011 at <http://www.axeb.dk/documents/Cent101.pdf>

[3.10]. Coleparmer (2011) [online]. Last visist 25 October 2011 at <http://www.coleparmer.co.uk>

[3.11]. Sparkman,O.David (2000). Mass Spectroscopy desk reference. Pitsburg, Global view Publication.

[3.12]. British Standard (BS 2782-8:Method 820A:1996). Method of testing Plastics part 8: Other properties, Method 820A: Deteremination of water vapour transmission rate (dish method).

[3.13]. Menard,K.P. (1999). Dynamic Mechanical Analysis A Practical Introduction. Wasington, CRC Press.

[3.14]. Strobl G. (1997). The Physics of Polymers. Berlin, Springer.

[3.15]. Griffiths, P. and de Hasseth, J.A. (2007). Fourier Transform Infrared Spectrometry (2nd editon). Wiley-Blackwell.

[3.16]. Jenkins, Ron (1999). X-ray Fluorescence Spectrometry (2nd edition). John Wiley and Sons, Inc.

[3.17]. Hore, P.J. (1995). Nuclear Magnetic Resonance. Oxford, Oxford University Press.

4.1. PVOH/clay nanocomposites

All nanocomposites presented in this report were prepared by solution-casting. The clay sample was sodium MMT supplied by Southern Clay Products with the tradename Cloisite Na⁺ and has a CEC = 92.5 meq/100g. The desired amount of clay was dispersed in 14 ml of deionised water in a glass container at room temperature by stirring with a magnetic/heater stirrer. The desired amount of PVOH (*Mw* 30,000) obtained from Aldrich was stirred in 6 ml of distilled water in a flask heated at 90 °C to allow for complete dissolution [4.1]. After two hours the clay suspension was added to the dissolved PVOH, the total amount of solids for each sample being 1 g. The PVOH/clay suspension was then kept at 90 °C and stirred for a further four hours before casting 2 ml suspension onto a glass slide and 18 ml suspension into a Petri dish. All the suspensions were dried in an oven at 40 °C for 24 hours before being analysed by XRD, TGA, DMA, FTIR, TGMS and XRF.

4.2. PEG, PPG, M600/clay nanocomposites

For PEG/clay nanocomposites, 1 g of clay was mixed with 14 ml deionised water and stirred for 2 hours at room temperature using a magnetic/heater stirrer. The desired amount of PEG (*Mw* 600, or *Mw* 2000) obtained from Aldrich was mixed with 6 ml deionised water also at room temperature. Clay suspension and PEG solution were then mixed and stirred for a further 4 hours at room temperature before casting a 2 ml aliquot on to a glass slide and 18 ml suspension into a Petri dish.

The procedure for PEG/clay composites was also used to prepared PPG (*Mw* 725 and *Mw* 2000)/clay nanocomposites and M600/clay nanocomposites.

4.3. PVOH/PEG600/clay nanocomposites

For the tertiary nanocomposite systems, 1 g clay was dispersed and stirred in 14 ml deionised water for 2 hours at room temperature. The desired amount of PEG600 was dissolved in 2 ml of water at room temperature, whereas the desired amount of PVOH was dissolved in 4 ml distilled water at 90 °C. Three different routes of mixing were implemented for the tertiary system. In route 1, the PEG600 solution was mixed and stirred with the PVOH solution for 4 hours before the clay suspension was added and stirred for another 4 hours. In route 2, the PVOH solution was mixed with the clay suspension for 4 hours before PEG600 solution was added and stirred for another 4 hours. In route 3, the PEG600 solution was mixed with the clay suspension for 4 hours, before the PVOH solution was added and stirred for another 4 hours. In these three routes, the mixing and stirring of the components were performed at 90 °C. The total volume of water for each sample was 20 ml. A 2 ml aliquot of the PVOH/PEG600/clay suspension was cast onto a glass slide and the remaining 18 ml suspension into a Petri dish.

The same procedure as that in route 1 was used to prepare PVOH/M600/clay nanocomposites.

4.4. Quaternized M600/Clay nanocomposites

The method for the quaternization of polytheramines with the tradename Jeffamine M600 was adapted from similar procedures obtained from the literature [4.2-4.4]. M600 (< 21 g), sodium bicarbonate (< 8.8 g), and methyl iodide (< 14.8 g) was dissolved and heated in 200 ml methanol under reflux for 75 hours. Whilst heating under reflux additional methyl iodide (< 14.8 g) was added to the reaction mixture after 24 and 48 hours. The reaction mixture was

cooled and filtered to remove solid (inorganic salts), then evaporated to dryness under reduced pressure using the rotatory evaporator. The residue was dissolved in deionised water (< 100 ml) and using a separating funnel any impurities were extracted using a diethyl ether wash (< 200 ml) three times. Finally, the aqueous solution was evaporated to dryness under reduced pressure at 40 °C using the rotatory evaporator. The product (QM600) also contained NaI as a by-product, it was not possible to precipitate this using hot chloroform and so during the cation exchange reaction with sodium MMT to produce QM600-MMT both were present.

The cation exchange process for QM600-clay was achieved using the following procedure: 1 g of clay was mixed with 14 ml distilled water and stirred for 2 hours at room temperature using a magnetic stirrer. The desired amount of QM600 was mixed with 6 ml distilled water also at room temperature. Then QM600/clay suspension was mixed and stirred for a further 4 hours at room temperature. Any NaI present after the cation exchange process (either resulting from the by-product of the QM600 synthesis or the cation exchange process) was washed with deionised water 6 times. After each wash the QM600/clay suspension was centrifuged at 15,000 rpm for 1.5 hours (see section 3.2.4). From the final wash 2 ml suspension was cast on to a glass slide and 18 ml suspension was placed into a Petri dish.

4.5. PVOH/QM600/Clay nanocomposites

For the preparation of PVOH/QM600/clay nanocomposite systems, the washed QM600/clay suspension (see section 4.4) was added to the desired amount of prepared PVOH solution. The mixing and stirring of the components was performed at 90 °C for 4 hours. The total volume of water for each sample

was 20 ml. A 2 ml aliquot of the PVOH/QM600/clay suspension was cast onto a glass slide and the remaining 18 ml suspension into a Petri dish

4.6. References

- [4.1]. Ngui, M. O. and Mallapragada, S. K. (1998). Understanding isothermal semicrystalline polymer drying: Mathematical models and experimental characterization. *Journal of polymer science part B: polymer physics*, **36** (15), 2771-2780.
- [4.2]. Cope, A. C., Ciganek, E., Fleckenstein, L.J. and Meisinger, M.A.P. (1960). Tertiary amines from methiodides and lithium aluminum hydride. *Journal of the American chemical society*, **82** (17), 4651-4655.
- [4.3]. Mitsunobu, O., Wada, M., Sano, T. (1972). Stereospecific and stereoselective reactions. I. preparation of amines from alcohols. *Journal of the american chemical society*, **94**(2), 679-680.
- [4.4]. Mongondry, P., Plaisance, C.B. Jean, M. and Tassin, J.F. (2003). Mild synthesis of amino-poly(ethylene glycol)s. Application to steric stabilization of clays. *Macromolecular rapid communication*, **24** (11), 681-685.

**Competitive and synergistic adsorption
of PVOH and PEG600 on Clay**

5.1. Clay dispersion

This section discusses the extent of clay dispersion, as determined by XRD, when present in binary systems, i.e. clay in PVOH or plasticizer (PEG600) or when present in tertiary systems, i.e. clay in PVOH and PEG600. The sequence of adding PVOH or PEG600 to clay is also discussed. The results from variable temperature x-ray diffraction (VT-XRD) of samples established at different humidities are presented. Finally, the amounts of PEG600 and/or PVOH adsorbed on clay in the binary and tertiary systems are presented.

5.1.1. PVOH and clay binary system

A wide range of PVOH and clay mixtures with different concentrations ranging from 0 to 100 wt% clay have been investigated by XRD and their traces are presented in Figures 5.1, 5.2 and 5.3. The peak at $7.42^\circ 2\theta$ (11.9 \AA) in the XRD trace of the clay film (Figure 5.1 a) represents the initial d_{001} -spacing. The addition of PVOH to clay results in producing either intercalated or exfoliated structures and is dependant on the amount added. The XRD traces showing two peaks indicate that clay layers are intercalated with two different polymer amounts (e.g. trace d and e in Figure 5.1) or a combination of layers with and without PVOH present (e.g. trace b and c in Figure 5.1).

As the concentration of PVOH increases from 2 to 15 wt%, step changes occur as the gallery expands from a depleted single layer (trace b: $\sim 6.51^\circ 2\theta$ [$d_{001} \sim 13.6 \text{ \AA}$]) through to a single layer (trace c: $\sim 6.37^\circ 2\theta$ [$d_{001} \sim 13.9 \text{ \AA}$]) and then a combined single and bilayer system (traces d-e: $\sim 4.87^\circ 2\theta$ [$d_{001} \sim 18.1 \text{ \AA}$]). A single layer refers to clay containing an even coverage of PVOH molecules within the clay gallery that is one layer thick, whereas a bilayer refers to the same but with two layers thick. These assignments are based the

dimensions of the polymer chains, their anticipated surface coverage and the gallery height (for a schematic representation, see Figure 2.4, which shows structure of intercalated surfactants). At 2-15 wt% PVOH loadings, the amount of polymer present is not enough to exfoliate any layers of the clay. When PVOH loading increases from 9 to 15 wt% (Figure 5.1 d to f), the peak with the higher d_{001} -spacing, attributed to the bilayer, is found to increase in intensity, while the peak attributed to the single layer decreases in intensity. The position of the peak indicating the presence of a single polymer layer shifts to lower angle slightly with increasing PVOH loading (6.51 to 6.21 $^{\circ}2\theta$), whilst the peak position of higher spacing (4.87 $^{\circ}2\theta$) does not vary with PVOH loadings up to 15 wt%.

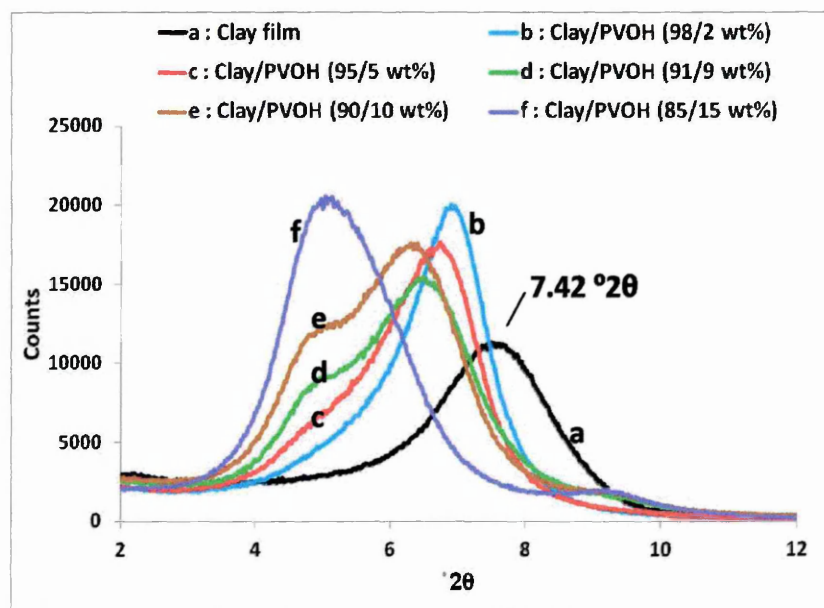


Figure 5.1. XRD traces from PVOH/Clay composites at low PVOH content.

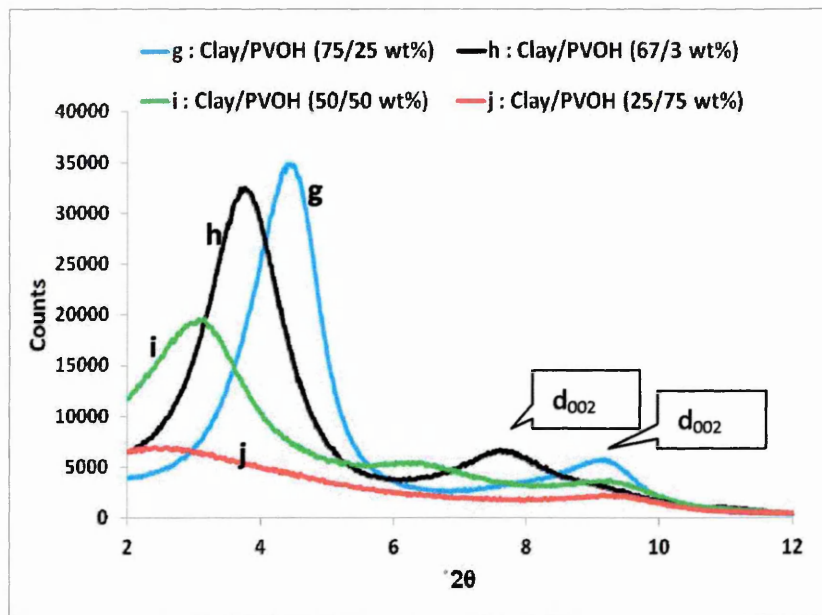


Figure 5.2. XRD traces from PVOH/Clay composites at intermediate PVOH content.

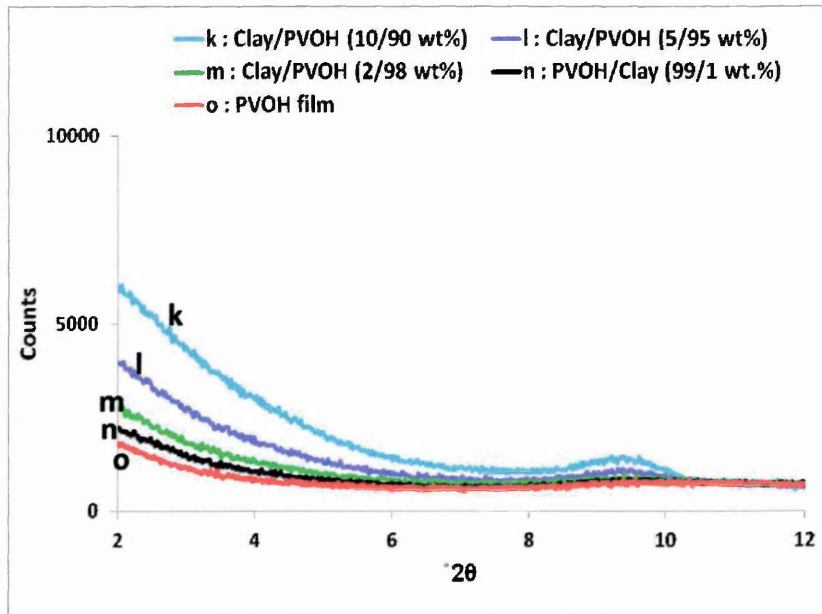


Figure 5.3. XRD traces from PVOH/Clay nanocomposites at high PVOH content.

PVOH loadings between 25 to 50 wt% (Figure 5.2, curves g-i) result in multilayered intercalated structures ($>4.36^\circ 2\theta$ [$d_{001} > 20.3 \text{ \AA}$]) with highly ordered clay layers as indicated by the high intensity of the d_{001} -peak. The peaks observed at $9.1^\circ 2\theta$ and $7.6^\circ 2\theta$ for the 25 wt% and 33 wt% PVOH samples, respectively are due to the d_{002} -spacing and also show that the clay

layers are highly ordered (the d_{003} and d_{004} -spacings also exist at higher angles, but are not presented). The increase in the d-spacing observed with increasing PVOH loadings between 25 and 50 wt% is due to more and more polymer being available and being located in the clay gallery and making the layers more difficult to re-aggregate during the drying of the films. When the PVOH loading is 75 wt% (Figure 5.2 j) it is likely that a mixture of both intercalated and very well dispersed clay structures, if not exfoliated, are present. It is observed that the intensity of the d_{001} -peak increases as the concentration of PVOH increases to 25 wt% then decreases upon further PVOH loading. It is also observed that the full width half maximum (FWHM) value decreases when a fully loaded single layer or bilayer is created.

Further increases in PVOH loading from 90 wt% and above (see Figure 5.3 k-o) resulted in the formation of either intercalated structures with d_{001} -spacings larger than 44 Å, which are believed to be unlikely, or very well dispersed systems (if not exfoliated) as indicated by the sloping baseline towards lower angles. The peak observed at $9.3^\circ 2\theta$ is possibly due to the d_{002} -spacing of a portion of intercalated clay with a d_{001} -spacing around $4.5^\circ 2\theta$, which is not clearly observable due to the sloping baseline. XRD on its own gives insufficient information to fully resolve the structure of the nanocomposites, but in this instance it seems likely that both structures are present, but it is predominantly exfoliated.

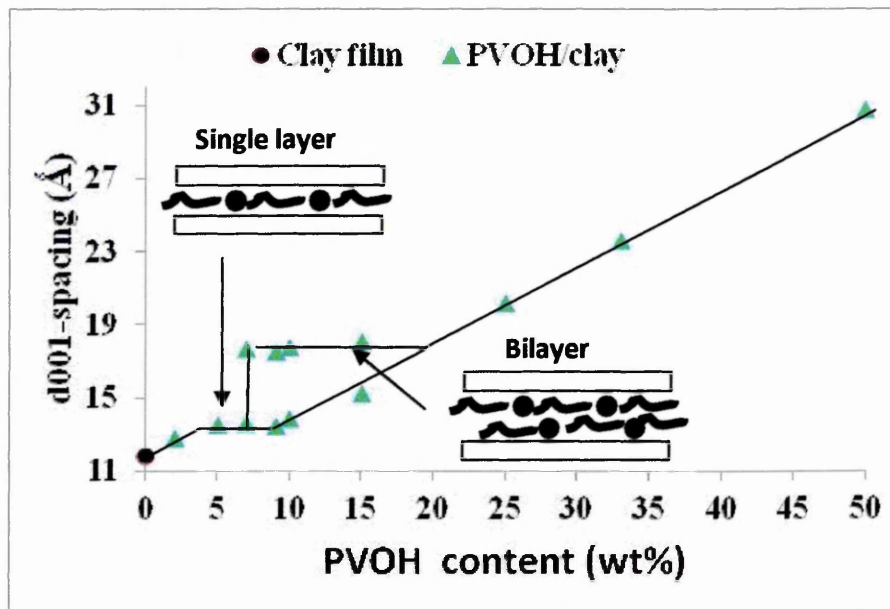


Figure 5.4. Summary of d-spacings from XRD traces of PVOH/Clay nanocomposites

A summary of the d_{001} -spacings of clay under the influence of PVOH loading is given in Figure 5.4 and shows that below 50 wt% PVOH, only intercalated structures are observed. The d-spacings of clay film and PVOH/clay systems shows that as the concentration of PVOH increases, step changes occur as the gallery expands from a depleted single layer through to a single layer and then a combined single and bilayer system. Mixed single layer and bilayer systems are indicated by the presence of two data points at the same PVOH loading. Multi-layers are then observed, which are followed by very well dispersed clay structures when the PVOH concentration is > 75 wt%. Data published for PVOH/clay nanocomposites by Strawhecker [5.1] and Doeppers [5.2] show similar trends in the structure dependence on clay loading, in which the systems become mostly intercalated as silicate loading increases beyond a clay loading ≥ 40 wt%.

5.1.2. Effect of thermal treatment and relative humidity on the d-spacing of in PVOH/clay composites.

The effect of temperature and relative humidity on the d-spacing of clay in PVOH composites has been investigated, since it can be significantly affected by any associated water. XRD traces were collected from samples after heating for 10 minutes at 80 °C and 150 °C and then after cooling and equilibrating for 24 hours at 20 °C and 50% RH, the samples were then equilibrated for 24 hours at 20 °C and 85% relative humidity. Note that any degradation to the clay or PVOH is unlikely to occur at these temperatures. The relative humidities of 50% and 85% were achieved by placing saturated magnesium nitrate and potassium chloride salt solution, respectively in a humidity chamber [5.3].

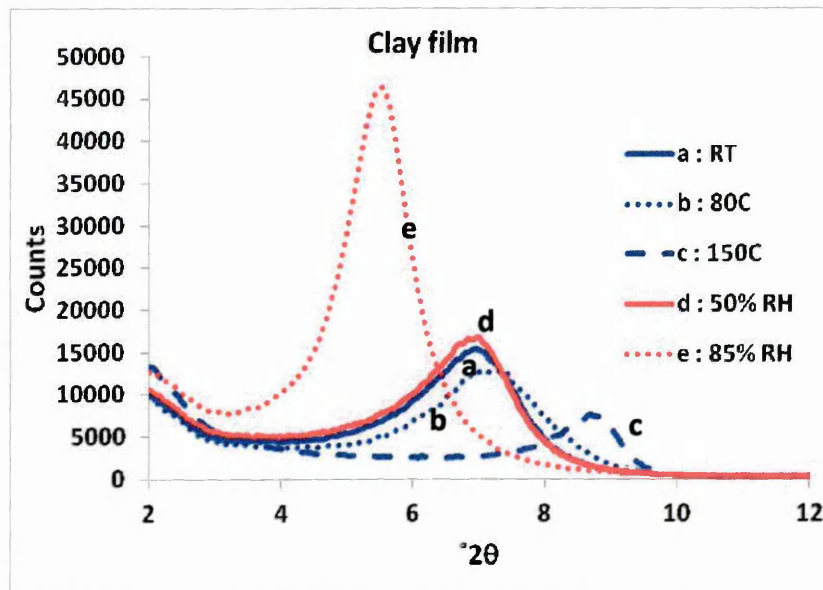


Figure 5.5. The influence of thermal treatment and relative humidity on the diffraction patterns of sodium clay

Figure 5.5 shows XRD traces of clay film collected at variable temperatures and humidities. RT represents the diffraction trace collected at

room temperature prior to any heat treatment i.e. at 20 °C and atmospheric humidity and several days after initially casting the film at 47 °C. After heating the clay film at 80 °C for 10 minutes, a slight shift to higher angle was observed at 7.25 °2θ (12.2 Å), but this was more significant when heated to 150 °C since the clay layers had collapsed from 7 °2θ (12.6 Å) at room temperature to 9.2 °2θ (9.6 Å). At this point very limited or even no water was present in the clay gallery due to adsorbed moisture and interlayer water being expelled from the clay. TGA data also shows (discussed below in section 5.2.1) most if not all physisorbed water had been removed. Investigation of the sample after cooling and equilibrating at 50% RH for 24 hours showed the effect was reversible since a very similar trace to that collected at RT was observed. This is as expected since the average atmospheric relative humidity is ~50%. Furthermore, the clay sample was able to swell to larger d-spacings when exposed to 85% RH as indicated by a shift in the peak to lower angles, 5.8 °2θ (15.0 Å). Increasing the amount of water available to the sample increased the peak intensity and narrowed the peak width indicating a more ordered system.

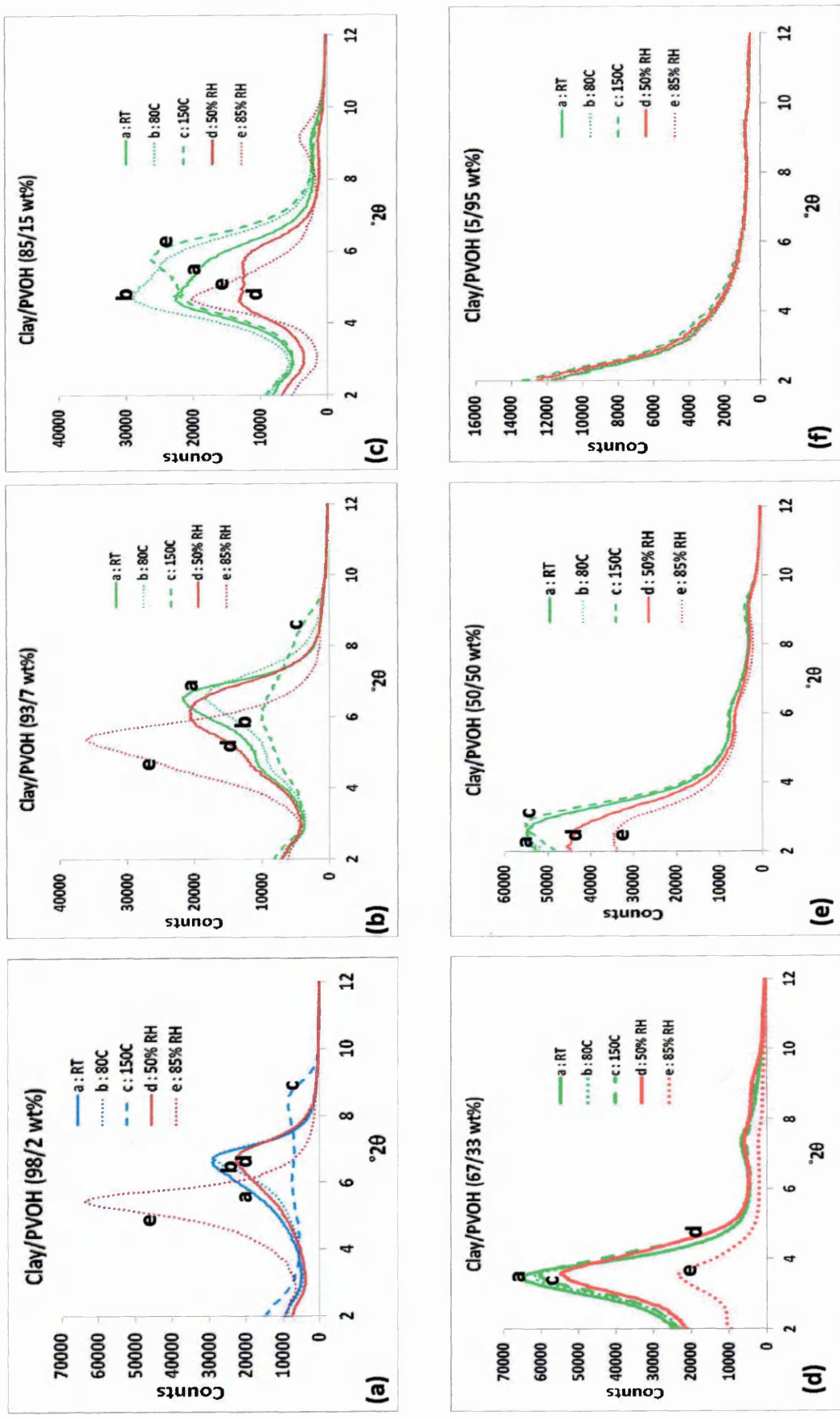


Figure 5.6. The influence of thermal treatment and relative humidity on the diffraction patterns of PVOH/clay nanocomposites

Figure 5.6 shows selected XRD traces collected from PVOH samples containing 5 to 98 wt% clay. Heating the samples to 80 °C did not have a significant effect on the d-spacing for most samples since only a small shift to higher 2θ or small change in relative intensities towards the higher 2θ peak was observed. Major effects were observed in samples with high clay loading, 98, 93, and 85 wt%, which are represented by Figures 5.6 a, b and c, respectively. When the samples with 98 to 93 wt% clay were heated to 150 °C a diffraction peak at 9.2 2θ (9.6 Å) was observed, together with a decrease in intensity of the peak near 6.3 2θ (14 Å). This indicates that there is little or no organic content in the clay gallery in the sample with 98 wt% clay and that both water and PVOH molecules are propping up the gallery. This becomes less apparent in the traces for the sample containing 93 wt% clay since the sample heated at 150 °C displays a small peak at 9.2 2θ and still has residual intensity at 6.3 2θ . For the composites that have a mixture of single and bilayer structures, for example 90 wt% (XRD trace not presented) and 85 wt% clay, heating to 150 °C reduced the intensity of the low angle peak associated with the bilayer structure whilst the intensity of the high angle peak associated with the single layer structure increased. This indicates that with samples containing greater than 85 wt% clay loading, the bilayer structures are not fully loaded with PVOH and that water is present and propping up the gallery. The movement of the peak to the lower 2θ at 85% RH supports the analysis which shows that the single layers are increased to the size of a bilayer by water propping up the gallery space.

Clay loadings of 75 wt% (XRD trace not presented), 67 wt% (Figure 5.6 d) and 50 wt% (Figure 5.6 e) achieved the best thermal and environmental

stability under the conditions investigated indicating that the gallery space is fully loaded with PVOH and little water is present.

For clay loadings of 5 wt% (Figure 5.6 f) and below were the nanocomposites are very well dispersed, the XRD traces do not provide sufficient information to elucidate the effect of thermal and relative humidity of water associated with clay layers. However, the absence of any peaks does show that no intercalated species are created at the various temperatures and humidities.

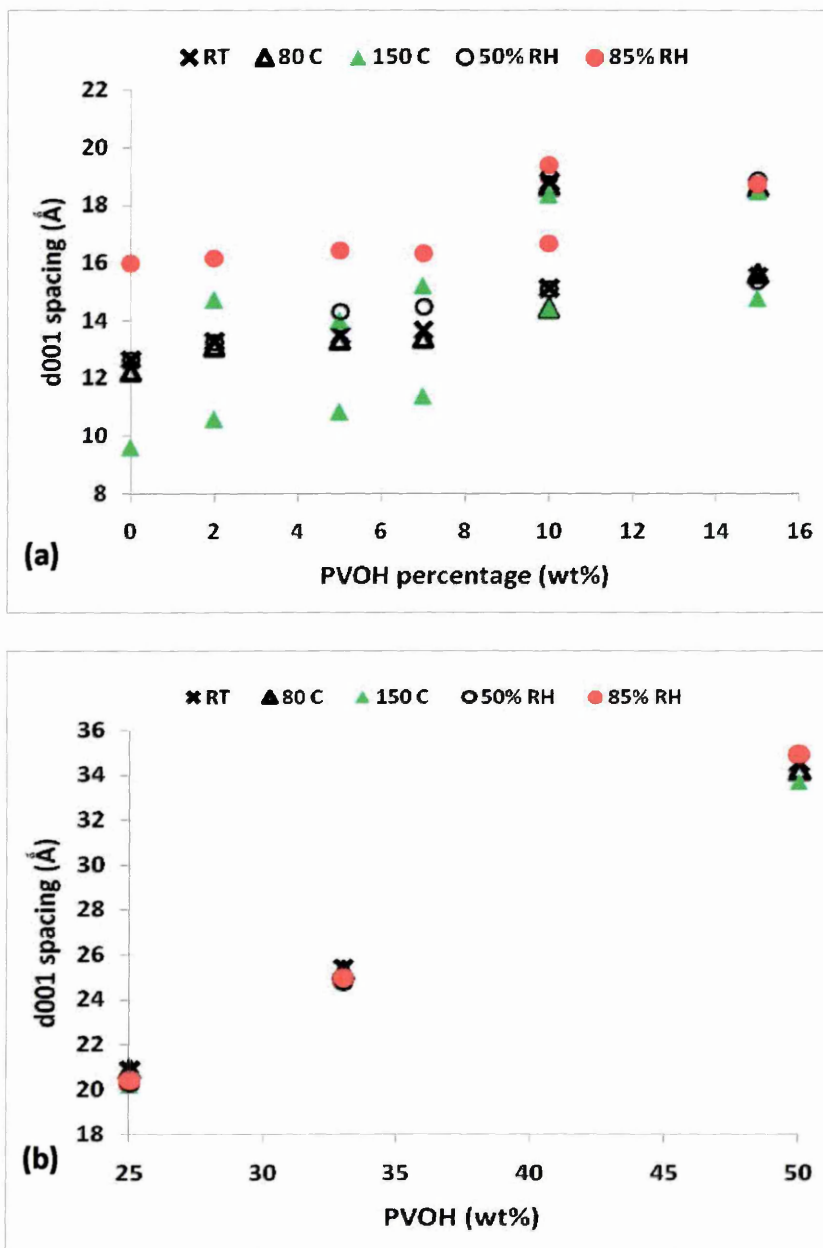


Figure 5.7. Summary of d-spacings from PVOH/clay composites under the influence of thermal treatment and relative humidity.

A summary of the d-spacings observed in the diffraction traces of PVOH/clay composites under the effect of temperature and relative humidities are shown in Figure 5.7. Two data points present at the same PVOH concentration for one experimental condition represent the presence of d_{001} -spacings from both single and bilayer structures. A brief survey of the general features displayed by the clay samples prepared using PVOH clearly show that the d-spacings of these simple systems is influenced by clay loading, the thermal history of the sample and their ability to rehydrate after heating. As the PVOH loading increases, the general extent of change of the d-spacings within the different conditions decreases showing less influence from the water is being experienced. This also suggests that less water is present in the clay gallery as more PVOH is added. At high clay loadings of 98 to 85 wt%, the single and bilayer structures are both present to different degrees depending upon the treatment that the particular sample has undergone, whilst at intermediate clay loadings of 75 to 50 wt% the intercalated structures show thermal and environmental stability. A reorientation of the polymer chains could be induced by the thermal treatment and hence contribute to a lowering of the d-spacing, however, this effect is not considered as significant as the affect of removing water.

5.1.3. PEG600/clay binary system

A wide range of clay loadings (0 to 95 wt%) with PEG600 have been investigated, their XRD traces are presented in Figures 5.8 and 5.9. Intercalated structures are observed for the whole range of clay loadings. Three steps can be used to describe the changes as the concentration of PEG600 increases:

- i) an increase to a depleted single layer at $\sim 6.64^\circ 2\theta$ ($\sim 13.1 \text{ \AA}$),
- ii) a depleted single layer to a fully loaded single layer at $\sim 6.4^\circ 2\theta$ ($\sim 13.8 \text{ \AA}$)
- iii) fully loaded single layer to a bilayer structure at $\sim 4.97^\circ 2\theta$ ($\sim 17.8 \text{ \AA}$).

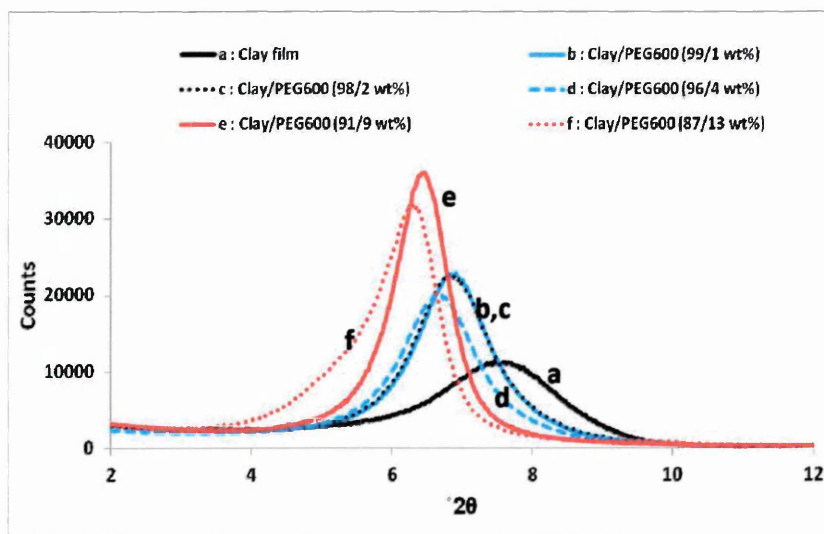


Figure 5.8. XRD traces for PEG600/Clay nanocomposites at low PEG600 content.

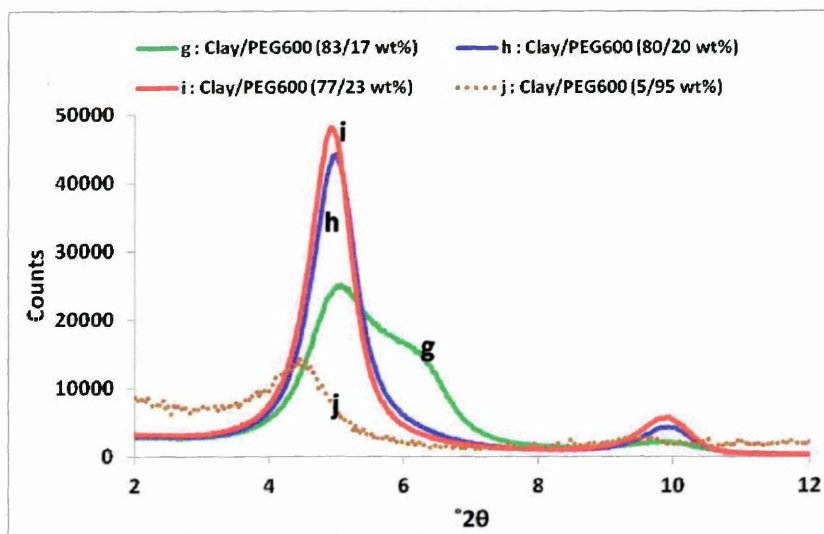


Figure 5.9. XRD traces for PEG600/Clay nanocomposites at low PEG600 content.

Even very small amounts of PEG600 (1 wt%) increase the d-spacing of the clay (Figure 5.8 b). The clays layers do not expand to a fully loaded single layer at 4 wt% PEG600 ($6.64^\circ 2\theta$ [13.3 \AA]) and only do so at 9 wt% PEG600

($6.40^\circ 2\theta$ [13.8 Å]). Further loading of PEG600 (13 wt%) results in a small portion of a bilayer structure and a the dominant single layer phase. A mixture of single and bilayer structures are also clearly observed with a PEG600 loading of 17 wt% (see Figure 5.9 g) since there are two peaks positioned at $6.17^\circ 2\theta$ (14.3 Å) and $5.07^\circ 2\theta$ (17.4 Å), at this stage the peak representing the bilayer structure is more intense than that of the single layer. The bilayer becomes fully loaded when the PEG600 loading reaches 20 wt%, as evidenced by the narrow distribution of d-spacings and the high intensity of the peak (Figure 5.9 h: $4.97^\circ 2\theta$ [17.78 Å]). Further loadings of PEG600 up to 95 wt% results in a slight peak shift to $4.43^\circ 2\theta$ (19.9 Å), this shows that the clay gallery does not continue to expand like clay dispersed in PVOH. The decrease in intensity is due to disorder within the clay layer and or a reduction in the amount of clay being analysed. The lack of expansion beyond a bilayer indicates a strong PEG600-clay interaction.

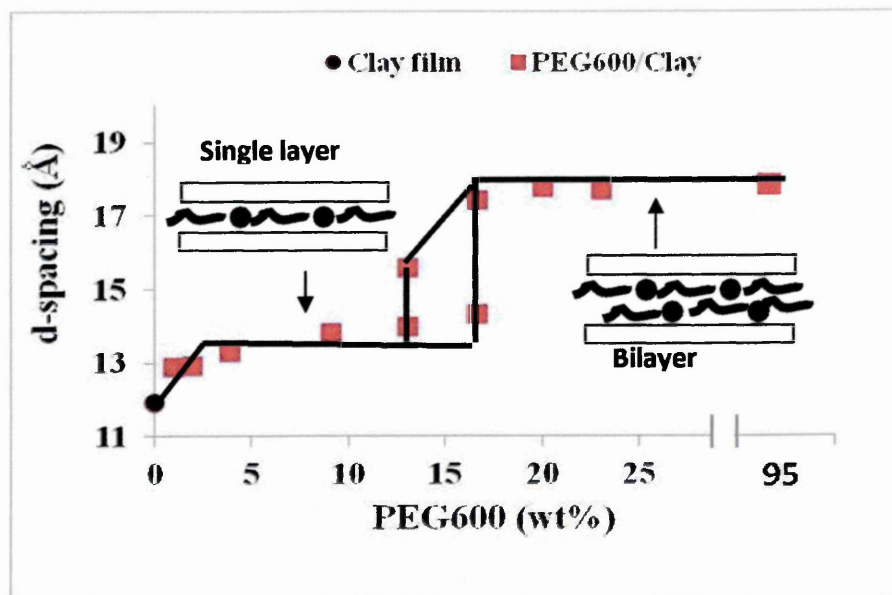


Figure 5.10. Summary of d-spacings observed in the XRD traces of PEG600/Clay composites

The d_{001} -spacings observed in the XRD traces of the PEG600 and clay composites are plotted in Figure 5.10 and shows that PEG600 resides in the gallery and forms only intercalated composites. As the concentration of PEG600 increases, step changes occur as the gallery expands from a depleted single layer to a fully loaded single layer and then a bilayer structure. A maximum d-spacing of $\approx 18.2 \text{ \AA}$ for PEG in clay was also reported by Chen [5.4] who studied PEG's with Mw's 300-20,000.

5.1.4. Effect of thermal treatment and relative humidity on the d-spacings of PEG600/clay composites.

The PEG600/clay composites were exposed to the same thermal and relative humidities as the PVOH/clay composites. The XRD trace collected at 150°C from the clay with 1 wt% PEG600 (Figure 5.11 a) is very similar to that of the base clay (Figure 5.5 a). The clay gallery has collapsed suggesting there is very little, if any, PEG600 present in the gallery. The trace for the clay sample treated with 4 wt% PEG600 and collected at 150°C (Figure 5.11 b), does exhibit a peak at $6.78^\circ 2\theta$ (13 \AA) indicating the present of PEG600 in the gallery. Heating the sample treated with 9 wt% PEG600 to 80°C or 150°C (Figure 5.11 c) does not displace the peak at $6.78^\circ 2\theta$ nor significantly diminish its intensity, which shows that the gallery contains little water and enough PEG600 to create a fully loaded single layer. For the samples with 1 to 9 wt% PEG600 that are exposed to higher humidity (85% RH) the peak position shifts to higher spacing at $5.7^\circ 2\theta$ (15.3 \AA). Here, the gallery has swollen with water to a spacing similar to that of a fully loaded bilayer.

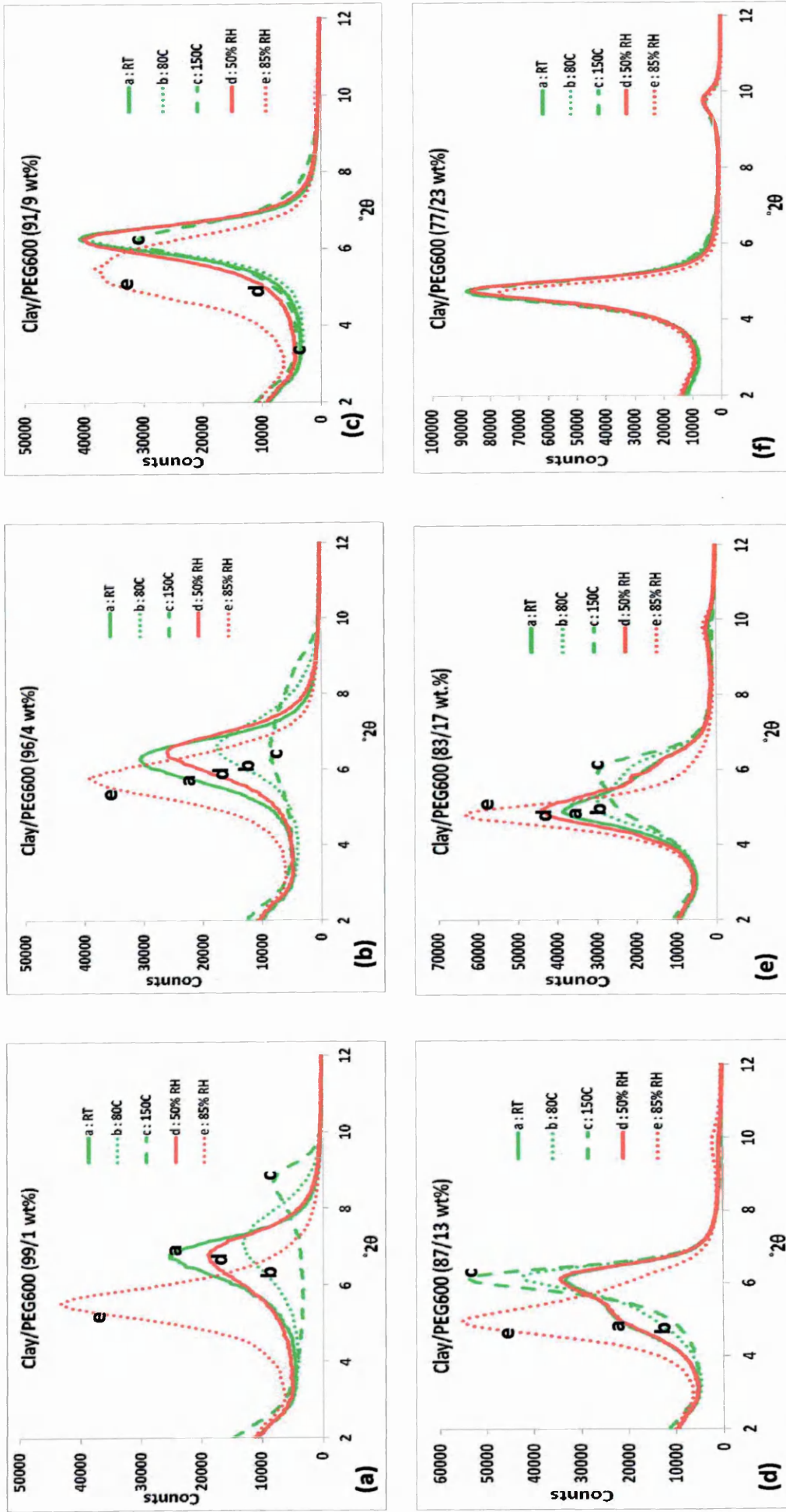


Figure 5.11. Influence of thermal treatment and relative humidity on the diffraction patterns of PEG600/clay composites

Heating samples which have both a single and bilayer structure (13 wt% and 17 wt% PEG600) results in the intensity of the peak relating to the bilayer decreasing suggesting the bilayer structure is not yet fully loaded. Conversely, increasing the amount of water available to the sample reduces the intensity of the single layer and increases the intensity of the bilayer. The bilayered structure created by treating the clay with 17 wt% PEG600 has better thermal stability than that with 13 wt% PEG600.

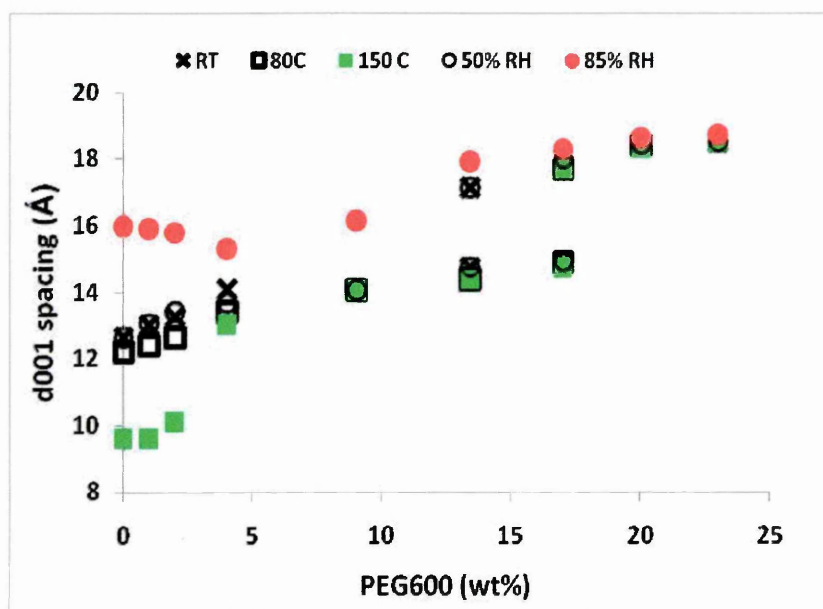


Figure 5.12. Summary of d-spacings of PEG600/clay composites under the influence of thermal treatment and relative humidity.

A summary of the changes in d-spacings observed in the clay/PEG600 samples under the influence of temperature and rehydration are plotted in Figure 5.12. It is clear that below a loading of 4 wt% PEG600 the d-spacing collapses upon heating at 150 °C, that by 13 wt % PEG600 a fully loaded single layer is formed, while by 17 wt % PEG600 a bilayer is formed. Above 17 wt % PEG600 the spacing gradually increases and is probably due to extra PEG600 or water molecules entering the gallery.

5.1.5. PVOH/PEG600/clay tertiary systems and different sequence of mixing

A wide range of different PEG600 (1, 2, 4, 10, 15, 20, 25 and 30 pph) and PVOH (2, 5, 10, 15 and 50 pph) concentrations with clay (100 pph) have been investigated. A selection of XRD traces are presented in Figure 5.13, which show the d-spacings increase with increasing PEG600 and PVOH content. The structure changes from an intercalated structure to a well dispersed clay structure when the PVOH content is increased above 70 wt% and the PEG content is 20 wt%. Pinnavaia [5.5] showed that if the d-spacing of a 2 component (A and B) (d_{AB}) intercalated clay gallery is not equal to the d-spacing of the individual intercalated components of A or B (d_A or d_B) and also not equal to the total d-spacing of A and B ($d_A + d_B$) then both component A and B are located in the same clay gallery. Therefore, in our case both PEG600 and PVOH are present within the clay gallery, as evidenced by increased d-spacings relative to those of the individual component. For example (see Figure 5.13), the d-spacing of PEG600/PVOH/clay 30:10:100 is higher than the individual d-spacing of PEG600/clay 30:100 and PVOH/clay 11:100 and not equal to the total d-spacing of their individual d-spacings.

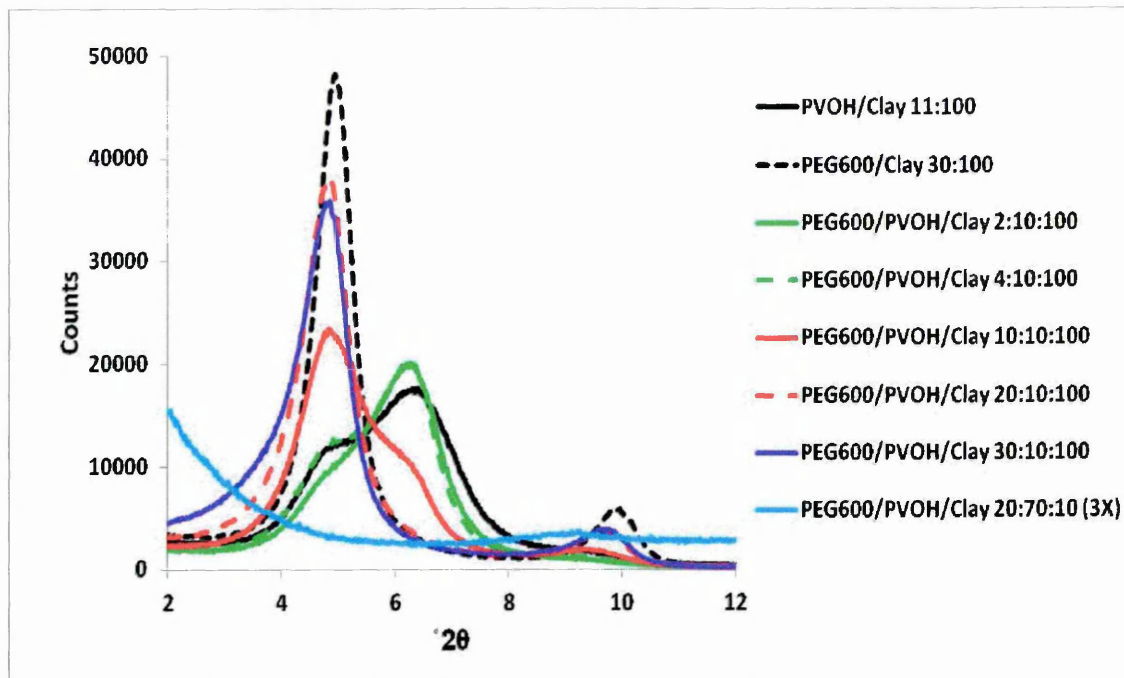


Figure 5.13. XRD patterns from tertiary systems of PEG600/PVOH/clay composites for moderate PVOH content (10 pph)

The d-spacings of PEG600/PVOH/clay mixtures under study are given in Figure 5.14 a-e, which shows the d-spacings change in steps from a depleted single layer to a fully loaded single layer, a combined single and bilayer and then a full bilayer structure. Multi-layers are then observed.

Figure 5.14 a and b show that with loadings of 2 or 5 pph PVOH and PEG600 (15 pph)/clay an increase in the portion of bilayer structure occurs as indicated by an increase in the d-spacing of the higher d-spacing portion. A mixed single and bilayer structure in PEG600 (20 pph)/clay changes into full bilayer structure in the PEG600/PVOH/clay system when only 2 pph PVOH is added. At higher amounts of PEG600, i.e. 25 and 30 pph, additional loading of 2 and 5 pph PVOH does not significantly change the d-spacings. Figure 5.14 c and d show that the d-spacing of PEG600/clay (1-4 pph) changes from depleted single layer to a mixed single and bilayer structure in the PEG600/PVOH/clay system when PVOH is offered at 10 or 15 pph. Loading 10 pph PVOH into

PEG600 (10 pph)/clay results in an increase of d-spacing from a single layer into a mixed single and bilayer structure (Figure 5.14 c), whilst loading 15 pph PVOH results in a full bilayer structure (Figure 5.14 d). Loading 10 or 15 pph PVOH to 15 and 20 pph PEG600/clay results in a full bilayer from a mixed single and bilayer structure. Loading 10 or 15 pph PVOH to 25 and 30 pph PEG600/clay results in a pseudo trilayer. Figure 6.14 e shows that loading 50 pph PVOH to any PEG/clay system results in a multilayer structure. It is interesting to note that even at high PEG600 concentrations (25 or 30 pph), when the gallery is believed to exist as a fully loaded bi-layer and does not expand upon further addition of PEG600 (Figure 5.10), the d-spacing does continue to increase in the presence of 'additional' PVOH (see Figure 5.14 c-e). This shows that the platelet-platelet interactions in the PEG600-clay systems can be overcome by the ingress of PVOH. PEG600 is therefore unable to 'control' the d-spacing by limiting the swelling in the presence of PVOH.

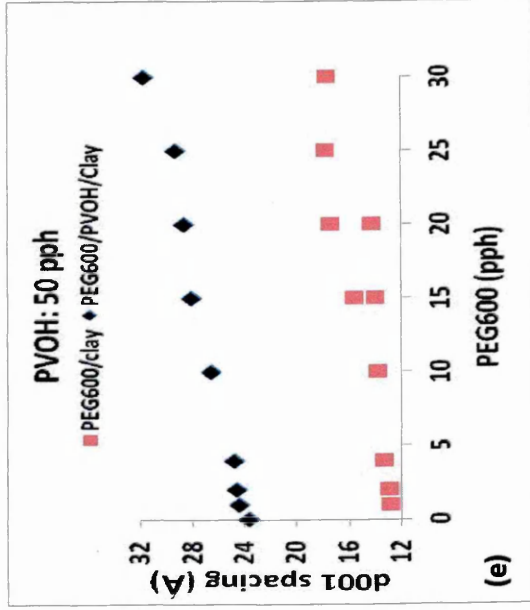
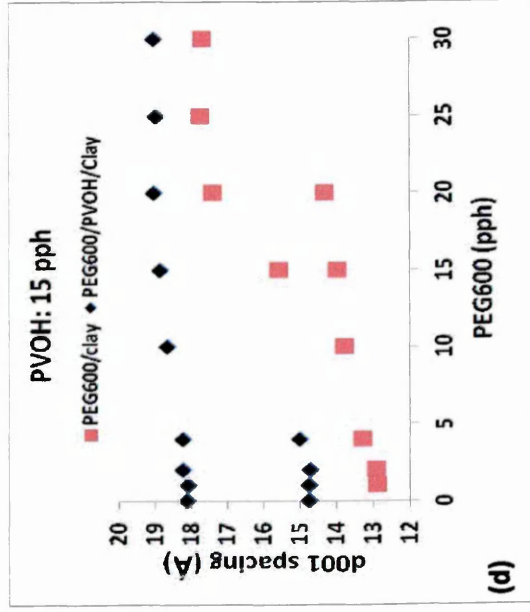
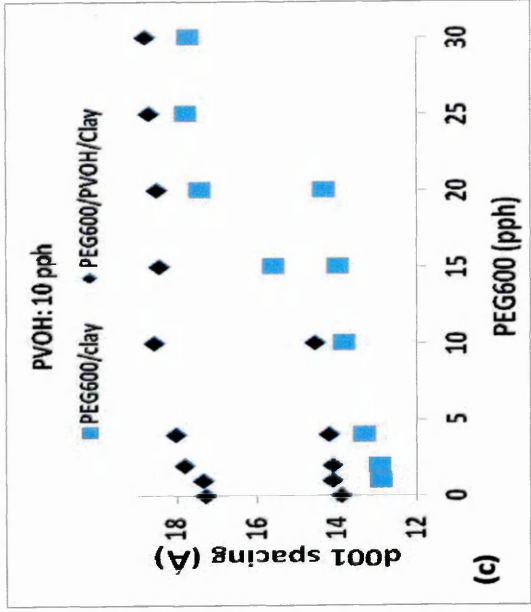
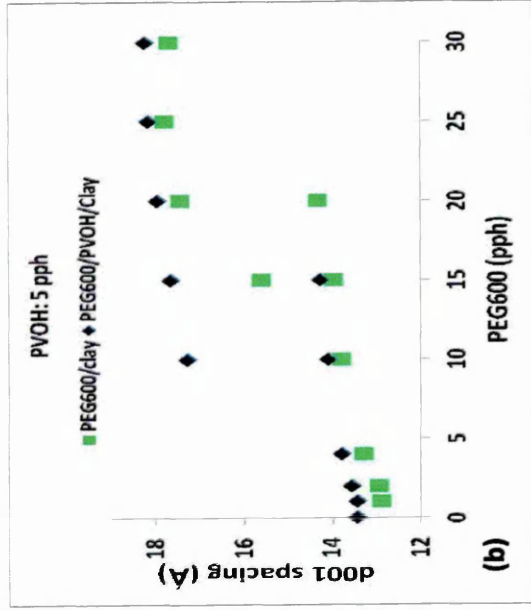
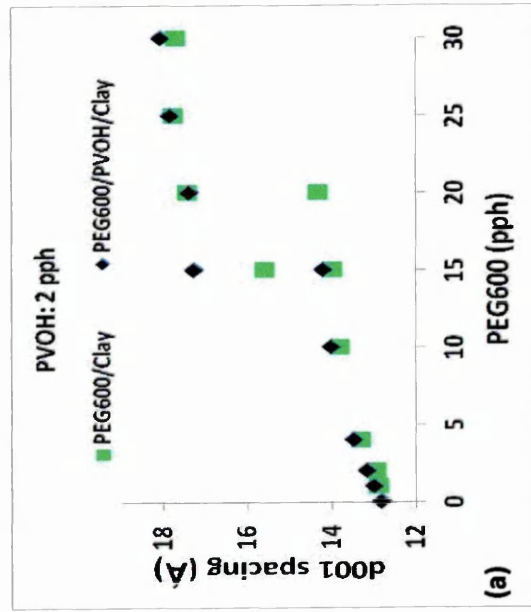


Figure 5.14. The d-spacing of PEG600/PVOH/clay composites when PVOH content of 2 pph (a), 5 pph (b), 10 pph (c), 15 pph (d) and 50 pph (e) along d-spacing of PEG600/clay

For the competitive absorption study, different sequences of mixing PEG600 and PVOH were employed (see experimental section 4.3). In route 1, the PEG600 was mixed with the PVOH before the clay was added. In route 2, the PVOH was mixed with the clay before PEG600 was added. In route 3, the PEG600 was mixed with the clay, before the PVOH was added. The results showed that regardless of mixing sequence both PEG600 and PVOH were present in the gallery together even at low organic loading (Figure 5.15 a) as shown by increases in the d-spacing when compared to the relative amounts of PEG600 and PVOH added. For example, in the PEG600/PVOH/clay 10:50:100 pph sample the d-spacing for routes 1 and 2 was 27 Å (3.27 °2θ) and for route 3 it was 28.9 Å (3.05 °2θ) as shown in Figure 5.15 f, this is not equal to the d-spacing of PEG600/clay 10:100 (6.43 °2θ [13.7 Å]) nor PVOH/clay 50:10 pph (3.75 °2θ [24 Å]) and also not equal to the sum of d-spacings due to PEG600/clay and PVOH/clay, i.e. 13.7 Å + 24 Å = 37.7 Å. When the content of PEG600 is higher than that of PVOH (see Figure 5.15 a and d) the peak positions are closer to those of the PEG600/Clay binary system, whereas when the content of PVOH is higher than that of PEG600 (see Figure 5.15 c, e & f) the peak positions are closer to those of the PVOH/Clay binary system.

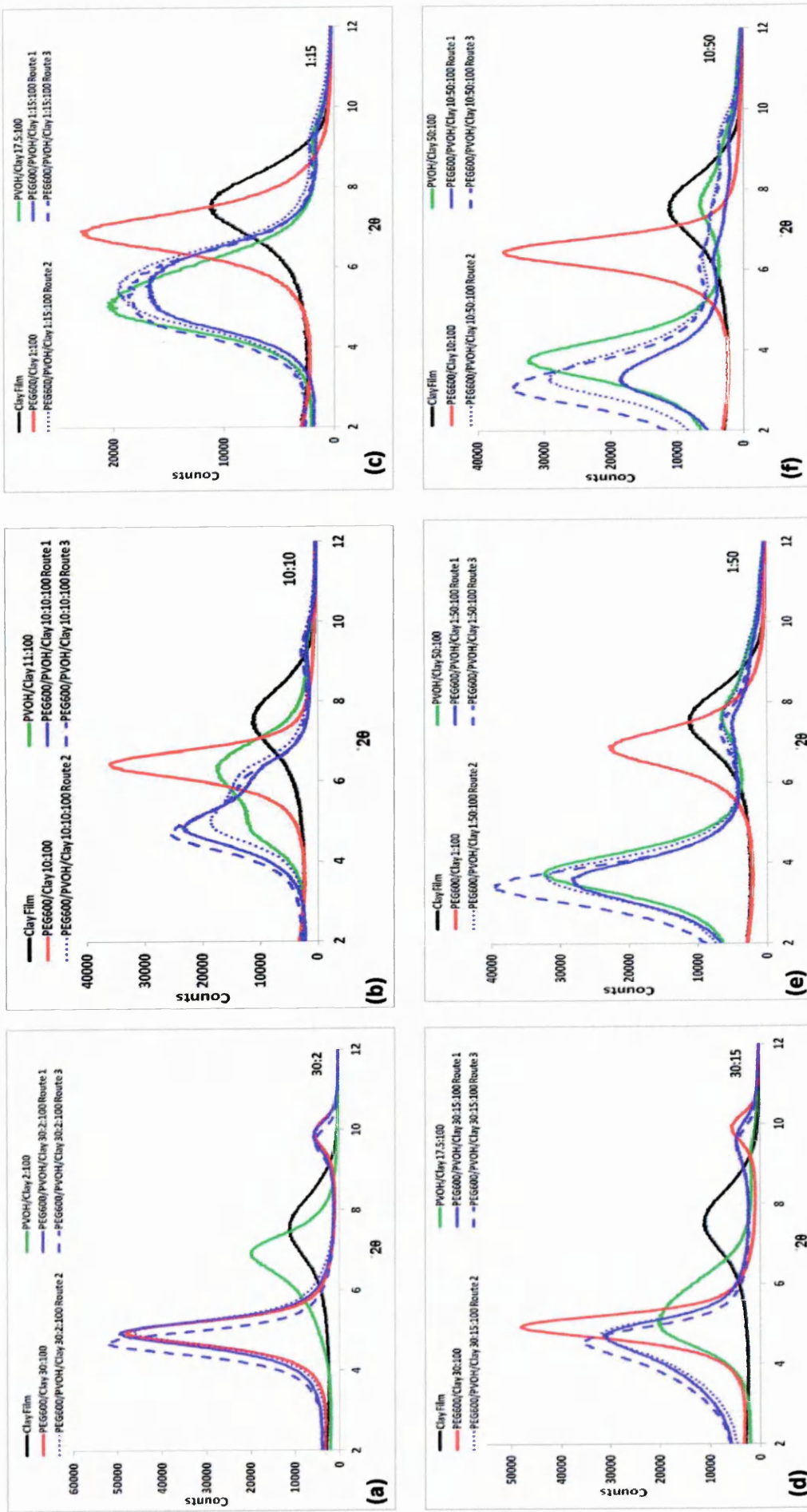


Figure 5.15. XRD patterns from PEG600/PVOH/clay composites

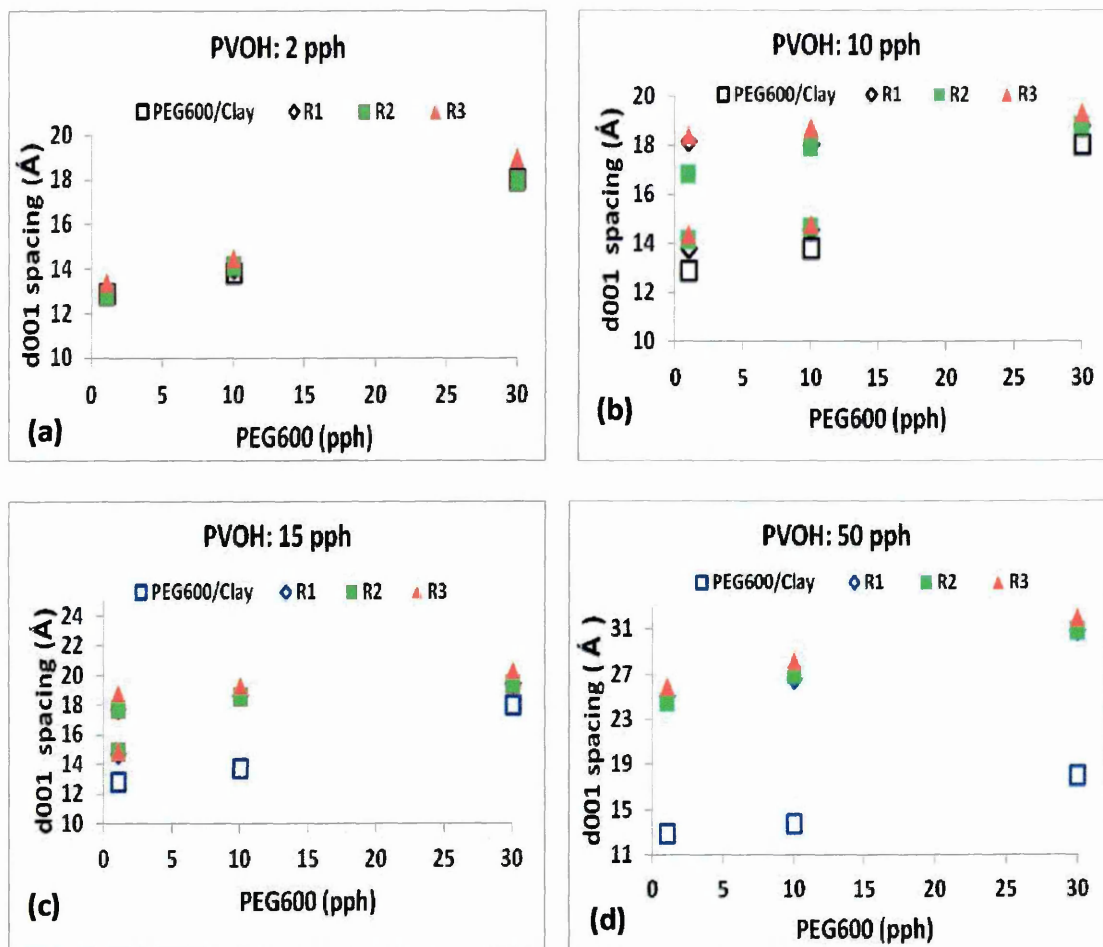


Figure 5.16. The d-spacings of PEG600/PVOH/clay composites prepared in route 1 (R1), route 2 (R2) and route 3 (R3) when PVOH content is (a) 2 pph, (b) 10 pph, (c) 15 pph and (d) 50 pph along with the d-spacings of PEG600/clay

A comparison of the XRD results collected from the from the different sequences of addition (Figures 5.15 and 5.16) showed that samples prepared using route 3 (PEG600 to clay then PVOH) consistently exhibited slightly higher d₀₀₁-spacings, in addition their peak intensities were higher when compared to the corresponding samples prepared by either route 1 or 2. The current hypothesis for this behaviour is based on the strong PEG600–clay interactions, their immobility when adsorbed to the clay surface and the subsequent irregular packing of the bulkier PVOH molecules leading to an increased number of molecular chains overlapping and as a result an increased d₀₀₁-spacing. Conversely, when PVOH is allowed to adsorb on the clay surface first, the

smaller PEG600 molecules are possibly able to neatly fill any spaces thus resulting in a better packing density and hence lower d_{001} -spacings.

To summarise, both PEG600 and PVOH reside in the gallery as evidenced by the increase in d-spacings when compared to the respective binary systems. In general, XRD traces of tertiary systems prepared by route 3 show clay galleries that are more ordered and have slightly larger d-spacings.

5.1.6. Effect of thermal treatment and relative humidity on the clay dispersion in PVOH/PEG600 clay nanocomposites.

The tertiary systems (PEG600/PVOH/clay) prepared via route 1 were also exposed to the same thermal and relative humidity treatments as for the binary systems. For low loading of PEG600 (1 pph) and PVOH (2 pph) (see Figure 5.17 a), heating the sample at 80 °C did not significantly change the d-spacing peak position. When heating at 150 °C, the peak intensity at $6.7^\circ 2\theta$ (13.5 Å) reduced whilst the intensity of the peak at $\sim 8.7^\circ 2\theta$ (10 Å) increased, suggesting only a fraction of the clay contained organic material in the gallery. The portion of bilayer increased, as shown by an increase in intensity at low angle ($5.5^\circ 2\theta$ [16.1 Å]), when exposed to 85% relative humidity whilst the PVOH loading remained at 2 pph and PEG600 loading increased to 10 pph (Figure 5.17 b) or 30 pph (Figure 5.17 c).

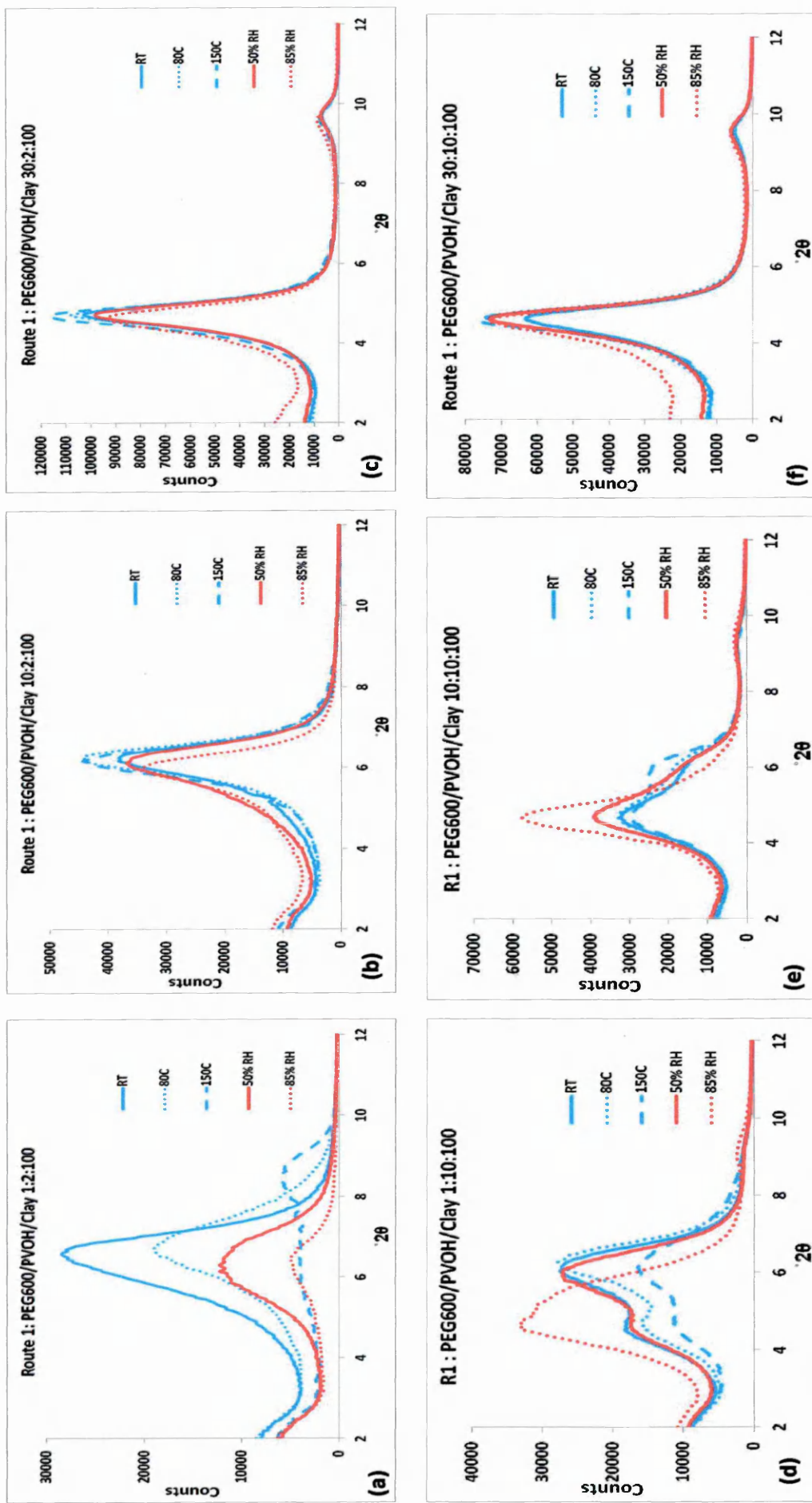


Figure 5.17 Influence of thermal treatment and relative humidity on the d-spacings of PEG600/PVOH/clay composites prepared via route 1, a-c) contain low PVOH levels (2 pph), d-f) contain medium PVOH levels (10 pph) (continued on next page)

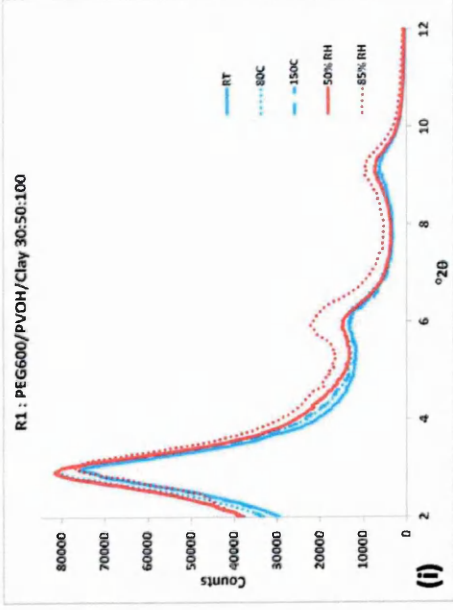
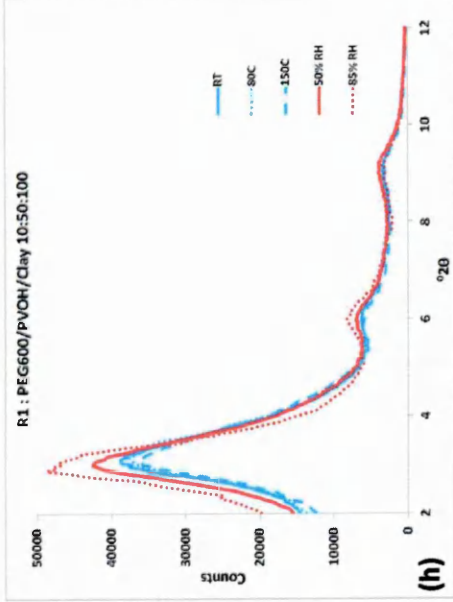
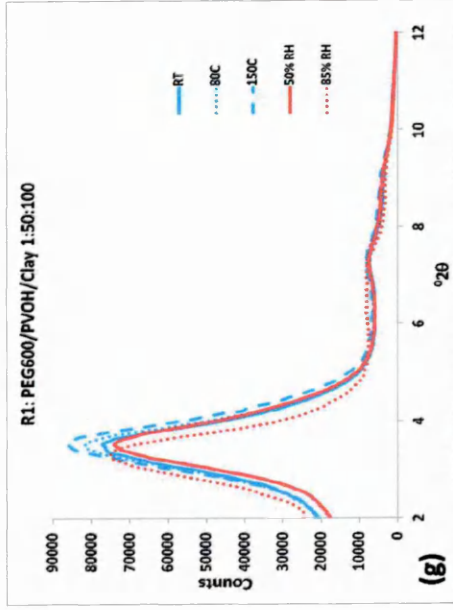


Figure 5.17 Influence of thermal treatment and relative humidity on the d-spacings of PEG600/PVOH/clay composites prepared via route 1, g-i) contain relatively high PVOH levels (50 pph) (continued from previous page).

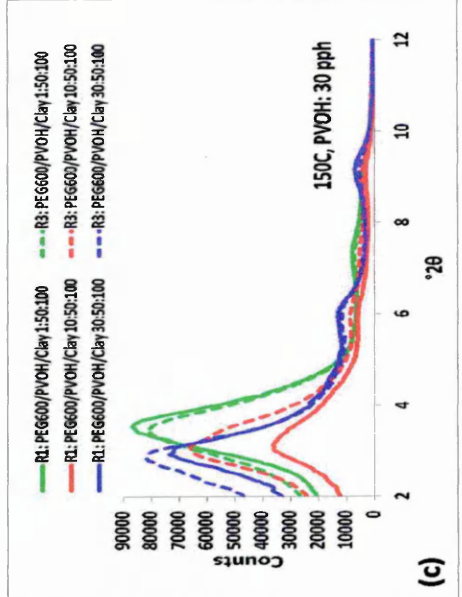
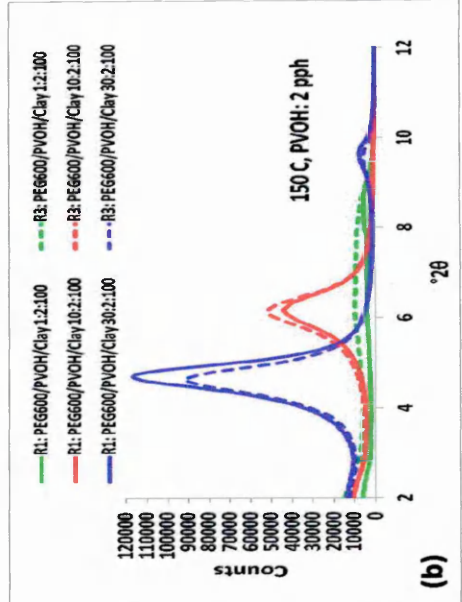
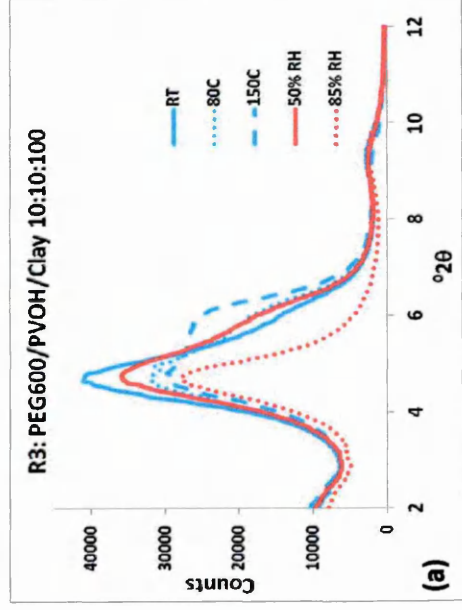


Figure 5.18. a) selected XRD patterns collected from samples prepared via route 3 and at various temperatures and humidities. Selected XRD traces of composites heated at 150 °C prepared via b) route 1 and c) route 3.

Heating the tertiary system containing PEG600/PVOH/clay (1:10:100 pph) (Figure 5.17 d) to 150 °C did not change the peak positions but slightly reduced the portion of the low angle peak ($4.66\text{ }^{\circ}2\theta$ [19\AA]). Assuming the change is not due to thermal rearrangement of the organic material present, this suggests that some water molecules are still present in the bilayer part of the gallery. At 85% RH, the portion contributing to the higher d-spacing ($4.66\text{ }^{\circ}2\theta$ [19\AA]) increases and dominates the system, suggesting either the single layer portion swells with water to produce the bilayer structure or the bilayer structures are not fully loaded with PEG600 and PVOH. At high organic loadings (i.e. PVOH at 50 pph, Figs. 5.17 g-i) good stability to thermal and humidity treatment is observed, regardless of the amount of PEG600 added (1, 10 or 30 pph). Stability to thermal and humidity treatment is best achieved when the PEG600/PVOH/clay ratio reaches 30/10/100 pph.

The influence of thermal treatment and relative humidity on the d-spacings of PEG600/PVOH/clay composites prepared via route 3 follow the same trends as those prepared via route 1, a selection of XRD patterns collected from samples prepared via route 3 are given in Figure 5.18 a. Typical XRD traces of composites heated at 150 °C prepared via route 1 and route 3 are given in Figure 5.18 b and c. They show that PEG600/PVOH/clay composites prepared via route 3 still (as previously shown in section 5.15) have higher d-spacings than those samples prepared via route 1 when heated at 150 °C suggesting that samples prepared using route 3 (PEG600 1st) are not higher simply due to a higher amount of water being present.

5.2. THERMAL STABILITY

The thermal stability of the binary and tertiary nanocomposites were investigated using TGA.

5.2.1. Effect of clay concentration on the thermal stability of PVOH/clay composites

Selected thermograms and their negative derivatives collected from PVOH and PVOH/clay composites are presented in Figures 5.19 a and b, respectively. In general, major weight losses are observed in the range 200 – 500 °C for both PVOH and PVOH/clay composites, which mostly relates to structural decomposition of the polymer (some water loss and low temperature dehydroxylation of the clay may also occur). Above 600 °C, relatively little weight is lost, but dehydroxylation of the clay does occur in this region [5.6].

A change in the rate at which weight is lost is represented as peaks in the negative derivative curve as shown Figure 5.19 b. Three temperature regions are noted in the derivative thermograms (DTGs) of the PVOH and PVOH/clay composites. The first weight loss region between 35 and 150 °C corresponds to the removal of water. The second weight loss region occurs between 200 and 385 °C, with the maxima around 284 °C for PVOH alone. The onset of thermal degradation for the PVOH shifted to higher temperatures with the incorporation of clay, which is the general trend for most polymers [5.7]. The increase in thermal stability is partly due to the restriction in mobility of polymer chains and suppression in the degradation reaction of the chains, decomposition therefore occurs at higher temperatures [5.8]. The clay also acts as a heat shield and slows down heat transfer into the polymer bulk. Although, no oxygen was present during the TGA experiment clay can restrict the ingress of oxygen into the polymer and therefore slow down the breakdown of polymer

due to oxidation. Clay can also restrict any gases produced during degradation from leaving the polymer, which slows down the degradation process. The weight loss in the second region (200 to 385 °C) is about 75 wt% of PVOH alone (Figure 5.20 b), and corresponds partly to the side chain removal of OH from PVOH [5.9] (which theoretically contributes to 38 wt% of PVOH) and partly from degradation products from the main chain [5.10], here the weight loss increases with increasing PVOH content. The third weight loss region between 400 °C and 550 °C, with the maxima around 485 °C for PVOH film, corresponds to the decomposition of the PVOH main chain to yield carbon and hydrocarbons [5.11]. Carrado [5.12] reported PVOH (Mw 50,000) decomposition maxima temperatures at 270 °C & 440 °C, while Doeppers [5.2] reported that the maxima of PVOH (Mw 30,000) were at 275 °C & 450 °C.

The amount of water removed from the clay and clay/PVOH composites (1st region) is plotted in Figure 5.20 a. The amount of physisorbed water in clay is about 4 wt%, which is 1.3% lower than that reported by Chen [5.6]. The amount of physisorbed water decreases as the amount of PVOH is increased from 2-10 wt% and then increases when the amount of PVOH is increased above 10 wt%. It is likely that at low PVOH loadings (<10 wt%) the water associated with sodium cations in the gallery is gradually removed and replaced by PVOH. When a fully loaded single layer is present (10 wt% PVOH) the least amount of water is adsorbed. With higher PVOH loadings (10-20 wt%), when a bilayer is present, the amount of water begins to increase, but does not return to that of the original clay. With even higher PVOH loadings (35-98 wt%), when multilayer structures are present, the PVOH appears to become more like that of the bulk PVOH since the amounts of associated water are similar.

Figure 5.20 b shows that the weight loss in the second region (200 – 385 °C) increases as PVOH content increases and appears to occur in two steps, i.e. step A from 0 to 75 wt% PVOH where the structures are intercalated and step B from 75 wt% and above where the structures are very well dispersed. The relatively higher amounts of weight loss in step B to those in the step A reflect the action of clay acting as a barrier for PVOH degradation. Selected m/z chromatograms from TGMS data of PVOH and PVOH/clay (50 wt%) in the range 240 to 400 °C are shown in Figure 5.21. Holland [5.10] showed that several degradation products were evolved within this temperature range, for example, m/z = 41 ($C_3H_5^+$), m/z = 43 ($C_3H_7^+$), m/z = 69 ($C_4H_6O^+$, e.g. 2-butenal) and m/z = 77 ($C_6H_5^+$, phenyl). As anticipated the intensity of the m/z ions are lower in the PVOH/clay composite than the pure PVOH since there is less PVOH present. The reverse is noted for the m/z ion = 18, which represents the detection of water and suggests a higher amount is lost from the PVOH/clay (50/50 wt%) sample than the pure PVOH. Higher amounts of water could result from more water molecules being strongly associated with the PVOH (in the gallery or bulk), water strongly associated with the exchangeable cations or water from the dehydroxylation of the clay which is promoted due to the degradation of PVOH. Note that the intensity of the m/z chromatograms do not necessarily equate to the amount of species present since varying levels of responses can be observed from different m/z ions.

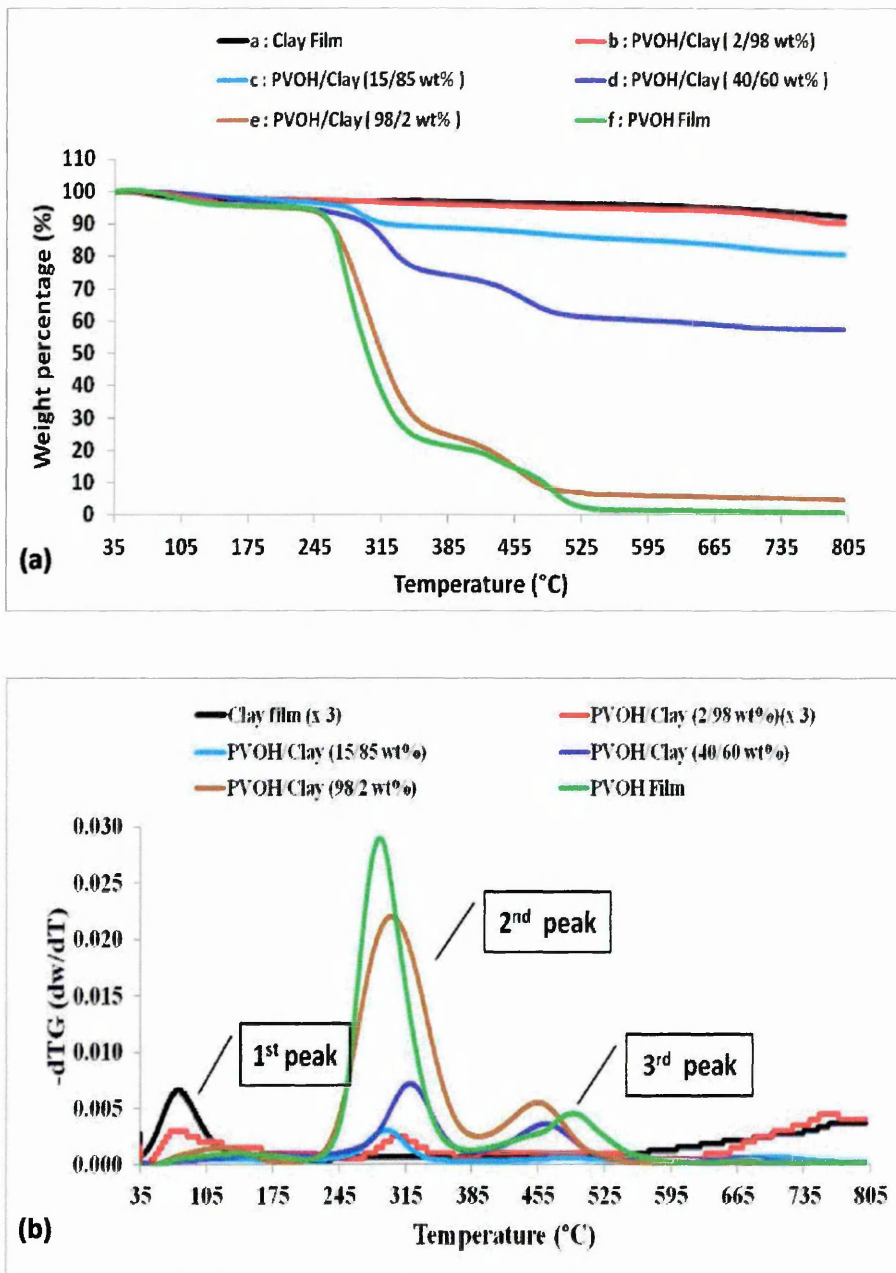


Figure 5.19. Thermograms (a) and their negative derivatives (b) of PVOH/clay composites and PVOH film.

The weight losses in the 3rd region (400 to 500 °C) are shown in Figure 5.20 c. Three distinct areas are observed, which can be related to single and bilayer structures (area A), multilayer structures (area B) and well dispersed structures (area C). It shows that a relatively higher amount of weight is lost in the multilayer structures than in the other types of structures. It shows that a smaller amount of PVOH was degraded in the single and bilayer structures than

that of the multilayer structures but larger than that in the exfoliation structures. The reason for a larger or smaller amount could be that in a particular type of structure more is lost in region 2 rather than region 3 and vice versa. The maximum rate of degradation of PVOH within the 3rd region appears to occur at lower temperatures as clay content increases as shown in Figure 5.22 b suggesting that the clay helps this degradation region to occur at lower temperatures.

The total weight loss of PVOH within the 2nd and 3rd regions is given in Figure 5.20 d and shows that it increases linearly with increasing PVOH content.

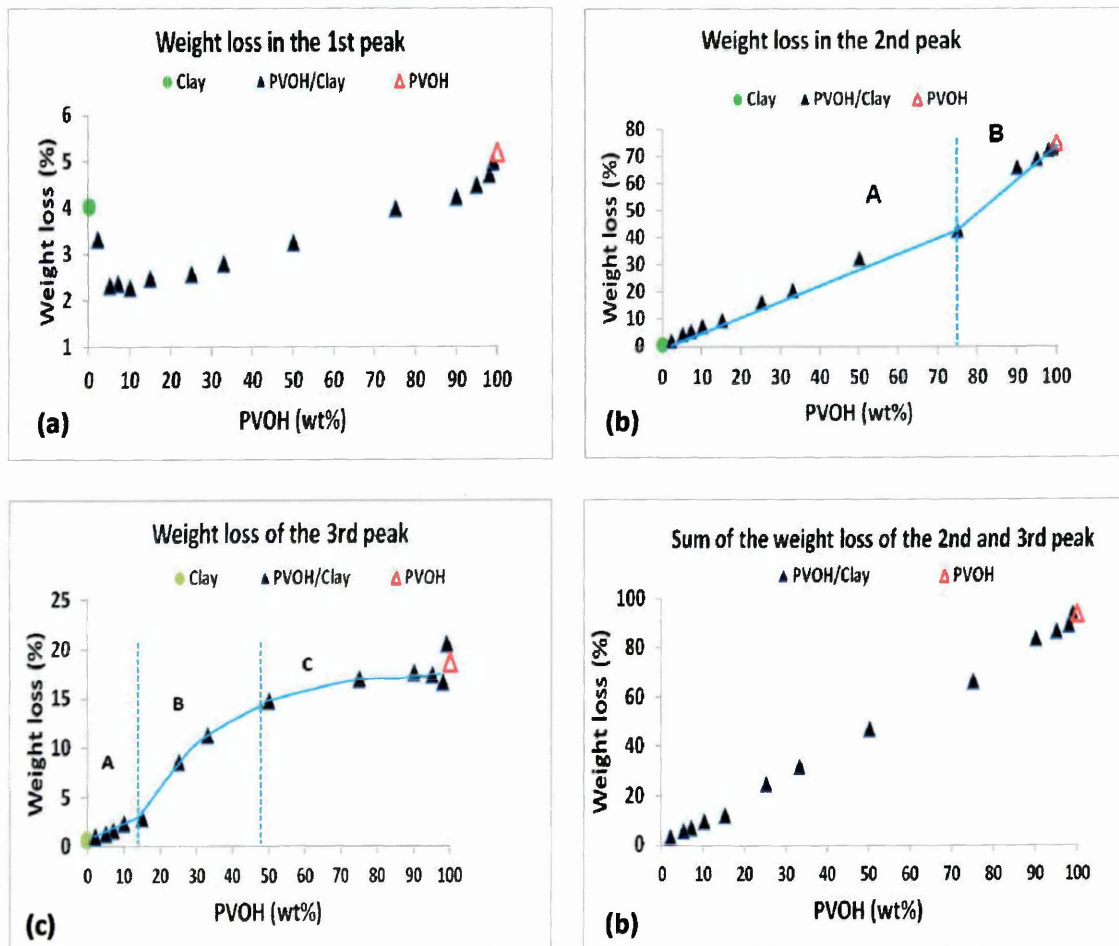


Figure 5.20. Weight loss in a) the first region (35-150 °C), b) second region (200 – 385 °C), c) third region (400-550 °C) and the sum of second and third regions for clay, PVOH and PVOH/clay mixtures.

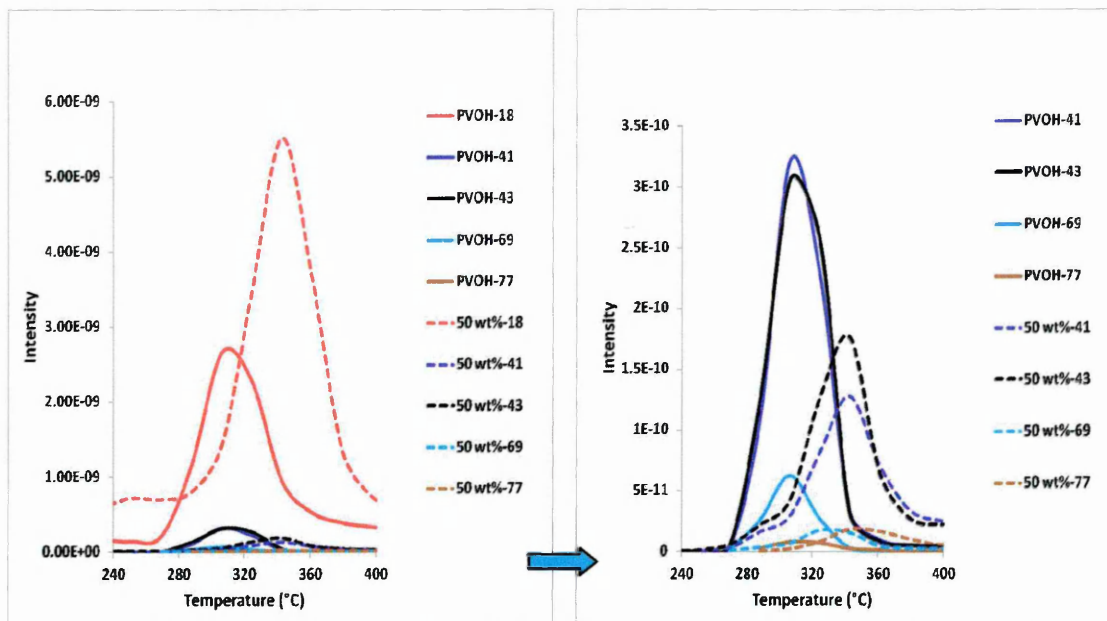


Figure 5.21. Mass chromatograms for volatile degradation products during the thermal degradation of PVOH.

A plot of the temperature at which the maxima in the second weight loss region (210-385 °C) occurs for the PVOH/clay composites is shown in Figure 5.22 a. The data shows that addition of a small amount of PVOH (1 wt%) results in a higher thermal stability than that of pristine PVOH, which then decreases to that of pristine PVOH when it reaches 9 wt%. This coincides with the formation of a depleted single layered structure and may suggest a that portion of the PVOH is outside the gallery. Alternatively, water in the gallery may promote the hydrolysis of the OH groups on the PVOH. When the PVOH concentration increases from 9 to 50 wt% the thermal stability also increases. This coincides with the formation of single and bilayer structures and may suggest that the majority of PVOH is inside the gallery and therefore more thermally stable. When the PVOH concentration increases from 50 to 99 wt% the thermal stability decreases, this coincides with the formation of exfoliated structures and as the clay concentration decreases the thermal stability becomes more like that of the pristine PVOH. A plot of the temperature at which the maxima in the

third weight loss region (400-550 °C) occurs for the PVOH/clay composites is shown in Figure 5.22 b. It almost shows opposing trends to the peak temperature of the second peak apart from the higher PVOH amounts (>50 wt%). Perhaps the improved thermal stability of the first degradation products results in a lower thermal stability of the second degradation products.

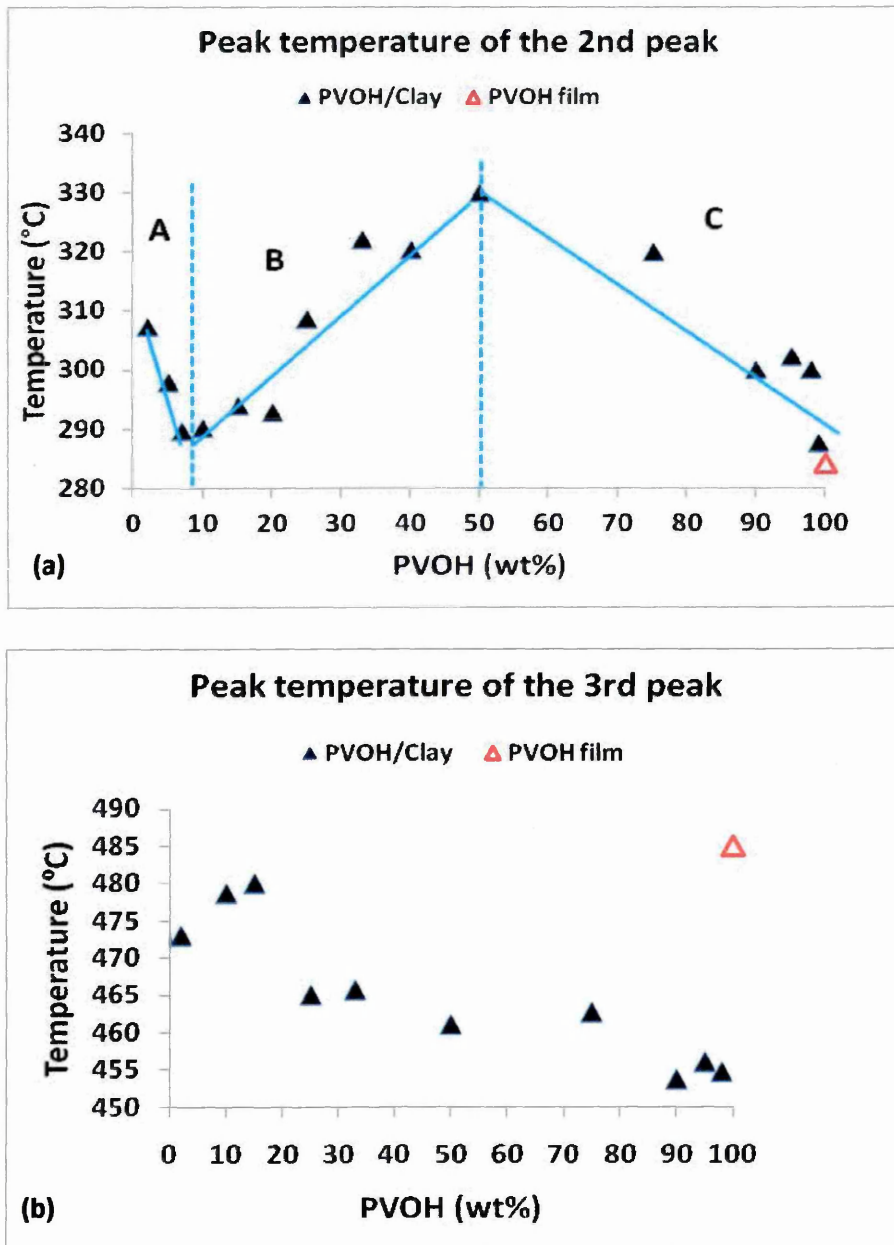


Figure 5.22. Summary of thermal stability (derivative peak maxima) of a) the 2nd peak and b) the 3rd peak for PVOH and PVOH/clay

5.2.2. Effect of clay concentration on the thermal stability of PEG600/clay composites

The thermograms and negative derivatives collected from PEG600 and PEG600/clay composites are presented in Figure 5.23. They show that PEG600 degradation occurs in one step. The thermograms in Figure 5.23 a show that the final weight loss in the samples at 800 °C decreases with the increase of clay loading. Two temperature regions can be identified over which most of the weight change occurs (Figure 5.23 b). The first major weight loss occurs between 35 and 150 °C and corresponds to the removal of water, the amounts are plotted in Fig 5.24 a and show that the amount of water decreases as the PEG concentration increases from 0 to 25 wt%. This indicates that water present in clay is replaced by PEG600. The second major weight loss occurs between 150 and 460 °C, the onset of thermal degradation in this region shifts to higher temperatures when clay is added to PEG600. This suggests that clay acts as a barrier to thermal degradation of PEG600. The weight loss in this region increases linearly with increasing PEG600 content as shown in Figure 5.24 b. The mechanism of PEG degradation is not well understood [5.13]. One of the proposed mechanisms for the degradation involves homolytic cleavage of the C-O and C-C bonds and is believed not to involve intramolecular transfer of hydrogen, but homolytic cleavage of the polymer backbone to produce radicals. These radicals are then postulated to unzip to form smaller molecules and/or monomer products such as diethyleneglycol ($C_4H_{10}O_3$), ethanol, 2-(2-methoxyethoxy) ($C_6H_{14}O_3$) and ethylene oxide (C_2H_4O) [5.11].

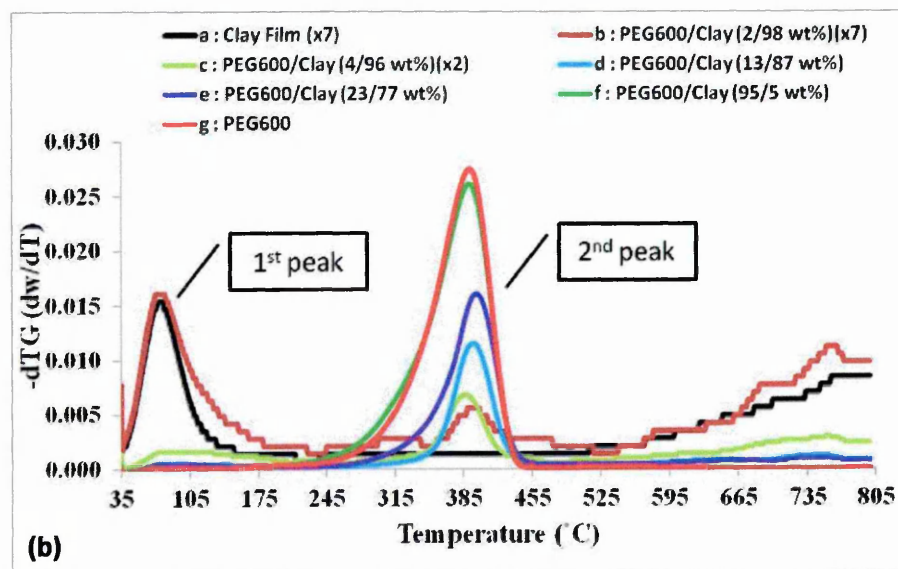
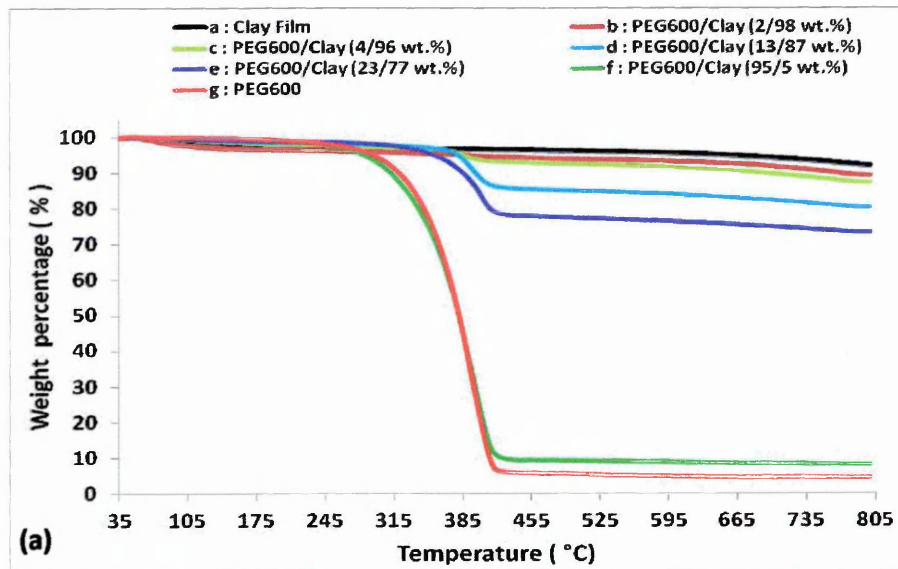


Figure 5.23. a) Thermograms and b) their derivatives of PEG600/clay composites and PEG600.

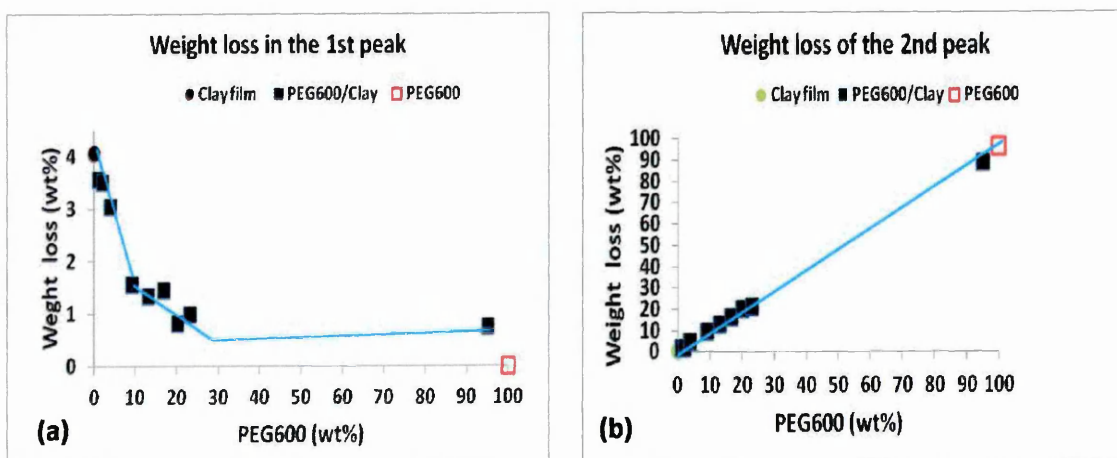


Figure 5.24. a) Weight loss in the first peak (35-150 °C) and b) second peak (150-460 °C) for clay, PEG600 and PEG600/clay composites

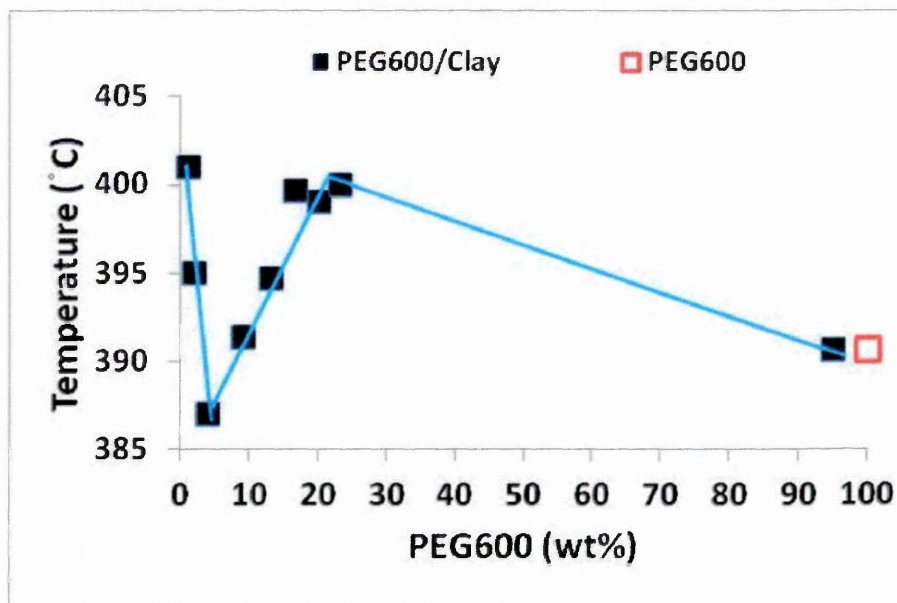


Figure 5.25. Summary of thermal stability (derivative peak maxima) for PEG600 and PEG600/clay composites.

The temperature at which the maxima occur in the DTGs obtained from PEG600/clay composites are plotted against PEG600 content in Figure 5.25. The data suggests that a portion of the PEG600 resides outside the gallery when present at loadings between 2 and 13 wt% as indicated by a decrease in the peak maximum temperature towards that of PEG600 alone. This correlates with the change in gallery occupation from a depleted single layer to a fully loaded single layer as shown in the XRD data (Figure 5.10). It appears that a small amount of PEG600 (1 wt%) is able to prop the gallery open, and a complete single layer is only formed after a critical concentration of PEG600 is added (> 9 wt%). It is believed the PEG600 inside the gallery contributes to the higher thermal stability and follows the same trend as the PVOH data.

5.2.3. Effect of clay concentration on the thermal stability of PVOH/PEG600/clay composites

The DTGs of PEG600, PVOH and their binary systems with clay are shown in Figure 5.26. They show that degradation of PEG600 and PEG600 with clay mostly occurs above 350 °C whereas for PVOH and PVOH with clay it mostly occurs below 350 °C. For PEG600 and PVOH mixtures (i.e. no clay) the PEG600 still appears to mostly degrade above 350 °C and the PVOH still mostly degrades below 350 °C, as evidenced by an increase in the maximum intensity above 350 °C in the presence of increased PEG600 content (and vice versa). However, it should be noted that some degradation of PEG600 does occur in the 210-350 °C region. It is therefore hypothesised that in the tertiary systems, the weight loss below 350 °C is mostly due to PVOH, whereas above 350 °C it is mostly due to PEG600.

Further analysis of TGMS data in Figure 5.27 shows that in the absence of clay the degradation pathway of PVOH is not affected by the degradation pathway of PEG600 when present as a mixture, and vice versa. The TGMS data provides a response from the volatile degradation products evolved during their thermal degradation. It is shown that the m/z ions = 79, 81, 82, 84, 91, 95, 96, 105 and 106 are only released by PVOH whereas the m/z ion = 73 is only released by PEG600. The ion chromatograms follow the same pattern when PVOH or PEG600 is present on its own. Voorhess [5.13] also stated that PEG/PVOH mixtures degraded independently of each other and there was no effect from the alumina crucible on their degradation. In another polymer system i.e. polyhydroxybutyrate PHB, Parra [5.14] reported that the addition of plasticizer did not alter the thermal stability of PEG/PHB blends.

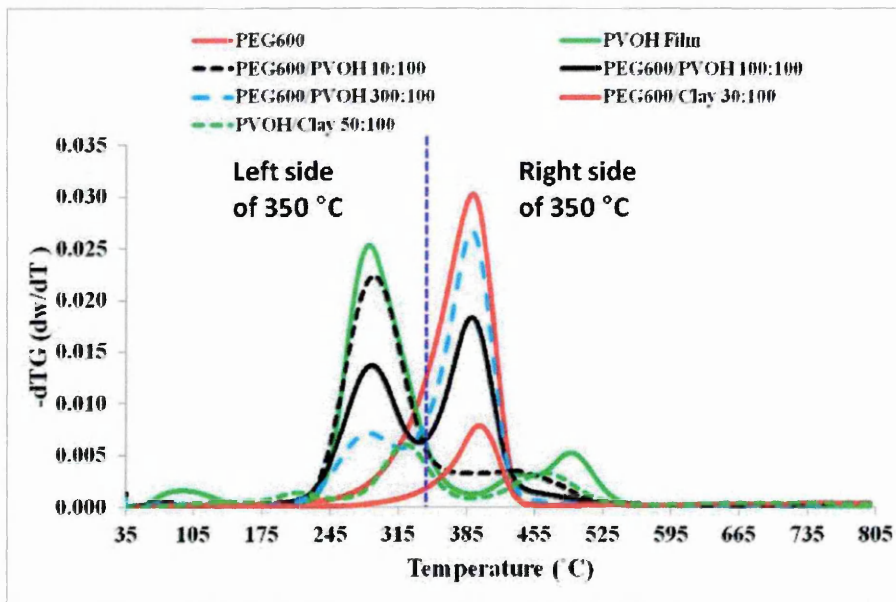


Figure 5.26. Negative derivative thermograms for PEG600, PVOH, PEG600/PVOH, PEG600/clay and PVOH/clay

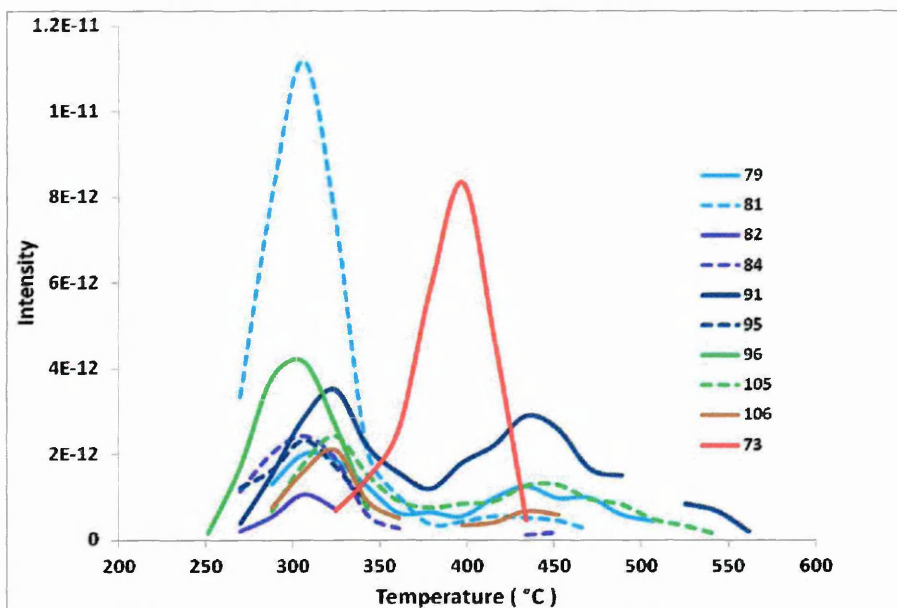


Figure 5.27. Mass chromatograms obtained from volatile degradation products during the thermal degradation of a PEG600/PVOH mixture (50 wt %).

Two main degradation pathways, represented by the maxima below and above 350 °C, were also observed in the tertiary systems of PEG600/PVOH/clay. The negative derivative thermograms of the tertiary systems as a function of increasing PEG600 concentration, whilst PVOH and

clay concentrations are kept constant, are given in Figure 5.28 a and shows that the intensity of the maxima at temperatures lower than 350 °C remain mostly constant whereas the intensity of maxima at temperatures higher than 350 °C increase with increasing PEG600 content. The converse is observed in the negative derivative thermograms of samples with increasing PVOH content whilst PEG600 content is kept constant (Figure 5.28 b). It is interesting to see that the peak position of maxima at temperatures greater or lower than 350 °C move to a slightly higher temperature with increasing PEG600 or PVOH content, respectively suggesting some interaction or possible delay in degradation due to both PVOH and PEG600 being within the confined area of the clay gallery. This analysis will be further discussed in Chapter 5.3 with reference to the quantitative adsorption data obtained via the centrifugation approach.

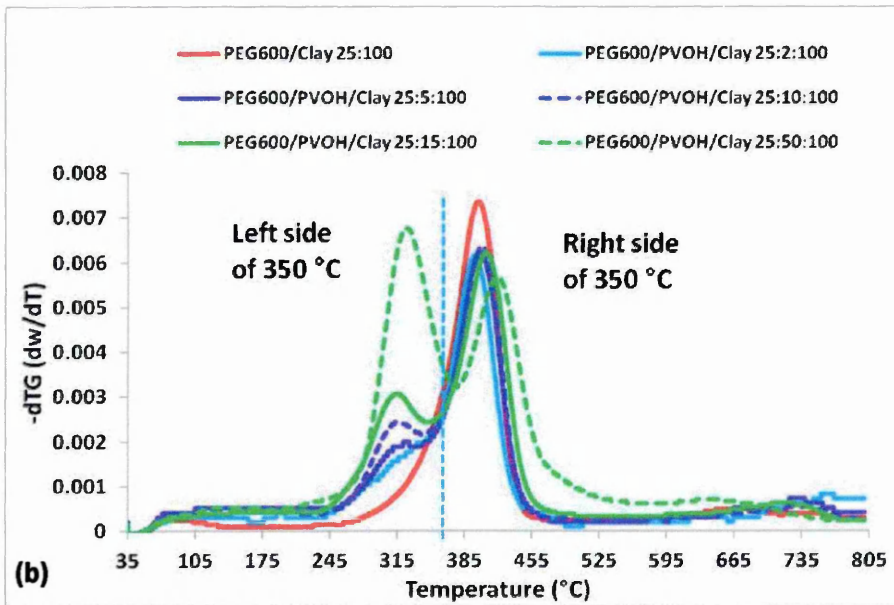
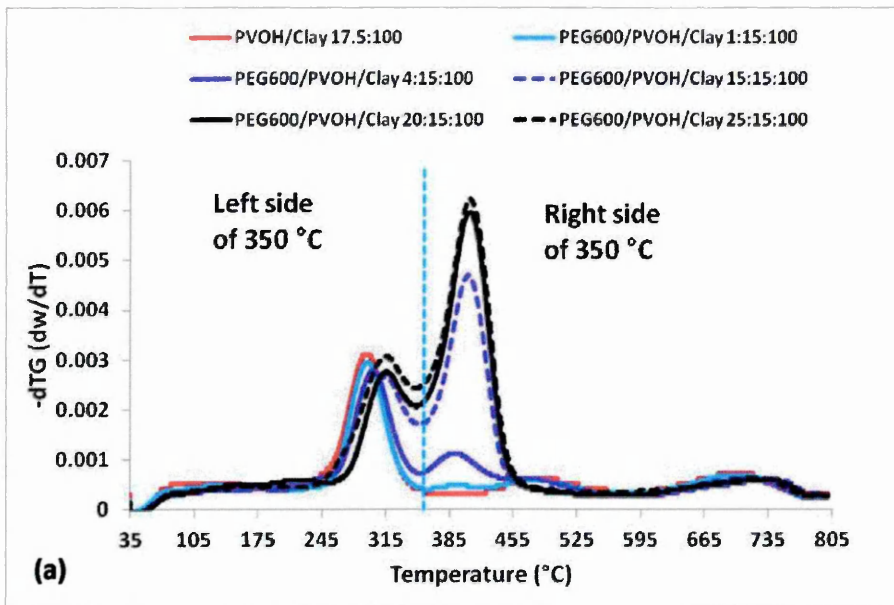


Figure 5.28. Derivative thermograms for PEG600/PVOH/clay nanocomposites with fixed amounts of PVOH (a) and PEG600 (b).

5.3. Competitive adsorption and effect of different route of mixing

Quantification PVOH and PEG600 adsorbed on clay was determined via a centrifugation approach alongside characterisation of the interlayer spacing by XRD.

5.3.1. Quantification of the amount of PVOH and PEG600 adsorbed by clay

The amount of polymer and/or plasticizer adsorbed on clay was obtained by using TGA to analyse the organic content in the supernatant collected from centrifuged aqueous polymer-clay-plasticizer suspensions. The experimental detail of this technique is discussed in Chapter 3.2 and 3.3. For binary suspension systems (i.e. PVOH/clay or PEG600/clay), the amount of PEG600 or PVOH adsorbed by the clay was calculated by the amount of organic offered to the clay minus the amount determined gravimetrically in the supernatant (free organic) after evaporation of the water. It has been shown previously in section 5.2.3 that the weight loss below 350 °C is predominantly due to the degradation of PVOH, whereas above 350 °C it is due to the degradation of PEG600 and the second degradation stage of PVOH. If the weight loss of the 1st peak (132-b °C) in the TGA data collected from PEG600/PVOH mixtures is plotted as a function of the actual PVOH content (Figure 5.29) a linear response is obtained, the relationship is described in the following equation:

$$y=0.7597x+0.5919 \quad (5.1)$$

where x is the PVOH content, and y is the weight loss of the first peak from (132-b °C). The starting temperature is fixed at 132 °C since it is not dependant on PEG or PVOH concentration whereas the end temperature, b , is both PVOH and PEG concentration dependent. The end temperature, b , for each PEG/PVOH mixture is the temperature at the minimum between the second and

third maxima. The amount of PEG600 in the supernatant is obtained from the total amount of free organic in the supernatant, which is determined gravimetrically minus the amount of PVOH in the supernatant, which is determined via the TGA method. The relative amounts of PEG600 and PVOH associated with the clay is then calculated by subtracting the respective amounts offered from the amounts of PEG600 and PVOH in the supernatant. The above equation has been tested and shows very good prediction power. The error in each determination is less than ± 0.5 wt%. The error was determined by comparing the weight loss between the "known" PVOH concentration and that calculated using equation 5.1. Five samples were used to test the error, one at each of the concentrations shown in Figure 5.29.

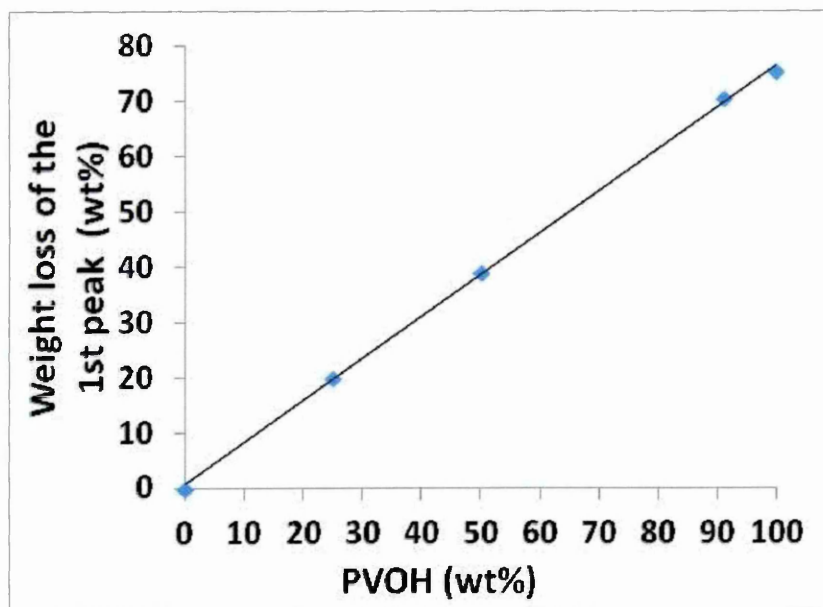


Figure 5.29. Weight losses from the 1st maximum as a function of actual PVOH content in PEG600/PVOH mixtures.

5.3.2. Adsorption of PVOH onto clay from aqueous solution

A wide range of PVOH concentrations offered (2 to 95 wt%) to clay have been investigated. The XRD traces of samples collected from full suspension

and from sediment after centrifugation are presented in Figures 5.30 a and b, and show that the amount of PVOH associated with clay increases with the amount of PVOH offered to clay as indicated by the increasing d-spacings. Both intercalated and exfoliated structures are observed in the films prepared from the full suspension, but only intercalated structures are observed in those from the sediment after centrifugation. It is evident that the d-spacings of films containing greater than or equal to 40 wt% PVOH and prepared from the sediment are lower than the respective d-spacings prepared from the full suspension indicating that some free PVOH is present in the full suspension (represented by that in the supernatant) and enters the clay gallery as the films are dried. Note that the traces of the films collected from full suspension are essentially repeats of those presented in Figures 5.1, 5.2 and 5.3, the traces are effectively the same and thus show the repeatability of the method.

When the amount of PVOH offered to clay is below 25 wt% (Figure 5.30 a and b) the amount of excess PVOH in the supernatant, if any, is very small as evidenced by the similarity in XRD traces of films collected from the full suspension and sediment. The diffraction traces of films collected from full suspension containing 75 wt% PVOH or greater indicates that the clay is very well dispersed, whereas the respective sediment films show that they are intercalated. This shows that the excess PVOH that is removed in the supernatant of the sediment films contributes to the good dispersion of the clay in the full suspension films.

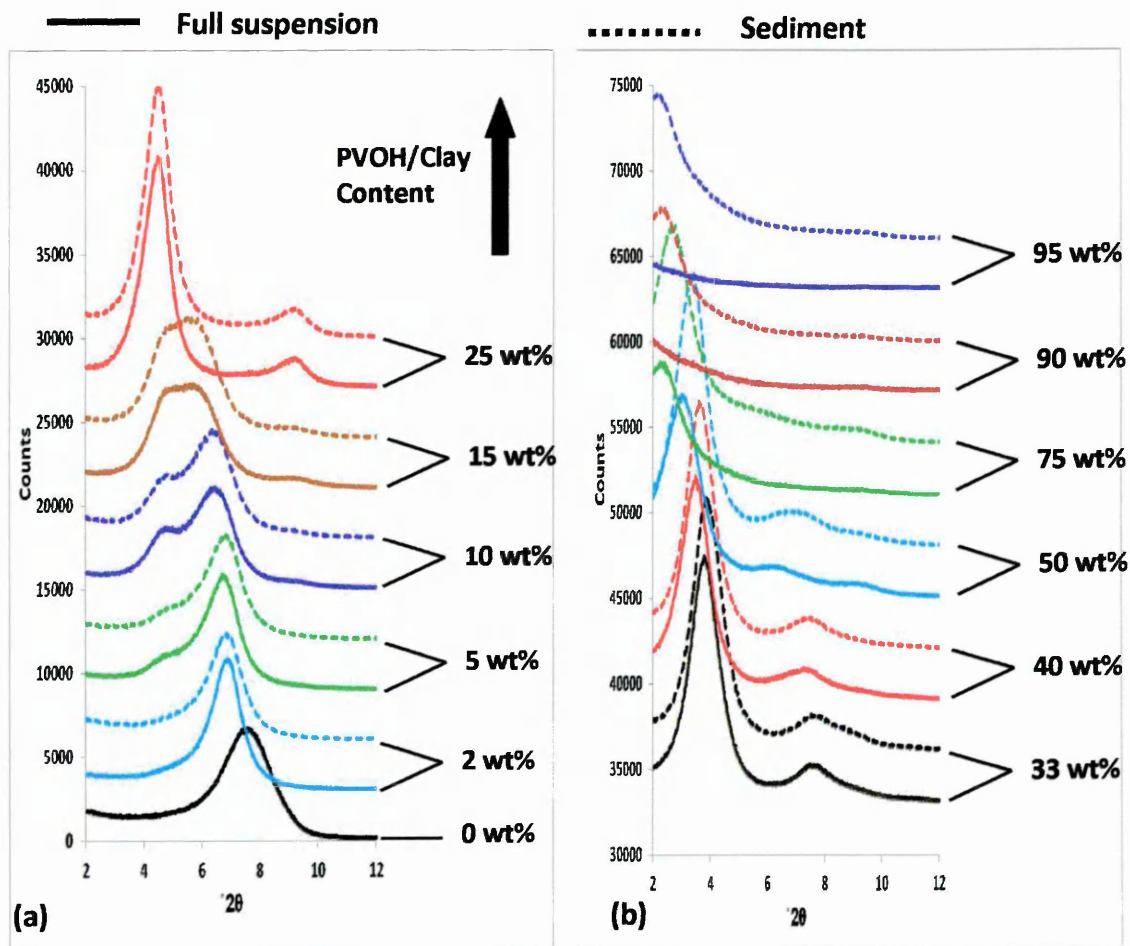


Figure 5.30. XRD patterns of PVOH/Clay a) 2-25 wt% PVOH and b) 23-95 wt% PVOH composites prepared from suspension (full line) and from sediment (dashed line) after centrifugation.

A summary of the d-spacings observed in the XRD traces of the PVOH and clay composites prepared from the full suspension and sediment are plotted in Figure 5.31 and shows more clearly that the amount PVOH residing in the clay gallery increases as the amount of PVOH offered to clay increases.

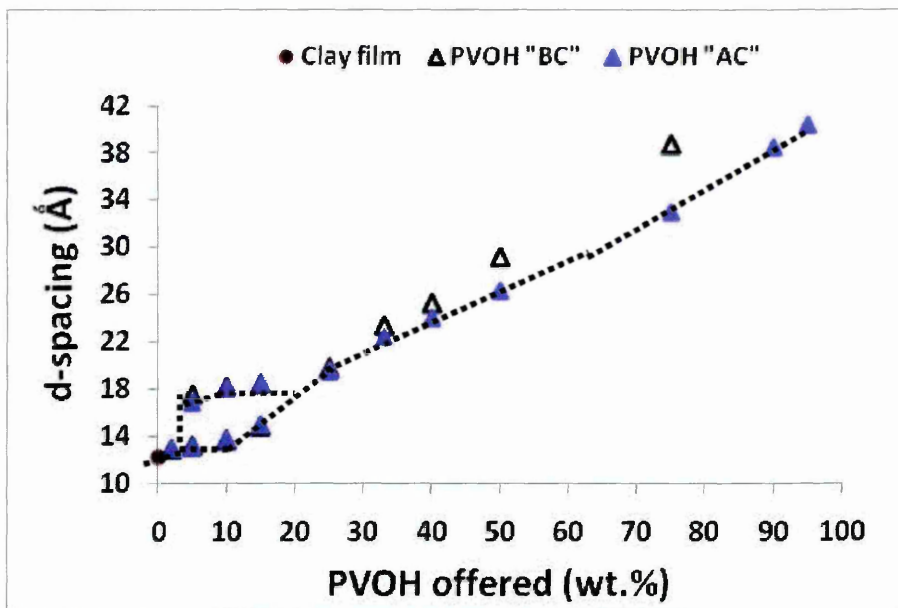


Figure 5.31. Summary of d-spacings observed in the XRD traces of PVOH/Clay composites prepared from full suspension (BC) and sediment (AC)

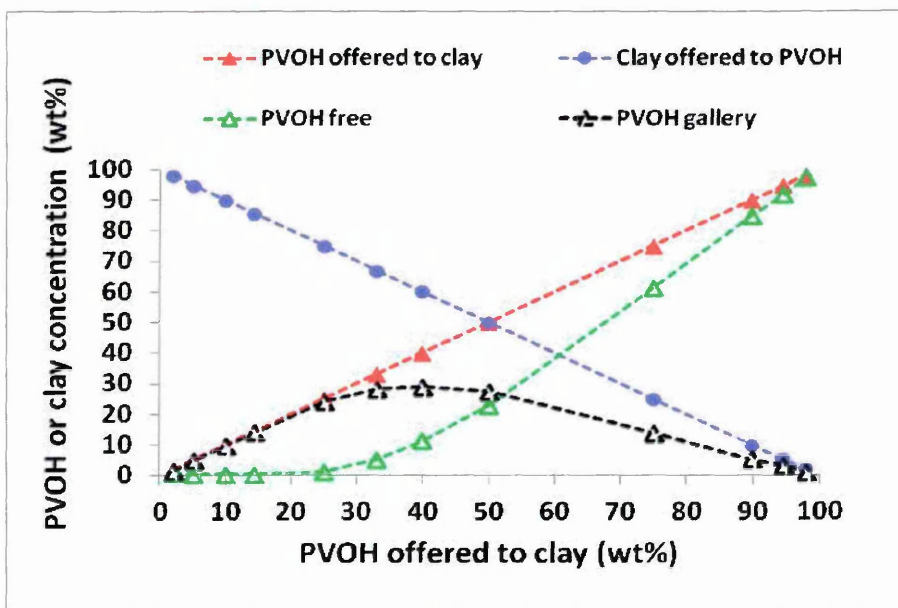


Figure 5.32. Adsorption data of PVOH onto clay from aqueous solution calculated via the centrifugation approach

Figure 5.32 shows the adsorption data of PVOH onto clay from aqueous solution obtained via the centrifugation approach. Free PVOH, i.e. that in the supernatant, is only observed when the concentration reaches between 25-33 wt% and greater, which is also reflected by the point of deviation in plots of AC

and BC in the XRD results (Figure 5.30 a and b). At concentrations greater than 25 wt%, free PVOH increases significantly with increasing amounts of PVOH offered to clay. At ~53 wt% PVOH offered and greater the amount of PVOH in the supernatant (PVOH free) is greater than that adsorbed by clay. The interaction between PVOH and clay could occur by i) hydrogen bonding between the hydroxyl groups of PVOH and the oxygen atoms of the clay layers, ii) by direct interaction of the oxygen atoms in the hydroxyl groups of PVOH to the sodium cations, or iii) hydrogen bonding of the hydroxyl groups of PVOH to the sodium cations via bridging water molecule/s [5.11,5.15,5.16]. The most likely scenarios are types i) and iii) since the interaction of water with the sodium cations is very strong and difficult to remove.

5.3.3. Adsorption of PEG600 onto clay from aqueous solution

XRD traces from PEG600/clay (1-95 wt% PEG600) composites prepared from full suspension and from sediment are presented in Figures 5.33 a and b. They show that the amount of PEG600 associated with clay increases with the amount of PEG600 offered to clay. Only intercalated structures are observed for the whole range of PEG600 concentrations and also whether prepared from full suspension or sediment. As already shown in Figures 5.8 and 5.9 three steps are observed in the changes in d-spacing as the amount of PEG600 offered is increased; i.e. a depleted single layer to a fully loaded single layer and then to a bilayer structure. The three steps are observed in both full suspension and sediment films.

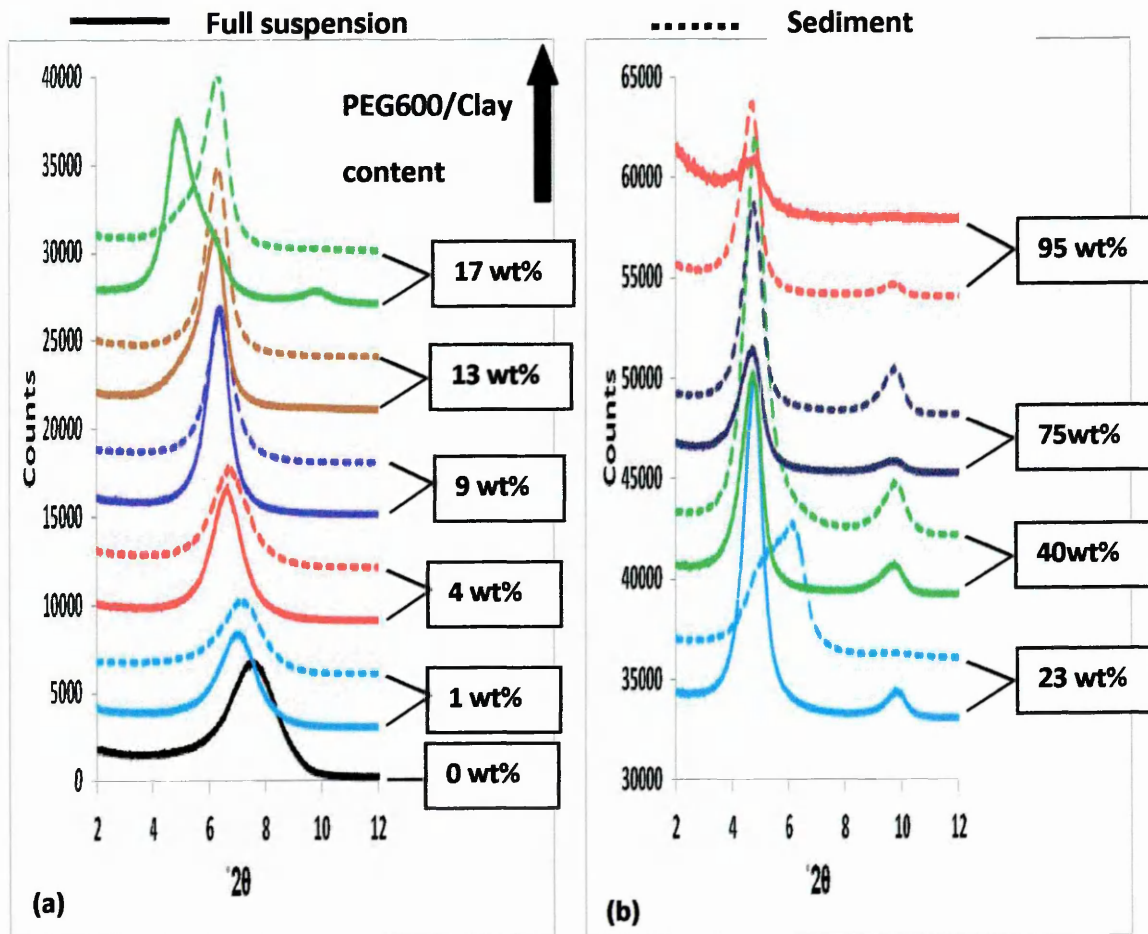


Figure 5.33. The XRD patterns of PEG600/Clay a) 1-17 wt% and b) 23-95 wt% composites prepared from full suspension (full line) and from sediment (dashed line)

The data shows that the amount of free PEG600 is very small when 13 wt% or less of PEG600 is offered to clay (Figure 5.33 a). When 17 wt% PEG600 is offered, free PEG600 is present and is able to enter the clay gallery and increase the portion of bilayer structures to those of single layer structures. When 23 wt% PEG600 is offered to clay (Figure 5.33 b), the amount adsorbed is not enough to create a full bilayer structure when the excess PEG600 is removed in the supernatant. No dissimilarity of the d-spacings is observed in films prepared by either the full suspension or sediment when present at 40 wt% and above. The reason may be that the clay has adsorbed sufficient

PEG600 to create a full bilayer and no space is available for any excess PEG600 to enter.

The d_{001} -spacings observed in the XRD traces of the PEG600 and clay nanocomposites are plotted in Figure 5.34. It shows more clearly that as the concentration of PEG600 increases, step changes occur as the gallery expands from a depleted single layer to a fully loaded single layer and then a bilayer structure. Excess PEG600 can enter the clay gallery when 13-23 wt% PEG600 is offered to clay, below 13 wt% it suggests that all the PEG600 clay is adsorbed by the clay and no excess is present.

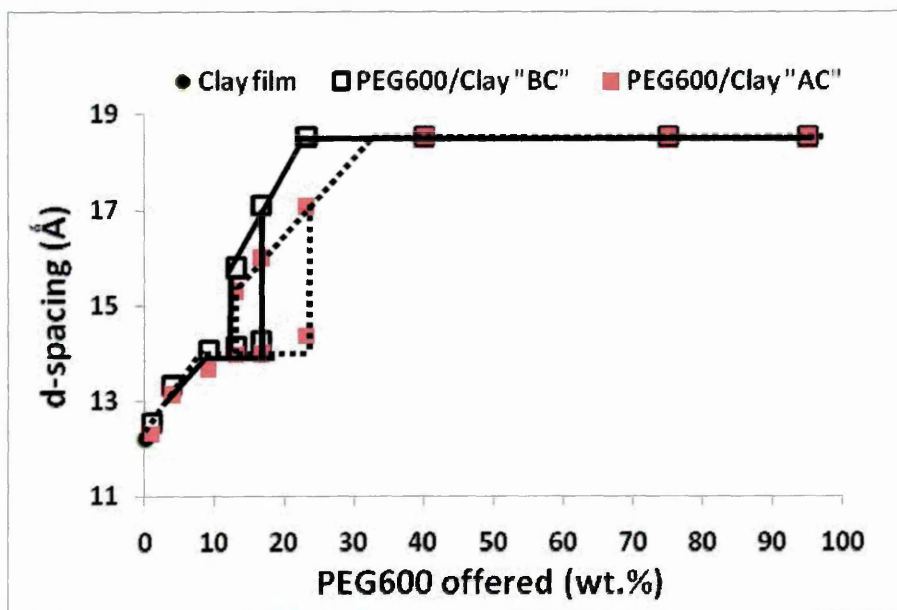


Figure 5.34. Summary of d-spacings observed in the XRD traces of PEG600/Clay composites prepared from full suspension (BC) and sediment (AC).

The adsorption data of PEG600 onto clay from aqueous solution via the centrifugation approach shown in Figure 5.35 demonstrates that all PEG600 is absorbed by clay when offered at levels below 13 wt%, which is also indicated by the XRD data (Figure 5.33 a). Above 23 wt% the amount in the supernatant significantly increases with the increase of PEG600 offered. Parfitt [5.17]

suggested that direct interaction between the exchange cations and PEG molecules was not responsible for the PEG adsorption, but due to the ether oxygen atoms of PEG and water molecules in the primary hydration shell of exchange cations, to give a water bridge.

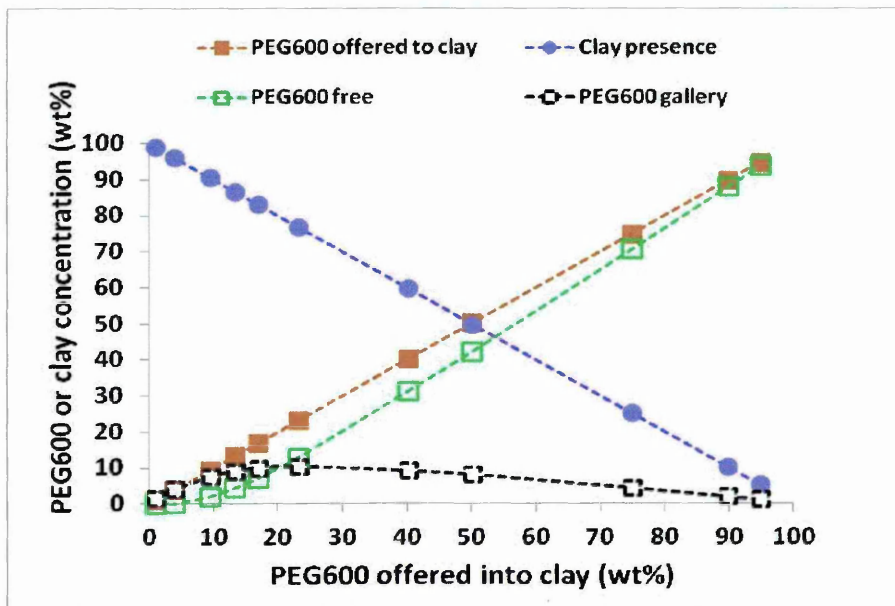
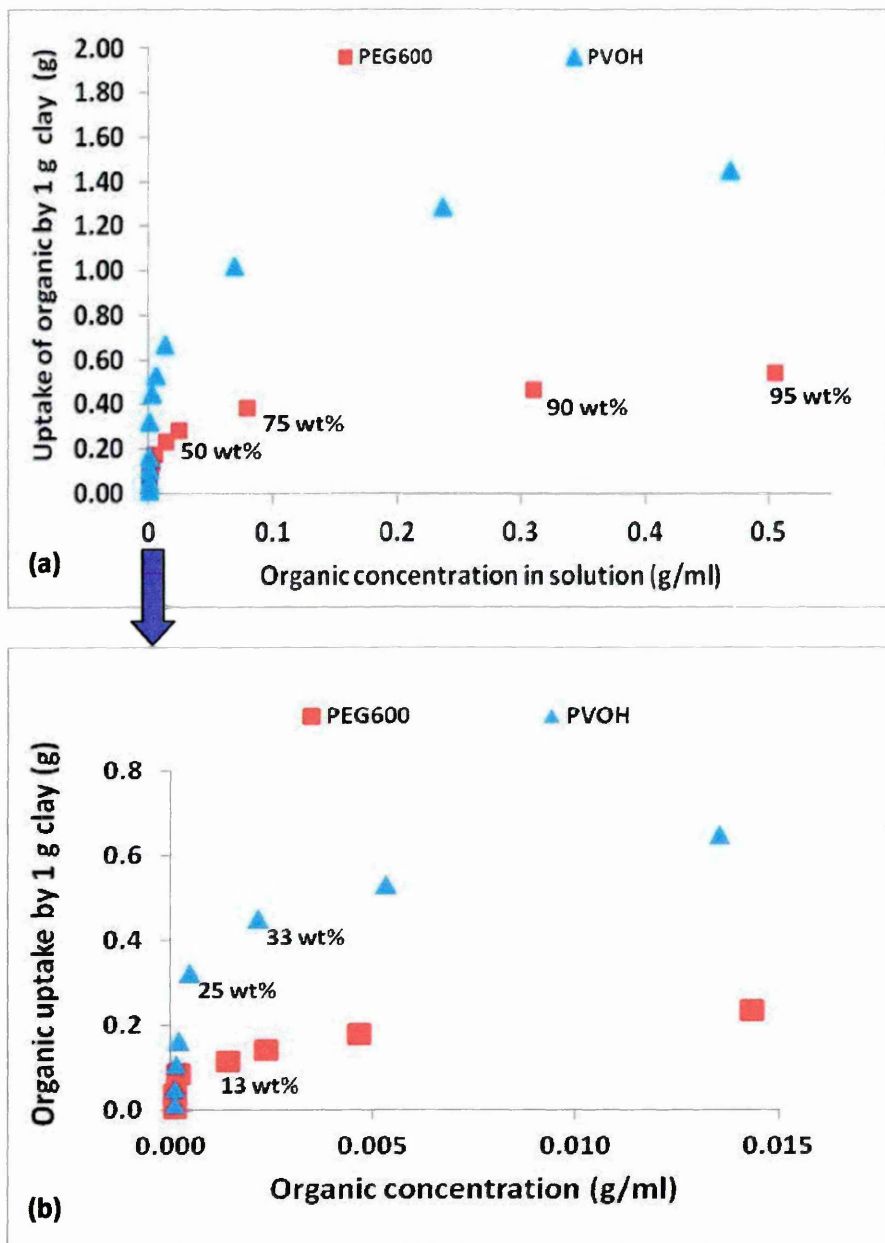


Figure 5.35. Adsorption data of PEG600 onto clay from aqueous solution (via centrifugation approach)

The adsorption data shown in Figures 5.32 and 5.35 is presented as a function of 'free organic' concentration in Figure 5.36 and shows that the amounts of PEG600 or PVOH associated with clay increases sharply as the amount offered increases and then continues to increase gradually as more is offered, the transitions for PEG600 and PVOH occur at ~ 0.0002 and ~ 0.0005 g/ml, respectively which relates to ~ 9 wt% for PEG600 and ~ 25 wt% for PVOH. Free PVOH or PEG is able to enter the clay gallery when the films from suspension are formed as shown by XRD data in Figure 5.30 a and b for PVOH and in Figure 5.33 a and b for PEG. The adsorption of PEG600 by clay follows

the L-type isotherm as described by Chen [5.4] and Parfitt [5.17] whilst the adsorption of PVOH by clay follows the H-type isotherm as described by Theng [5.18] and De Bussetti [5.19].



5.3.4. Competitive and synergistic adsorption of PVOH and PEG600 onto clay from aqueous solution

For the competitive adsorption studies a selected range of PEG600 (1, 10 and 30 pph) and PVOH (2, 5, 10, 15, 50 and 90 pph) concentrations were offered to clay. The XRD traces collected from films prepared from the full suspension and sediment are presented in Figures 5.37 a (low PEG600 concentration = 1 pph), 5.37 b (medium PEG600 concentration = 10 pph) and 5.37 c (large PEG600 concentration = 30 pph). All composite structures in this series were intercalated. The amounts of PEG600 and PVOH adsorbed by clay increased with the increasing amounts of PEG600 and PVOH offered as evidenced by the corresponding increases in d-spacing. A similar trend is observed in these tertiary systems when compared to those in the binary systems since the d-spacings of films prepared from sediment are lower than those prepared from full suspension. This also shows that any free organic in the full suspension will enter the clay gallery when the films are dried.

Figure 5.37 a shows that the d-spacings in the tertiary systems are only slightly higher than those of PVOH/Clay binary systems (2, 5, 11, 17, 50 and 100 pph) since the amount of PEG600 offered is only small. With higher amounts of PEG600 (10 and 30 pph) offered to clay in the tertiary systems (Figures 5.37 b and c) more significant increases in the d-spacings are observed. These increases are due to both PEG600 and PVOH being present in the clay gallery. The highest amounts of free organic, as indicated by the differences in respective AC and BC points, are observed when the amounts of PVOH offered to clay are 50 and 90 pph and that these differences are larger as more PEG600 is offered. The corresponding adsorption data shows an increase in the amount of PVOH adsorbed by clay but a decrease in the amount

of PEG600 adsorbed (Figure 5.38 and 5.39). Any free organic present when PVOH is offered to clay at 2-15 pph is due to PEG600 as evidenced in the adsorption data (Figure 5.38), no free PVOH is present in the tertiary systems when 2-15 pph PVOH is offered.

The combined amounts of PVOH and PEG600 adsorbed onto clay when the concentration of PVOH is variable and the concentration of PEG600 is fixed at 1, 10 and 30 pph are shown in Figure 5.38 a. The combined amounts adsorbed onto clay and that in solution increases as the amount of PVOH or PEG600 offered to the clay increases.

Competitive adsorption data of PVOH in the absence and presence of 1, 10 and 30 pph PEG600 is shown in Figures 5.38 b, c and d, respectively. The amount of PVOH adsorbed is very similar regardless of whether the amount of PEG600 is fixed at 1, 10 and 30 pph. At low loadings most of the PVOH that is offered is adsorbed it only begins to deviate at concentrations greater than 40 pph, in addition above this value more PVOH is adsorbed in the tertiary systems than the binary systems. For example, when 90 pph PVOH is offered in the presence of either 1, 10 or 30 pph PEG600, 79 pph PVOH is adsorbed, but in its absence 60 pph PVOH are adsorbed. This result shows that PEG600 promotes the adsorption of PVOH when the amount of PVOH offered is ≥ 50 pph.

PEG600/PVOH/Clay

———— Full suspension Sediment

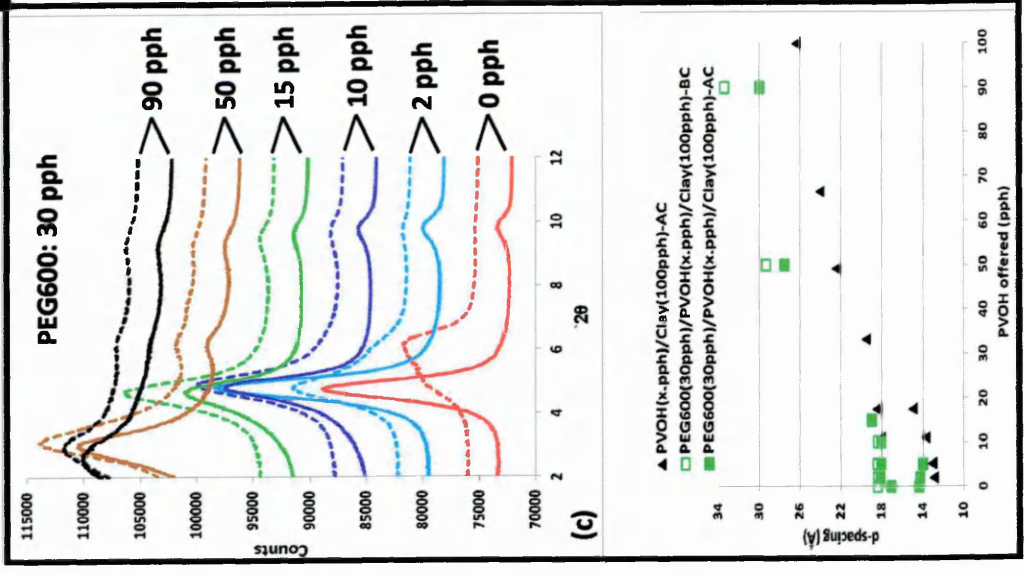
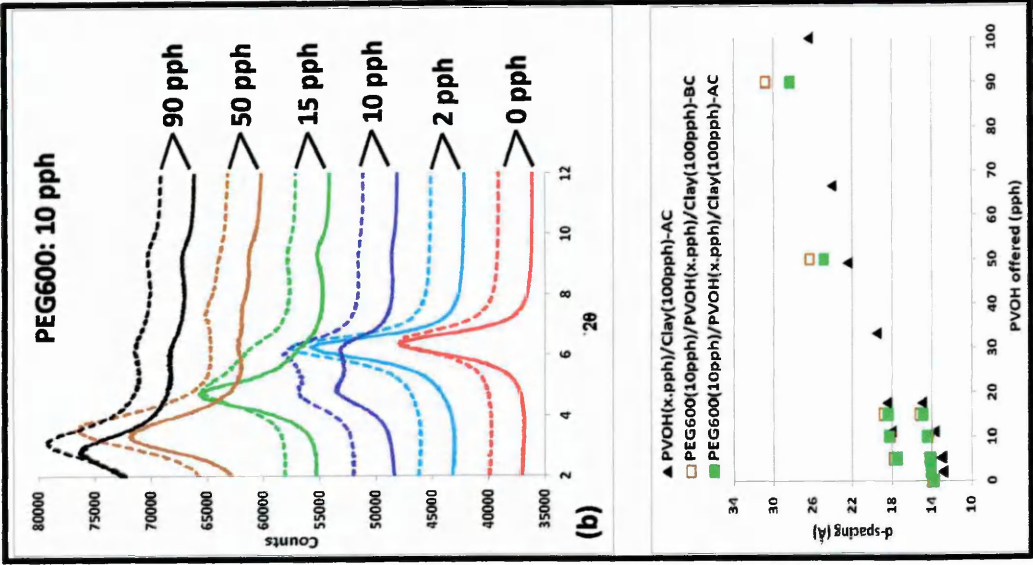
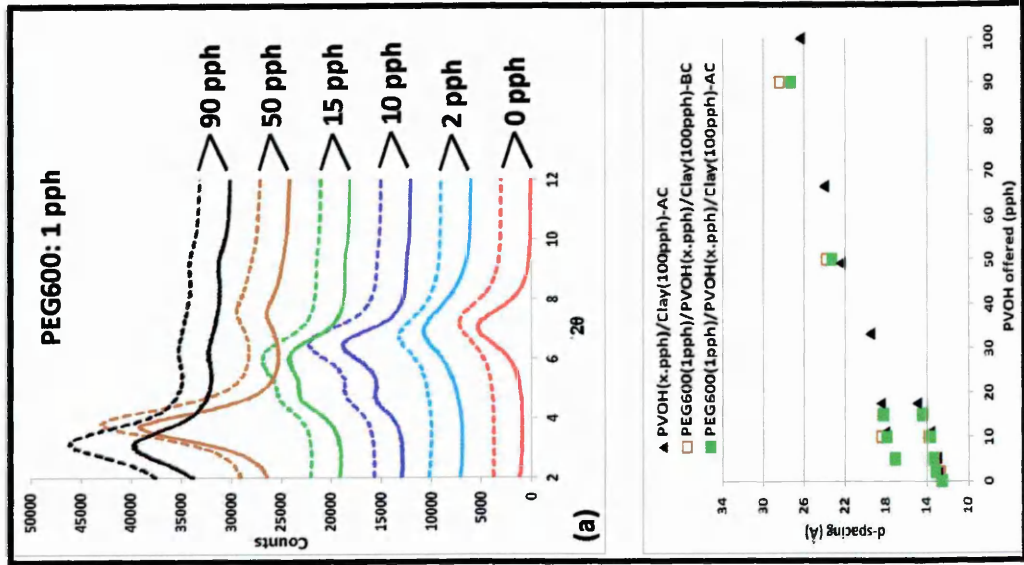


Figure 5.37. The XRD patterns and d-spacings of PEG600/PVOH/Clay nanocomposites when amount of clay is 100 pph and PEG600 are a) 1 pph, b) 10 pph and c) 30 pph prepared from suspension (BC) and from sediment (AC)

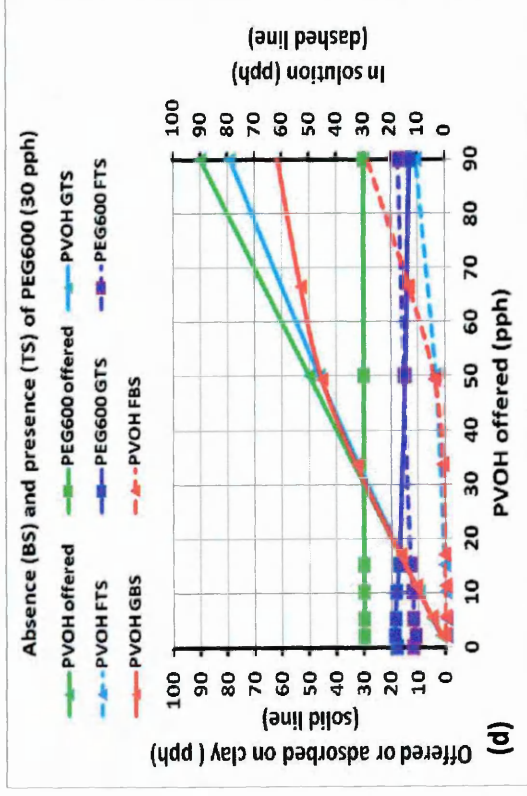
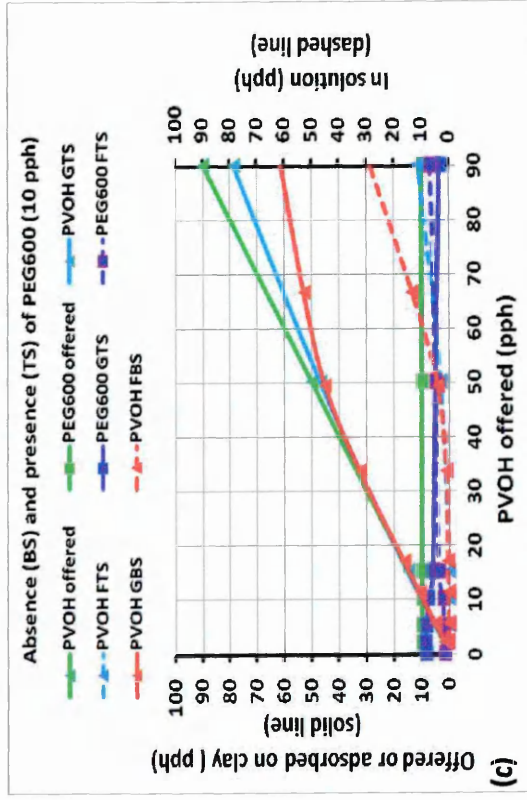
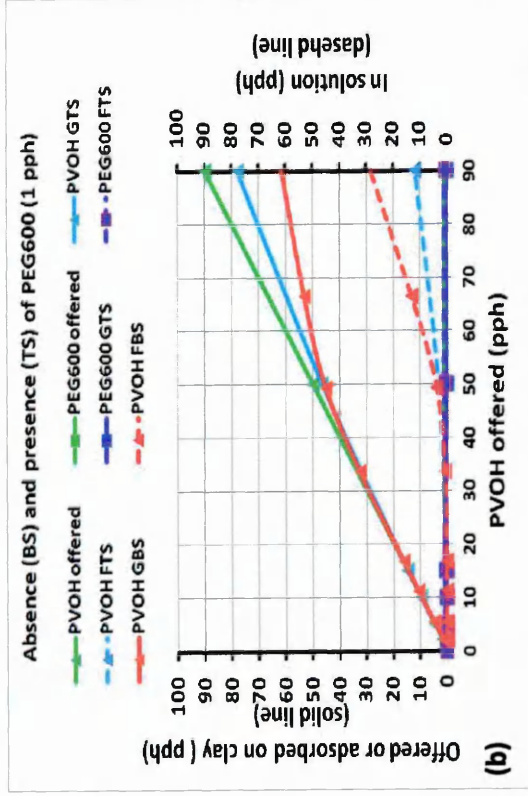
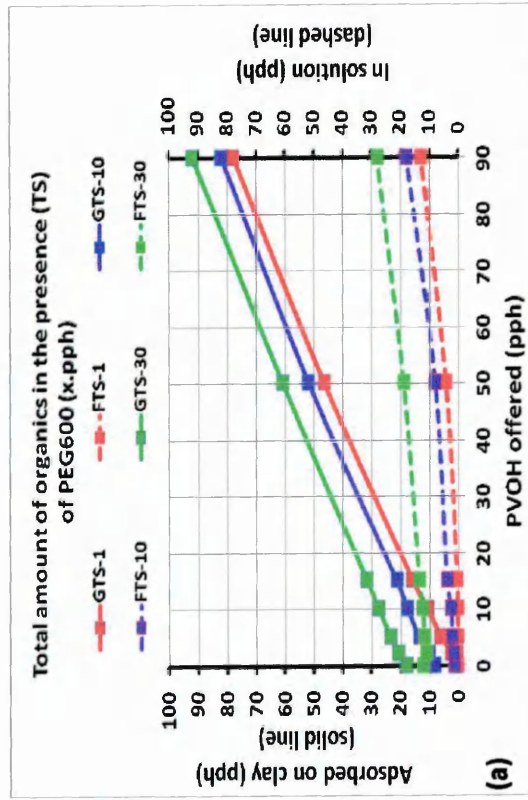


Figure 5.38. Competitive adsorption data of PVOH and PEG600 onto clay from aqueous solution in tertiary systems (TS) (a) and its comparator with binary system (BS) when the amount of PEG600 is constant 1 (b), 10 (c), and 30 pph (d). G refers to organic adsorbed by clay and F refers to organic in the supernatant.

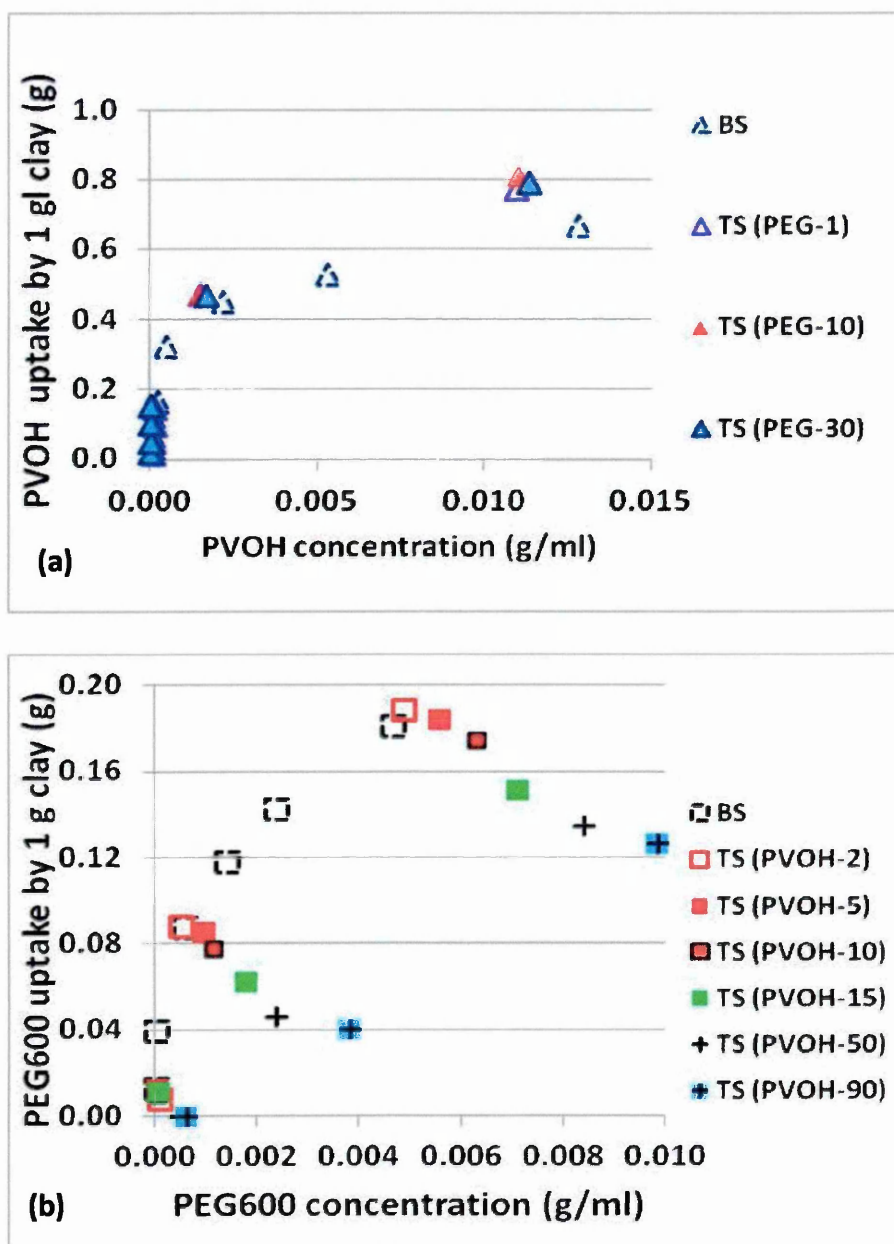


Figure 5.39. Summary of competitive adsorption data of PEG600 and PVOH onto clay from aqueous solution for binary (BS) and tertiary systems (TS). TS (PEG-1) represents the adsorption of PVOH in the presence of 1 pph PEG600 in the tertiary system. TS (PVOH-2) represents the adsorption of PEG600 in the presence of 2 pph PVOH in the tertiary system.

When 1 pph PEG600 is present most, if not all, of the PEG600 is absorbed by the clay and so any organic in solution is due to PVOH. When 10 or 30 pph PEG600 is offered, the amount of PEG600 adsorbed by clay is gradually reduced as the amount of PVOH offered to clay is increased (Figures

5.38 c and d); only 4 and 13 pph PEG600 are adsorbed from 10 and 30 pph PEG600 offered, respectively when 90 pph PVOH is offered. This data again shows that PVOH has a higher affinity for the clay than that of PEG600.

The adsorption data shown in Figure 5.38 is presented as a function of “free organic” concentration in Figures 5.39 a and b. The amount of PVOH adsorbed by clay increases sharply and then continues to increase gradually as more is offered, the transition occurs at ~ 0.0003 g/ml in the presence of 1, 10 or 30 pph PEG600. Since the transition occurred in the binary system at ~ 0.0005 g/ml, this result indicates that the amount of PVOH adsorbed by clay is increased in the tertiary system i.e. in the presence of PEG600. This can be seen over the whole PVOH concentration range in Figure 5.39 a, which shows the amount of PVOH adsorbed in the tertiary system (red line) is always higher than that in the binary system (black line). The increased amount of PVOH adsorbed by clay in the tertiary system compared to binary system may be due to small amounts of PEG600 allow more PVOH to adsorb on the clay by acting as a compatibilising agent. The amount of PEG600 adsorbed by clay is reduced when any amount of PVOH is introduced in the tertiary system (Figure 5.39 b). The reduced amount of PEG600 adsorbed in the tertiary system, compared to the binary system, may be due to the increased adsorption of PVOH will drive the PEG600 away due to less space being present. In addition, the presence of PVOH on the clay will make the clay environment less hydrophilic which drives the PEG600 into solution. Similar trends in the competitive interaction of hydrophilic polymers onto clay was also observed by Chen [5.20] who found that clay preferred to adsorb PEG with a higher molecular weight (M_w 35000) than that with lower molecular weight (M_w 5000). The preferential intercalation of clay to PVOH than that of PEG600 may be explained by Carrado [5.11] and

Bujdak [5.15] who reported that the basal Si-O groups in the spaces between hydrated cations in the clay interlayer are relatively hydrophobic and so PVOH is preferentially adsorbed on these sites as PVOH is more hydrophobic than PEG600.

5.3.5. Effect of sequence of addition on the adsorption of PVOH and PEG600 onto clay from aqueous solution

As discussed in the previous section (Figure 5.15) it was shown by XRD that for the tertiary systems, route 3 (PEG600 is mixed first with clay, then PVOH is added later) produced higher d-spacings than those of route 1 (PEG600 and PVOH is mixed first, then added to clay suspension) and route 2 (PVOH and clay is mixed first, then PEG600 is added later), it was also established by VT-XRD results (section 5.16) that the difference was not due to the presence of additional water. This result revises a question as to whether this is due to a higher amount of PEG600 or PVOH adsorbed by clay in route 3 than those of route 1 and route 2 or whether it's due to the molecular arrangement of PEG600 or PVOH within the clay gallery.

A wide range of PEG600 (1, 10 and 30 pph) and PVOH (2, 10, 15 and 50 pph) concentrations were offered to clay for routes 1, 2 and 3. Typical XRD patterns from PEG600/PVOH/Clay (10/50/100 pph) films prepared from full suspension and from sediment are shown in Figure 5.40. They show that the d-spacings from all films prepared from the sediment are lower than those of films prepared from full suspension indicating that free organic enters the clay gallery when the films are dried. As already discussed in the previous section (Figures 5.15 and 5.16) the d-spacing of films prepared from full suspension for route 3 are higher than those of route 2 and route 3, however, the d-spacing of films

prepared from sediment show no dissimilarity for all three routes suggesting that the route of mixing has no effect on the amount of organic adsorbed by clay when in suspension.

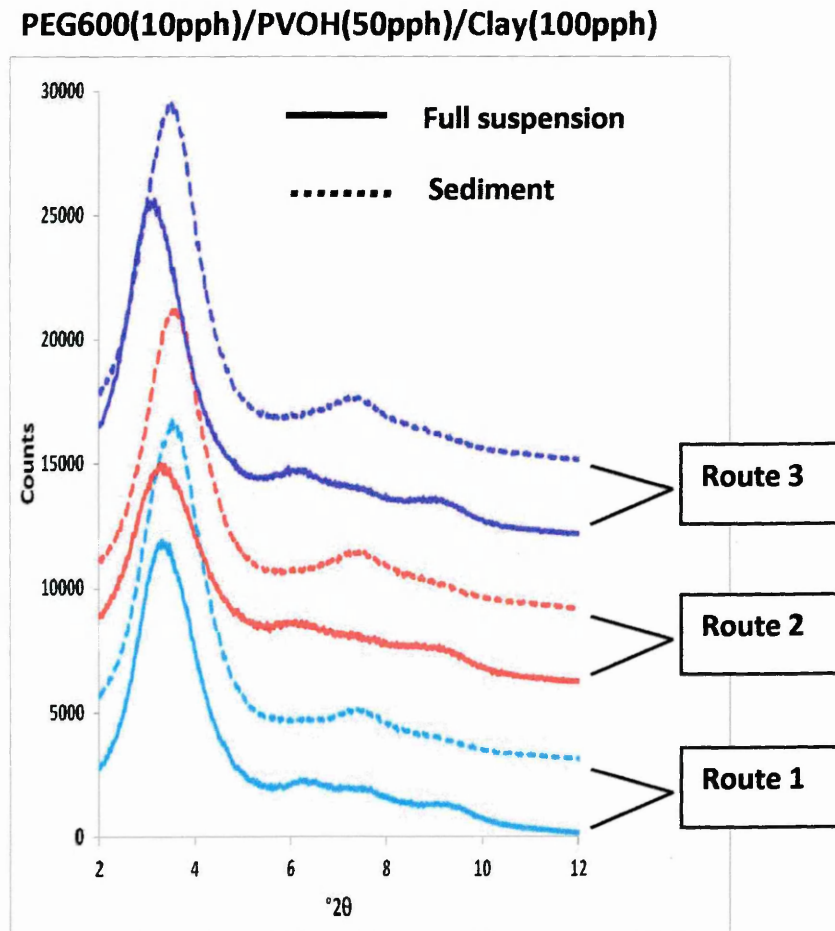


Figure 5.40. Typical XRD patterns from PEG600/PVOH/clay composites prepared by routes 1, 2 and 3. For each route the amount of PEG600, PVOH and clay are 10, 50 and 100 pph, respectively and prepared from full suspension or from sediment after centrifugation.

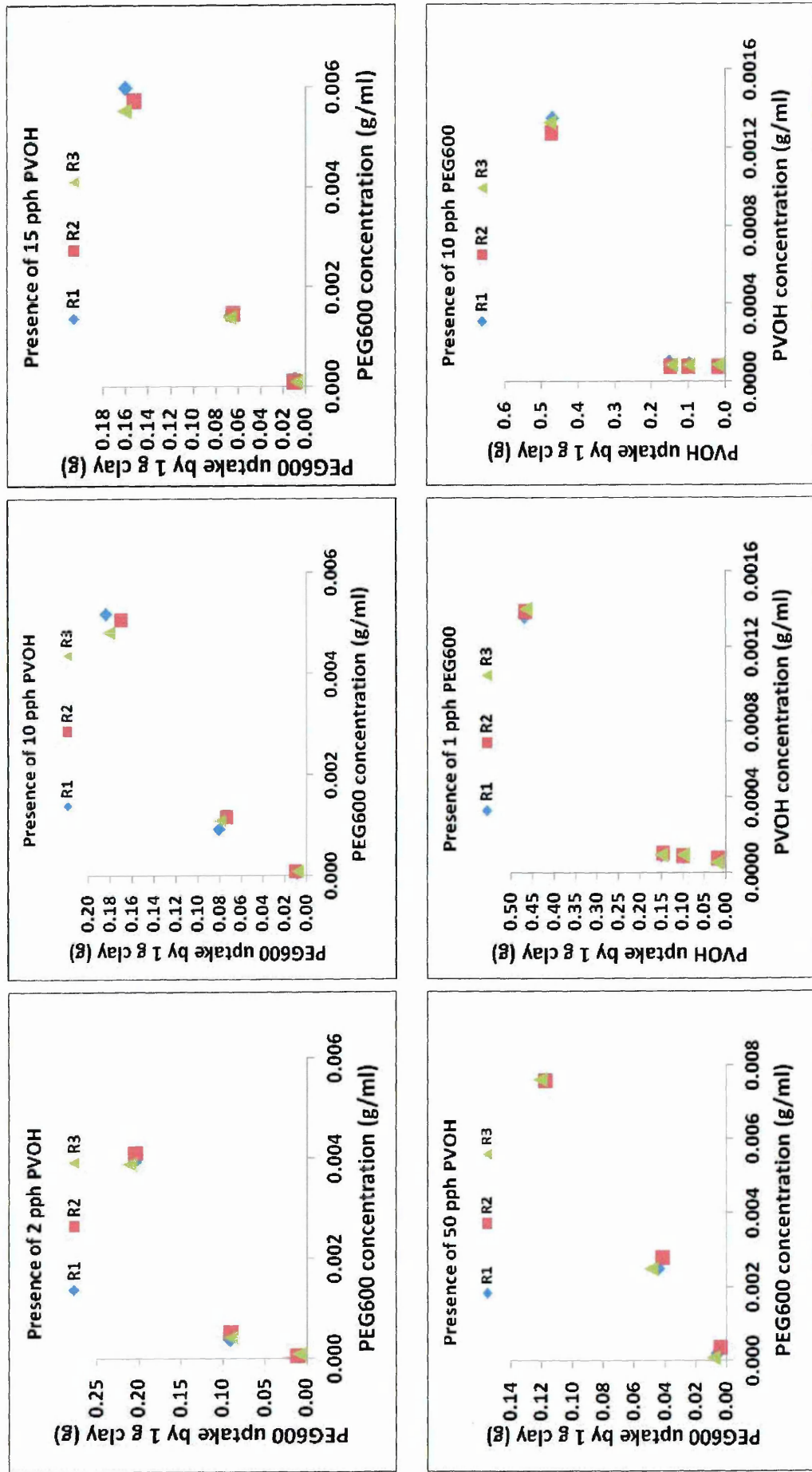


Figure 5.41. Competitive adsorption of PEG600 and PVOH onto clay from aqueous solution for route 1 (R1), route 2 (R2) and route 3 (R3) in tertiary system (continued on next page).

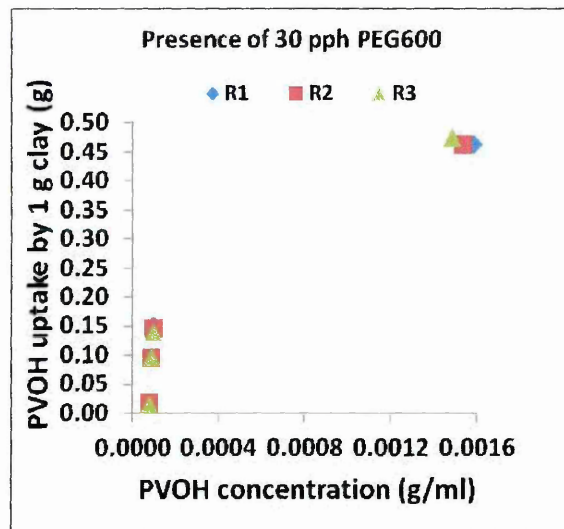


Figure 5.41. Competitive adsorption of PEG600 and PVOH onto clay from aqueous solution for route 1 (R1), route 2 (R2) and route 3 (R3) in tertiary system (continued from previous page)

The amounts of PEG600 and PVOH adsorbed by clay within the three routes are given in Figure 5.41, which shows that there are no significant differences in the amounts adsorbed by clay for either routes 1, 2 and 3. This suggests that the higher d-spacings from films prepared by route 3 than those of route 1 and route 2 via the full suspension are not due to higher amounts of PEG600 nor PVOH adsorbed by clay, but rather different molecular arrangements in which the free PEG600 or PVOH molecules are organized or associated with the clay upon drying. Perhaps the strong PEG600–clay interactions and their immobility when adsorbed to the clay surface and the subsequent irregular packing of the bulkier PVOH molecules leads to an increased number of molecular chains overlapping and as a result an increased d_{001} -spacing. The strong PEG600-clay interactions and their immobility is supported by the desorption experiment discussed in Chapter 6, which shows that PEG600 cannot be easily washed away (up to 10 washes with water) when present in the gallery as a full single layer. Conversely, when the bulkier PVOH (radius of gyration $R_g \approx 55 \text{ \AA}$ for 1 % PVOH solution in water [5.21]) is allowed to adsorb on the clay surface first, the smaller PEG600 ($R_g \approx 8\text{-}25 \text{ \AA}$ depends

on PEG concentration and the type of salt [5.22]) molecules are able to neatly fill any spaces thus resulting in a better packing density and hence lower d-spacings.

5.4. References

[5.1]. Strawhecker, K.E. and Manias, E. (2000). Structure and properties of poly (vinyl alcohol)/Na montmorillonite nanocomposites. *Chemistry of materials*, **12** (10), 2943-2949.

[5.2]. Doeppers, L.M. (2004). Preparation and characterisation of poly(ethylene terephthalate) and poly(vinyl alcohol)/clay nanocomposites. *Ph.D thesis*, Sheffield Hallam University-UK

[5.3]. Equilibrium relative humidity at
<http://www.omega.com/temperature/z/pdf/z103.pdf>

[5.4]. Chen, B. and Evans, J. R. G. (2005). X-ray diffraction studies and phase volume determinations in poly (ethylene glycol)-montmorillonite nanocomposites. *Polymer international*, **54** (5), 807-813.

[5.5]. Pinnavaia, T.J. and Wang, Z. (2002). Hybrid mixed ion clay structures for polymer nanocomposite formation. US patent no 6,414,069 B1

[5.6]. Chen, B. and Evans, J.R.G. (2005). On the thermodynamic driving force for polymer intercalation in smectite clays. *Philosophical magazine*, **85** (14), 1519-1538.

[5.7]. Ray, S.S. and Okamoto, M. (2003). Polymer/layered silicate nanocomposites: A review from preparation to processing. *Progress in polymer science*, **28** (11), 1539-1641.

[5.8]. Kuljanin, J., Comor, M.I., Djokovic, V. and Nedeljkovic, J.M. (2006).

Synthesis and characterization of nanocomposite of polyvinyl alcohol and lead sulfide nanoparticles. *Materials chemistry and physics*, **95** (1), 67-71.

- [5.9]. Yang, Y., Liu, C. and Wu, H. (2009). Preparation and properties of poly(vinyl alcohol)/exfoliated α -zirconium phosphate nanocomposite films. *Polymer testing*, **28** (4), 371-377.
- [5.10]. Holland, B. J. and Hay, J. N. (2001). The thermal degradation of poly(vinyl alcohol). *Polymer*, **42** (16), 6775-6783.
- [5.11]. Jia, X., Li, Y., Zhang, B., Cheng, Q. and Zhang, S. (2008). Preparation of poly (vinyl alcohol)/kaolinite nanocomposites via in situ polymerization. *Materials research bulletin*, **43** (3), 611-617.
- [5.12]. Carrado, K. A., Thiyagarajan, P. and Elder, D. L. (1996). Polyvinyl alcohol-clay complexes formed by direct synthesis. *Clays and clay minerals*, **44** (4), 506-514.
- [5.13]. Voorhess, K. J., Baugh, S. F. and Stevenson, D. N. (1996). The thermal degradation of poly (ethylene glycol)/poly (vinyl alcohol) binder in alumina ceramics. *Thermochimica acta*, **274**, 187-207.
- [5.14]. Parra, D. F., Fusaro, J., Gaboardi, F. and Rosa, D.S. (2006). Influence of poly (ethylene glycol) on the thermal, mechanical, morphological, physical-chemical and biodegradation properties of poly (3-hydroxybutyrate). *Polymer degradation and stability*, **91** (9), 1954-1959.
- [5.15]. Chang, S. H., Ryan, M.E., Gupta, R.K. and Swiatkiewicz, B. (1991). The adsorption of water-soluble polymers on mica, talc limestone, and various clay minerals. *Colloids and surfaces*, **59** (0), 59-70
- [5.16]. Bujdak, J., Hackett, E., and P. Giannelis, E.P (2000). Effect of layer charge on the intercalation of poly(ethylene oxide) in layered silicates: Implications on nanocomposite polymer electrolytes. *Chemistry of materials*, **12** (8), 2168-2174.

- [5.16]. Bajpai, A. K. and Vishwakarma, N. (2003). Adsorption of polyvinylalcohol onto fuller's earth surfaces. *Colloids and surfaces A: Physicochemical and engineering aspects*, **220** (1-3), 117-130.
- [5.17]. Parfitt, R.L. and Greenland, D.J. (1970). The adsorption of poly(ethylene glycol) on clay minerals. *Clay Minerals*, **8** (3), 305-315.
- [5.18]. Theng, B.K.G. (1982). Clay-polymer interactions: summary and perspectives. *Clays and clay minerals*, **30** (1), 1-10.
- [5.19]. De Bussette, S.G. and Ferreiro, E.A. (2004). Adsorption of poly(vinyl alcohol) on montmorillonite. *Clays and clay minerals*, **52** (3), 334-340.
- [5.20]. Chen, B. and Evans, J.R.G. (2004). Preferential intercalation in polymer-clay nanocomposites. *The journal of physical chemistry B*, **108** (39), 14986-14990.
- [5.21]. Garvey, M.J., Tadros, T.F. and Vincent, B. (1974). A comparison of the volume occupied by macromolecules in the adsorbed state and in bulk solution: Adsorption of narrow molecular weight fractions of poly(vinyl alcohol) at the polystyrene/water interface. *Journal of colloid and interface science*, **49** (1), 57-68.
- [5.22]. Thiyagarajan, P., Chaiko, D. J. and Hjelm, R. P. (1995). A neutron scattering study of poly(ethylene glycol) in electrolyte solutions. *Macromolecules*, **28** (23), 7730-7736

**Adsorption of PEG2000, M600 and QM600
onto clay in the absence and
presence of PVOH**

6.1. Adsorption of PEG2000 or M600 onto clay from aqueous solution in the absence of PVOH

A wide range of PEG2000 and M600 concentrations were offered (2 to 90 wt%) to clay and their XRD traces are presented in Figures 6.1 a and b, respectively alongside a plot of their respective d_{001} -spacings in Figure 6.1 c and d. They show the amount of PEG2000 or M600 associated with clay increases as the amount of PEG2000 or M600 offered to clay increases. As the concentration of PEG2000 or M600 offered to clay increases, step changes occur as the gallery expands from a depleted single layer to a fully loaded single layer and then a bilayer structure. Only intercalated structures are observed for the whole range of complexes prepared from full suspension or sediment after centrifugation. Only intercalated structures with a maximum of a bilayer structure for PEG was also reported by Chen [6.1].

When the amount of PEG2000 offered to clay is 23 wt% or when the amount of M600 offered to clay is 13 wt%, the d-spacings of the films prepared from the sediment (AC film) are lower than those prepared from full suspension (BC film). This indicates that excess PEG2000 or M600 present in the supernatant enters the clay gallery when the films from suspension are dried. At 13 wt% PEG600 and below or 9 wt% M600 and below, no significant differences are observed in the d-spacings between AC and BC films and so indicate that all PEG2000 or M600 is all adsorbed onto clay.

XRD data suggests excess PEG2000 or M600 no longer enters the clay gallery when offered at 50 wt% and above suggesting the clay is fully loaded with little space remaining to accommodate more molecules.

———— Before centrifugation : BC ······ After centrifugation : AC

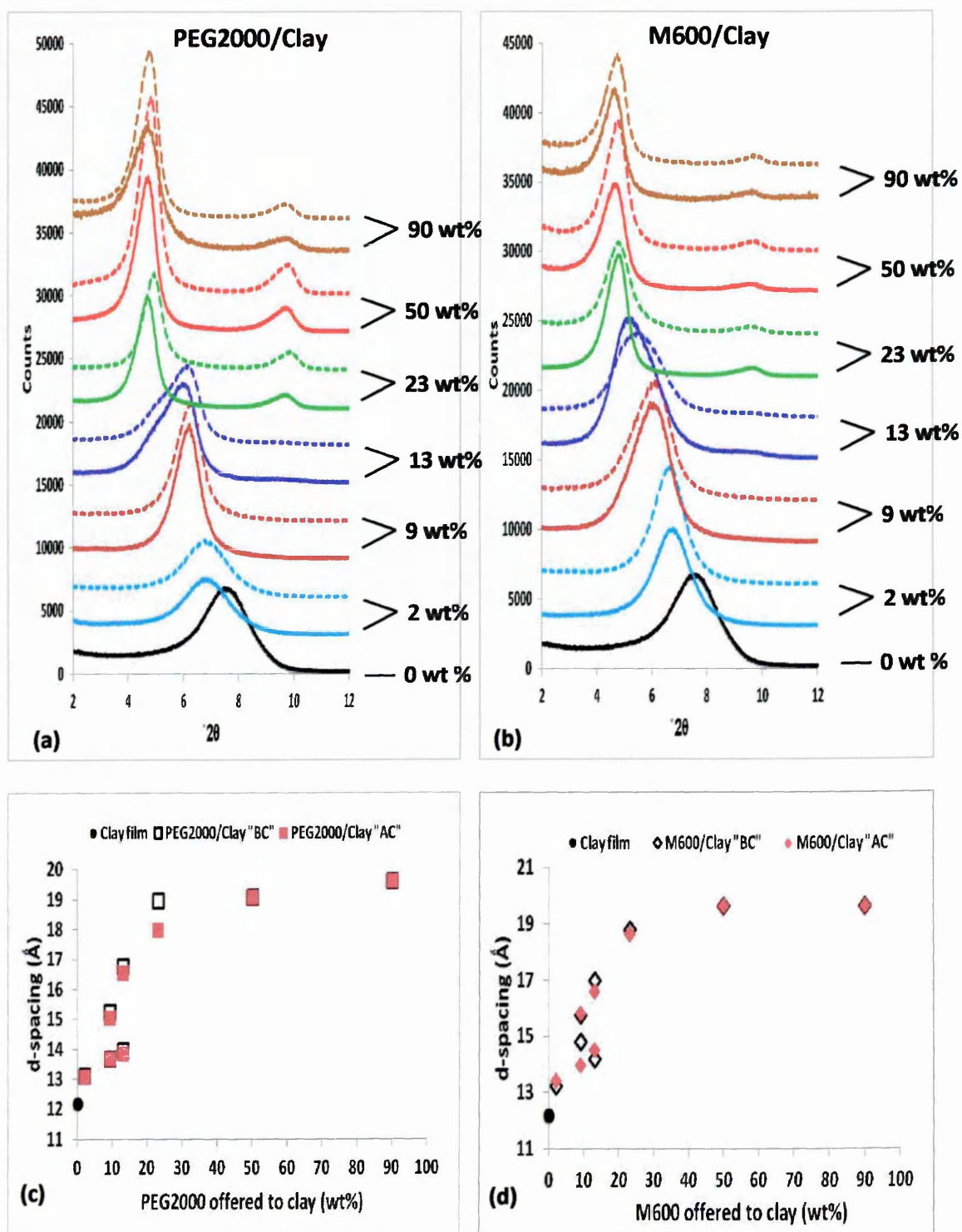


Figure 6.1. XRD patterns of a) PEG2000/clay and b) M600/clay composites prepared from full suspension (full lined traces: BC) or sediment after centrifugation (dashed traces: AC). Their respective d-spacings are plotted against concentration of c) PEG2000 or d) M600

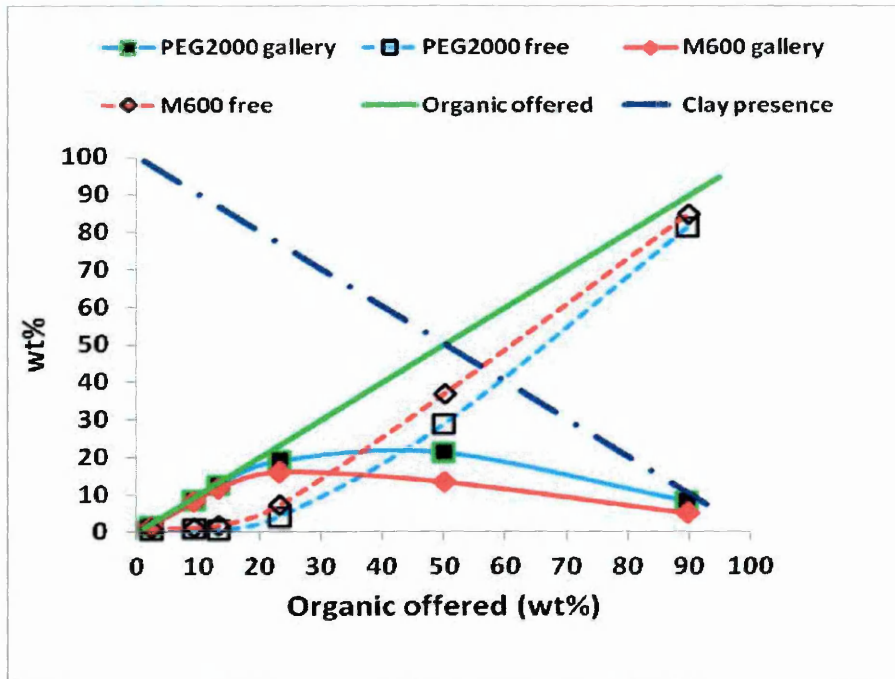


Figure 6.2. Data from adsorption experiment (centrifugation approach) of PEG2000 and M600 onto clay from aqueous solution

Figure 6.2 presents adsorption data of PEG2000 or M600 onto clay from aqueous solution obtained via the centrifugation approach, which shows that most, if not all PEG2000 or M600 is absorbed by clay when offered at 13 wt% or below. This result is supported by XRD data (Figure 6.1), which shows that there is free organic in the supernatant when offered to clay at around 13 wt% for M600 and around 23 wt% for PEG2000. The percentage of free PEG2000 or M600 is higher than that in the gallery when offered at concentrations ~45 wt% and ~33 wt%, respectively. This relates to the observation in XRD traces (Figure 6.1) which suggests free PEG2000 or M600 no longer enters the clay gallery when offered at ≥ 50 wt%. The results show that the amount of PEG2000 adsorbed by clay is higher than that of M600 suggesting that PEG2000 has a higher affinity to clay than M600.

6.2. Comparison of PVOH and plasticizer (PEG600, PEG2000, and M600)

adsorption onto clay in binary systems from aqueous solution

Figure 6.3 compares XRD traces of PVOH/clay and plasticizer/clay composites films prepared from sediment after centrifugation and shows that all structures are intercalated. The highest d-spacings observed in PEG600, M600, or PEG2000/clay composites indicate bilayer structures are present, whilst those for PVOH indicate multilayer structures are present. The d-spacings of PEG600/clay composite systems are generally the lowest, whilst those of PVOH/clay composites are only the highest when loadings are greater than 9 wt%. At 23 wt% and below, the d-spacings of M600 are higher those of PEG2000 and PEG600, but at 50 wt% and above the d-spacings of PEG600, M600 and PEG2000 composites become similar.

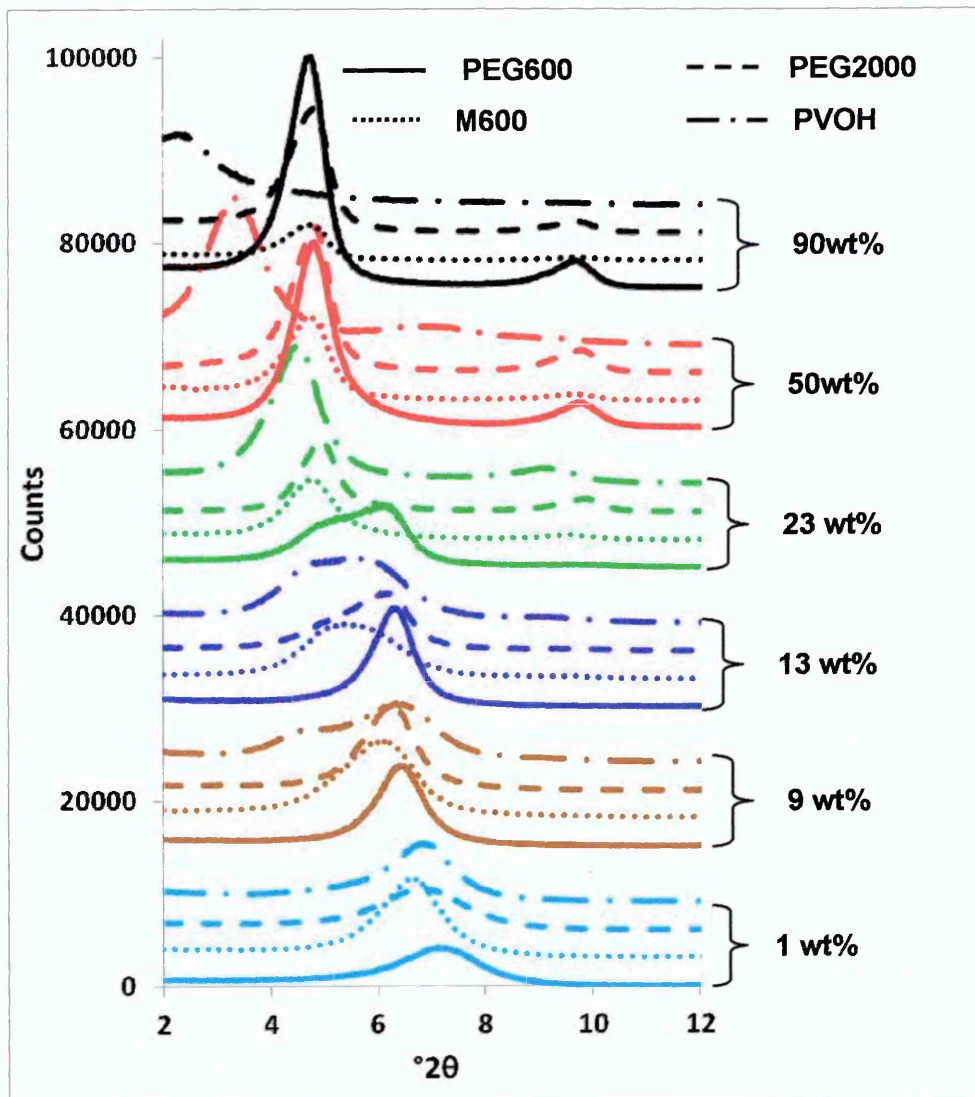


Figure 6.3. XRD traces of organic/clay binary systems for PEG600, M600, PEG2000 and PVOH from films prepared from sediment after centrifugation. Traces are offset for clarity

The amounts of PVOH and plasticizers; PEG600, M600 and PEG2000 adsorbed by clay as a function of organic offered are given in Figure 6.4. They shows that all the PVOH or plasticizers are adsorbed when offered at concentration ≤ 9 wt%. The respective XRD traces, Figure 6.3, show that even though the composites have the same organic loadings, the d-spacings are different. This reflects the differences in how the molecules are arranged within the gallery and will be discussed in more detail later. At all concentrations above 10 wt%, the amounts of PVOH adsorbed by clay are always higher than those of the plasticizers. Also more PEG2000 is adsorbed than M600 and the least

amount adsorbed is always PEG600. These results are not generally reflected in the XRD traces since those of M600/clay complexes show higher d-spacings than those of PEG2000, even though higher amounts of the latter are adsorbed. This again reflects the arrangement of the molecules within the gallery, rather than the amounts adsorbed by the clay. PVOH always shows a higher d-spacing, presumably due to both molecular arrangement and higher amounts adsorbed. The opposite is observed for the PEG600 complexes where the d-spacings of PEG2000 are always higher than those of PEG600. The reason may be due to either PEG2000 having fewer terminal OH groups or the longer chains have a different molecular arrangement and radius of gyration. In summary, PVOH has the highest affinity to clay, followed by PEG2000, then M600 and finally PEG600.

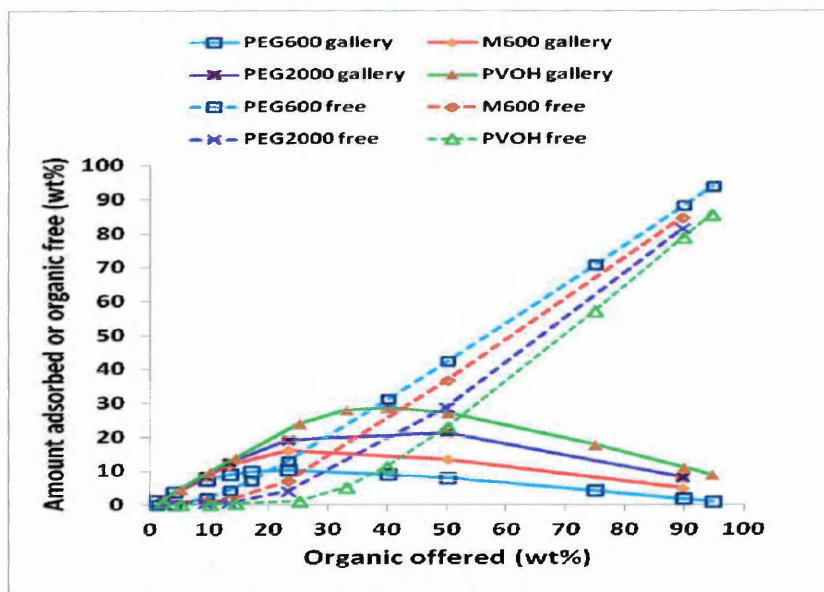


Figure 6.4. Comparison of adsorption data for organic gallery and free organic as a function of organic offered.

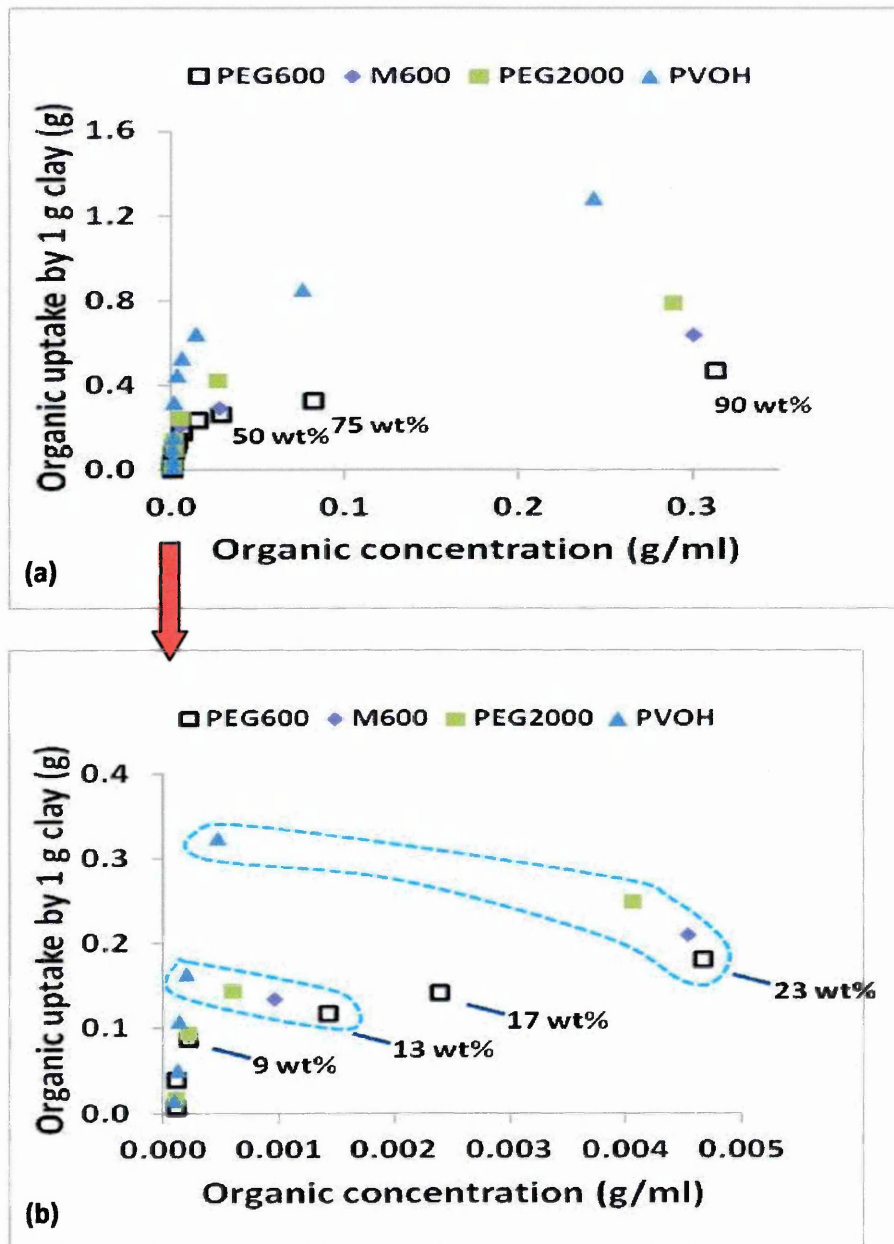


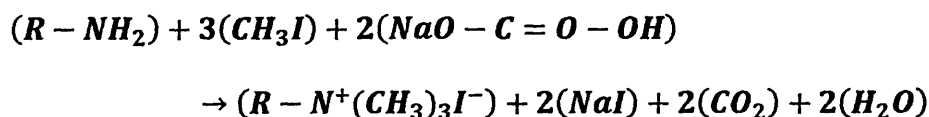
Figure 6.5. Organic uptake by clay as a function of "free organic" concentration ranges up to a) 0.5 g/ml and b) 0.005 g/ml

The adsorption data of PVOH and plasticizers onto clay plotted as a function of free organic concentration (Figures 6.5 a and b) shows Langmuir-type adsorption, since the amount of organic associated with the clay increases sharply as the amount offered increases and then continues to increase gradually as more is offered. Free PVOH is observed at concentrations of 23 wt% and above whilst free plasticizer it is observed at concentrations of 13 wt%

and above. Preferential intercalation of PEG to clay (MMT) was also reported by Parfitt [6.2] who reported that PEG with high molecular weight has a higher affinity to the clay than that of PEG with a lower molecular weight.

6.3. Adsorption of Quaternized M600 (QM600) onto clay from aqueous solution in the absence of PVOH

Quaternization methods of amino PEGs have been described in the literature [6.3-6.5] and the chemical reaction can be stated as follows:



The raw chemicals for the reaction are R-NH₂ (M600), CH₃I (methyl iodide) and NaHCO₃ (sodium bicarbonate). The main product is R-N⁺(CH₃)₃I⁻ (QM600) with by-products NaI (sodium iodide), H₂O (water) and CO₂ (carbon dioxide). The by-product (sodium iodide) was unable to be washed from QM600 using either diethyl ether or hot chloroform. Although the washing procedure was performed the sodium iodide was still present in the main product (QM600) as shown by Na analysis using XRF (3.4 wt% Na₂O) and ICP-MS (performed by Medac Ltd) (2.51 wt%). Therefore, any amount of product (QM600) offered to clay accounted for the by-product. The successful quaternization of M600 was evidenced by NMR and FTIR. The differences in the ¹H NMR spectra of M600 and QM600, highlighted in Table 1, indicated that QM600 had been produced as shown by the disappearance of peaks due to N-H and the appearance of a peak due to protons in the group N-(CH₃)₃. The formation of the N-(CH₃)₃ group appeared in the QM600 sample as a singlet at 3.45 in deuterated chloroform and 3.1 ppm in deuterated water, respectively. There was no evidence in the NMR data to suggest that the intermediate products R-NH(CH₃) or R-N(CH₃)₂

were present, either the reaction went to completion or these were removed during the washing stages. NMR results are supported by FTIR data presented in Figures 6.6 a and b. Figure 6.6 a shows that the N-H stretching bands of M600 (at 3358, 3278 and 3168 cm^{-1}) [6.6] are not clearly present in that of QM600. QM600 is very hygroscopic and so the O-H stretching bands of the associated water make it difficult to confirm the disappearance of the N-H bands, this was also the case when the majority of water was removed by heating the sample to 60 °C. Supporting evidence for the quaternisation reaction is the C-H stretching band from $\text{N}-(\text{CH}_3)_3$ located at 2995 cm^{-1} , which is observed in QM600 and not M600. The intensity ratios of the C-H stretching bands (from CH_3 , CH_2 , O- CH_2) [6.6] do change, but it is not possible to infer the conversion of M600 to QM600 from them. Figure 6.6 b shows i) that the band at 1392 cm^{-1} relating to $-\text{N}(\text{CH}_3)_3$ symmetric bending [6.6] only appears in QM600, ii) the band at 1105 cm^{-1} in M600, which relates to the C-N stretching vibration of the CH-NH_2 group and or C-O anti-symmetric stretching [6.6] is prominent, whilst those are prominent at 1119 and 1078 cm^{-1} in QM600 and iii) the N-H deformation band at 1579 cm^{-1} is present in M600, but not clearly present in QM600.

Table 1. Characteristic chemical shifts in the ^1H NMR spectra of M600 and QM600 when using CDCl_3 or D_2O as solvent

H NMR				
Bruker Avance ^{III} , 400				
	CDCl_3		D_2O	
	M600	QM600	M600	QM600
$\text{N-(CH}_3)_3$	n/a	3.45 (s)	n/a	3.1*
NH_2	expected 1.8-2.8, but no peak ⁺	n/a	Becomes deuterated therefore disappears.	n/a
* observed at 3.65 for the similar α -amino- ω -methoxy-PEGs that were quaternized in Mongondry's paper [6.5].				
⁺ solubility effects were considered the reason for absence of peaks.				

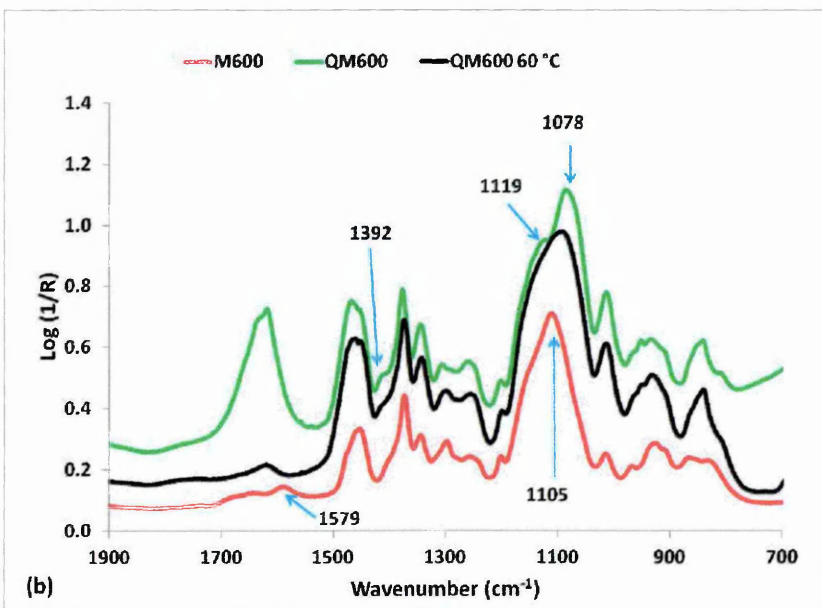
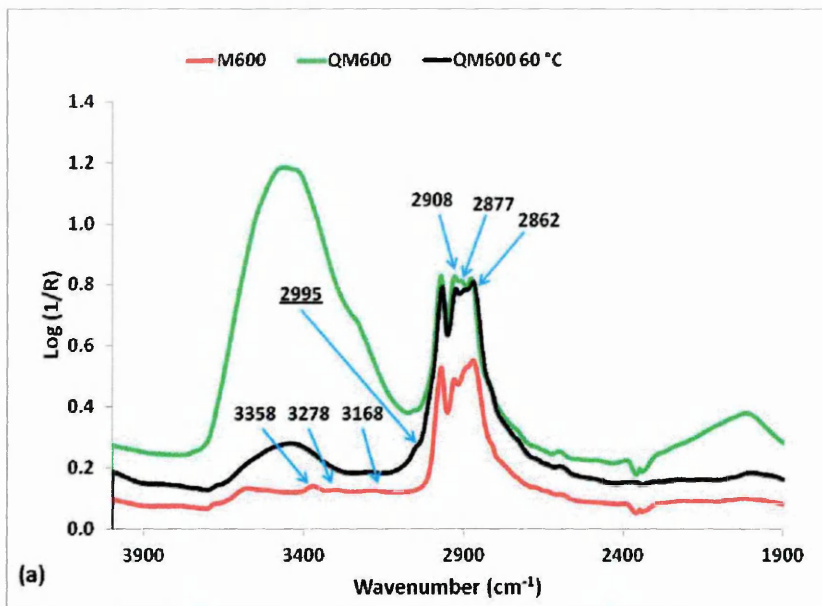


Figure 6.6. FTIR spectra of M600, QM600 and QM600 heated at 60 °C

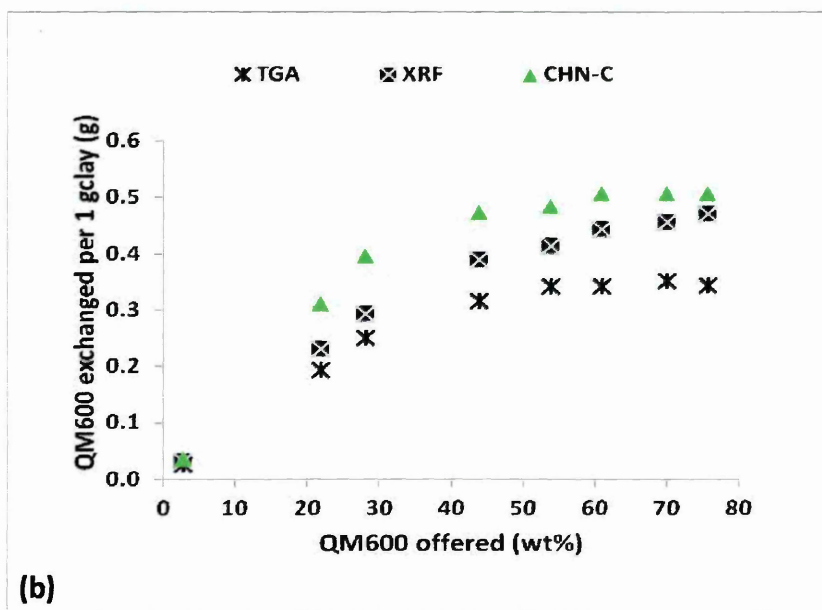
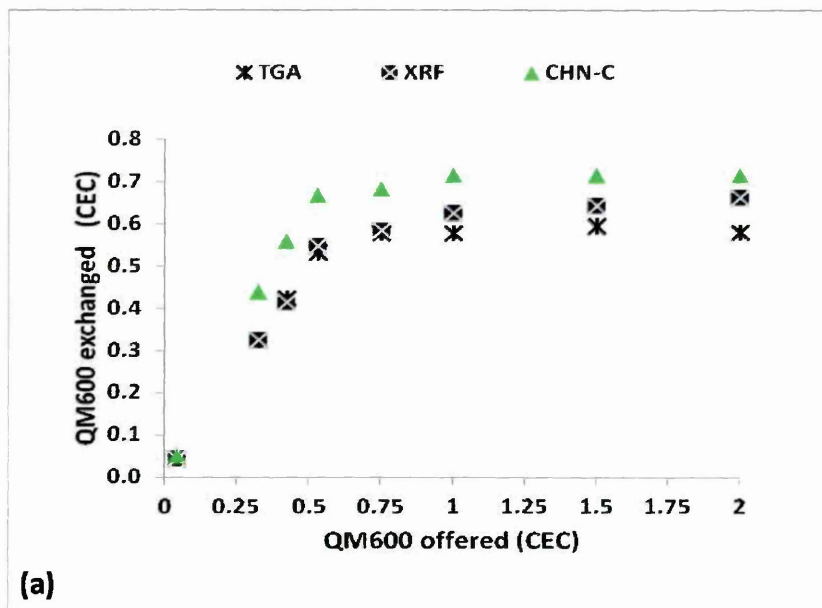


Figure 6.7. Amounts of QM600 exchanged as a function of QM600 offered expressed as CEC (a) and gram/gram of clay (b) and determined by either TGA or XRF measurement.

The amounts of QM600 exchanged on clay as a function of QM600 offered is presented in terms of cation exchange capacity (CEC) and g/g clay in Figure 6.7 a and b, respectively. TGA, XRF and CHN analysis were used to determine the amounts exchanged. XRF determines the amount by differences in Na ion content, TGA by the weight loss in the region due to degradation of QM600 and CHN analysis by determining their relative amounts by combustion analysis and elemental analysers (performed by Medac Ltd). Figures 6.7 a and

b show that the amount of QM600 exchanged increases as the amount of QM600 offered is increased, but levels off when $\sim 0.75 \times \text{CEC}$ or 42 wt% of QM600 is offered. There are discrepancies within each technique used to calculate the amounts adsorbed, due to errors associated with each technique e.g. sensitivity and errors related to unknown water content, but it is accepted that approximately a maximum of about $0.65 \times \text{CEC}$ or 0.43 g/g clay of QM600 is able to be exchanged onto the clay.

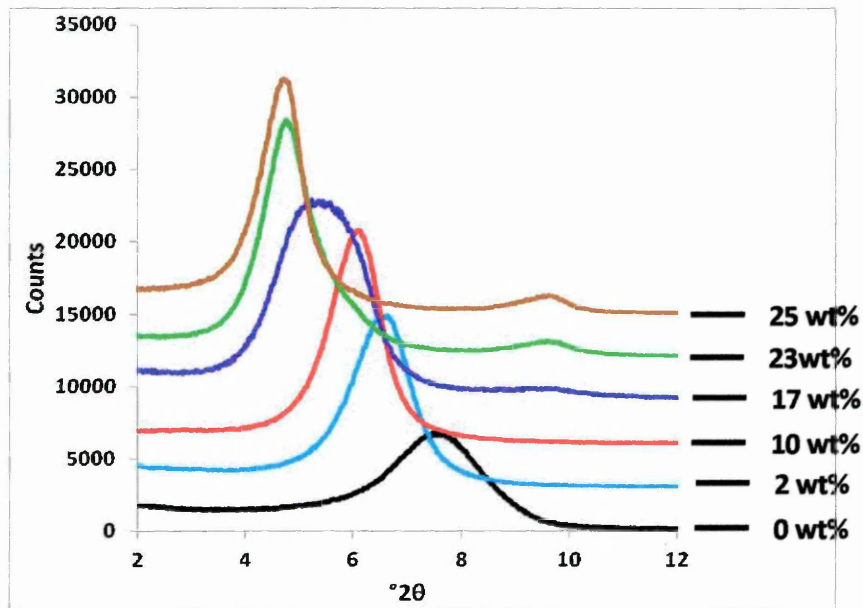


Figure 6.8. XRD patterns of QM600 exchanged clay

XRD traces collected from QM600/clay complexes are presented in Figure 6.8 and show that QM600 has entered the gallery for the whole range of clay loadings. The QM600/clay samples were prepared from aqueous suspensions that had been washed after mixing and are therefore more comparable to previous PEG, M600 and PVOH samples prepared from the sediment after centrifugation. Also, the amounts of QM600 offered to clay are much higher in comparison to the amounts of PVOH and other plasticizers

added. Three steps are observed in the d-spacings as the concentration of QM600 increases, a depleted single layer (at 2 wt%) to a fully loaded single layer (at 10 wt%) and then a bilayer structure (≥ 23 wt%).

6.4. Competitive adsorption of PVOH and M600 onto clay from aqueous solution

Adsorption experiments via a centrifugation approach along with XRD was used to investigate the amounts of PVOH and M600 adsorbed by clay.

6.4.1. Quantification of the amount of PVOH and M600 adsorbed by clay

The amount of M600 adsorbed by clay in the binary suspension systems was calculated by the amount of M600 offered to the clay minus the amount gravimetrically determined in the supernatant (free M600). It is shown in the TGA data of M600, PVOH and M600/PVOH mixtures (Figure 6.9) that the weight loss below 300 °C is predominantly due to PVOH, whereas that above 300 °C is due to M600 and a secondary degradation product of PVOH. If the weight loss of the 1st peak (132-b °C) is plotted against the actual PVOH content a linear relation is noted, which is described in the following equation:

$$y=0.3142x + 44.562 \quad (2)$$

where y is the PVOH content, and x is the weight loss of the first peak (132-b °C). The reason for the starting temperature is fixed at 132 °C as it does not depend on M600/PVOH concentration whilst the end temperature (b) is PVOH and PEG concentration dependent. The end temperature (b) value for each PEG/PVOH mixture is the minimum temperature between the second peak and the third peak. The amount of M600 in the supernatant of the tertiary systems is obtained from the total amount of free organic in the supernatant, which is

determined gravimetrically, minus the amount of PVOH in the supernatant determined by TGA. The relative amounts of M600 and PVOH associated with the clay are then obtained. The above equation has been tested and the error in each determination is less than $\pm 1\%$.

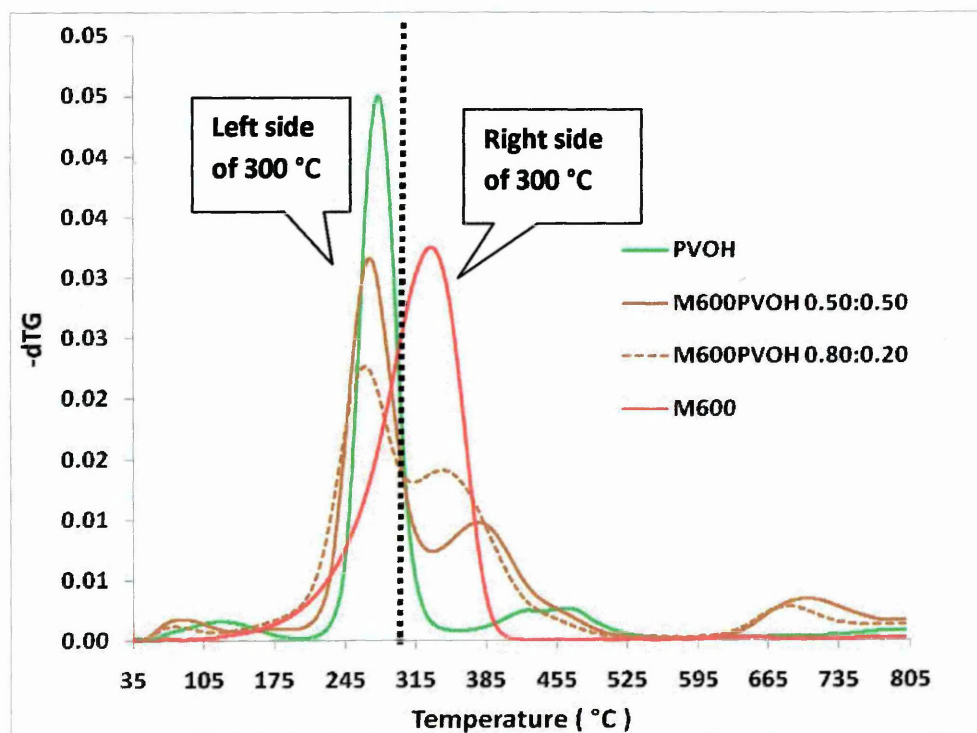


Figure 6.9. DTG's of M600, PVOH and PEG600/PVOH mixtures

6.4.2. Adsorption of PVOH and M600 onto clay from aqueous solution

For the competitive studies, a selected range of M600 (1, 10 and 30 pph) and PVOH (2, 10, 15 and 50 pph) concentrations were offered to clay. The XRD traces and d-spacings are presented in Figures 6.10 a (low M600 concentration; 1pph), 6.10 b (medium M600 concentration; 10 pph) and 6.10 c (large M600 concentration; 30 pph). Only intercalated structures were observed whether prepared from the full suspension or sediment after centrifugation. The amounts of M600 and/or PVOH adsorbed by clay increases with the amount of

M600 and/or PVOH offered as evidenced by the increases in d-spacing, the exception is when PVOH is offered between 2-15 pph at 30 pph M600. When comparing the d-spacings of the tertiary systems with those of the PVOH/clay binary systems (2, 5, 11, 17 and 50 pph PVOH), it shows that they are only slightly higher when the amount of M600 offered is only small (1 pph). When higher amounts of M600 (10 and 30 pph) are offered to clay in the tertiary systems (Figures 6.10 b and c) more significant increases in the d-spacings are observed. These increases are due to both M600 and PVOH being present in the clay gallery.

XRD traces of films from the full suspension are very similar to those from the sediment when the concentration of M600 is 1, 10 and 30 pph and the concentration of PVOH is between 2-15 pph. This suggests little excess M600 or PVOH is present in the supernatant.

Figure 6.10 c shows that the d-spacings of the tertiary systems are only slightly higher than the M600/clay binary system (M600 = 30 pph and PVOH = 0 pph) when the amount of PVOH offered to clay is between 2-15 pph, suggesting that these amounts of PVOH and M600 are not enough to expand the clay gallery. However, significant increase in d-spacing is observed when the amount of PVOH offered is 50 pph.

M600/PVOH/Clay

— Full suspension

..... Sediment

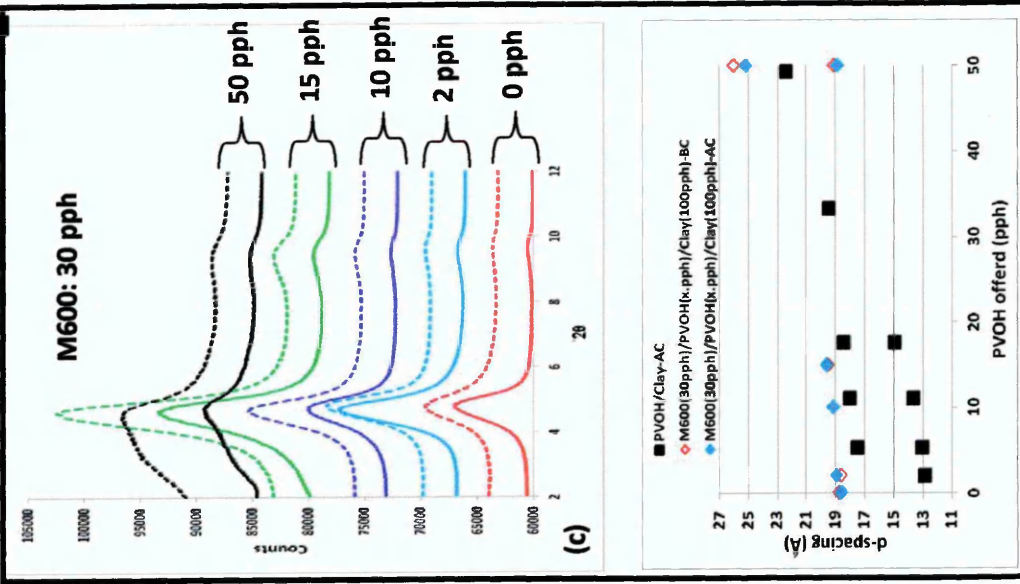
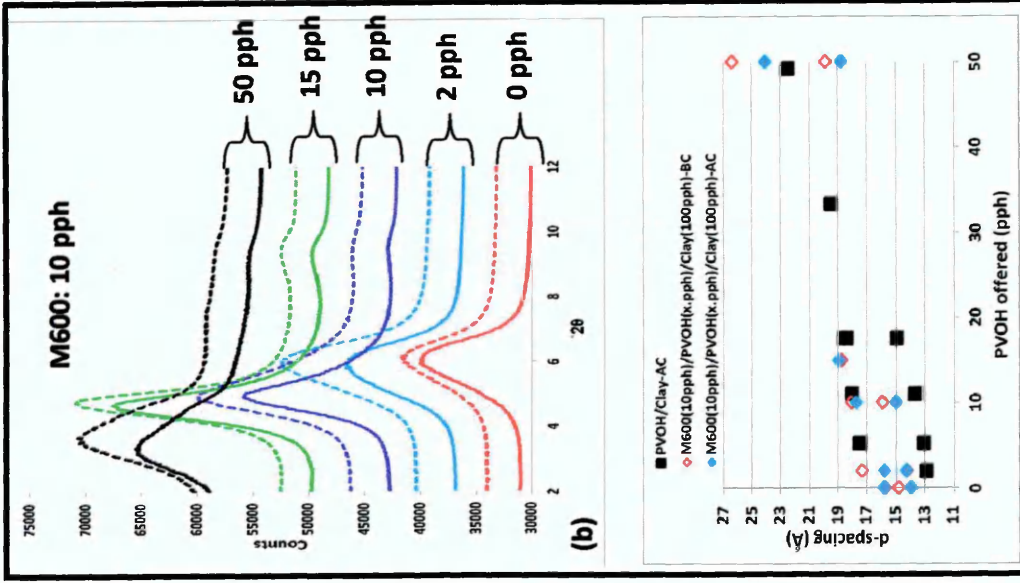
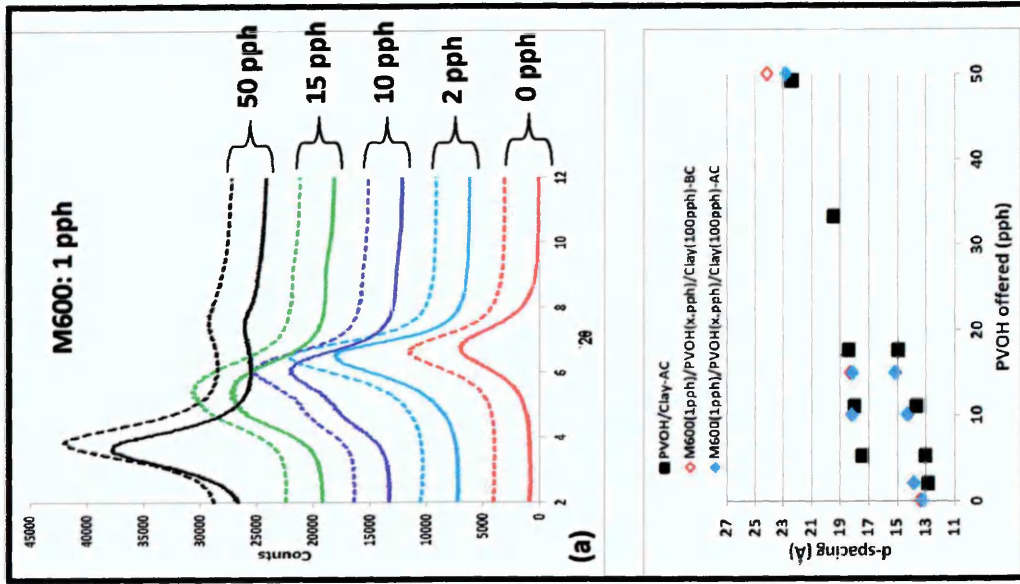


Figure 6.10. XRD patterns and d-spacings of M600/PVOH/Clay nanocomposites prepared from suspension (BC) and from sediment (AC) when amounts of clay is 100 pph and M600 are a) 1 pph, b) 10 pph and c) 30 pph.

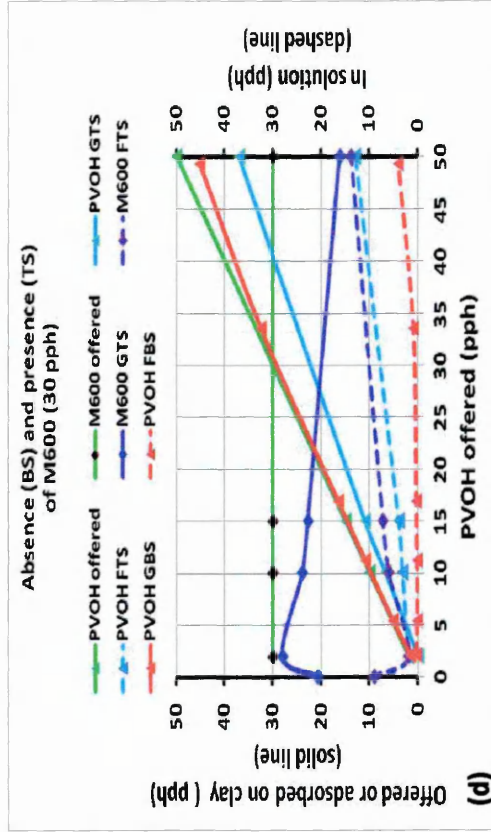
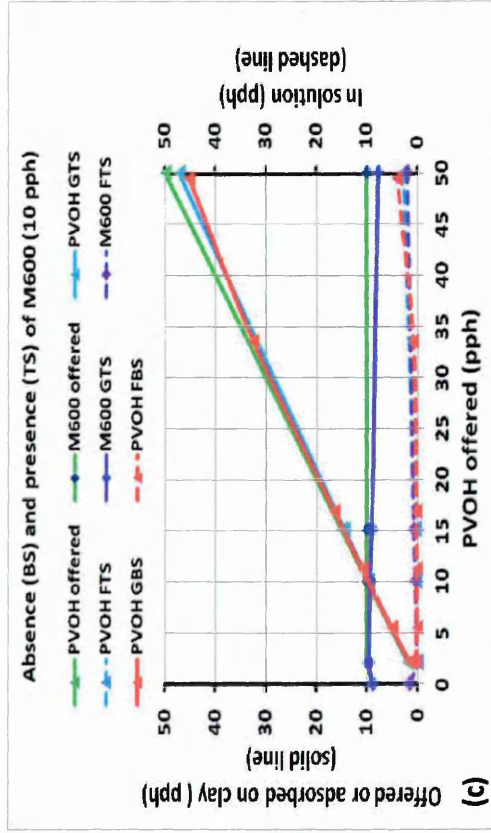
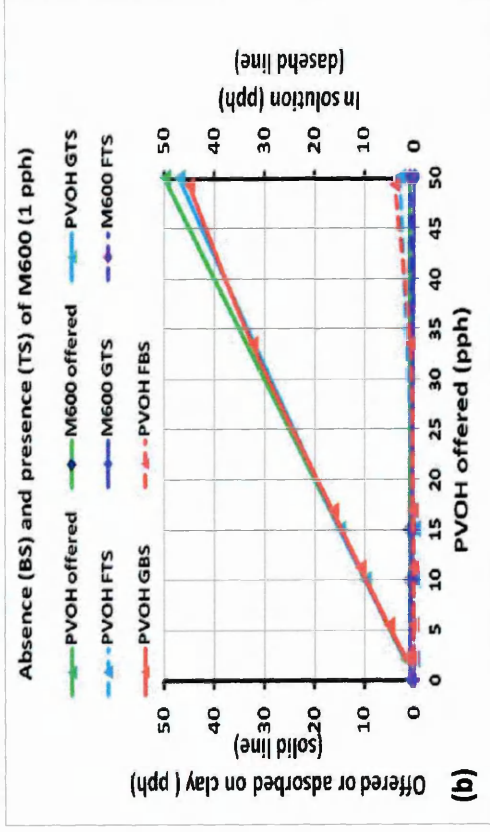
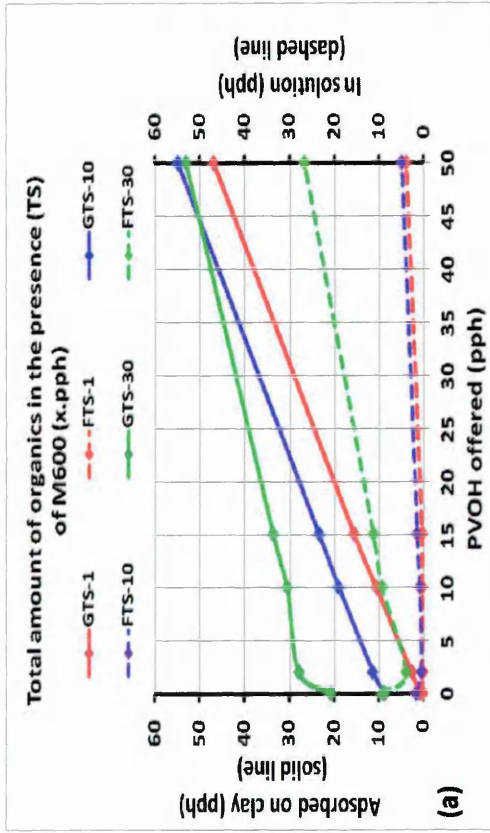


Figure 6.11. Competitive adsorption data of PVOH and M600 onto clay from aqueous solution in tertiary system (TS) (a) and its comparison with PVOH/clay binary system when the amount of M600 is constant; 1 (b), 10 (c), and 30 pph (d)

The combined amounts of PVOH and M600 adsorbed onto clay when the concentration of M600 is fixed at 1, 10 and 30 pph are shown in Figure 6.11 a. In general, the combined amount of PVOH and M600 adsorbed onto clay and that in solution increases as the amount of PVOH or M600 offered to the clay increases. The exception appears to occur when 50 pph PVOH and 30 pph M600 are offered to the clay since the combined amount adsorbed (53 pph) is slightly lower than that when 50 pph PVOH and 10 pph M600 are offered (55 pph). Although the data points for these two experiments are quite similar and perhaps within the error of the experiment, the respective XRD traces presented in Figures 6.11 b and c (after centrifugation) show that on average a larger d-spacing is observed when 10 pph M600 (22.7 Å) is present compared to when 30 pph M600 (21.3 Å) is present indicating more adsorption on the former. It is interesting to note that when the concentration of M600 is constant at 30 pph the excess of total organic reduces when only 2 pph PVOH is offered to clay, showing that PVOH encourages the adsorption of M600. The total organic in solution then increases again when PVOH is offered above 2 pph.

The individual amounts of PVOH and M600 adsorbed on clay when M600 concentration is kept constant at 1, 10 and 30 pph is shown in Figures 6.11 b, c and d, respectively. When the amount of M600 is fixed at 1 pph (Figure 6.11 b) the amount of PVOH adsorbed is very similar to that offered and only begins to slightly deviate (i.e. less is adsorbed by clay) at concentrations greater than 35 pph; only 4 pph PVOH are in solution when 50 pph PVOH are offered. Most, if not all, of the M600 is absorbed by the clay and so any organic present in solution is due to PVOH.

The amounts of PVOH adsorbed onto clay are very similar when the amount of M600 is fixed at either 1 or 10 pph (Figure 6.11 b and c, respectively).

In the tertiary systems most of the M600 is adsorbed when offered at a concentration of 10 pph; at 15 and 50 pph PVOH only 1.5 and 3 pph M600 remains in solution, respectively, which is similar to that of PVOH alone. Also, the amounts of PVOH adsorbed in the presence of 1 and 10 pph M600 are very similar with those in the absence of M600, the amounts of PVOH in solution only begin to be observed at concentrations greater than 35 pph.

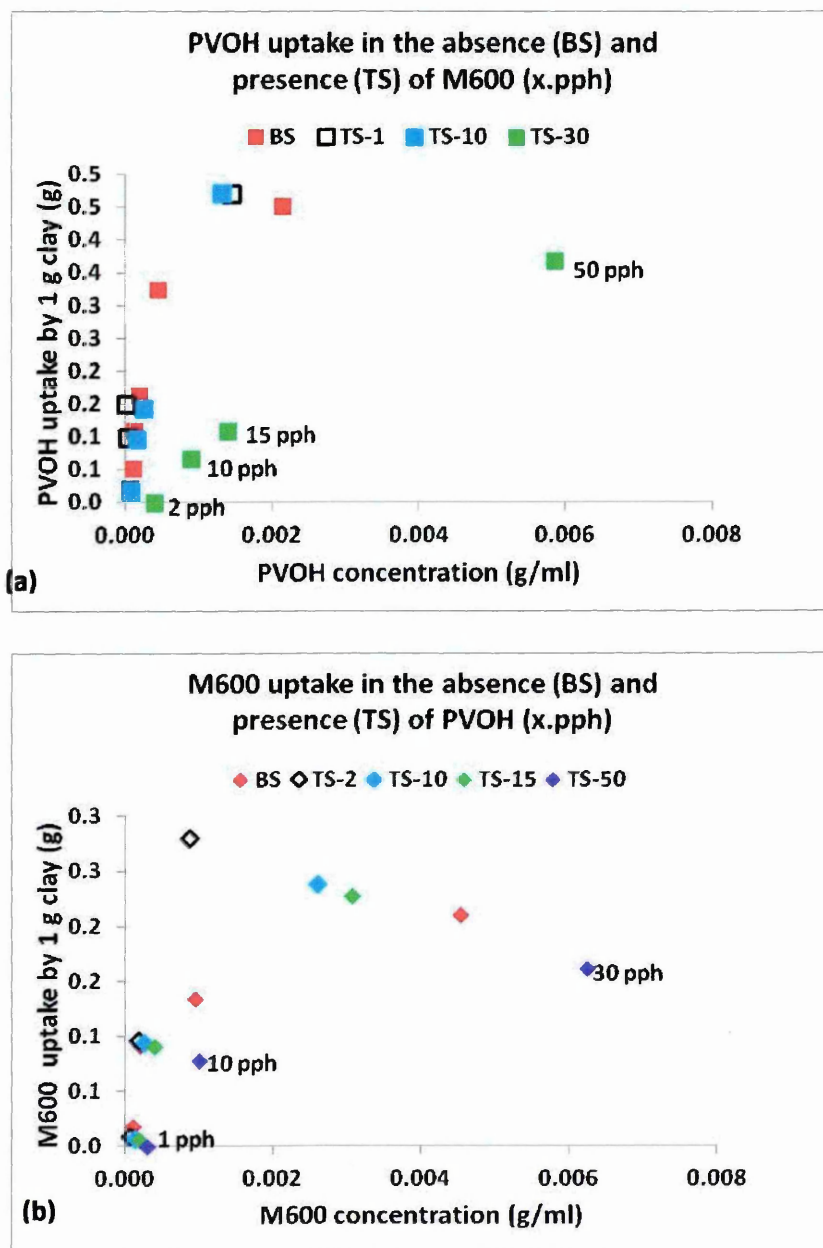


Figure 6.12. Competitive adsorption data of M600 and PVOH onto clay from aqueous solution. TS represents the tertiary systems, whereas BS represents the binary systems, the associated numbers represent the concentrations of PVOH or M600 offered.

When 30 pph M600 (Figure 6.11 d) is offered in the tertiary system the amounts of PVOH adsorbed are greatly reduced, when 50 pph PVOH is offered 12 pph PVOH remain in solution. The amount of M600 adsorbed by clay in the presence of PVOH is higher than in the absence of PVOH when PVOH offered is below 20 pph, only a small amount of PVOH (2 pph) is required to entice the M600 onto the clay. At higher concentrations of PVOH (>20 pph) the portion of the 30 pph M600 adsorbed by clay, relative to the binary system, is reduced such that 15 pph M600 remain in solution when 50 pph PVOH is offered.

The same competitive adsorption data of M600 and PVOH on clay is given in Figure 6.12 a and b, but presented as a function of "free organic" concentration. Generally, the amount of PVOH or M600 adsorbed by clay increases with increasing amount PVOH or M600 offered. The amount of PVOH adsorbed is not affected significantly when M600 is present at 1 and 10 pph, but does decrease considerably when the amount of M600 offered is 30 pph. When M600 is present at 30 pph a certain amount of PVOH is needed before it is adsorbed onto clay since no PVOH is absorbed when offered at 2 pph (Figure 6.12 a), this amount is between 2 and 10 pph PVOH.

6.5. Adsorption of PVOH onto cation-exchanged QM600-clay

The adsorption of PVOH (2, 10, 15, 50 and 90 pph) on clay that has been modified with different amounts of QM600 (2, 10 and 30 pph) has been investigated. The concentrations of QM600 (2, 10 and 30 pph) refer to the amounts exchanged after washing and were derived from TGA, XRF and CHN analysis, they equate to modifications equal to 0.04, 0.32 and 0.42 x CEC, respectively (Figure 6.7). The XRD traces and corresponding d-spacings are presented in Figure 6.13 a (low QM600 concentration 2 pph), Figure 6.13 b

(medium QM600 concentration 10 pph) and Figure 6.13 c (large QM600 concentration 30pph). All composites prepared from either the full suspension or sediment showed intercalated structures. The increases in d-spacings suggest that the amounts of PVOH adsorbed on QM600/clay increase as the amount of PVOH offered is increased.

Figure 6.13 a shows that the d-spacings increase significantly when QM600 is present at 2 pph when compared to those in its absence showing that the immobility of QM600 in the clay gallery promotes the adsorption of PVOH within gallery. The replacement of sodium cations and their hydrated shells by QM600 presumably makes the gallery more hydrophobic and thus a more attractive environment for the PVOH. It needs to be emphasised that XRD only indicates the amount of organic adsorbed in the gallery and not the total amount adsorbed since organic material can adsorb at the edges of clay layers, and also at the top and bottom of clay stacks.

Lower d-spacings are only observed in films prepared from sediment, when compared to those from suspension, when the concentration of QM600 is 2 pph QM600 and that of PVOH is between 2-90 pph Figure 6.13 a) and also 10 pph QM600 and between 2-90 pph PVOH (Figures 6.13 b) suggesting that excess PVOH in the supernatant enters the clay galley when the films are dried. With 10 pph QM600, little difference in d-spacings are observed between films prepared from full suspension and sediment at PVOH concentrations of 50 and 90 pph suggesting that little excess PVOH is present.

QM600/PVOH/Clay

— Full suspension

..... Sediment

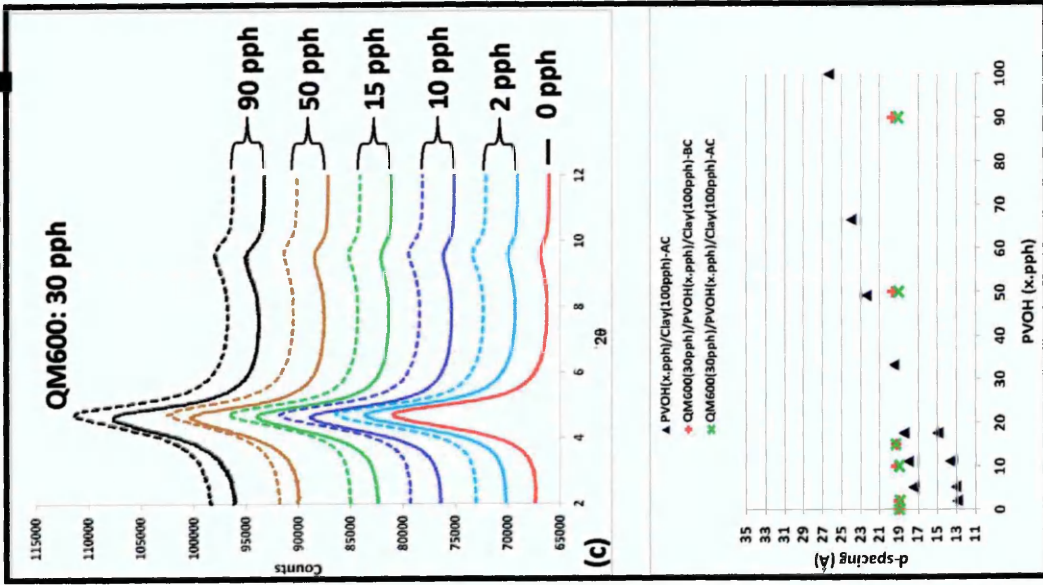
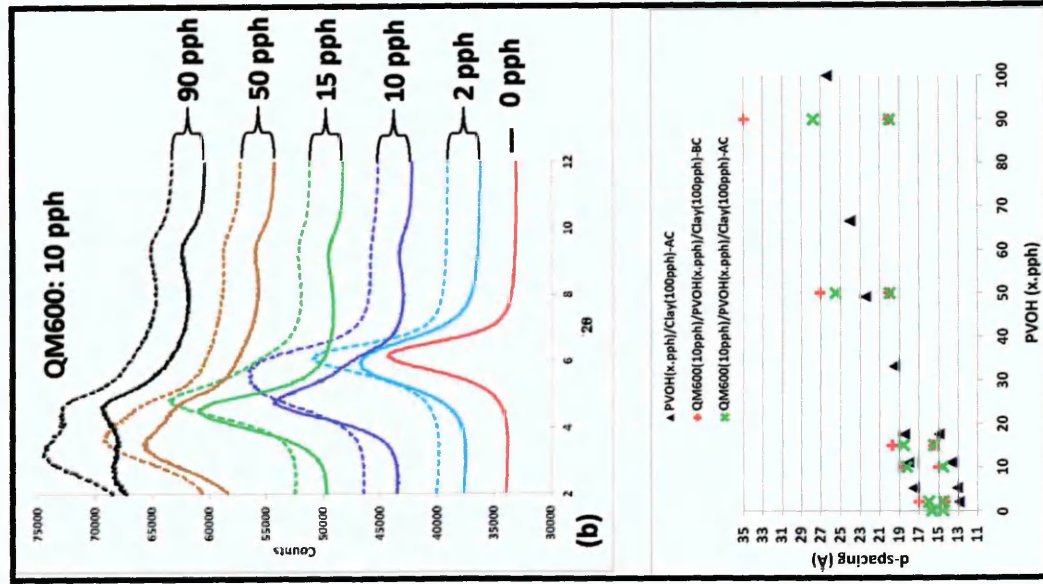
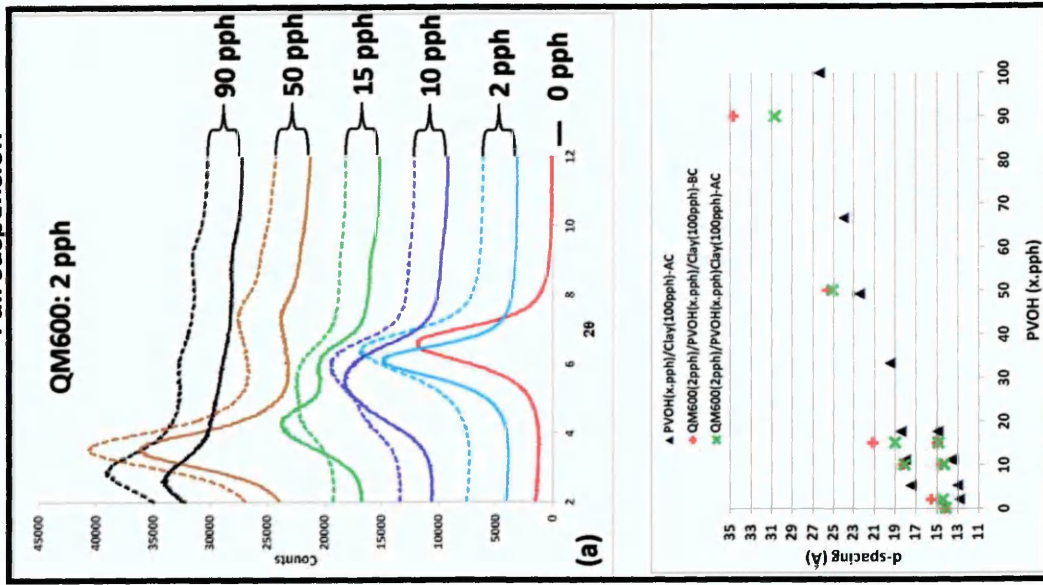


Figure 6.13. The XRD patterns and d-spacing of QM600/PVOH/Clay composites where the amount of clay is 100 pph and QM600 is constant, i.e. a) 2, b) 10 pph and c) 30 pph, respectively prepared from suspension (BC) and from sediment (AC)

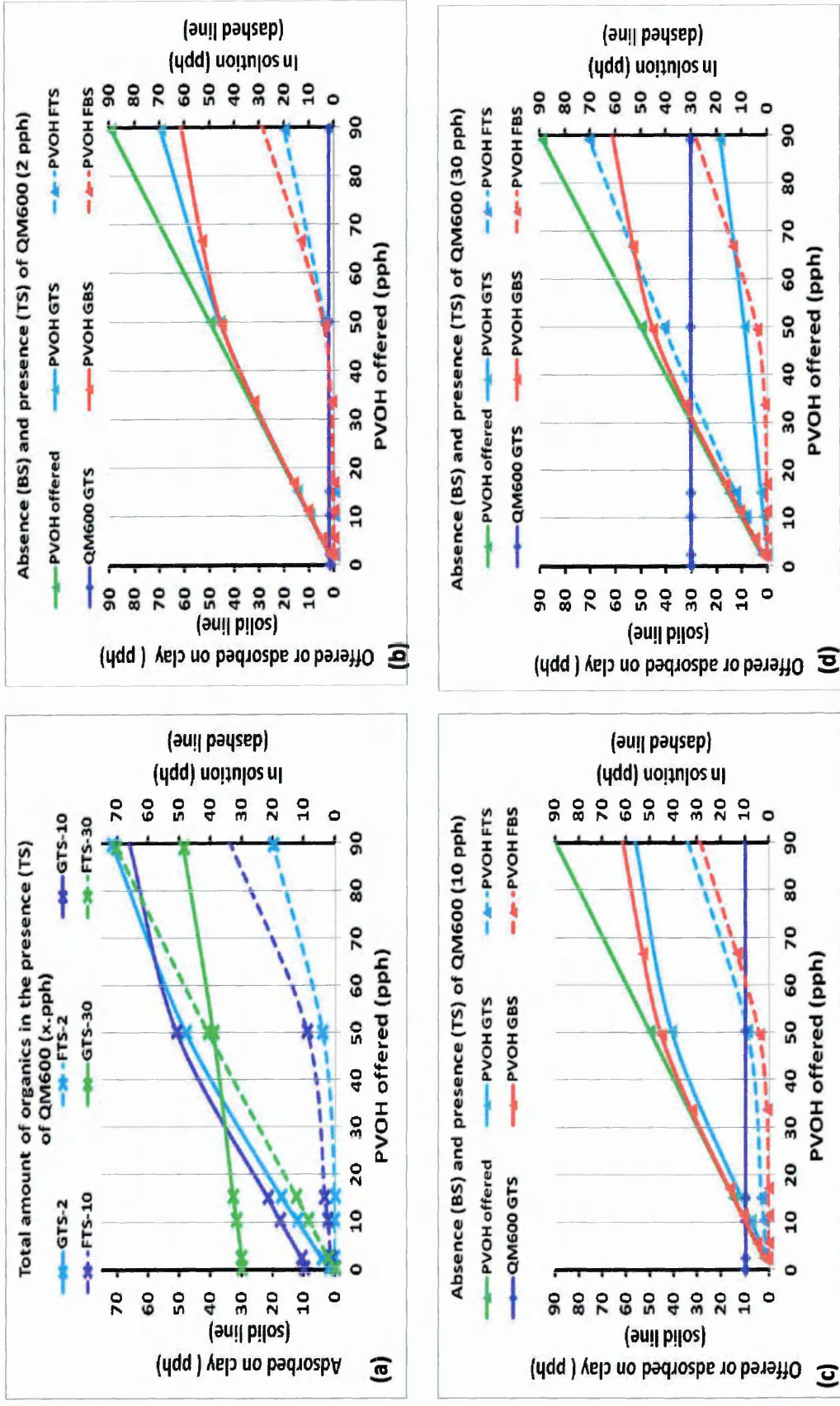


Figure 6.14. Adsorption of PVOH onto clay from aqueous solution in the presence of QM600 (a) and its comparison with binary system (BS) when the amount of QM600 is constant; 2 (b), 10 (c), and 30 pph (d)

No differences in d-spacings between films prepared from full suspension and sediment were observed when 30 pph QM600 and 2-90 pph PVOH were present (Figure 6.13 c) suggesting that QM600 is the dominant phase in the clay gallery, this is not too surprising since it is anchored in position. It suggests that the presence of 30 pph QM600 creates a gallery that is difficult for PVOH to enter the gallery, which may be due to strong interactive forces created by the QM600 in the gallery keeping the silicate layers together or it creates a too hydrophobic environment for the PVOH to enter. A balance between the amount of QM600 and PVOH present may need to be met in order for gallery expansion to be greater than 20 Å.

The combined total amounts of PVOH and QM600 adsorbed on clay which have been modified with constant amounts of QM600, i.e. 2, 10 and 30 pph are shown in Figure 6.14 a. In general, the combined amounts of PVOH and QM600 adsorbed onto clay and that in solution increase as the amount of PVOH is increased and QM600 kept constant. Up to a concentration of 50 pph PVOH, the highest amount of total organic adsorbed occurs when 10 pph QM600 is present, whereas the least occurs when 30 pph QM600 is present. When PVOH is present at a concentration of 90 pph and QM600 is present 2 pph the combined amount adsorbed (72 pph) is higher than those when 10 and 30 pph QM600 are offered (66 and 49 pph, respectively). This is reflected in the respective XRD traces presented in Figure 6.13 a, b and c (after centrifugation), which show that a larger d-spacing at 90 pph PVOH is observed when 2 pph QM600 (30.7 Å) is present compared to when 10 pph QM600 (average d-spacing of 26.9 Å) and 30 pph QM600 (19.1 Å) indicating more adsorption on the former.

The individual amounts of PVOH adsorbed during the competitive adsorption of PVOH in the absence and presence of 2, 10 and 30 pph QM600 are shown in Figures 6.14 b, c and d, respectively. When the amount of QM600 is fixed at 2 pph (Figure 6.14 b) the amounts of PVOH adsorbed are very similar to those offered as the concentration of PVOH is increased, but deviates at concentrations greater than 35 pph; 20 pph PVOH are in solution when 90 pph PVOH are offered. The amount of PVOH adsorbed in the presence of 2 pph QM600 is greater than that in the absence of QM600 when PVOH concentration is greater than 50 pph showing that the presence of QM600 promotes the adsorption of PVOH onto clay.

When the amount of QM600 is fixed at 10 pph (Figure 6.14 c) the amount of PVOH adsorbed is less than that in the absence of QM600; 33 pph PVOH are in solution when 90 pph PVOH are offered in the presence of QM600, but only 27 pph in its absence. The amount of PVOH adsorbed, when offered at 90 pph is also reduced from 70 to 57 pph when the presence of QM600 is increased from 2pph to 10 pph.

When the amount of QM600 is fixed at 30 pph (Figure 6.14 d) the amounts of PVOH adsorbed are less than when QM600 is fixed at 2 or 10 pph and considerably less when in the absence of QM600. PVOH concentration in solution is greater than those adsorbed on clay. The amount of PVOH adsorbed is greatly to 20 pph when QM600 is present 30 pph.

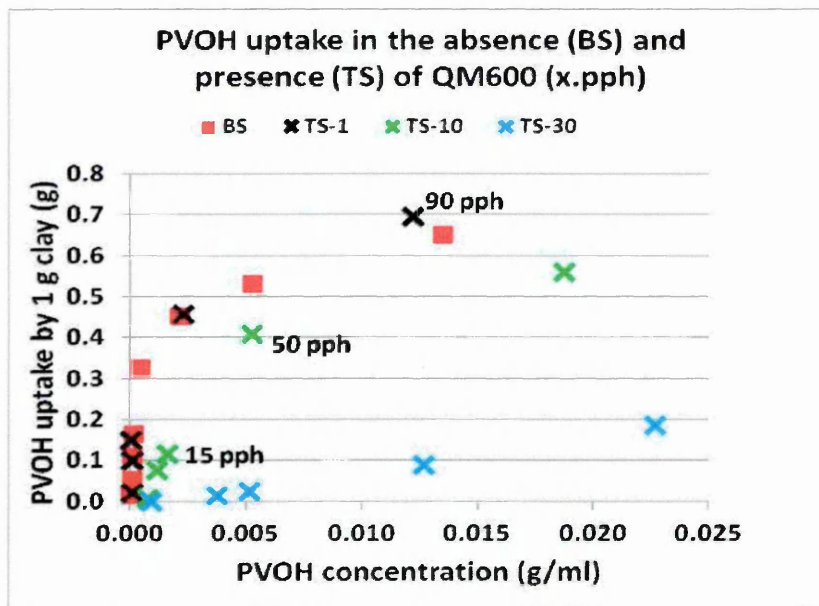


Figure 6.15. Competitive adsorption of PVOH onto clay from aqueous solution in the present of QM600 (tertiary system-TS) and its comparison with that in the binary system (BS).

The same adsorption data of PVOH on clay in the absence (binary system) and presence of QM600 (tertiary system), but presented as a function of “free organic” concentration is given in Figure 6.15. Generally, the amount of PVOH adsorbed by clay increases with increasing amount of PVOH offered. The amount of PVOH adsorbed on clay in the tertiary system is lower than that in the binary system when QM600 is present at 10 pph and 30 pph, whereas it is similar when QM600 is present at 2 pph, the exception is when 90 pph PVOH is present which shows a higher amount of PVOH adsorbed.

6.6. Comparison of PVOH adsorption from aqueous solution in the presence of PEG600, M600 and QM600

Several XRD traces of PEG600/PVOH/clay, M600/PVOH/clay and QM600/PVOH/clay films prepared from sediment after centrifugation are presented in Figures 6.16 a, b and c, respectively. Figure 6.16 a shows that when small amounts of plasticizer (PEG600 and M600 = 2pph and QM600 = 1 pph) are mixed with PVOH and clay the highest d-spacings are always

pph) are mixed with PVOH and clay the highest d-spacings are always observed with QM600. Figure 6.16 b shows that with medium amounts of plasticizer (10 pph) and PVOH amounts of 2-15 pph the highest d-spacings are observed with M600, followed by QM600 and then PEG600, but when the amounts of PVOH offered are between 50-90 pph, the highest are observed with PEG600, followed by QM600 and then M600. Figure 6.16 c shows that with high amounts of plasticizer (30 pph) and PVOH amounts of 2-10 pph the highest d-spacings are observed with M600, followed by QM600 and then PEG600, but when the amount of PVOH offered is 15 pph similar d-spacings are observed with QM600 and PEG600 and that these are higher than with M600.

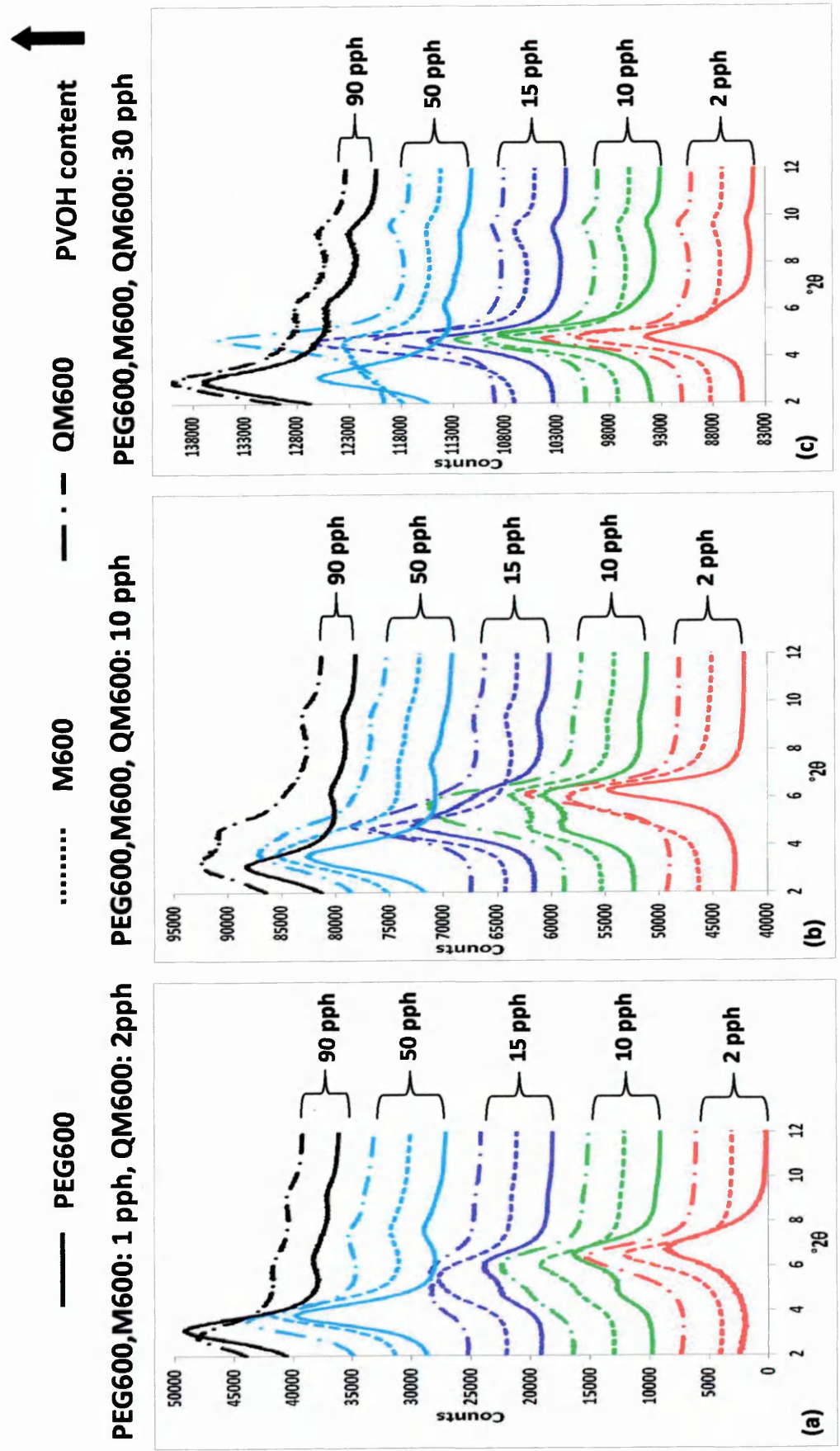


Figure 6.16. Comparison of XRD traces from PEG600/PVOH/clay, M600/PVOH/clay and QM600/PVOH/clay films prepared from sediment (AC films). The amounts of PEG600 and M600 are fixed at 1pph and that of QM600 at 2 pph in a) all plasticizer concentrations are fixed at 10 pph in b) and 30pph in c).

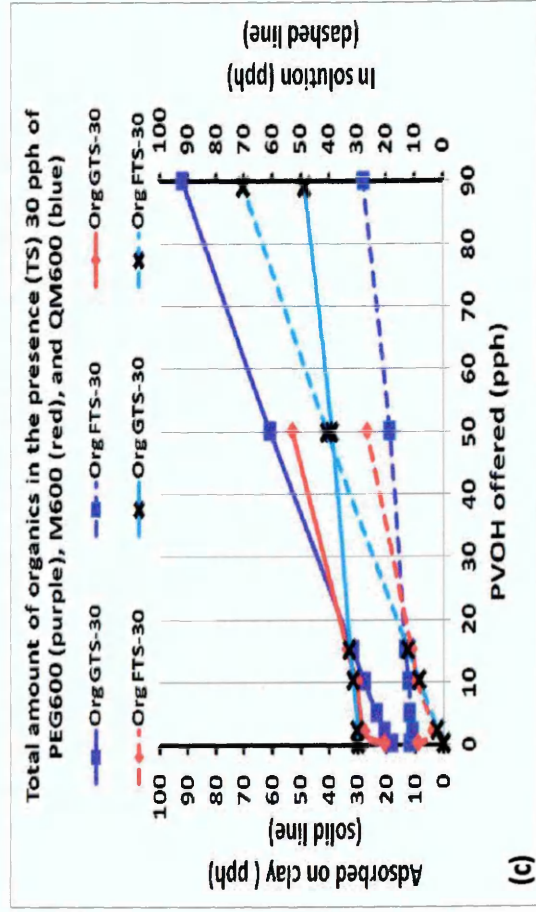
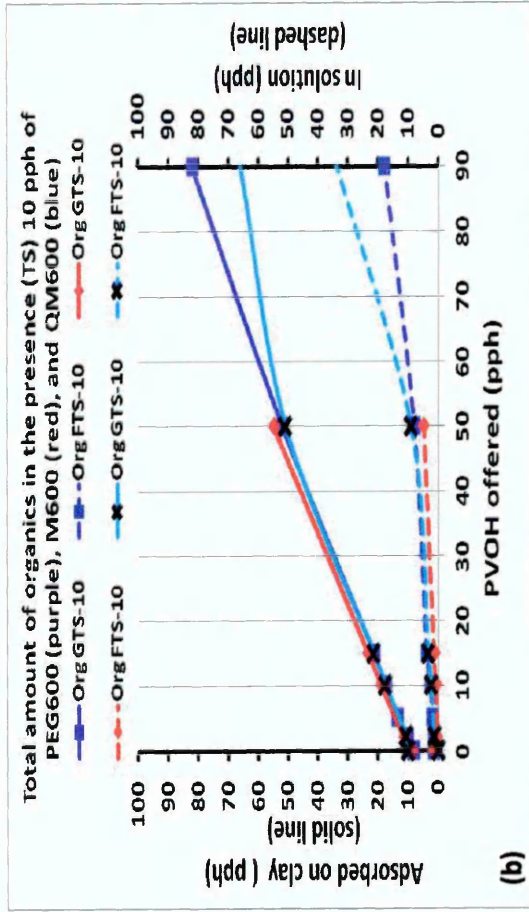
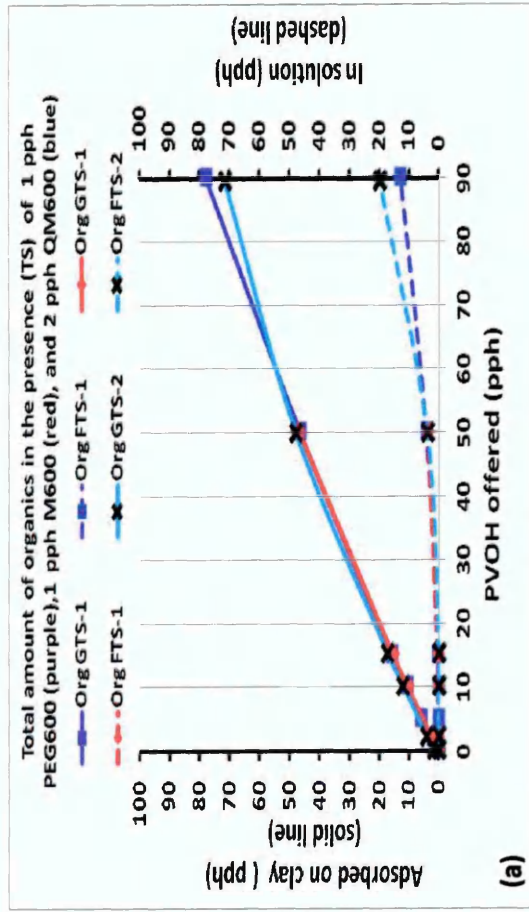


Figure 6.17. Comparison of the combined amounts of PVOH and plasticizer adsorbed onto clay from aqueous solution in the presence of fixed amounts of PEG600, M600, and QM600 i.e. a) 1 pph for PEG600 and M600 and 2 pph for QM600, b) 10 pph and c) 30 pph

Figures 6.17 a, b and c show that the combined amounts of PVOH and plasticizer adsorbed on clay increase with increasing amount of PVOH offered when the amount of each plasticizer remains constant. The combined amounts of PVOH and plasticizer adsorbed on clay are very similar when the concentration of PEG600, M600 or QM600 is ≤ 10 pph and the amount of PVOH is ≤ 50 pph (Figure 6.17 a and b). However, when the amount of PVOH offered is 90 pph the combined amount of PVOH and PEG600 is greater than that of PVOH and QM600; i.e. 79 pph are observed when the amount of PEG600 is 10 pph, whereas only 67 pph are adsorbed with 10 pph QM600. Figure 6.17 c shows that when the plasticizer concentration is fixed at 30 pph and the amount of PVOH offered is below 12 pph the combined amounts of PVOH and plasticizer adsorbed by clay are lower in the presence of PEG600 than those in the presence of M600 or QM600, but higher when the amount of PVOH offered is above 12 pph.

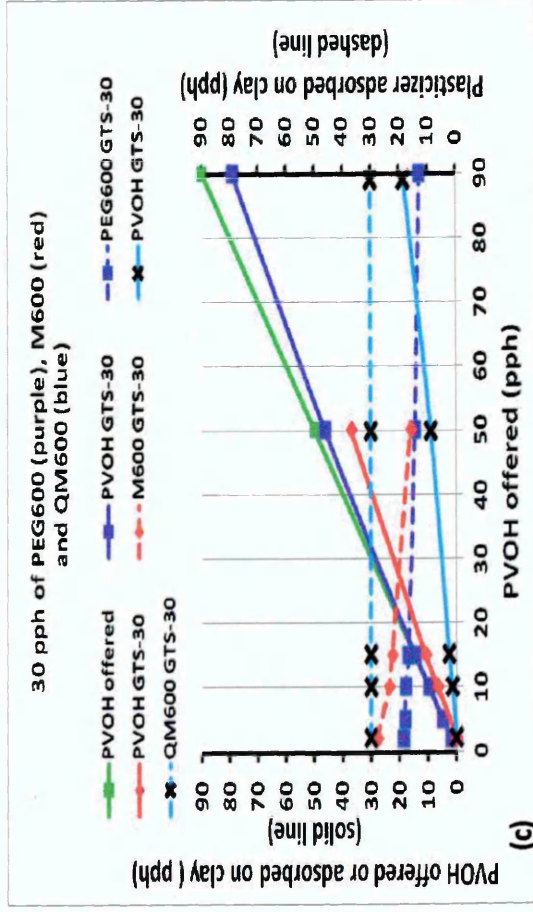
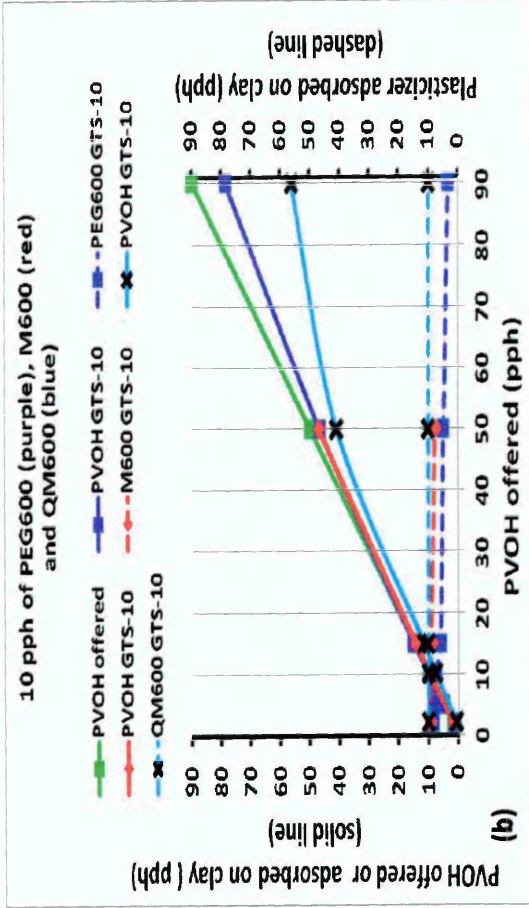
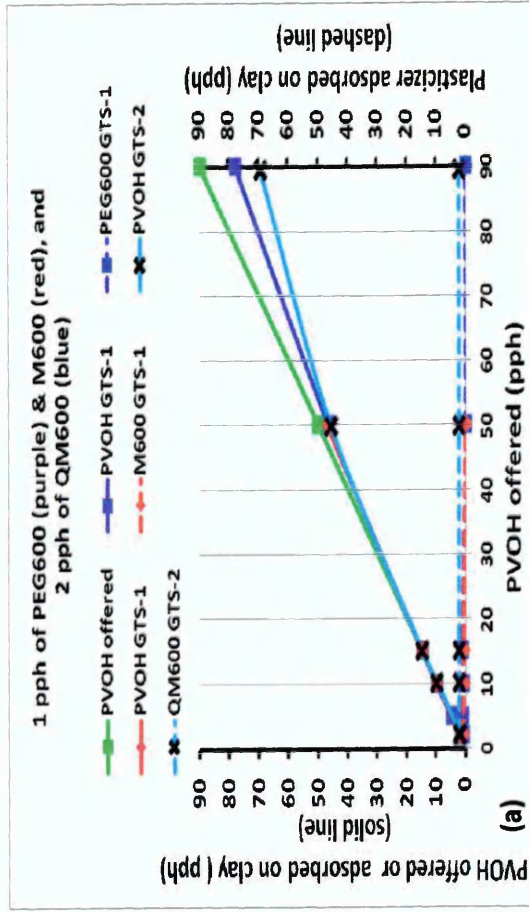


Figure 6.18. Competitive adsorption data of PVOH and plasticizer onto clay from aqueous solution in the presence of fixed amounts of PEG600, M600, and QM600 i.e. a) 1 pph for PEG600 and M600 and 2 pph for QM600, b) 10 pph and c) 30 pph. The amounts in solution are not presented.

Further explanation of the data in Figure 6.17 is given in Figure 6.18, which presents the individual amounts of PVOH and plasticizer (PEG600, M600 and QM600) adsorbed by the clay. The amounts in solution are not presented. The data shows that more PVOH is adsorbed by clay when PEG600 is present and that PEG600 is the lowest amount of plasticizer adsorbed by clay in the presence of PVOH.

Figure 6.18 a shows that when PVOH offered is ≤ 15 pph its adsorption by clay is not affected by the presence of small amounts of plasticizers (1 pph PEG600, 1 pph M600 or 2 pph QM600) and the amount adsorbed only decreases from that offered when at concentrations higher than ~ 50 pph. When PVOH offered is 90 pph, the amount of PVOH adsorbed is higher in the presence of 1 pph PEG600 (i.e. 79 pph) than 2 pph QM600 (i.e. 70 pph). The amounts of plasticizer at these low levels that are adsorbed by clay are very similar since most, if not all, is adsorbed in the PVOH range of 2-90 pph.

Figure 6.18 b shows that when the amounts of PVOH offered are ≤ 50 pph the amounts of PVOH adsorbed by clay are similar in the presence of 10 pph PEG600 or M600, and less in the presence of 10 pph QM600.

Figure 6.18 c shows that with high plasticizer concentrations (30 pph) the amounts of PVOH adsorbed by clay are quite different, with respect to each plasticizer, even when PVOH is offered at ≤ 15 pph. The amount of PVOH adsorbed in the presence of QM600 is considerably lower than that in the presence of PEG600 or M600. A noticeable difference is also observed between the amounts of PEG600 and M600, in which more PVOH is adsorbed in the presence of PEG600.

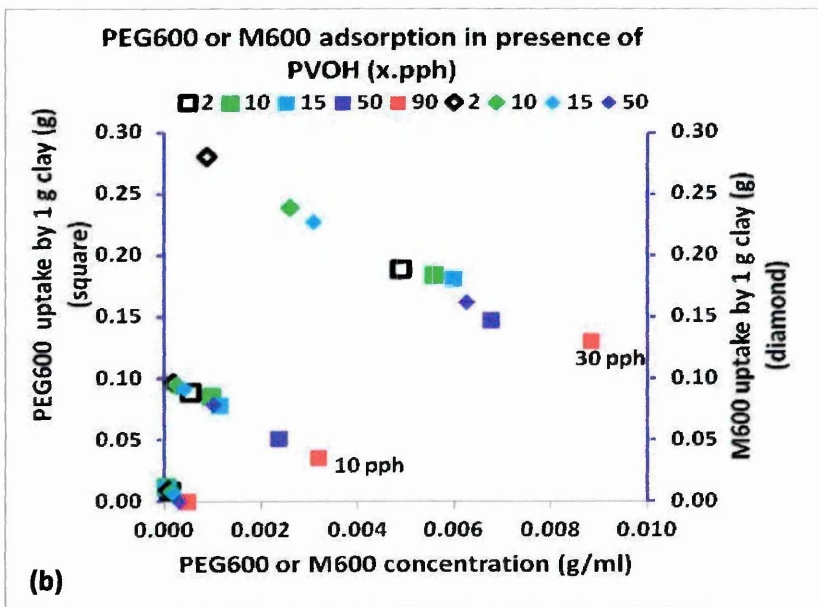
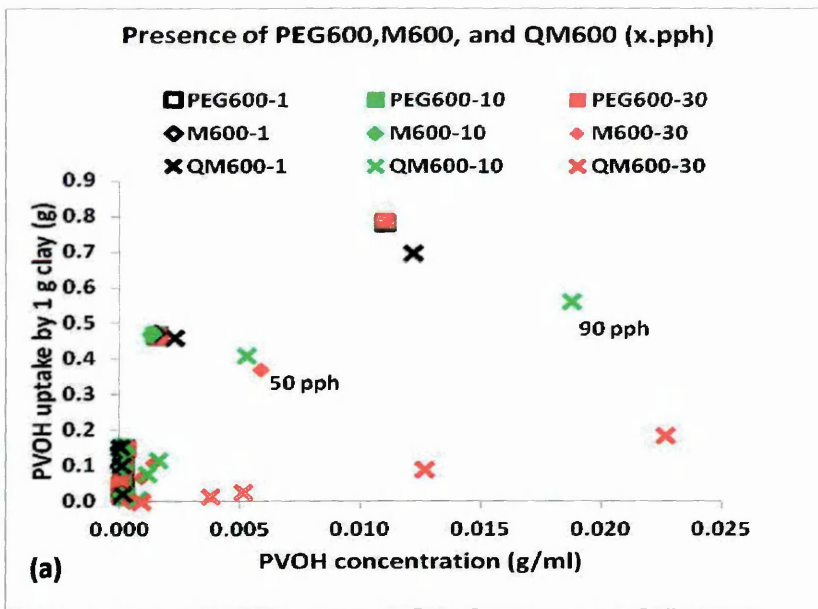


Figure 6.19. Adsorption data of a) PVOH from aqueous solution in the presence of varying plasticizer (PEG600, M600 and QM600) concentrations and b) adsorption data of PEG600 and M600 from aqueous solution in the presence of varying PVOH concentrations

The adsorption data of PVOH in the presence of plasticizers (PEG600, M600 and QM600) as a function of solution concentration is shown in Figure 6.19 a and shows that the amount of PVOH adsorbed by clay is not affected by the concentration of PEG600, but does reduce when the concentration of M600 is increased to 30 pph. A reduction in PVOH adsorption is also observed, in comparison to those of PEG600 and M600, when the concentration of QM600

is increased from 1 to 10 and then 30 pph. Figure 6.19 b shows that the amount of PEG600 or M600 adsorbed by clay is reduced when the amount of PVOH offered is increased, and that the amount of PEG600 adsorbed is lower than M600 when equal amounts of PVOH are offered. The adsorption of these plasticizers in the presence of PVOH follows the same trend as in the absence of PVOH i.e. the amount of M600 adsorbed by clay is higher than PEG600 (Figure 6.5)

6.7. Desorption of organics from aqueous solution

Desorption of selected organics, PEG600, PPG725, PPG2000 and PVOH from clay after being treated with a loading of 16.7 wt% by washing 10 times with aliquots of deionised water has been investigated by XRD (Figures 6.20 and 6.21). Figure 6.20 a shows that after only one wash the mixed single and bilayer structure for PEG600/clay reduces to a single layer structure. Figure 6.20 b shows that after one wash the bilayer structure for PPG725/clay changes to a mixed bilayer and single layer structure, whereas Figure 6.21 a shows that the bilayer structure of PPG2000/clay does not change even after 10 washes. Figure 6.21 b shows that the mixed bilayer and single layer structure for PVOH/clay does not change even after 10 washes.

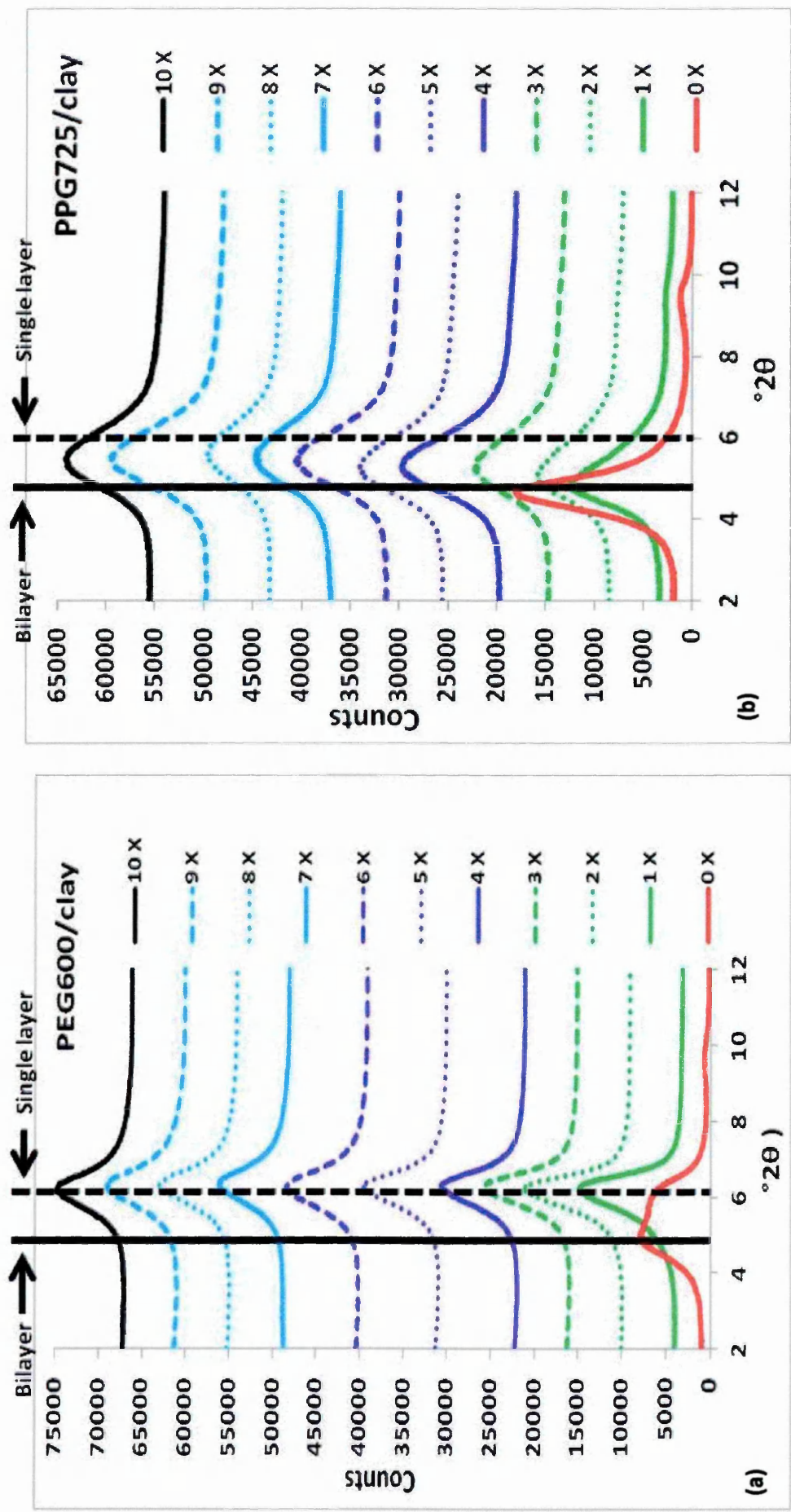


Figure 6.20. XRD traces of a) PEG600 and b) PPG725 after being offered at 16.7 wt% loading (from full suspension) and after being washed 1 – 10 times (from sediment after centrifugation).

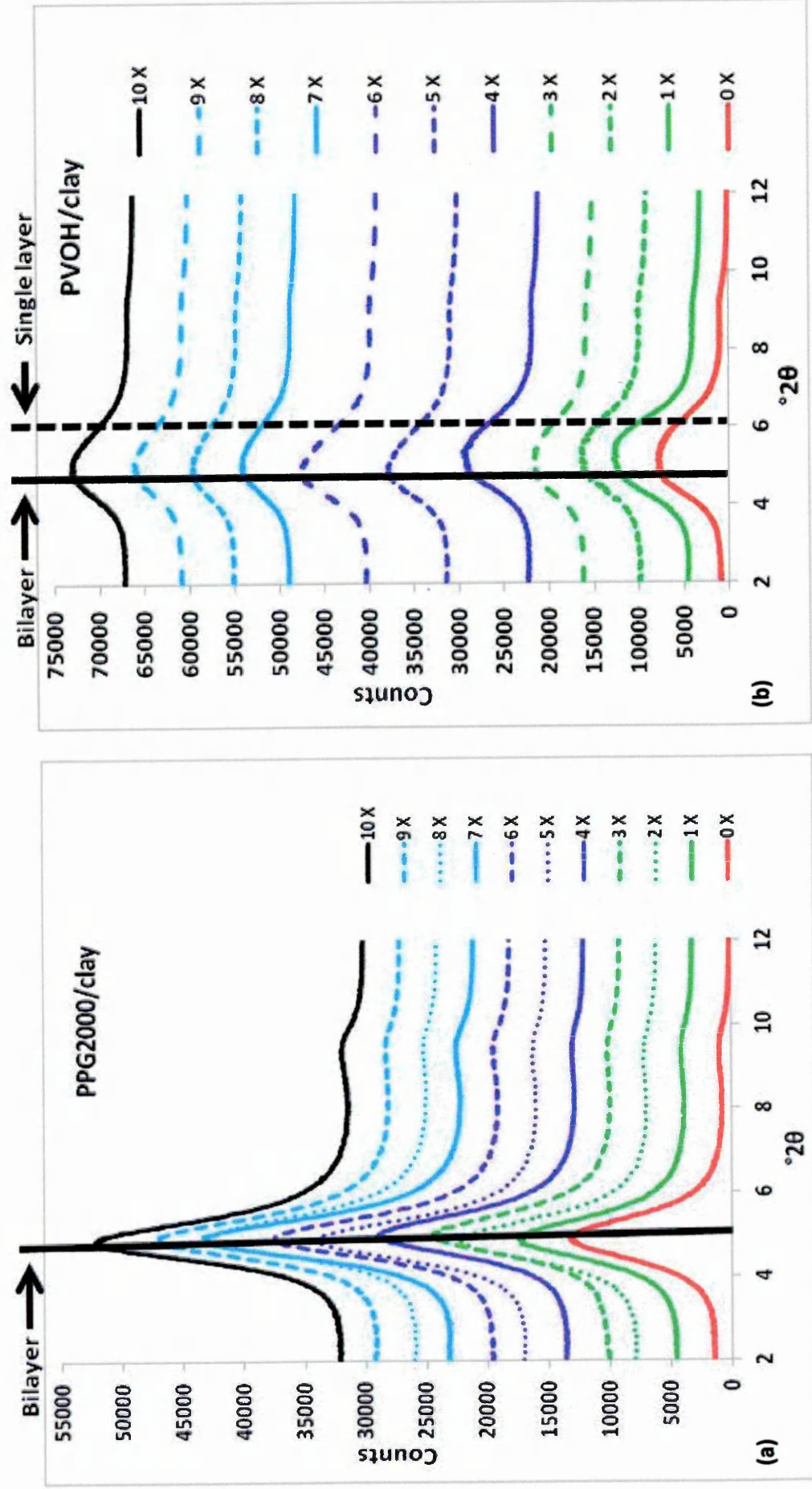


Figure 6.21. XRD traces of a) PPG2000 and b) PVOH after being offered at 16.7 wt% loading (from full suspension) and after being washed 1 – 10 times (from sediment after centrifugation).

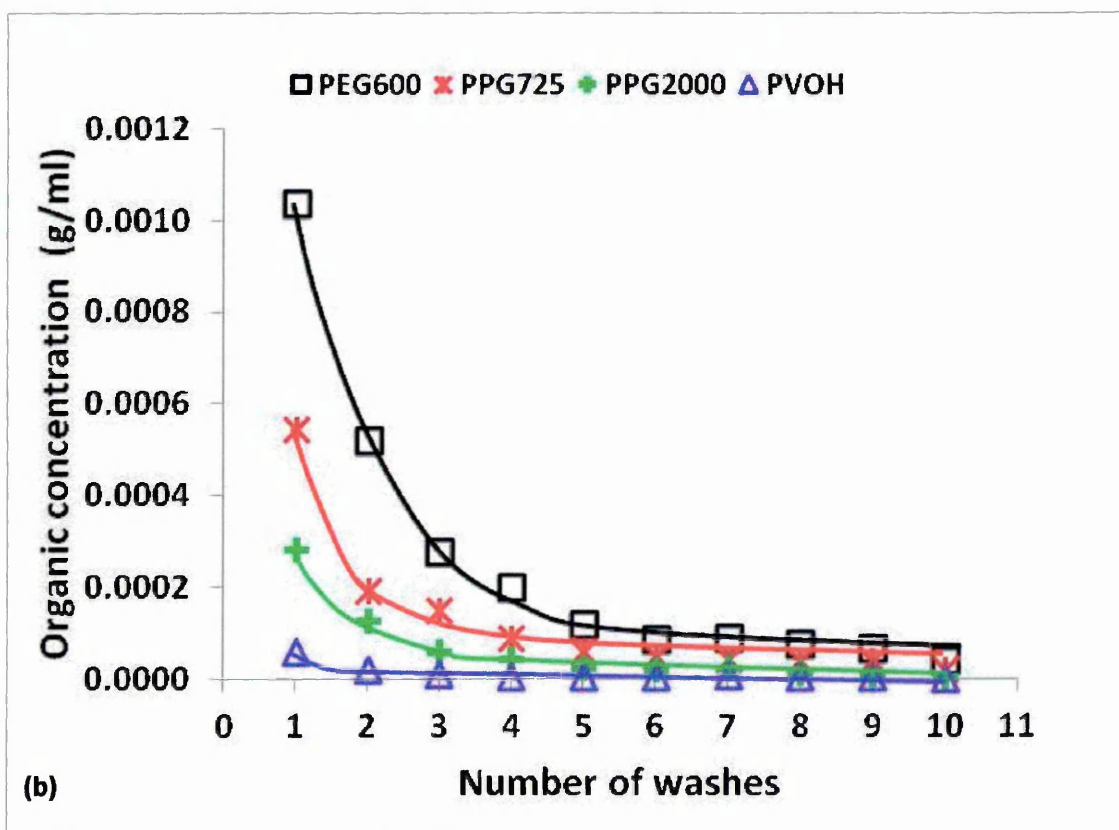
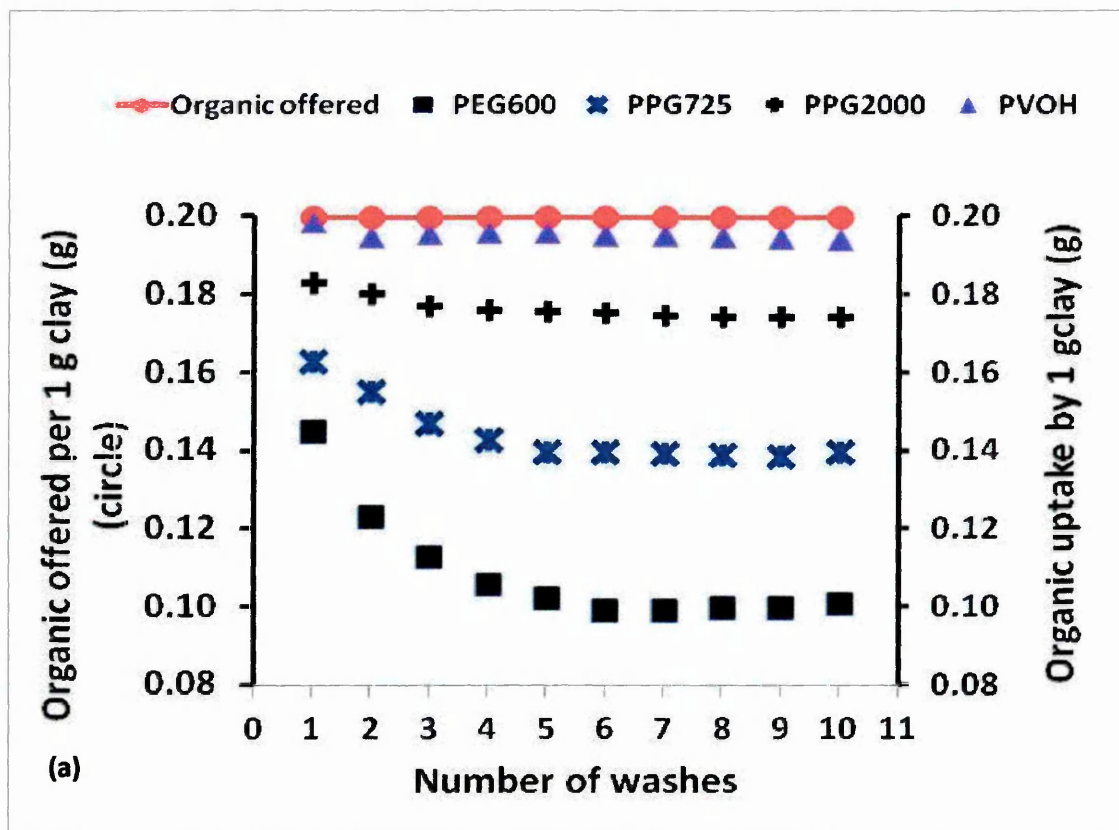


Figure 6.22. a) Amounts of PEG600, PPG725, PPG2000 and PVOH adsorbed on clay before and after washing (numbers in graph represent the final wt% of organic remaining on the clay) and b) concentrations of PEG600, PPG725, PPG2000 and PVOH removed from the organic/clay complexes during successive washings.

After 10 washes none of the organic/clay complexes collapsed to a d-spacing equal to the initial clay showing that once organic is adsorbed by clay it is very difficult (or even not possible) to be removed all by using water alone. It is shown in Figure 6.22 a that the amount of PVOH, PPG2000, PPG725 or PEG600 remaining on clay that could not be washed away is 16.3, 14.8, 12.2 and 9 wt% respectively. This behaviour was also observed in PVOH/clay complexes by Chiellini [6.8] and De Bussetti [6.9] who found that the adsorption process was almost irreversible as evidenced by no detectable amounts of PVOH being released from clay samples.

The amount of organic removed in the supernatant as a function of number of washes is presented in Figure 6.22 b, which shows that the organic concentrations reduced dramatically then levelled off after 6 washes for PEG600, 5 washes for PPG725, 3 washes for PPG200 and 2 washes for PVOH. The total amount of organic removed after 10 washes for PEG600, PPG725, PPG2000 and PVOH is 0.1176, 0.0760, 0.0330 and 0.0058 g per 1 g clay, respectively. The total amount of PPG725, PPG2000 and PVOH removed is 1.55, 3.56 and 20.2 times lower than that of PEG600. Also it shows that in the 1st wash, the highest amount of organic removed was with PEG600, followed by PPG725, PPG2000 and then PVOH. It is believed that most of the PEG600 or PPG725 removed after one wash is adsorbed within the clay gallery, which is supported by the XRD traces in Figure 6.20 which show reductions in d-spacing. Since no reduction in d-spacing is observed after 2 washes, but organic is still being removed it could be presumed that this organic is located at the top and the bottom of clay stacks or at the edges of clay layers. This cannot be ascertained with certainty using XRD, but it suggest that the organic removed in the later washes doesn't significantly contribute to the d-spacing of

the gallery and if present in the gallery are not as strongly adsorbed as those that remain. These same comments can also be applied to the PPG2000 and PVOH systems, since no changes in d-spacing are observed throughout the 1-10 washes. De Bussetti [6.9] and Strawhecker [6.10] showed adsorbed PVOH molecules were located not only in the clay gallery but also on the external surfaces. In summary, the order of affinity of organic to clay is PEG600 < PPG725 < PPG2000 < PVOH.

6.8. References

- [6.1]. Chen, B. and Evans, J. R. G. (2005). X-ray diffraction studies and phase volume determinations in poly (ethylene glycol)-montmorillonite nanocomposites. *Polymer international*, **54** (5), 807-813.
- [6.2]. Parfitt, R.L. and Greenland, D.J. (1970). The adsorption of poly(ethylene glycol) on clay minerals. *Clay Minerals* **8** (3), 305-315.
- [6.3]. Cope, A. C., Ciganek, E., Fleckenstein, L.J. and Meisinger, M.A.P. (1960). Tertiary amines from methiodides and lithium aluminum hydride. *Journal of the American chemical society*, **82** (17), 4651-4655.
- [6.4]. Mitsunobu, O., Wada, M., Sano, T. (1972). Stereospecific and stereoselective reactions. I. preparation of amines from alcohols. *Journal of the american chemical society*, **94**(2), 679-680.
- [6.5]. Mongondry, P., Plaisance, C.B. Jean, M. and Tassin, J.F. (2003). Mild synthesis of amino-poly(ethylene glycol)s. Application to steric stabilization of clays. *Macromolecular rapid communication*, **24** (11), 681-685.
- [6.6]. Science and fun (2011) [online]. Last visit 25 October 2011 at <http://www.science-and-fun.de>.
- [6.7]. Borodko, Y., Jones, L., Lee, H., Frei, H., and Somorjai, G. (2009). Spectroscopic study of tetradecyltrimethylammonium bromide Pt-C₁₄TAB nanoparticles: structure and stability. *Langmuir*, **25** (11), 6665-6671

[6.8]. Chiellini, E., Corti, A., Politi, B. and Solaro, R. (2000).

Adsorption/desorption of polyvinyl alcohol on solid substrates and relevant biodegradation. *Journal of polymers and the environment*, **8** (2), 67-79

[6.9]. De Bussette, S.G. and Ferreiro, E.A. (2004). Adsorption of poly(vinyl alcohol) on montmorillonite. *Clays and clay minerals*, **52** (3), 334-340

[6.10]. Strawhecker, K.E. and Manias, E. (2001). AFM of poly (vinyl alcohol) crystals next to an inorganic surface. *Macromolecules*, **34** (24), 8475-8482.

**Physical and barrier properties of PVOH films
in the absence and presence of clay
and/or PEG600**

7.1. Mechanical properties of PVOH/clay films

The mechanical properties of PVOH films with different amounts of clay loading (1, 3, 5, 10, 20 and 30 wt%) have been investigated by dynamic mechanical analysis (DMA) using a tension set up and within the temperature range of -50 to 150 °C. The samples were equilibrated in the humidity oven at 23 °C and 85 % relative humidity (RH) for 24 hours before performing the DMA experiment. The sample was immediately transferred to the DMA from the oven and the experiment started, the humidity within the DMA chamber was not controlled and susceptible to atmospheric conditions during the cooling and heating cycle. The plot of tensile storage modulus (E') as a function of temperature for PVOH and PVOH/clay composites are shown in Figure 7.1 a, which shows that in general the E' increases over the whole temperature range as the amount of clay added is increased. For example with introduction of 30 wt% clay, the E' at -50 °C increases from $\approx 3 \times 10^9$ to 14.3×10^9 Pascal (Pa), which is 4.76 times higher than pure PVOH. Also at 150 °C, E' increases from 6×10^8 to 2.2×10^9 Pa, which is 3.66 times higher than pure PVOH.

The plot of $\log E'$ as a function of temperature is given in Figure 7.1 b and shows that for PVOH alone, the $\log E'$ gradual decreases as it is heated from -50 to 5 °C (which relates to β transition), then sudden decreases as it is further heated to 50 °C (which relates to α transition) and then gradually increases as it is heated to 110 °C (which relates to the rearrangement of polymer molecules due to loss of water [7.1]), it is finally followed by a further decrease when heated above 120 °C which relates to its softening point. Generally, the same trends are observed for the samples containing clay, but the extent of decrease between 5 to 50 °C and the extent of increase between ≈ 50 to 100 °C become less as clay loading increases. At 20 and 30 wt% clay,

little increase is observed between ≈ 50 to 100 °C. The general background increase in tensile storage modulus between 50 to 100 °C is due to the incorporation of the clay and is simply due to the rigidity of clay. Specific increases around 110 °C are due to loss of water. Less water has already been shown to be removed from the samples as the amount of clay is added (Section 7.3, Figure 7.18). Water acts as plasticizer for PVOH and so the loss of water increases the rigidity of PVOH.

A decrease in tensile storage modulus of PVOH is observed in two steps i.e. around 10 °C which is related to the glass transition temperature and around 120 °C which is related to the softening of PVOH. Coffin [7.1] observed that the softening point of PVOH (Mw 50,000) was around 135 °C, whereas Peng [7.2] observed it at 115 °C (Mw 70,000). The decrease in storage modulus around the softening point becomes weaker as more clay is added, and finally disappears when clay is added at 20 wt% and more. The weaker decrease of storage modulus as more clay is added is due to the mechanical properties of the composites being controlled by clay (rigidity) at high clay content, whereas at low clay content the mechanical properties are controlled by PVOH (flexibility).

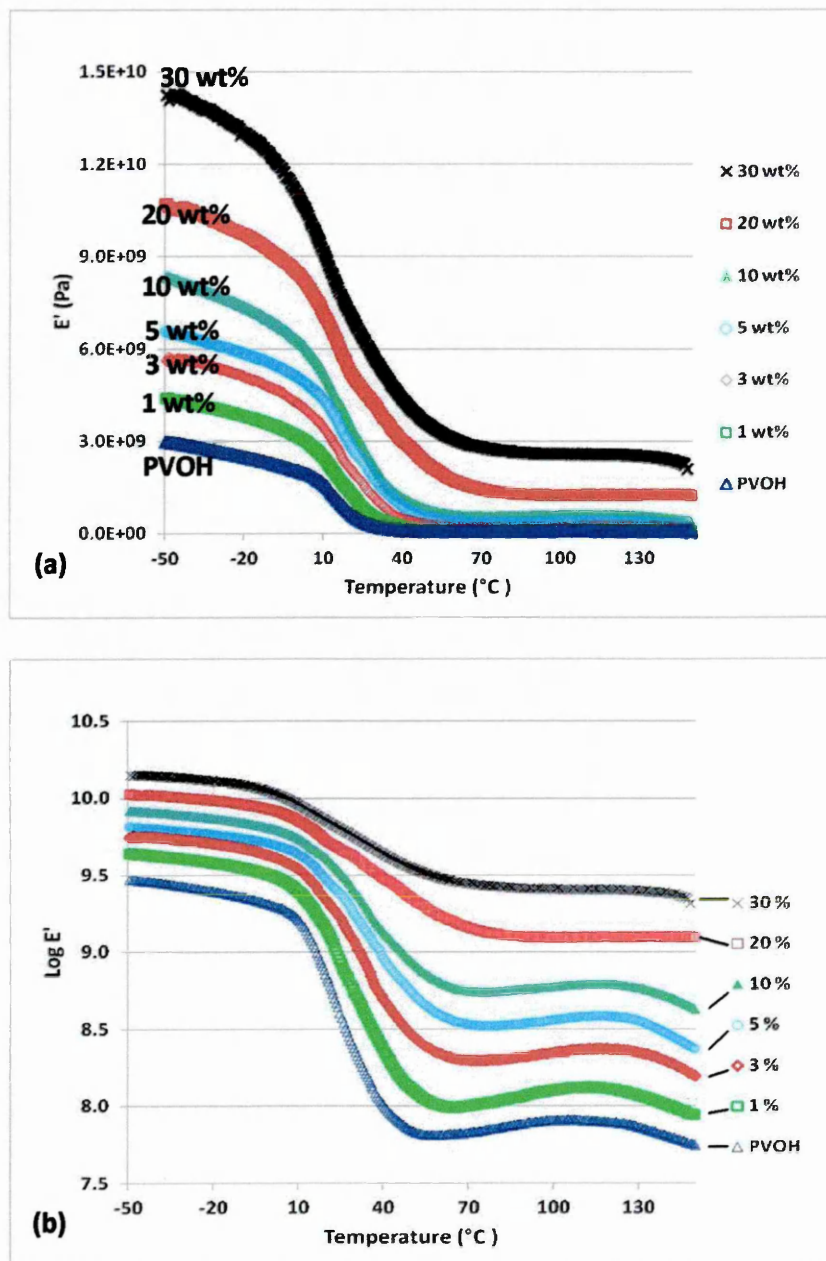


Figure 7.1. a) Tensile storage modulus, E' and b) $\log E'$ for PVOH and PVOH/clay composites as a function of temperature (Frequency 1 Hz). The samples were equilibrated in the humidity oven at $23^{\circ}C$ and 85 % relative humidity (RH) for 24 hours before performing the DMA experiment.

Tan δ as a function of temperature for PVOH and PVOH/clay composites is given in Figure 7.2. For PVOH alone, three peaks are observed. The first peak is the termed β transition and is associated with the local twisting motions around main chain bonds or conformational changes of the PVOH side group

[7.3, 7.4] and can often be related to the toughness of a polymer [7.5] and is affected by adsorbed moisture [7.6] and clay content [7.7] in the samples. As the clay content is increased, the β transition becomes more apparent, especially with 20 wt% clay and more. The peak of β transition is related to the sample toughness and shows that the toughness decreases with the increase of clay content. Similar result was reported by Strawhecker [7.5]. The β transition temperature for PVOH observed by other researches was $-3\text{ }^{\circ}\text{C}$ [7.3] and $35\text{ }^{\circ}\text{C}$ [7.6]. The second peak (i.e. the main peak) at $27\text{ }^{\circ}\text{C}$ is termed the α transition which corresponds to the glass transition temperature (T_g) and is related to chain movement [7.5]. The T_g value for PVOH observed by other researchers was $65\text{ }^{\circ}\text{C}$ (Mw 70,000, $f=5\text{ Hz}$) [7.2], $55\text{ }^{\circ}\text{C}$ (Mw 94,000, $f=3\text{ Hz}$) [7.3] and $86\text{ }^{\circ}\text{C}$ (Mw 124,000, $f = 1\text{ Hz}$) [7.4]. The T_g is affected by several factors such as the Mw of a polymer, moisture content and the applied frequency and hence the reason why the T_g observed in the PVOH of this study (Mw - 30,000) is different. The third peak, around $120\text{ }^{\circ}\text{C}$, is related to the slip of molecular chains [7.2,7.5].

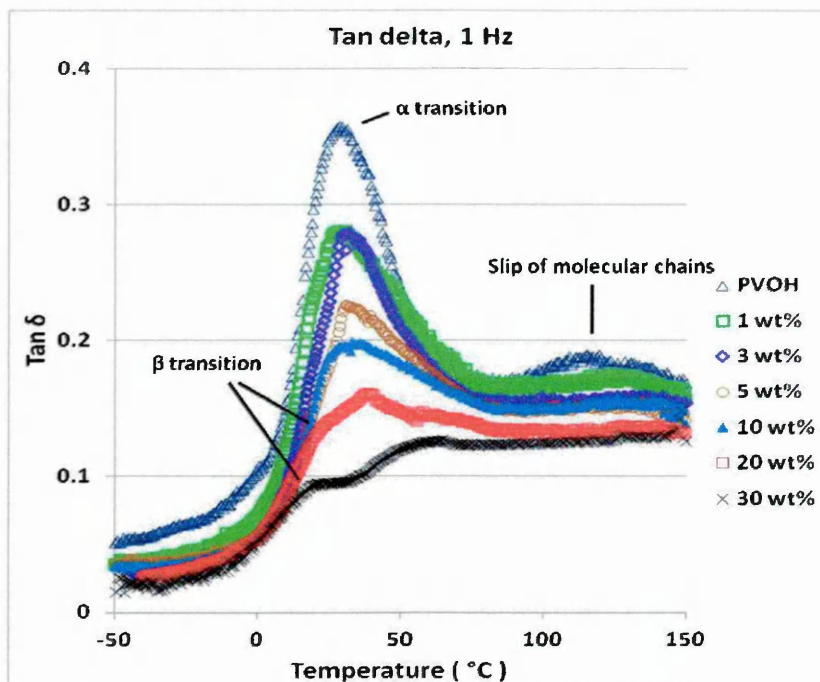


Figure 7.2. Tan δ of PVOH and PVOH/clay nanocomposites as a function of temperature (Frequency 1 Hz).

Analysis of data in Figure 7.2 is explored further and given in Figure 7.3 which plots the intensity of the tan δ at T_g (Figure 7.3 a) and the peak temperature of the α transition (T_g) (Figure 7.3 b) as a function of clay content. Figure 7.3 a shows that the intensity of tan δ at T_g decreases with increasing clay content. Tan δ is a measure of the damping properties of the material [7.4]. PVOH has a higher tan δ than the PVOH/clay composites and can therefore absorb more energy under the acute strain environment. Higher accumulated energy adsorbed by PVOH leads to more thermal degradation and further reduces the mechanical property of PVOH than those of PVOH/clay composites. Therefore, introduction of clay to PVOH results in a better thermal stability than that of pure PVOH. This is supported by previous results in section 5.2.1 that show the introduction of clay increases the thermal stability of PVOH. Figure 7.3 b shows that the T_g is lowest for PVOH and increases with increasing clay content. The change in T_g due to introduction of clay in PVOH suggests a

strong interaction between clay and PVOH, which becomes more apparent as clay content increases. This is supported by the results in section 5.3.1, which show that the amount of PVOH associated with clay increases with increasing clay content. As a result, introduction of clay will restrict the chain mobility of PVOH resulting in an increase in T_g of PVOH. The slip of PVOH molecular chains decrease with increasing clay content due to strong polymer clay interactions, thus the peak at $\approx 120^\circ\text{C}$ (Figure 7.2) gradually decreases as clay content increases.

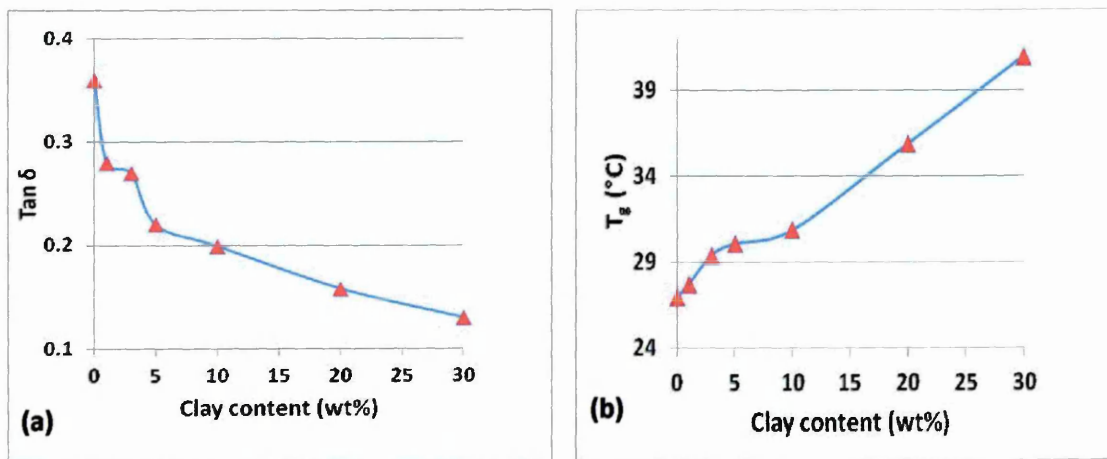


Figure 7.3. a) $\text{Tan } \delta$ at transition (T_g) measured at peak height and b) peak temperature (T_g) as function of clay content

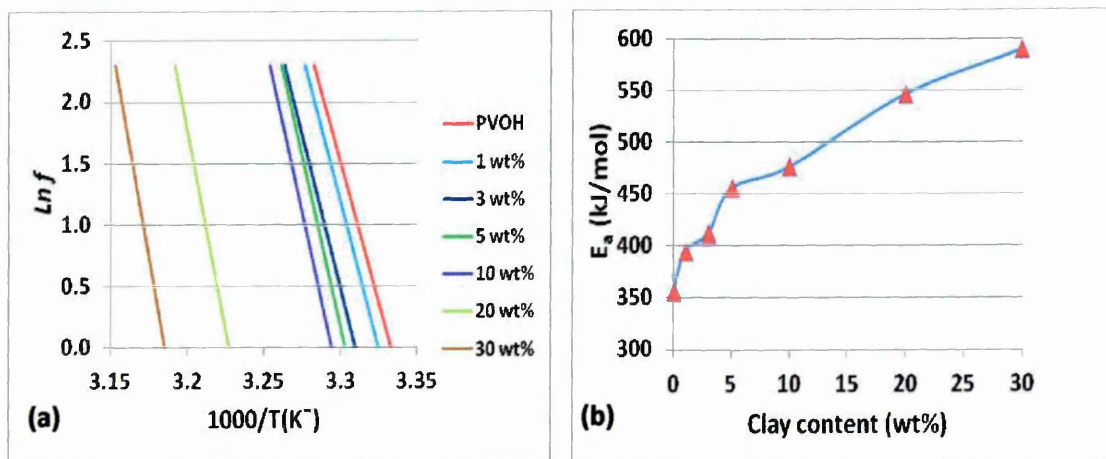


Figure 7.4. Logarithmic frequency as a function of temperature (a) and activation energy E_a as function of clay content (b)

To ensure that the transition observed in Figure 7.3 b is a T_g , the analysis is performed by scanning at different frequencies and calculating the activation energy for a T_g transition [7.8]. The temperature dependence of the characteristic relaxation time, $\tau(T)$, is given by the Arrhenius equation which relate the changes of the T_g with the applied frequency as follow [7.9]:

$$f \propto \frac{1}{\tau(T)} = A \exp \frac{-E_a}{RT} \quad (7.1)$$

or

$$\ln f = \ln A - \frac{E_a}{RT} \quad (7.2)$$

where f is the applied frequency, A is a constant, T is the absolute glass transition temperature (K), R is the universal gas constant (8.31446121 J/mol K) and E_a is the activation energy. A plot of logarithmic frequency as a function of $1/T_g$ is presented in Figure 7.4 a, which shows that the T_g shifts to higher temperature when applied frequency is increased. The activation energy E_a , which is obtained from the gradient in Figure 7.4 a, as a function of clay content is presented in Figure 7.4 b. Our calculation of the activation energy E_a for pure PVOH showed about 356.5 kJ/mol. This value was close to the reported activation energy for PVOH i.e. 377.5 kJ/mol (Mw 70,000) by Peng [7.2] and 410 kJ/mol (Mw 94,000) by Cendoya [7.3]. The difference is likely to be due to the lower molecular weight PVOH used in these experiments (MW = 30,000). An introduction of clay resulted in a significant increase in the activation energy of PVOH. For example, incorporation of 30 wt% clay into PVOH increased the activation energy of PVOH by 65 %. The increase of the activation energy will increase the glass transition temperature, as shown by similar trend of T_g in Figure 7.3 b, and this is due to the restricted movement of PVOH chains. As a result, higher energy is needed during relaxation of PVOH/clay than pure PVOH.

7.2. Water vapour barrier properties of PVOH and PVOH/clay films in the absence and presence of PEG600

7.2.1. PVOH/clay films in the absence of PEG600

Water vapour barrier properties of PVOH films (thickness $\approx 65 \mu\text{m}$) with different amounts of clay loading (1, 3, 5, 7, 10, 20, 30 and 50 wt%) have been investigated using Payne cups at 23 °C and 85 % relative humidity (RH). The samples were also tested using less harsh conditions (23 °C and 50 % RH) and were shown to be very good barriers ($<1.7 \text{ g/m}^2\cdot\text{day}$). However, no significant differences were observed between samples, which was due to the lack of sensitivity within the test for these test conditions. The amount of water vapour transmitted through the films versus time is given in Figure 7.5 and shows that it increases linearly with time, but decreases relatively with increasing clay content. The water vapour transmission rate (WVTR) values obtained from this data (Figure 7.5) and calculated using equation 3.4 (section 3.5) are plotted in Figure 7.6. It shows that the WVTR decreases with increasing clay content. With 50 wt% clay, the WVTR decreases from 300 to 37 $\text{g/m}^2\cdot\text{day}$, which is an 8 times improvement. This enhancement in the water permeability comes from the increased path tortuosity of the water molecules forced from the presence of well dispersed clay layers in the PVOH matrix (see section 2.6.2).

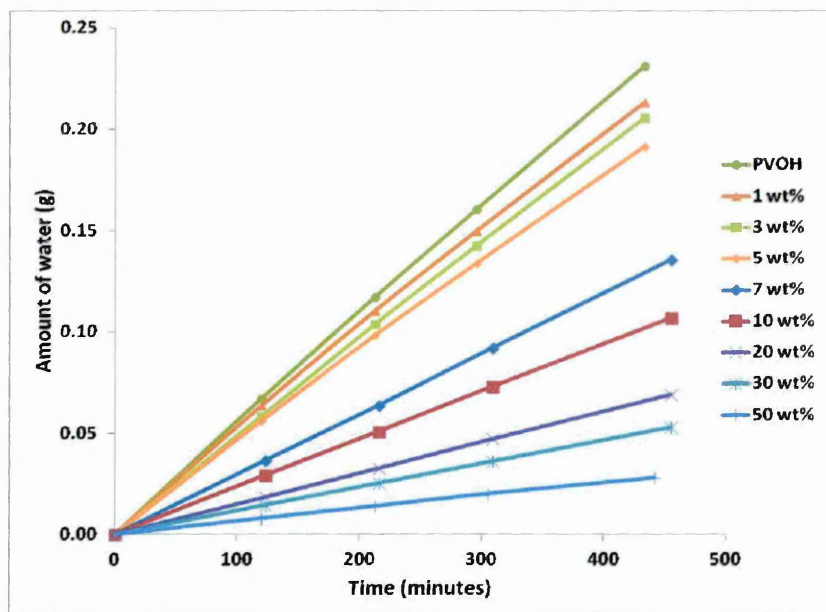


Figure 7.5. Amount of water (g) transmitted through PVOH and PVOH/clay nanocomposites

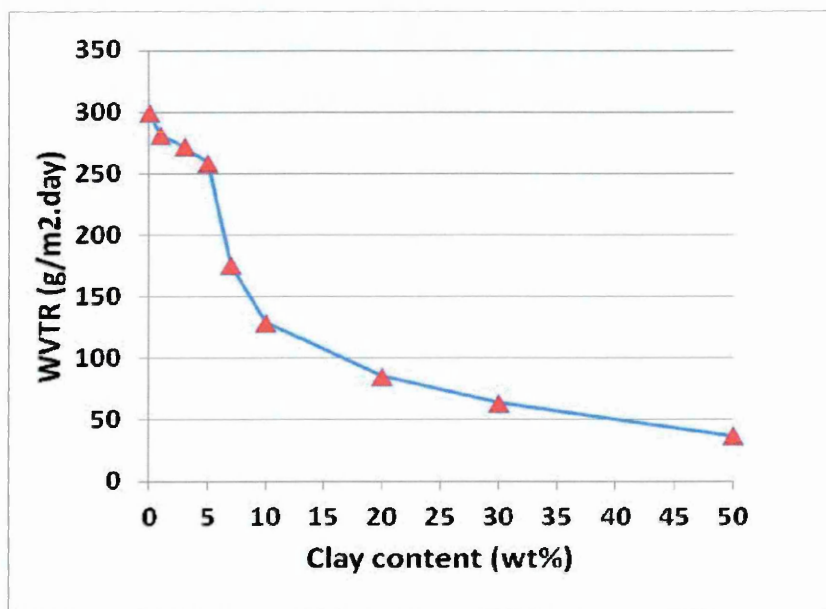


Figure 7.6. Water vapour transmission rates for PVOH and PVOH/clay nanocomposites

Figure 7.6 shows that the WVTR values decrease gradually when clay content is increased from 1 to 5 wt%, and then decreases more significantly when clay content is increased from 5 to 10 wt %. A more gradual decrease is

observed when clay content is increased from 10 to 50 wt%. XRD traces (section 4.1.1) indicate that when clay is present between 1 to 5 wt% only exfoliated (or very well dispersed) structures are observed and that as the clay content is increased from 5 to 10 wt% the amount of intercalated structures increases. With a higher amount of clay layers the packing density increases and thus the ability of clay to rotate in the PVOH matrix becomes restricted. The physical hindrance of the clay layer is therefore believed to lead to more intercalated structures. The larger decrease in WVTR values between 5 and 10 wt% clay may be due to the optimum dispersion of both intercalated and exfoliated clay that leads to the optimum path tortuosity. Further increases in clay content, and thus a higher ratio of intercalated to exfoliated structures, leads to only gradual improvements.

7.2.2. PVOH/clay films in the presence and absence of PEG600

The amount of water that passed through PVOH films (thickness $\approx 65 \mu\text{m}$) containing 20 wt% PEG600 and different amounts of clay loading (1, 3, 5, 7, 10, 20, 30 and 50 wt%) at 23 °C and 85 % relative humidity (RH) are presented in Figure 7.7. They show that the amount of water vapour passing through the PVOH/PEG600 and PVOH/PEG600/clay nanocomposites increases linearly with time, but decreases relatively with the increase in clay content. The water vapour transmission rate (WVTR) values are given in Figure 7.8 and show that the WVTR values decrease with increasing clay content. With the introduction of 20 wt% PEG600 to PVOH the WVTR value is 1305 g /m².day, which is 4.4 times greater than that of PVOH alone (300 g/m².day, Figure 7.6). PEG600 also increases the water permeability of PVOH samples containing clay, for example, with 10 wt% clay the water permeability of PVOH/PEG600/Clay is 5.48 faster than that of PVOH/clay. The water

permeability of PVOH films after addition of PEG600 recovers with the introduction of ~23 wt% clay. Figure 7.9 shows that the increase in water permeability due to 20 wt% PEG600 is highest when clay content is below 7 wt% and gradually improves as clay content is increased. Plasticizer (in this case PEG600) plays an important role in affecting the properties of the PVOH-clay composites. It provides lubrication and promotes chain mobility by reducing intra-molecular hydrogen bonds [7.9]. It was shown previously (section 5.3.4) that with low amounts of clay most of the PEG600 resides outside the clay gallery, this would lead to a higher probability of PEG600 disturbing the intra molecular bonds of PVOH resulting in the reduction of PVOH chain packing. Further increases in the amount of clay results in a higher portion of PEG600 relative to PVOH in the bulk matrix (due to more PVOH being adsorbed in the gallery of clay) and therefore consequently a reduction of PVOH chain packing occurs. Comparison of the water permeability of respective PVOH/PEG600/clay and PVOH/clay (Figure 7.9) films shows that the differences reduce more significantly when the amount of clay present is ≤ 20 wt % and that it remains constant when the amount of clay is ≥ 30 wt%.

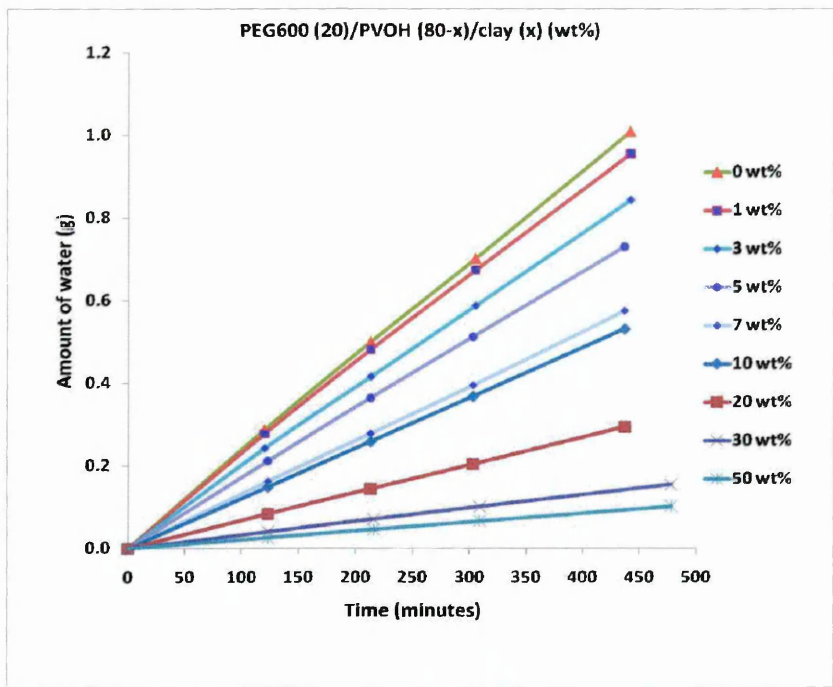


Figure 7.7. Amount of water transmitted through PVOH(80-x)/clay(x wt%)/PEG600(20) films.

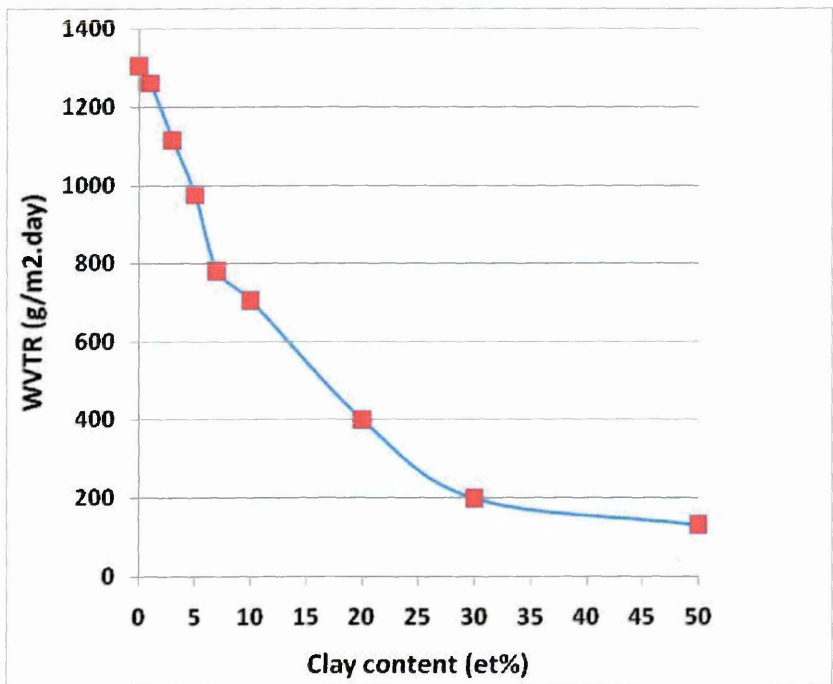


Figure 7.8. Water vapour transmission rate (WVTR) values for PVOH/PEG600/clay nanocomposites films

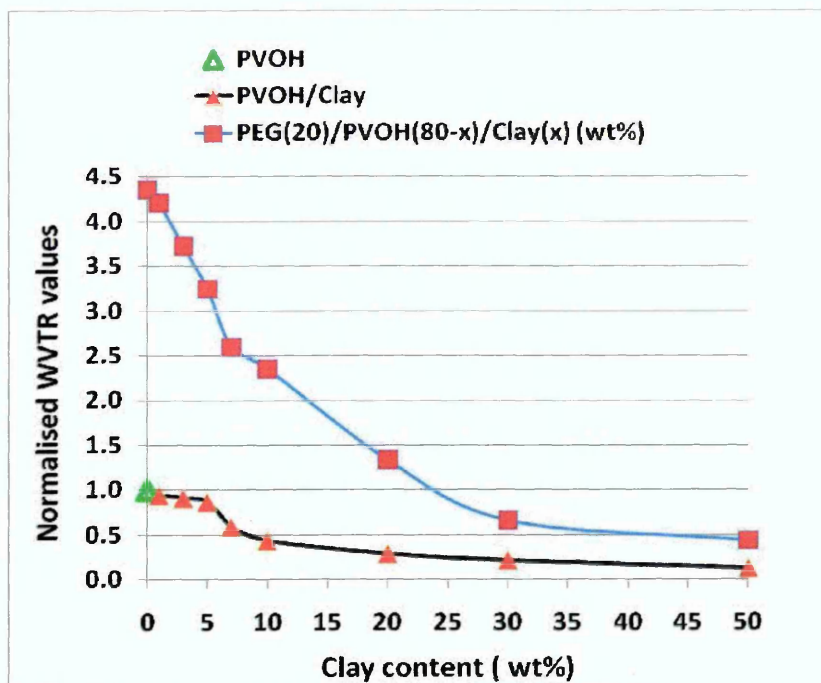


Figure 7.9. Comparison WVTR from PVOH/clay and PVOH/clay/PEG600 after normalisation to that of PVOH alone

7.3. Effect of PVOH crystallinity on water vapour barrier properties in the absence and presence of clay

The effect of PVOH crystallinity on the water vapour transmission rate (WVTR) of films in the absence and presence of clay (5 and 10 wt%) was investigated. The crystallinity of the films was modified by heating at 160, 180, 200 and 220 °C for 10 minutes before immediately determining the WVTR at 23 °C and 85 % RH. This measurement was identified as being recorded on day 1 (D1). The WVTR was also measured again on day three (D3) and day 52 (D52). Before and after any heat treatment, and before and after any WVTR measurement the crystallinity of the films were investigated using XRD and FTIR. The heating parameters were chosen specifically to avoid any visible discolouration in the films, a phenomenon that commonly occurs in PVOH films,

even though higher temperatures and heating times can induce greater extents of crystallinity.

Figure 7.10 shows the WVTR values of PVOH and PVOH/clay films on D1, D3 and D52 as a function of the temperature used to modify the crystallinity. It shows that the WVTR values of the films decrease with increasing crystallisation temperature. For example, the WVTR value of the PVOH before heating (D1-23 °C) decreased from 300 g/m².day to ≈151 g/m².day when heated at 220 °C. The respective WVTR values for PVOH/clay (5 wt%) were 225 to 92 g/m².day and for PVOH/clay (10 wt%) were 148 to 55 g/m².day. These values correspond to a % decrease of 51, 41 and 37 % respectively. It is interesting to see that there is a relatively large drop in the WVTR values for the PVOH samples heated at 160 and 180 °C. There is possibly a similar effect in the PVOH/clay 5 wt% sample, but it is not as evident. The large drop in the WVTR may due to the removal of water in the film as shown later (Figure 7.18). Figure 7.10 also shows that the WVTR values decrease with increasing clay content for both unheated and heated samples. Moreover, the WVTR values of all the films increase with time suggesting that their crystallinity decreases with time when maintained at 23 °C and 85 % RH. For example, the WVTR values of the PVOH films heated at 220 °C increase from 151 on D1 to 186 g/m².day on D52. The respective changes for the PVOH/clay (5 wt%) and PVOH/clay (10 wt%) samples are 92 to 121 g/m².day and 55 to 74 g/m².day. This suggests that water disturbs the crystalline structure. It is interesting to note that the WVTR values did not return to their original value (i.e. without heating) after remaining at 23 °C and 85 % RH for 51 days as it was perceived that the PVOH would lose its crystallinity more rapidly. Mallapragada [7.11] reported that the presence of water reduced the crystallinity

of PVOH but the crystallinity was formed again by rearrangement as the water evaporated, showing that this is a reversible process.

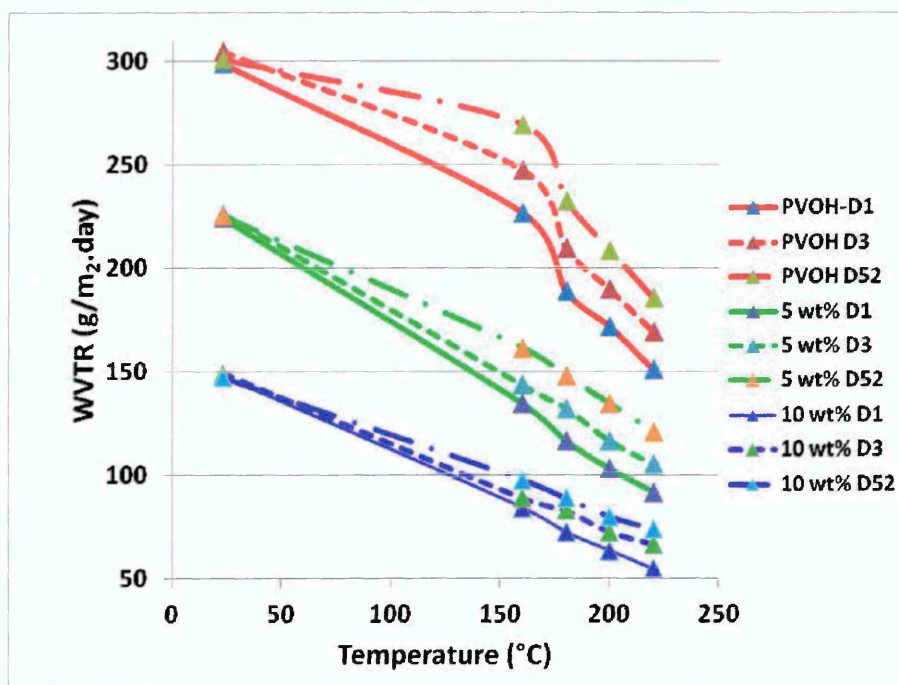


Figure 7.10. Water vapour transmission rate (WVTR) values for PVOH/clay composites

Further analysis of the data shows that on D1 the water permeability of pure PVOH when heated between 180-220 °C are lower than that of unheated PVOH/clay (5 wt%). Also those of PVOH/clay (5 wt%) when heated between 160-220 °C are lower than that of unheated PVOH/clay (10 wt%). This data shows that good water vapour barrier properties can be achieved by introducing clay into the polymer matrix and/or by heating the samples to induce crystallinity changes.

Figure 7.11 depicts FTIR spectra of unheated and heated PVOH films collected on D1 and shows that the intensity of the band at 1142 cm^{-1} increases with increasing crystallisation temperature, whilst the intensity of the band at 2942 cm^{-1} remains constant. Figure 7.12 depicts FTIR spectra of PVOH films heated at 200 °C on D1, D3 and D52 and shows that the intensity of the band at

1142 cm^{-1} decreases with time whilst the intensity of the band at 2942 cm^{-1} remains constant. Figure 7.13 depicts FTIR spectra of PVOH, PVOH/clay (5 wt%) and PVOH/clay (10 wt%) heated at 200 °C on D1 and shows that the intensity of the bands at 1142 cm^{-1} and 2942 cm^{-1} decrease with increasing clay content. Crystallinity of PVOH is related to the band at 1142 cm^{-1} [7.11-7.14]. Quantitative information about the crystallinity of PVOH films can be obtained from the intensity ratio of the bands at 1142 cm^{-1} and 2942 cm^{-1} . The 1142 cm^{-1} band occurs as a result of the symmetric C-C stretching mode [7.14], which increases as the degree of the PVOH crystallinity increases [7.12,7.13].

The intensity of the band at 2942 cm^{-1} occurs due to the C-H stretching vibration [7.15] and does not change with change in degree of PVOH crystallinity. The intensity ratios of the band at 1142 cm^{-1} and 2942 cm^{-1} from all films are given in Figure 7.14 and shows that the ratios increase with increasing crystallisation temperature and clay content, but decrease with time. The ratios of the bands are shown to slightly increase after performing the WVTR measurements on D3 and D52, suggesting some recovery of the crystallinity, this may be due to the films slightly drying as the films were taken out of the controlled humidity environment and their weights recorded on the weighing balance. This also highlights the sensitivity of the films to water. Increases in PVOH crystallinity with temperature treatment have been reported by other researchers [7.11,7.12,7.16].

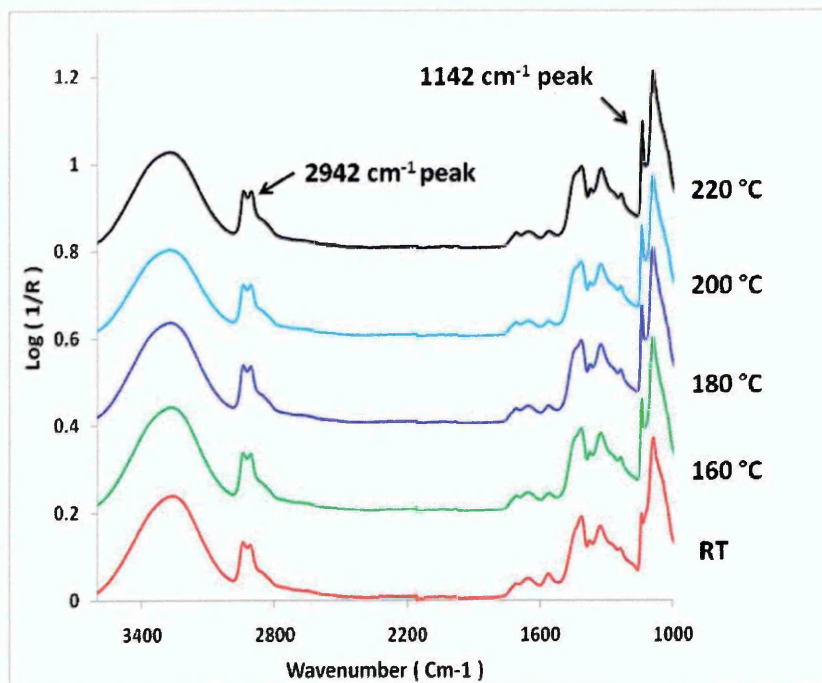


Figure 7.11. FTIR spectra collected on D1 of PVOH films treated at different temperature

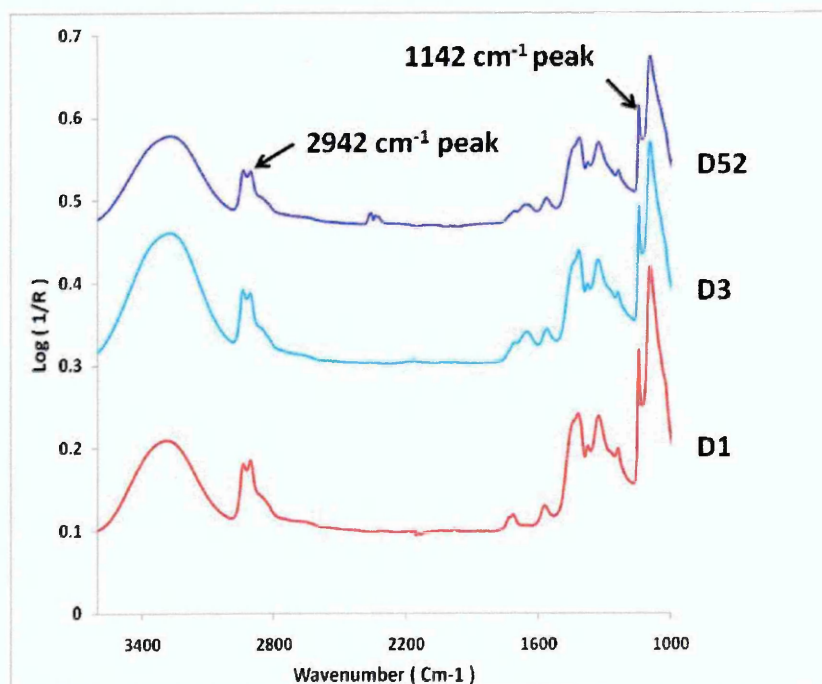


Figure 7.12. FTIR spectra of PVOH films heated at 200 °C on D1, D3 and D52

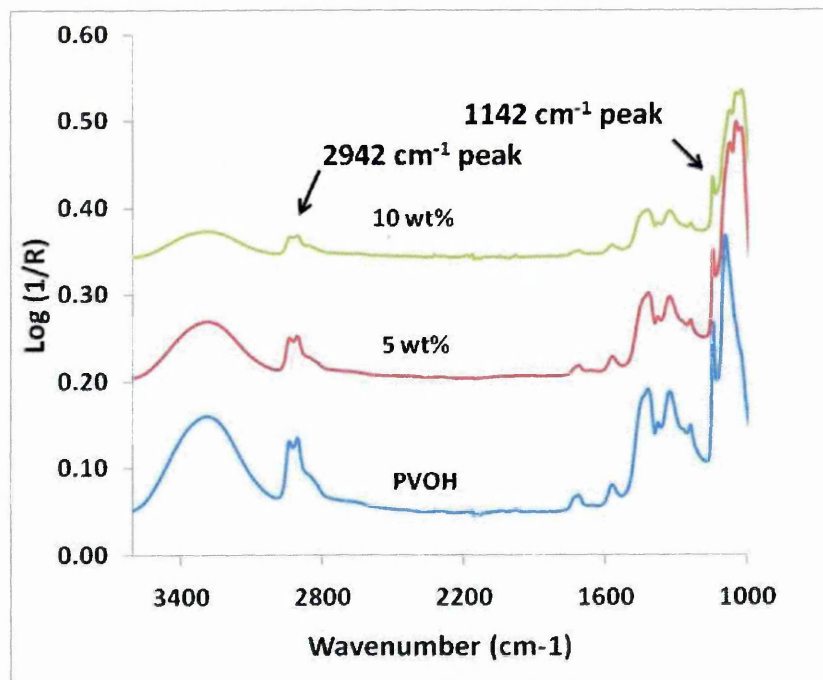


Figure 7.13. FTIR spectra of PVOH, PVOH/clay 5 wt% and PVOH/clay 10 wt% heated at 200 °C on D1

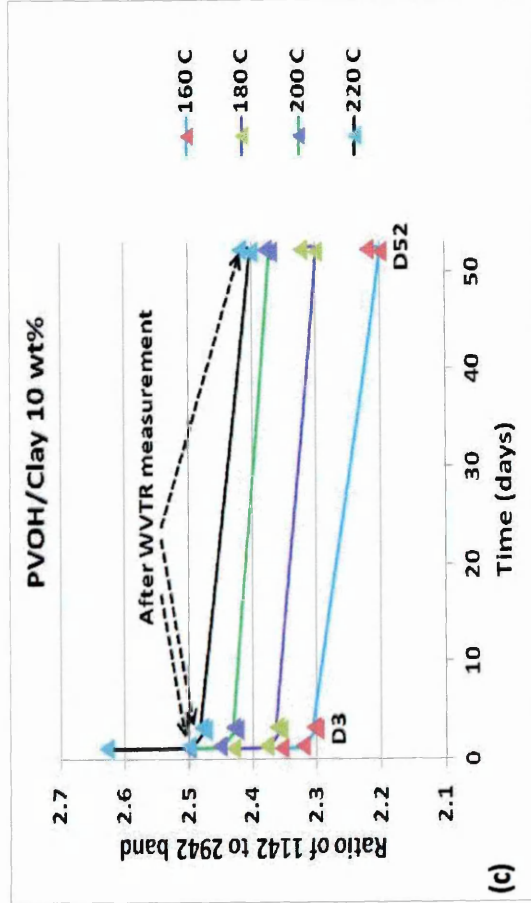
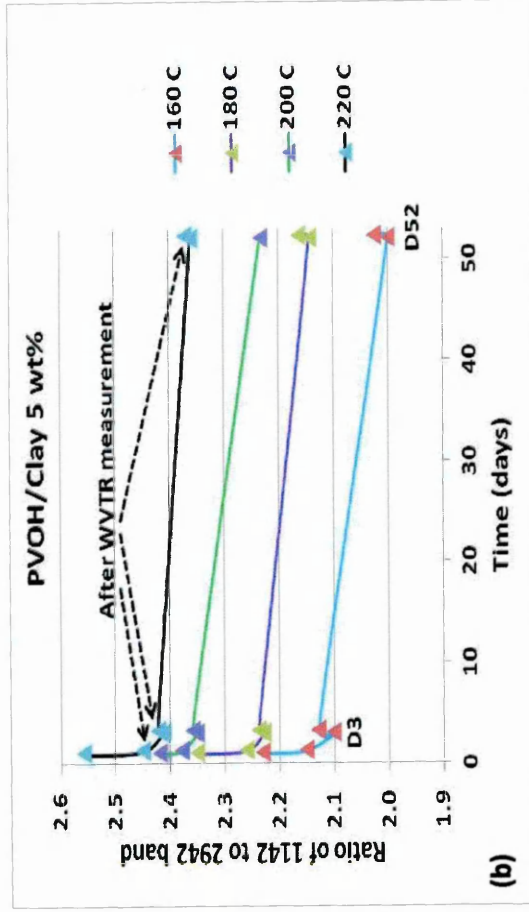
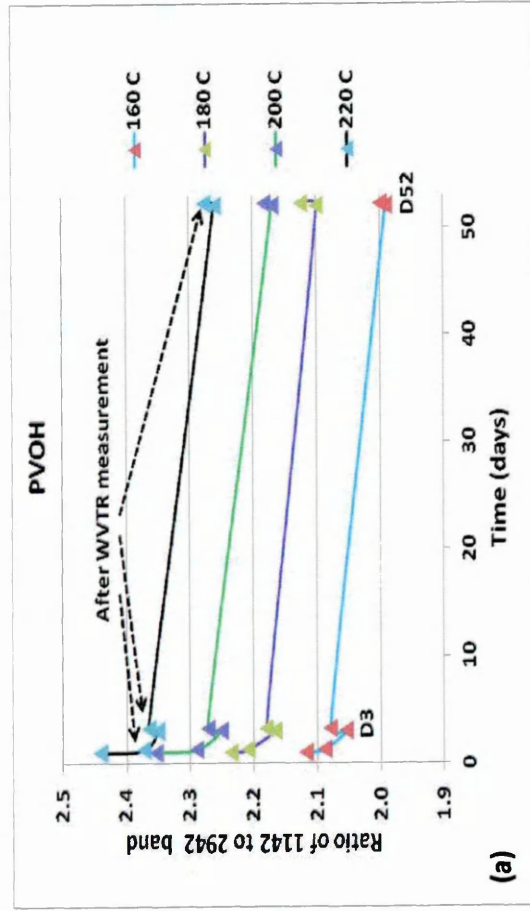


Figure 7.14. intensity ratios of 1142 to 2942 cm^{-1} bands from PVOH (a) and PVOH/clay 5 wt% (b) and PVOH/clay 10 wt% (c) as a function of time (days)

It should be noted that since ATR-FTIR was used, which is a surface sensitive technique, the spectra only represent $\approx 2\text{-}10\ \mu\text{m}$ of the film surface whereas the actual film thickness were $\approx 65\ \mu\text{m}$. The WVTR values and FTIR results are supported by XRD traces, which are shown in Figures 7.15-7.17. Figure 7.15 presents XRD traces of unheated and heated PVOH films and shows that the intensity of the peak at $\approx 19^\circ 2\theta$ increases with increasing crystallisation temperature. Similar observations were also observed in the XRD traces collected from PVOH/clay 5 wt% and PVOH/clay 10 wt% (data not shown), which suggests that clay does not have a significant effect on the crystallinity of the films under the particular heating parameters studied. Figure 7.16 presents XRD traces of PVOH films heated at 200°C on D1, D3, and D52 and shows that the intensity of the peak at $\approx 19^\circ 2\theta$ decreases with time. The peak at $\approx 19^\circ 2\theta$ is related to the crystallinity of pure PVOH [7.16,7.17]. Therefore the decrease in intensity at $\approx 19^\circ 2\theta$ with time indicates a decrease in PVOH crystallinity and so supports the FTIR interpretation (Figure 7.14 a). Hodge [7.17] reported the intensity at $\approx 19^\circ 2\theta$ in XRD traces decreased with increasing water content of PVOH, then collapsed when water content was ≥ 46 wt% and so claimed that water destroyed the crystallinity of PVOH. The collapsed intensity at $\approx 19^\circ 2\theta$ was not found in the XRD traces of our samples even at D52.

Figure 7.17 presents XRD traces of PVOH, PVOH/clay 5 wt% and PVOH/clay 10 wt% and shows that the background intensity increases between 2 and $7^\circ 2\theta$ as the amount of clay increases and is due to the dispersion of the clay layers as an exfoliated structure (if not exfoliated then very well dispersed). There is little difference in crystallinity between the PVOH, PVOH/clay 5 wt% and

PVOH/clay 10 wt% films when heated at 200 °C since there is little difference between the peak intensity at $\approx 19^\circ 2\theta$.

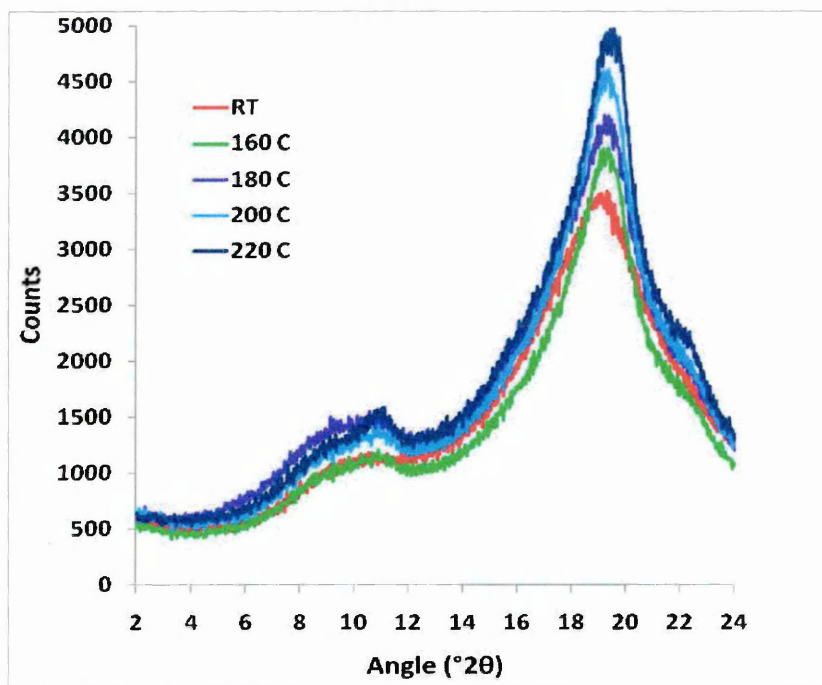


Figure 7.15. XRD traces of unheated and heated PVOH films on D1

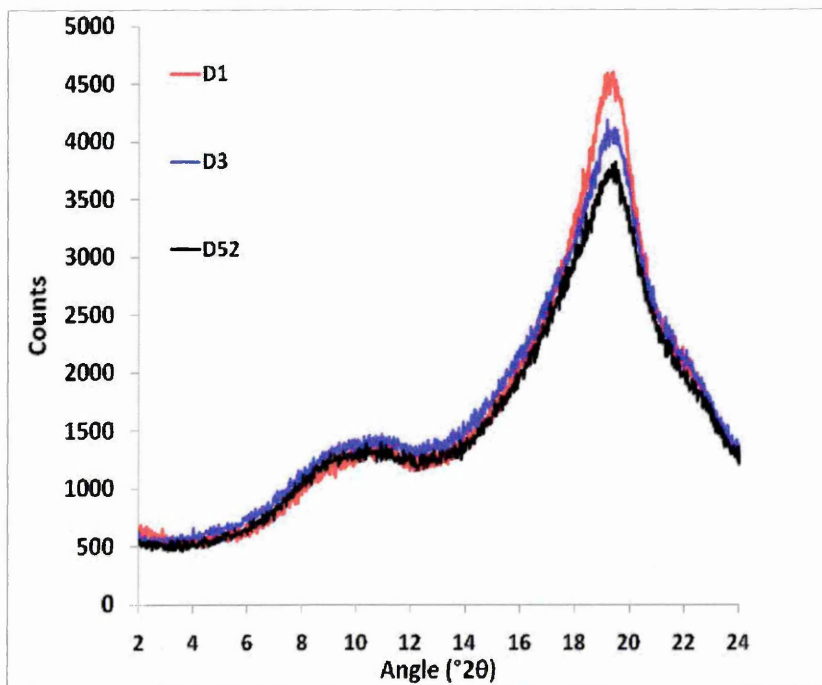


Figure 7.16. XRD traces of PVOH films heated at 200 °C on D1, D3 and D52

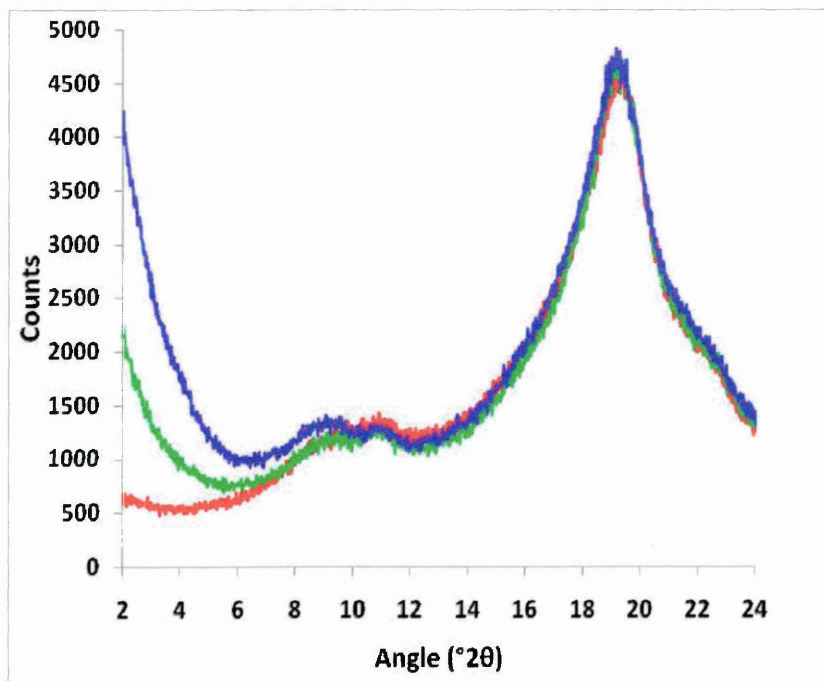


Figure 7.17. XRD traces of PVOH and PVOH/clay 5 wt% and PVOH/clay 10 wt% heated at 200 °C on D1

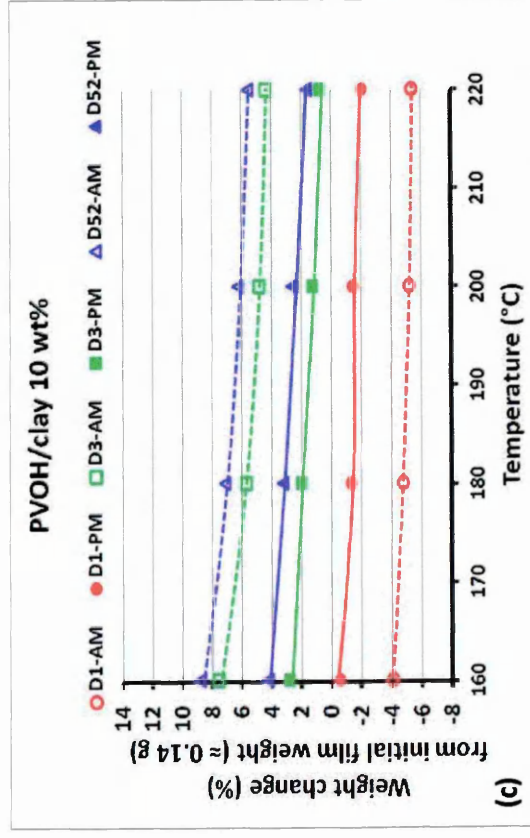
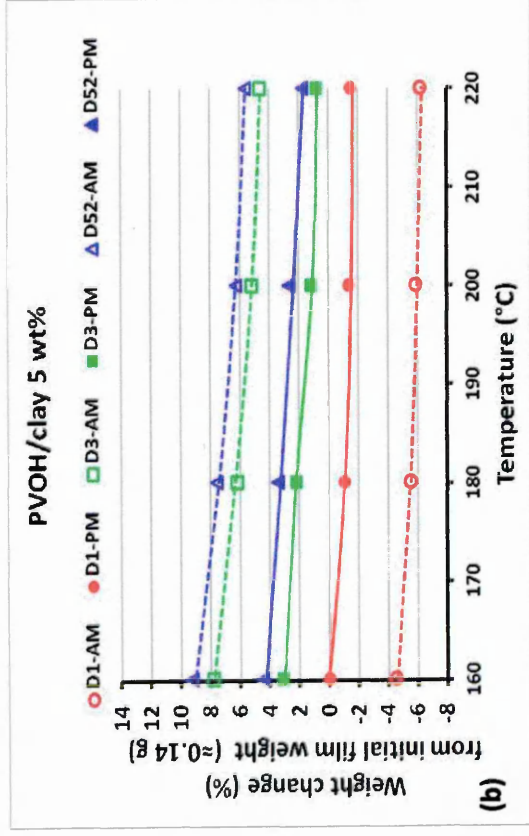
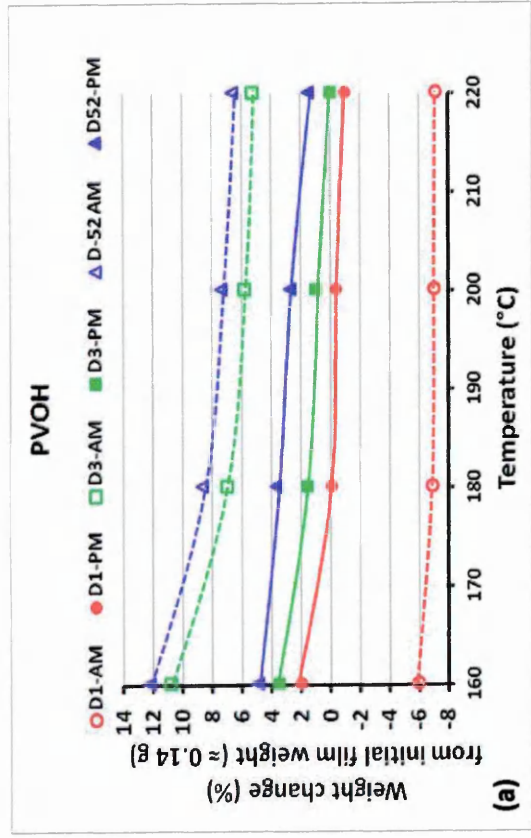


Figure 7.18. a) Percentage weight change from initial weight (≈ 0.14 g) of a) PVOH, b) PVOH/clay 5 wt% and c) PVOH/clay 10 wt% films

The percentage weight changes, which are related to water content, relative to the initial weights (≈ 0.14 g) of PVOH, PVOH/clay 5 wt% and PVOH/clay 10 wt% films, as they are heated and further exposed to 23 °C and 85% RH are given in Figure 7.18. For example, the amount of water lost from PVOH (Figure 7.18 a), PVOH/clay 5 wt% (Figure 7.18 b) and PVOH/clay 10 wt% (Figure 7.18 c) films after heating at 160 °C (D1-AM) were ≈ 5.9 , 4.5 and 4%, respectively. When the films are heated at 160 or 180 °C, the amount of water lost in the PVOH films is greater than those of PVOH/clay 5 wt% and PVOH/clay 10 wt%, this could be due to less water being present in the PVOH/clay samples (as evidenced in Figure 5.19 a) as well as a slower diffusion of water from the films due to the tortuosity effect of the clay. The relative amount of water adsorbed by the PVOH film heated at 160 °C on D1 is higher than those in the PVOH/clay films and may explain the relatively higher WVTR value for this film as observed in Figure 7.10.

The amount of water in all films generally increase with time, but on D3 and D52 the amount of water reduces after performing the WVTR experiment (i.e. D3-PM or D52-PM) compared to those before (i.e. D3-AM or D52-AM, respectively). This result is coincident with the slightly increase in intensity ratio of the bands at 1142 cm^{-1} and 2942 cm^{-1} after doing the WVTR on D3 and D52 (Figure 7.14). Mallapragada [7.11] reported that the crystallinity of PVOH returned by rearrangement as water evaporated. Assuming most of the water had been removed from the films upon heating, the highest amount re-adsorbed on D52 was by the films heated at 160 °C, for PVOH, PVOH/clay 5 wt% and PVOH/clay 10 wt% the amounts were ≈ 18.2 , 13.4 and 12.9 %, respectively. These amounts of water are much lower than the amount of water (≥ 46 wt%) observed in Hodge's PVOH films, which showed the collapse of the XRD peak

at $19.2^\circ 2\theta$ [7.17]. The amount of water adsorbed in the films on D3 and D52 are higher than those in the initial films (before heating), but the corresponding WVTR values did not return to their initial values (Figure 7.10). This shows that although the amount of water present in the film is likely to affect the water vapour barrier properties some of the PVOH crystallinity is still retained.

7.4. References

[7.1]. Coffin, D.R., Fishman, M.L., and Ly, T.V. (1996). Thermomechanical properties of blends of pectin and poly(vinyl alcohol). *Journal of applied polymer science*, **61** (1), 71-79.

[7.2]. Peng, Z., Kong, L.X. and Li, S.D. (2005). Dynamic mechanical analysis of poly(vinyl alcohol)/silica nanocomposite. *Synthetic metals*, **152** (1-3), 25-28.

[7.3]. Cendoya, I., López, D., Alegría, A. and Mijangos, C. (2001). Dynamic mechanical and dielectrical properties of poly(vinyl alcohol) and poly(vinyl alcohol)-based nanocomposites. *Journal of polymer science part B: Polymer physics*, **39** (17), 1968-1975.

[7.4]. Cassu, S.N. and Fellisberti, M.I. (1999). Poly(vinyl alcohol) and poly(vinylpyrrolidone) blends: 2. study of relaxations by dynamic mechanical analysis. *Polymer*, **40** (17), 4845-4851.

[7.5]. Menard, K.P. (1999). *Dynamic Mechanical Analysis A Practical Introduction*. Washington, CRC Press.

[7.6]. Cendoya, I., López, D., Alegría, A. and Mijangos, C. (2001). Dynamic mechanical and dielectrical properties of poly(vinyl alcohol) and poly(vinyl alcohol)-based nanocomposites. *Journal of polymer science part B: Polymer physics*, **39** (17), 1968-1975; Reference therein.

[7.7]. Strawhecker, K.E. and Manias, E. (2000). Structure and properties of poly (vinyl alcohol)/Na montmorillonite nanocomposites. *Chemistry of materials*, **12** (10), 2943-2949.

[7.8]. PerkinElmer, Inc. (2008). Introduction to Dynamic Mechanical Analysis A Beginner's Guide. USA

[7.9]. Gedde, U. W. (2001). Polymer Physics. London, Kluwer Academic Publishers.

[7.10]. Hodge,R.M., Bastow,T.J.,Edward,G.H., Simon, G.P and Hill,A.J. (1996). Free volume and the mechanism of plasticization in water-swollen poly (vinyl alcohol). *Macromolecules*, **29** (25), 8137-8143.

[7.11]. Mallapragada,S.K. and Peppas, N.A. (1996). Dissolution mechanism of semicrystalline poly(vinyl alcohol) in water. *Journal of polymer science part B: Polymer Physics*, **34** (7), 1339-1346

[7.12]. Ngui, M. O. and Mallapragada, S. K. (1998). Understanding isothermal semicrystalline polymer drying: Mathematical models and experimental characterization. *Journal of polymer science part B polymer physics*, **36** (15), 2771-2780.

[7.13]. Wong, S. S, Altinkaya, S. A. and Mallapragada, S. K. (2007). Crystallization of poly(vinyl alcohol) during solvent removal: Infrared characterization and mathematical modeling. *Journal of polymer science part B: Polymer physics*, **45** (8), 930-935.

- [7.14]. Tadokoro, H., Seki, S. and Nitta, I. (1956). Some information on the infrared absorption spectrum of polyvinyl alcohol from deuteration and pleochroism. *Journal of polymer science*, 28 (102), 563-566.
- [7.15]. Mangala, E., Kumar, T.S., Baskar, S., and Rao, K.P. (2003). Development of chitosan/poly(vinyl alcohol) blend membranes as burn dressings. *Trend biomaterial artificial organs*, 17(1), 34-40
- [7.16]. Assender, H.E. and Windle, A.H. (1998). Crystallinity in poly(vinyl alcohol). 1. an X-ray diffraction study of atactic PVOH. *Polymer*, 39 (18), 4295-4302.
- [7.17]. Hodge, R.M., Edward, G.H. and Simon, G.P. (1996). Water absorption and states of water in semicrystalline poly (vinyl alcohol) films. *Polymer*, 37 (8), 1371-1376.

8.1. Introduction

This chapter focuses on the overall conclusions of the work that was done and discussed through the course of the thesis. Conclusions for Chapters 5, 6 and 7 are given in Sections 8.2, 8.3 and 8.4, respectively. Future work is given in Section 8.5.

8.2. Competitive and synergistic adsorption of PVOH and PEG600 on clay

It has been shown that the dispersion of clay in PVOH created both intercalated and exfoliated structures, which were dependant on clay concentration, while in PEG600 only intercalated structures were formed. As the concentration of PEG600 or PVOH increased, step changes occurred in the gallery as it expanded from a depleted single layer through to a full single layer, then a combined single and bilayer system, and finally a full bilayer system. For PVOH, multi-layers were observed, which continued to form mostly exfoliated structures when the PVOH concentration was > 75 wt%.

The effect of thermal treatment and relative humidity on the d-spacing of PVOH/clay composites showed that as the PVOH loading increased, the extent of change in the d-spacings within the different conditions tested decreased suggesting less influence from the water was being experienced and less water was present in the gallery as more PVOH was added. The intercalated structures showed thermal and environmental stability when clay loading was between 50-75 wt%. For PEG600/clay composites, with a loading of 4 wt% PEG600 and below the d-spacing collapsed upon heating at 150 °C.

In the competitive adsorption studies, it was shown that both PEG600 and PVOH are present within the clay gallery, the amounts of PEG600 and PVOH present increase with the amount of PEG600 and PVOH offered, and the

platelet-platelet interactions in the PEG600-clay systems can be overcome by the ingress of PVOH. With different orders of mixing PEG600 and PVOH with clay, it was shown that samples prepared using route 3 (PEG600 mixed with clay, before adding PVOH) consistently exhibited slightly higher d_{001} -spacings and peak intensities when compared to the corresponding samples prepared by either route 1 (PEG600 mixed with PVOH before adding clay) or 2 (PVOH mixed with clay before adding PEG600). Thermal treatment showed that the higher d_{001} -spacings observed in route 3 were not affected by the presence of water.

TGA data showed the thermal stability of PVOH in clay decreased with increasing PVOH content up to 9 wt%, then increased when the PVOH concentration increased from 9 to 50 wt%, this further decreased when the PVOH concentration increased from 50 to 99 wt%. For PEG600 in clay, the thermal stability decreased with an increase of PEG600 content up to 9 wt%, increased when PEG600 content increased from 9 to 23 wt% and then decreased when PEG600 content increased above 23 wt%. It suggested that when PVOH or PEG600 was inside the gallery it contributed to the higher thermal stability. With PEG600, PVOH, clay and their mixtures, it was shown that degradation of PEG600 and PEG600 with clay mostly occurred above 350 °C whereas for PVOH and PVOH with clay it occurred below 350 °C. For PEG600 and PVOH mixtures (i.e. no clay) the PEG600 still appeared to mostly degrade above 350 °C and the PVOH still mostly degraded below 350 °C, the degradation pathway of PVOH was therefore not greatly affected by the degradation pathway of PEG600 when present as a mixture, and vice versa.

The adsorption of PEG600 or PVOH on clay follows a Langmuir-type adsorption isotherm, the amount of PEG600 or PVOH associated with the clay increased sharply as the amount offered increased and then continued to increase gradually as more was offered. In PEG600/PVOH/clay mixtures, the amounts of PEG600 and PVOH adsorbed increased with the amounts of PEG600 and PVOH offered. The amount of PVOH adsorbed by clay was slightly increased by the presence of PEG600 offered to clay, whilst the amount of PEG600 adsorbed was reduced when the amounts of PVOH offered were increased. It showed that PEG600 promotes the adsorption of PVOH on clay when PVOH offered is ≥ 50 pph. Further investigation confirmed that the higher d-spacings from films prepared by route 3 than those of route 1 and route 2 via the full suspension was neither due to a higher amount of PEG600 nor PVOH adsorbed by clay, but rather different ways in which PEG600 or PVOH molecules were organized or associated on the clay.

8.3. Adsorption of PEG2000, M600 and QM600 in the absence and presence of PVOH onto clay

The adsorption of PEG2000 and M600 followed a Langmuir-type adsorption; the amount of PEG2000 and M600 adsorbed on clay increased sharply as the amount offered increased and then continued to increase gradually as more was offered. Compared to PEG600 and PVOH, the order of affinity to clay was PVOH, PEG2000, M600 and PEG600.

Amino PEG600 was quatinized successfully as evidenced by ^1H NMR and FTIR, which showed the disappearance of peaks due to N-H and the appearance of $\text{N}-(\text{CH}_3)_3$ in QM600. Steric stabilization on clay by QM600

showed the amount of QM600 exchanged increased as the amount offered increased, but only a maximum of ~ 60% of the CEC was exchanged.

The competitive adsorption of M600 and PVOH on clay showed that generally the amount of PVOH or M600 adsorbed by clay increased sharply and then continued to increase gradually as more was offered. The amount of PVOH adsorbed was not affected significantly when M600 was present at 1 and 10 pph, but decreased when the amount of M600 offered was 30 pph. The amount of M600 adsorbed by clay in the absence of PVOH was lower than when PVOH was present at 15 pph and below, but higher when PVOH was present at 50 pph.

The adsorption of PVOH on clay in the presence of QM600 showed that generally the amount of PVOH adsorbed by clay increased sharply and then continued to increase gradually as more was offered. The amount of PVOH adsorbed on clay in the presence of 10 pph and 30 pph QM600 was lower than in its absence. The amount of PVOH adsorbed on clay in the presence of 2 pph QM600 was similar to that in its absence. An exception was observed when PVOH was present at 90 pph which showed higher amount of PVOH were adsorbed in the presence of 2 pph QM600.

Comparison of PVOH adsorption in the presence of plasticizers (PEG600, M600, and QM600) showed that the amount of PVOH adsorbed by clay was slightly increased by the presence of PEG600, but reduced in the presence of 30 pph M600 and 1, 10 and 30 pph QM600, whilst the amount of PEG600 or M600 adsorbed by clay was reduced when the amount of PVOH offered was increased. The amounts of PEG600 adsorbed were lower than M600 when equal amounts of PVOH were offered.

Desorption from clay of selected organics PEG600, PPG725, PPG2000, and PVOH by repeatedly washing the suspension 10 times after treatment with a loading of 16.7 wt% showed that after one wash the structures for PEG600/clay changed from a mixture of bilayer and single layer structures to only a single layer, whereas for PPG725/clay it changed from bilayer to a mixture of bilayer and single layer structures. For PPG2000/clay and PVOH/clay the structures did not change even after 10 washes. The order of affinity of organic to clay was PEG600 < PPG725 < PPG2000 < PVOH. Moreover, after 10 times of washing the d-spacing of organic/clay did not collapsed to a d-spacing of clay on its own; 16.3, 14.8, 12.2 and 9 wt% of PVOH, PPG2000, PPG725 and PEG600, respectively remained adsorbed to the clay.

8.4. Physical and barrier properties of PVOH films in the absence and presence of clay and PEG600

The tensile storage modulus increased over the whole temperature range as the amount of clay added was increased. Four events were observed relating to changes in the tensile modulus; i) a gradual decrease from -50 to 5 °C relating to β transition, ii) a sudden decrease from 5 to 50 °C relating to α transition, iii) a gradual increase to 110 °C relating to loss of water, and iv) a further decrease after 120 °C relating to the softening point. The temperature of the β and α transition increased with clay content, the increase due to loss of water decreased with clay content and the softening point was weaker with increasing clay content. The toughness and damping properties of the samples decreased with increasing clay content suggesting clay improved the thermal stability of PVOH. The activation energy for PVOH is about 356.5 kJ/mol and

increased with increasing clay content where the trend of the E_a was similar to the T_g confirming the transition observed was a T_g .

Introduction of clay into PVOH resulted in a reduced water permeability in the nanocomposites; an 8 times reduction was observed when clay content was 50 wt%. The trends in reduction with clay content were gradual from 1-5 wt%, but a more significant decrease was observed when increasing to 10 wt%, this was then followed by a more gradual reduction as clay was increased to 50 wt%. The reductions related to the structure change of the nanocomposites, i.e. from an exfoliated structure to the optimum dispersion of both intercalated and exfoliated clay, leading to the optimum path tortuosity. Further increases in clay content led to more intercalated and less exfoliated structures resulting in only gradual reductions.

The opposite trend was observed when PEG600 was introduced to the PVOH; 20 wt% PEG600 increased the water permeability of PVOH 4.4 times, which was due to PEG600 reducing the PVOH chain packing. Introduction of clay to PVOH/PEG600 reduced the water permeability and \approx 23 wt% clay was needed to return the value to that of PVOH alone. It was shown that with the addition of clay the ratio of PEG600 to PVOH in the bulk rather than that in the clay gallery decreased and therefore probably contributed to the improved water vapour barrier properties.

Besides clay, the crystallinity of PVOH was shown to reduce the water permeability of the nanocomposites. Water permeability reduced with increasing modifying temperature for films of PVOH, PVOH/clay 5 wt% and PVOH/clay 10 wt%. Furthermore, the water permeability of all the films increased with time when maintained at 23 °C and 85% RH. The levels of PVOH crystallinity were identified using FTIR from the intensity ratio of the bands at 1142 cm^{-1} and 2942

cm⁻¹. In all the samples the ratio increased with heating temperature and clay content but decreased with time. In addition, the intensity of the XRD peak at $\approx 19^\circ 2\theta$, which relates to PVOH crystallinity increased with temperature and decreased with time for all films. The sample crystallinity was very affected by water content, as shown by comparing the trends in water content and sample crystallinity. However, the induced crystallinity was not completely lost after being maintained at 23 °C and 85 % RH for 51 days.

8.5. Future work

Although, lots of research has been performed by many scientists as evidenced by the ever-growing number of publications in the literature there are still many issues that need to be resolved. One such issue, which has been addressed to some extent in this thesis, is the location and competitive interaction of plasticizer and polymer onto the clay. The future work presented here aims to complete some of the finer details within the thesis that need addressing further and to encompass the general forward direction of the research.

TGA was successfully developed to quantify the amount of PVOH and plasticizer that associated with clay gallery when present simultaneously. This simple and time-efficient technique could be further applied to several other polymer composite systems, which have similar degradation temperatures such as starch (320 °C) [8.1], cellulose (365 °C) [8.1], chitosan (355 °C) [8.2,8.3] and PLA (376.5 °C) [8.4]. Comparing the competitive adsorption of plasticizers within different polymer-matrix systems would allow further understanding of the competitive adsorptions processes that occur.

Due to time constraints within the project, the use of PEG2000, M600, QM600 and other hydrophobic plasticizers such as PPG in PVOH and their effect on the water vapour barrier properties was not assessed. Whether these could be used to improve the barrier properties would be assessed and related to their effect on clay dispersion. It was found that these plasticizers can have very negative effects on the film forming properties of PVOH and so this would need to be overcome. The quaternization of amino PEG600 and its cation exchange onto clay resulted in a maximum d-spacing of $\approx 19 \text{ \AA}$. Lin [8.5,8.6] created organo-clays with much higher d-spacings (92 \AA) using protonated polyetheramines. It would be very interesting to investigate the mechanical and barrier properties of PVOH films containing these very well ordered structures since it would represent a unique type of clay dispersion. The hydrophobic environment and presumably ordered structure of the alkyl chains within the clay gallery may significantly contribute to the barrier properties.

As shown in this thesis the extent of crystallinity and water content in PVOH films is crucial for good water vapour barrier properties, better knowledge of the re-adsorption processes of water into the film, especially in the presence of clay, is therefore important. Since PVOH is very sensitive to water, it becomes imperative that the techniques used to monitor the changes in properties don't actually change the properties of the films, This was noted in the WVTR results of this thesis in which the films began to dry out whilst the WVTR analysis was being formed. Performing the experiments in a controlled and closed environment could overcome these problems.

It was shown that that route 3 (PEG 1st) created a higher d-spacing than those of route 1 and 2. The permeability of PVOH nanocomposites in the presence of 20 wt% PEG600 prepared via route 1 have been investigated, It

would be interesting to investigate the water permeability of PVOH nanocomposites prepared via route 3 in order to determine whether an effect would be observed.

The mechanical properties of PVOH/clay using dynamic mechanical analysis (DMA) were only tested in a tension set up. An investigation into the flexibility of these films using either single or dual cantilever mode in a controlled humidity and temperature environment could then be correlated to location of plasticizer within the film and as well as plasticizer content, clay content and clay dispersion.

8.6. References

- [8.1]. Alvarez, V. A. and VÁZQUEZ, A. (2004). Thermal degradation of cellulose derivatives/starch blends and sisal fibre biocomposites. *Polymer degradation and stability*, **84** (1), 13-21.
- [8.2]. Wang, S. F., Shen, L., Tong, Y.J., Chen, L., Pang, I.Y., Lim, P.Q. and Liu, T.X. (2005). Biopolymer chitosan/montmorillonite nanocomposites: Preparation and characterization. *Polymer degradation and stability*, **90** (1), 123-131
- [8.3]. Hong, P.Z., Li, S.D., ou, C.Y., Li, C.P., Yang, L. and Zhang, C.H. (2007). Thermogravimetric analysis of chitosan. *Journal of applied polymer science*, **105** (2), 547-551.
- [8.4]. Ohkita, T. and Lee, S.H. (2006). Thermal and biodegradability of Poly(lactic acid)/corn starch biocomposites. *Journal of applied polymer science*, **100** (4), 3009-3017.
- [8.5]. Lin, J.J., Cheng, I.J., Wang, R., and Lee, R.J. (2001). Tailoring basal spacings of montmorillonite by poly(oxyalkylene)diamine intercalation. *Macromolecules*, **34** (26), 8832-8834.
- [8.6]. Lin, J. J., Chen, I. J. and Chou, C. C. (2003). Critical conformational change of poly (oxypropylene) diamines in layered aluminosilicate confinement. *Macromolecular rapid communications*, **24** (8), 492-495.

A1. Award and presentation in seminar and conferences

1. 1st Prize Winner for "The Best Oral Presentation" at MERI Student Presentation Day, Sheffield Hallam University-UK, 20 May 2009.
2. Khairuddin, Francis Clegg, Chris Breen "Understanding the synergistic and competitive interactions between clay, polymer and plasticizers in nanocomposites", Oral Presentation at EUROCLAY 2011 Conference, Antalya, Turkey, 26 June - 1 July 2011.
3. Khairuddin, Francis Clegg, Chris Breen "Competitive Adsorption of Polymer and Plasticizer into the Clay Gallery ", Poster Presentation at Trilateral Meeting on Clays, Seville, Spain, 8-11 June, 2010
4. Khairuddin, Francis Clegg, Chris Breen "Exploring the Competitive Adsorption of Starch and Plasticizers in The Clay Interlayer and Its Influence of the Barrier Properties of Starch Nanocomposite Paper Coatings", Oral Presentation at Trilateral Meeting on Clays, Seville, Spain, 8-11 June, 2010
5. Khairuddin, Francis Clegg, Chris Breen "X-ray Diffraction Studies of Plasticized Poly(vinyl alcohol)/Montmorillonite Nanocomposites^{Part 2} ", Poster Presentation at MERI Student Presentation Day, Sheffield Hallam University, UK, 26 may 2010
6. Khairuddin, Francis Clegg, Chris Breen "X-ray Diffraction Studies of Plasticized Poly(vinyl alcohol)/Montmorillonite Nanocomposites^{Part 1} ", Poster Presentation at the Futuroclays Meeting, Newcastle, UK, 14-16 December, 2009
7. Khairuddin, Francis Clegg, Chris Breen "The Interaction between Plasticizer and Clay in Poly(vinyl alcohol) Nanocomposites", Poster

Presentation at the XIV International Clay Conference, Italy, 14-20 June

2009

8. Khairuddin, Francis Clegg, Chris Breen "Optimisation of Clay Polymer Plasticizer Mixtures for Packaging Application", Oral Presentation at MERI Student Presentation Day, Sheffield Hallam University, UK, 20 May 2009

A2. Conference and seminars attended:

1. The 197th Infra Red and Raman Discussion Group Christmas Meeting, London, UK, 20th December 2011.
2. EUROCLAY 2011 Conference, Antalya, Turkey, 26 June - 1 July 2011.
3. MERI Student Presentation Day, Sheffield Hallam University, UK, 25 May 2010.
4. The 194th Infra Red and Raman Discussion Group Christmas Meeting, London, UK, 16th December 2010.
5. Seminar on Bio-Plastic Food Packaging, Newport Shropshire, UK, 23 June 2010.
6. The TMC "Trilateral Meeting on Clays": General Meeting and Symposium in Seville, Spain, 8-11 June 2010.
7. MERI Student Presentation Day, Sheffield Hallam University, UK, 26 May 2010.
8. Macro Group Young Research Meeting' 2010, Nottingham, UK, 29-30 April 2010.
9. The Futuroclays Meeting, Newcastle, UK, 14-16 December, 2009.
10. The XIV International Clay Conference, Castellaneta Marina, Italy, 14-20 June 2009.
11. MERI Student Presentation Day, Sheffield Hallam University, UK, 20 May 2009.
12. Weekly MERI and PCAS Seminars, Sheffield Hallam University, UK, October 2008 – to date.